MECHANISTIC PHASE INVERSION OF SATURATED FATTY ACID-BASED *IN SITU* FORMING MATRIX FOR PHARMACEUTICAL APPLICATIONS
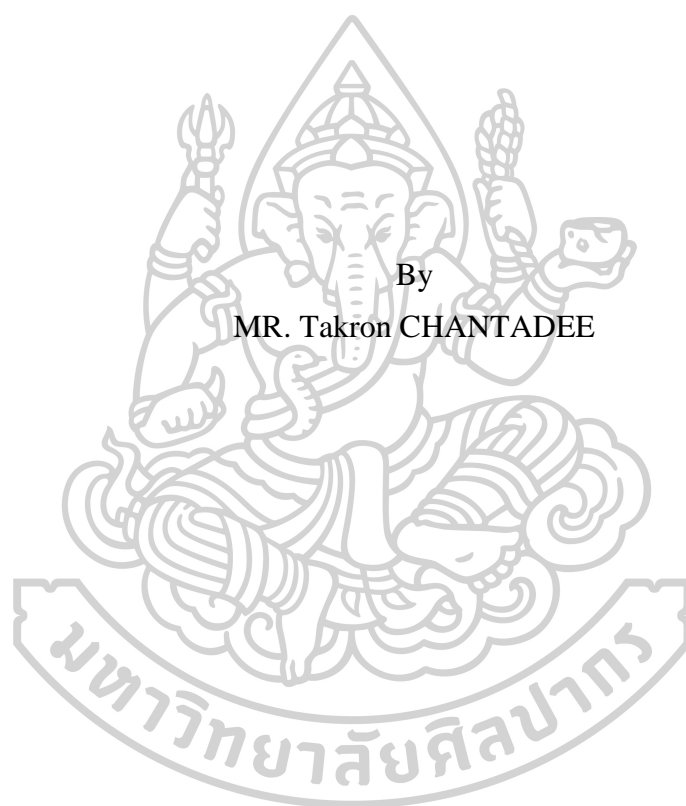
By

MR. Takron CHANTADEE

A Thesis Submitted in Partial Fulfillment of the Requirements
for Doctor of Philosophy (PHARMACEUTICAL TECHNOLOGY)
Department of PHARMACEUTICAL TECHNOLOGY
Graduate School, Silpakorn University
Academic Year 2020
Copyright of Graduate School, Silpakorn University

กลไกการกลับวัฏภาคของเมทริกซ์ก่อตัวเองจากกรดไขมันอิ่มตัวสำหรับการประยุกต์ใช้ทางเภสัชกรรม

โดย
นายฐกร จันทะดี

วิทยานิพนธ์นี้เป็นส่วนหนึ่งของการศึกษาตามหลักสูตรปรัชญาดุษฎีบัณฑิต
สาขาวิชาเทคโนโลยีเภสัชกรรม แบบ 1.2 ปรัชญาดุษฎีบัณฑิต
ภาควิชาเทคโนโลยีเภสัชกรรม
บัณฑิตวิทยาลัย มหาวิทยาลัยศิลปากร
ปีการศึกษา 2563
ลิขสิทธิ์ของบัณฑิตวิทยาลัย มหาวิทยาลัยศิลปากร

MECHANISTIC PHASE INVERSION OF SATURATED FATTY ACID-BASED *IN SITU* FORMING MATRIX FOR PHARMACEUTICAL APPLICATIONS

By

MR. Takron CHANTADEE

A Thesis Submitted in Partial Fulfillment of the Requirements
for Doctor of Philosophy (PHARMACEUTICAL TECHNOLOGY)
Department of PHARMACEUTICAL TECHNOLOGY
Graduate School, Silpakorn University
Academic Year 2020
Copyright of Graduate School, Silpakorn University

Title	Mechanistic phase inversion of saturated fatty acid-based *in situ* forming matrix for pharmaceutical applications
By	Takron CHANTADEE
Field of Study	(PHARMACEUTICAL TECHNOLOGY)
Advisor	Associate Professor Thawatchai Phaechamud , Ph.D.

Graduate School Silpakorn University in Partial Fulfillment of the Requirements for the Doctor of Philosophy

.... Dean of graduate school
(Associate Professor Jurairat Nunthanid, Ph.D.)

Approved by

.... Chair person
(Associate Professor Sontaya Limmatvapirat , Ph.D.)

.... Advisor
(Associate Professor Thawatchai Phaechamud , Ph.D.)

.... Committee
(Assistant Professor Pawaris Wongprayoon , Ph.D.)

.... Committee
(Assistant Professor Jitnapa Sirirak , Ph.D.)

.... External Examiner
(Associate Professor Wiwat Pichayakorn , Ph.D.)
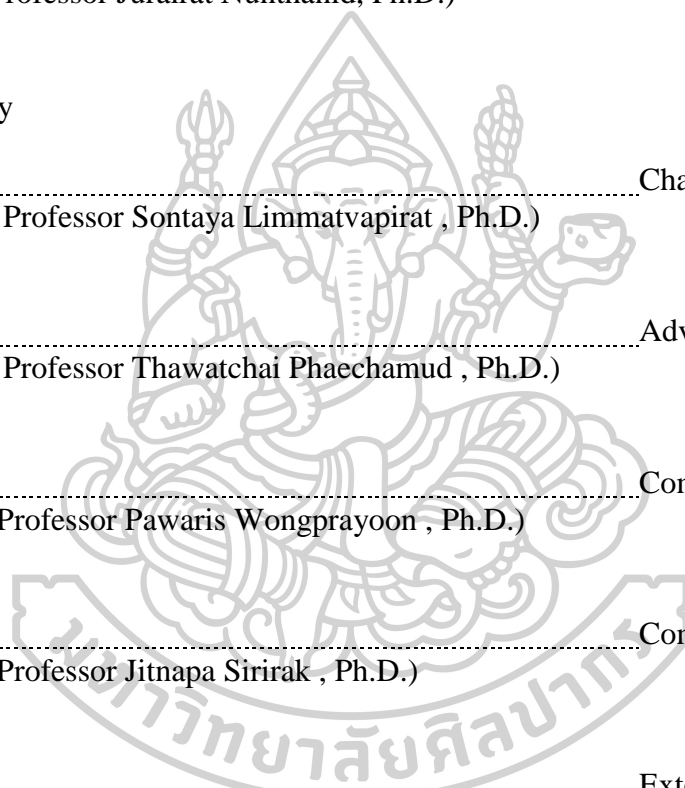
60353803 : Major (PHARMACEUTICAL TECHNOLOGY)
Keyword : In situ forming matrix, Saturated fatty acid, Vancomycin hydrochloride, Local drug delivery system, Molecular dynamics simulation

        MR. TAKRON CHANTADEE : MECHANISTIC PHASE INVERSION OF SATURATED FATTY ACID-BASED *IN SITU* FORMING MATRIX FOR PHARMACEUTICAL APPLICATIONS THESIS ADVISOR : ASSOCIATE PROFESSOR THAWATCHAI PHAECHAMUD, Ph.D.

        Saturated fatty acids of different chain lengths (C_8–C_{18}) were studied as matrix forming agents in this investigation as the localised injectable vancomycin HCl (VCM)-loaded solvent exchange-induced *in situ* forming matrices (ISM). The fatty acid-based ISM showed a low viscosity with high injectability. Their phase transition and matrix formation at the microscopic and macroscopic levels depended on the chain length of fatty acids, fatty acid concentration and solvent type. The VCM release pattern depended on the nucleation/crystallization, solvent exchange behaviours of the delivery system, aliphatic chain length of the fatty acid, and the environmental temperature. Molecular dynamics (MD) simulations completed the understanding *in situ* matrix formation process and movement/location of VCM. The developed VCM-loaded *in situ* forming systems presented efficient antimicrobial activities against standard microbes such as *Staphylococcus aureus* and Methicillin-resistant *S. aureus* (MRSA). Hence, VCM-loaded fatty acid-based ISM is a potential delivery system for the treatment of local Gram-positive infection sites, such as joint infection after total knee arthroplasty and periodontitis. The understanding for this mechanistic phase inversion serves as a fundamental knowledge for further development of ISM based on fatty acid for loading other drugs.

ACKNOWLEDGEMENTS

TABLE OF CONTENTS

Page

LIST OF TABLES

Page

LIST OF FIGURES

Page

LIST OF ABBREVIATIONS

%	percent
%v/v	percent volume by volume
%w/v	percent weight by volume
%w/w	percent weight by weight
°C/min	degree Celsius per minute
°C	degree Celsius
cm^{-1}	per centimeter
Å	Angstrom
α	alpha
β	beta
r^2	coefficient of determination
®	trademark
μg	Microgram(s)
μL	Microliter(s)
μg/mL	microgram per milliliter
μm	Micrometer(s)
k	release rate
n	solvent release exponent value
±	plus-minus
2θ	two theta
Abs	absorbance
ANOVA	way analysis of variance
ATCC	American Type Culture Collection
DMST	Department of Medical Sciences Thailand
cm	centimeter(s)
CO., LTD.	Company Limited
cPs	centipoise
CPL	Caprylic acid
CPR	Capric acid
BCS	biopharmaceutics classification system
DMSO	dimethyl sulfoxide
dL/g	deciliter per gram
DSC	Differential scanning calorimetry
DTG	differential thermogravimetric analysis
e.g. (Latin);	for example
Eq.	equation
et al.	and others
etc. et cetera	and other things/ and so forth
FE-SEM	field emission-scanning electron microscope
Fig.	figure
FT-IR	Fourier-transform infrared

g	gram (s)
g/kg	gram per kilogram
g/dL	gram per deciliter
G (needle)	gauge
GCF	gingival crevicular fluid
h	hour(s)
HCl	hydrochloride
HPLC	High-performance liquid chromatography
HSM	hot stage microscope
ISM	*in situ* forming matrix
KBr	Potassium bromide
KH_2PO_4	potassium dihydrogen phosphate
kV	killo volt(s)
L	liter(s)
LAU	Lauric acid
LD_{50}	median lethal dose
LSD	least significant difference
M	Molar
mg	Milligram(s)
MIC	Minimum inhibition concentration
mm	millimeter
mL/Kg	milliliter per kilogram
min	minute(s)
mL	milliliter(s)
mV	millivolt(s)
MW	molecular weight
MRSA	methicillin-resistant *Staphylococcus aureus*
msc	model selection criterion
MHA	Mueller-Hinton agar
MYR	Myristic acid
N	newton
mN/m	meter newton/meter
Nm	newton meter
nm	namometer(s)
NMP	N-methyl pyrrolidone
No.	number
ND	not determine
ns	nanosecond(s)
NSAIDs	non-steroidal anti-inflammatory drugs
o/o	oil in oil
o/w	oil in water
OH	hydroxyl
PAL	Palmitic acid
PB	phosphate buffer solution

PD	probing depth
pH	potentia hydrogenii (Latin); power of hydrogen
PI	plaque index
PLA	Poly(lactide)
PLGA	Poly(D,L-lactide-co-glycolide)
PYR	2-pyrrolidone
Rpm	revolutions per minute
sec	second(s)
S.D.	standard deviation
SEM	scanning electron microscopy
SPSS	statistical package for social sicence
STR	Stearic acid
TG	thermogravimetric
TGA	Thermogravimetric analysis
UV-vis	Ultraviolet-visible
UK	United Kingdom
USA	Uinted States of America
VCM	Vancomycin Hydrochloride
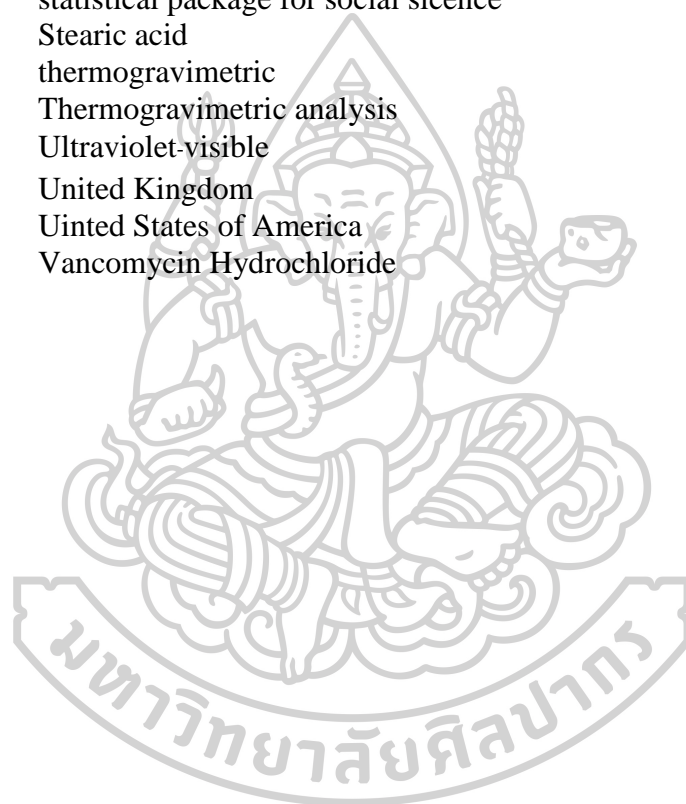
CHAPTER 1

INTRODUCTION

RATIONAL AND PROBLEM STATEMENT

The beneficial usages of antibiotic drugs with local drug delivery are side effect minimization, less potential antibiotic resistance and adequate/effective concentration at the target site. *In situ* forming systems are recognized as the one of useful pharmaceutical delivery systems due to their self-transformation into an expected state such as gel, solid, and microparticle after administrating into the target site for controlling drug liberation. Solvent-exchange induced *in situ* forming system is one of the various types of these systems. Drug-loaded solvent exchange-induced *in situ* forming matrices (ISM) were prepared by dissolving that active compound with water-insoluble polymers such as poly (D,L-lactide-co-glycolide) (PLGA) [1], ethyl-cellulose [2] and eudragit RS [3] in the biocompatible solvents such as *N*-methyl-pyrrolidone (NMP) or dimethyl sulfoxide (DMSO). The prepared drug-loaded polymeric solutions converts into a solid-like matrix after being exposed to an aqueous physiological environment [4,5] owing to the inward diffusion of the aqueous fluid from the target site and the outward solvent diffusion from the delivery system inducing phase inversion of water-insoluble material. The hydrophobic property seems to be a crucial factor to the designing of this system. Thus, another aqueous insoluble material such as lipid is of interest for using as a matrix former of the solvent exchange-induced ISM.

Fatty acids have been used as multipurpose natural nutrient/material such as the components in food, cosmetic and pharmaceutical products [6]. They could modify the properties of pharmaceutical product or drug molecule such as increasing dissolution, permeability, absorption, stability, and controlling drug release resulting in promoting higher clinical effectiveness. Saturated fatty acid nanoparticles have been used for loading podophyllotoxin [7] or as an aggregate to achieve a sustained drug release [8]. The mixture of hydrophilic polymer and saturated fatty acid was found to achieve a desired sustained drug release from the capsule [9]. Fatty acids are found typically in the human body and food [10-12]. Fatty acids can be metabolized in human body [13]. Some short and medium chain fatty acids exhibit the antimicrobial activity against various bacteria and fungi [14,15]. Thus, biocompatible, biodegradable, low-toxic and hydrophobic material such as saturated fatty acids were of interest as the core components of various drug delivery systems [16]. Owing to various length of aliphatic chain, they have different unique properties such as crystallinity and thermal properties [17] resulting in various outcome. For example, the release of metoprolol tartrate from behenic acid-based matrices was slower than stearic acid-based matrix [18]. Using longer aliphatic hydrocarbon chain fatty acid showed a lower drug/fatty acid interaction than the shorter one [19]. Thus, the type of fatty acid might affect to the *in situ* forming system such as self-transformation behavior and sustaining drug release ability. One of the main different characters of fatty acid from the most of polymers is the crystallinity property

which differentiate the properties of fatty acid-based from polymer-based *in situ* forming system. Nucleation and crystallization have been known as an important role in pharmaceutical field since they relate to the expected/unexpected properties of active ingredient and/or the formula which refer to the manufacturing process and quality of the product as well as in the delivery system development such as nanoparticles [20], microparticles [21] and macrostructure matrix [22]. The pattern of nucleation and crystallization influences on the polymorph of crystal affecting the mechanical, physical and thermal properties of materials [23,24]. Therefore, these might be a key parameter of various outcomes of fatty acid-based *in situ* forming system and play an important role on its matrix formation mechanism.

NMP, DMSO and 2-pyrrolidone (PYR) have been used as the solvents for ISM [25] because of their biocompatible and low toxic characters [1,26]. DMSO has been used in injection and subcutaneously implanted dosage forms and also been used as a solvent in *in situ* forming implant and *in situ* forming microparticles [27-29]. NMP is a thermally stable, biocompatible, high solubilizing power solvent [29,30] and it shows low toxicity both orally and parenterally [31]. PYR has been used as a solvent of ISM [25,32] and *in situ* forming microparticles 32],[33 and has been reported as a plasticizer to improve a mechanical properties and reduced a drug burst release of spider silk films [34]. It was suggested that the mixed solvent concept can be used to modify the properties of the formulation. Using the mixture of NMP and triacetin as a solvent for poly lactic acid-based *in situ* implants had a different effect on viscosity, matrix morphology and ability to sustain ivermectin and thymosin alpha1 release [35,36]. Thus, the paired solvent mixture of above three solvents might modify the physicochemical properties of prepared ISM.

Vancomycin HCl (VCM) is a suitable antibiotic for periodontitis treatment by direct administration to periodontal pocket due to its antimicrobial activity against pathogenic bacteria and its clinical use as VCM ointment in an oral cavity. Moreover, it has a very low oral bioavailability (<10%) and has potential cause of a serious side effect *via* an intravenous route [37,38]; therefore, the development into the local dosage form such as ISM is very interesting to keep a high drug concentration at the target site and thereafter minimize the side effect [39] with good patient compliance [40]. In cases of knee infection, it has been reported to be administered this drug *via* the intra-articular route [41]. Because of its very low oral bioavailability, the parenteral route is normally selected route for administration [42]. Both of the concentration of VCM and the therapeutic period are crucial factors for achieving an effective treatment for bacterial infections of joints [41]. Fatty acid-based ISM which could modify the drug release by varying fatty acid type and environmental temperature is of interest for applying to deliver of VCM for patients with joint infection after total knee arthroplasty.

The aims of this study were to prepare solvent exchange-induced ISM for antimicrobial agent delivery by using saturated fatty acids with different molecular

chain lengths as the matrix formers and to investigate the physicochemical characteristics of prepared formulas as a product for periodontitis treatment and joint infection after total knee arthroplasty treatments. To achieve the system modification, understanding the effect of component was needed. Thus, the influence of aliphatic chain length of fatty acid in various solvent systems on physicochemical characteristics of prepared ISM was studied. ISMs were prepared from six fatty acids including caprylic acid (CPL), capric acid (CPR), lauric acid (LAU), myristic acid (MYR), palmitic acid (PAL) and stearic acid (STR) in various solvent systems including DMSO, NMP, PYR and mixed solvent. Both of solution and the transformed state of prepared formulas were investigated such as viscosity, rheology, matrix formation behavior, solvent exchange mechanism, ability to prolonging drug release, crystallinity, morphology and thermal behavior. The profound explanation was established for the mechanistic phase transition of solvent-exchange induced saturated fatty acid ISM. In addition, the modeling interfacial interaction / solvent exchange with saturated fatty acid matrix formation of this delivery system was conducted. The molecular dynamics (MD) simulation was performed to understand and clarify the mechanism underlying this system, its macro/microscopic properties, and the initial step of the *in situ* formation process.

OBJECTIVES

1. To determine the mechanistic phase inversion of solvent exchange-induced saturated fatty acid ISM.
2. To investigate the physicochemical properties and transformation behaviors of saturated fatty acid-based ISM.
3. To develop VCM-loaded saturated fatty acid ISMs for periodontitis treatment and joint infection after total knee arthroplasty treatment.

HYPOTHESIS

1. The types of solvents, fatty acids molecular weight and their concentrations can influence the physicochemical properties and transformation behaviors of saturated fatty acid-based ISM.
2. The types of solvents, fatty acids molecular weight and their concentrations can influence the release pattern of vancomycin HCl from saturated fatty acid-based ISM.
3. The conductivity and ion of the environment can influence the nucleation and crystallization of saturated fatty acid-based ISM.

BENEFITS OF THIS STUDY

The fatty acid-based ISM showed markedly low viscosity and apparent high injectability promoting their ease for injection than the typical polymeric ISM and became more convenience for both patient and medical staff during administration. The fatty acid type, solvent type, fatty acid concentration, mixed ratio of fatty acid and

mixed ratio of solvent affected the transformation behaviors at both microscopic and macroscopic levels. The developed ISM prolonged the release of VCM for 6-7 days due to its hydrophobicity and high matrix tortuosity. The release pattern and drug release sustainability of ISM were differentiated by the fatty nucleation/crystallisation and the solvent exchange behavior, wherein the various interior structure were obtained. The VCM-loaded fatty acid ISM showed the efficient antimicrobial activities against various pathogens. The MD simulation of the low- and high-water-ratio regions elucidated the initial phenomenon of *in situ* formation process of developed VCM-loaded fatty acid-based ISM.

This study provided the fundamental information on further development of drug delivery sustems using various fatty acids as a matrix former for solvent exchange-induced *in situ* forming system. VCM-loaded saturated fatty acid ISMs can become suitable local antimicrobial delivery systems for treatment of various Gram-positive bacterial infection sites, such as joints, crevicular pockets and post-surgery sites. The administration amount can be adjusted based on the following considerations: the fluid volume at the target site, the minimum inhibition concentration of any bacteria at the infection site and the pharmacokinetics of VCM at the target site. This study provided fundamental information on further development using various fatty acids as a matrix former for solvent exchange-induced *in situ* forming system for other groups of active compound, wherein the drug release sustainability is required such as anticancer, anti-Alzheimer, immunoglobulin, hormonal drugs and other non-communicable disease drugs.

CHAPTER 2

LITERATURE REVIEW

Saturated fatty acid

Fatty acid is a carboxylic acid with a various aliphatic carbon chain which differ them from each other. Fatty acids containing straight chain with a single carbon-carbon bonds are called saturated fatty acid. Saturated fatty acids are separated by the length of carbon chain as shows in Table 1. Various saturated fatty acids are synthesized in the human body and found in human food [10-12]. They can be catabolised *via* ω-, α- or β-oxidation and the tricarboxylic acid cycle pathways [13]. The biocompatible and inert properties of these substances have been known [13,43]. These pointed out the safety of saturated fatty acid. MYR showed a low acute toxic in rat by orally and not induce mutation in bacterial and mammalian cells. No observed-effect level of LAU, MYR, STR and PAL has been reported at 12,000, >10,000, >5,000 and 5,000 mg/kg, respectively, when administered to rat *via* the oral route [13,44,45]. Short and medium chain fatty acids exhibit antimicrobial activity against several microbes such as *Propionibacterium acnes* [14], *Streptococcus mutans*, *Streptococcus gordonii*, *Streptococcus sanguis*, *Candida albicans*, *Aggregatibacter actinomycetemcomitans*, *Fusobacterium nucleatum* and *Porphyromonas gingivalis* [15]. The influence of low pH was used to explain this activity [46]. Moreover, fatty acids are known that they could dissociate bacteria membranes resulting in disorganization of them [46,47]. LAU was fused into PLGA matrix to form triple layered to promote an antimicrobial activity [48]. Anti-inflammatory of CPL *via* suppression of the IL-8 secretion was reported [49] in which used for promoting clinical effectiveness of mesalamine for inflammatory bowel diseases [50]. Since fatty acids could modify the properties of pharmaceutical product or drug molecule, they have been used in many pharmaceutical products [6]. The 12-18 carbon atom fatty acids could enhance the skin permeability of drug from transdermal delivery system by lipid layer interference and the increasing of lipid fluidity in stratum corneum [51,52].

Table 1 The thermal properties of fatty acids

Fatty acid	Molecular formulation	Melting temperature (°C)	Melting latent heat (J/g)	Reference
Caprylic acid (CPL)	$CH_3(CH_2)_6COOH$	16.10	144.2	[53]
Capric acid (CPR)	$CH_3(CH_2)_8COOH$	32.14	156.40	[54]
Lauric acid (LAU)	$CH_3(CH_2)_{10}COOH$	43.55	184.29	[55]
Myristic acid (MYR)	$CH_3(CH_2)_{12}COOH$	51.80	178.14	[56]
Palmitic acid (PAL)	$CH_3(CH_2)_{14}COOH$	60.42	233.24	[56]
Stearic acid (STR)	$CH_3(CH_2)_{16}COOH$	66.86	258.98	[56]

STR was used as a core component in nanoparticles drug delivery system for loading podophyllotoxin to achieve a sustained drug release [7]. The aggregation of STR and chitosan was developed to deliver doxorubicin which promoted the bioavailability of encapsulated drug [8]. Poorly water soluble drug such as prednisolone was loaded into stearic-based solid lipid nanoparticles for controlled the release pattern from buccal tablets [57]. Cationic aggregates were formed by using LAU resulting in a prolonged drug release from agar gel [58]. The sesame oil and soy oil oleogels were prepared by using STR as a gel former. The properties of oleogels such as spreadability and viscosity could be modified by varying the amount of STR [59]. The mixture of hydrophilic polymer such as povidone and hydroxyl propyl cellulose with a fatty acid such as LAU and STR was found to achieve a sustained drug release from the capsule. Sustained drug liberation from capsule was achieve by mixing hydrophilic polymer, fatty acid and the drug in capsule then exposed to 50°C [9]. High methotrexate loading nanoparticle was developed by using lipid and STR-valine conjugated as a core shell. The STR-valine conjugate acted as a biosurfactant for initial core shell forming during anti-solvation process [60]. Ibrutinib was encapsulated in nanocomplexes which were formed by using sialic acid (SA)–STR conjugate for targeted immunotherapy [61]. The slow drug release pattern from fatty acid-based matrix could be improved by adding water soluble agent. Benzoic acid release behavior was modified by adding lactose filler into STR-based compacts [62]. Sustaining release of high water soluble drug such as metoprolol tartrate was elevated by using high molecular weight polyethylene oxide and STR as the matrix components [63].

The various length of aliphatic chain incurs the different physicochemical properties of saturated fatty acid which differentiates them from each other. The longer aliphatic chain fatty acid presents a higher melting temperature and melting latent heat as shows in Table 1. The mixed fatty acid can cause eutectic which has a lower melting point than pure substance. The binary mixtures of 5:5 CPL:CPR, 5:5 CPR:LAU, 5:5 LAU:MYR, 5:5 MYR:PAL, and 6:4 PAL:STR showed an eutectic temperature at 3.58°C, 20.21°C, 34.95°C, 45.47°C, and 55.59°C, respectively [17]. The ternary mixture of 55.2% LAU, 24.8% MYR and 20% PAL exhibited an eutectics system with the melting temperature of 31.1 °C and the latent heat of 166.6 J/g [64]. The eutectic composed of 40% LAU and 60% 1-tetradecene exhibits the melting temperature on 24.33 °C, and its melting latent heat is 161.45 J/g [55].

Crystallinity is a remarkable property of saturated fatty acid. Single crystals of LAU were grown by a slow evaporation of its solution and the monoclinic crystal structure was confirmed by single-crystal X-ray diffraction and X-ray diffraction analysis [65,66]. It is known that crystallization can affect to the mechanical, physical and thermal properties of the formulas [23,24]. There are many factors that can affect to the pattern of fat crystallization resulting in a change of macroscopic characters of each formulation. Macroscopic mechanical properties are influenced by solid fat content and

the morphology and interaction of crystals [67,68]. The key phenomenon of the STR-based oleogel formation was heterogeneous nucleation with the one-dimensional growth of STR. The rate of crystallization and amount of crystal were according to the amount of STR in the formulation which affected the viscosity and mechanical properties [59], likewise, more amount of PAL in the formulation of complex fluid promoted more rapid crystallization resulting in different rheological behavior owing to a different crystal morphology and inter-particle interactions [69]. However, the crystallinity of fatty acids was not much different. There were no different physical properties between MYR, PAL and STR coated magnetite (Fe_3O_4) nanoparticles under powder X-ray diffractogram [70].

The different physicochemical properties between each of saturated fatty acids resulting in various outcomes which could be applied for many purposes. For example, the longer aliphatic chain could promote the release-sustaining ability [18] and minimize the drug/fatty acid interaction [19]. The thermal conductivity of the formulas decreased with a longer carbon part of fatty acid [70].

In situ forming systems

In the past, liquid to solid phase inversion of the pharmaceutical formulations after administration seems to be a valueless phenomenon since it was the term of unstable properties. Nowadays, the phase inversion idea has been applied in the drug delivery systems over decades, called "*in situ* forming system". *In situ* forming system is an interesting drug delivery system since it has special and unique behavior which is a liquid state at first then becomes a semisolid, or solid by itself *via* various mechanisms such as thermally trigger mechanism [71-73], pH trigger system [74], solvent exchange mechanism [75], chemicals reaction [74,76] and etc. For example, thermosensitive *in situ* forming gel was developed by using poloxamer 407 as a gelling agent. The gelling temperature and gelling time seem to be potential points for this kind of system. It was a liquid form at room temperature and then became a gel by thermally trigged at 27.5±0.5°C [71]. The poloxamer 407-based *in situ* forming gel could modify the gel formation pattern by using NMP as an additive [77]. Low methoxy pectins solution which can form into gel by the free calcium ions was applied to be a pH-triggered *in situ* forming system. The free calcium was released when the complexed calcium in the formulation was breakdown by acidic environment then induced the gel formation [74]. The *in situ* forming concept was also applied to the *in situ* forming microparticles. The emulsion and solvent exchange concept were applied for this development. The solution of poorly water-soluble polymer, such as bleach shellac and PLGA, dissolving in various solvents was used as an internal phase of oil in oil emulsion. The emulsion could self-participate into microparticles when it was triggered by the aqueous solution [78-80]. Recently, the *in situ* process was requested for nanoparticles formation [81].

The solvent exchange mechanism is the migration of solvent outward from the systems to the environment while the aqueous phase of environment migrates inward resulting in the phase inversion of the matrix component which is a poorly water-soluble material [4,5]. PLGA was used as a matrix former for *in situ* forming implants to carry typical antipsychotics such as risperidone and paliperidone, which required a long-term drug delivery system. The application with this delivery system showed a good result clinically since it could load the 50% antipsychotics and minimize the burst release together with sustainable drug release over 3 weeks [5]. Ethylcellulose, bleached shellac, and eudragit RS were used as the aqueous insoluble materials of solvent exchange-induced *in situ* forming gel systems. These polymers were dissolved in NMP then the prepared solutions were tested on viscosity, rheology, rate of water penetration, injectability, gel formation behavior and gel degradation. The rapid gel formation behavior was achieved after injected their solutions into the aqueous phase [2]. Thereafter, doxycycline hyclate, metronidazole, and benzoyl peroxide were used as the antimicrobial agents for the antimicrobial-loaded *in situ* forming gel systems and they were evaluated similarly as previously mentioned. The systems exhibited a sustainable drug release pattern together with the efficient antimicrobial activities against *Staphylococcus aureus, Escherichia coli, Candida albicans, Streptococcus mutans,* and *Porphyromonas gingivalis* [3]. The *in situ* forming gel of buprenorphine was formulated by using PLGA-PEG-PLGA (triblock) as a gel former together with NMP as a solvent for minimizing the burst release. The thermosensitive property of the triblock and H-bonding between the solvent and the PEG of the triblock minimized the rapidly outward diffusion of the solvent resulted in a limited burst release [82]. The PLGA/hydroxypropyl methyl cellulose-based *in situ* forming implants was developed to improve the physical key properties such as hardness, springiness, resilience and stickiness. The developed system exhibits a sticking to teeth' surfaces and greater mechanical strength than the commercial products. Chlo-site® showed less adhesion and quickly shrank while Parocline® showed less mechanically strength [83]. Alginate microspheres encapsulated with *in situ*-formed bismuth sulfide nanoparticles was developed for tumor therapy via embolization, hyperthermia and sustained doxorubicin release ability [81]. Recently, not only polymers but also lipids that were used for *in situ* forming system development as a matrix component. Cholesterol was used as a matrix former of *in situ* forming gel to deliver doxycycline hyclate at a periodontal pocket for periodontitis treatment [84]. Phospholipid-based phase transition gel was developed for prolonging the release of ropivacaine. The prepared solution containing phospholipid, medium chain triglyceride dissolved in ethanol transformed into gel state rapidly after subcutaneous injection and prolonged drug release subsequently [85]. Solvent exchange *in situ* forming system was also developed for the macromolecule delivery such as insulin in which the phospholipid was used as a gel former [86]. Some lists of *in situ* forming systems with different trigger mechanisms are presented in Table 2.

Drug-loaded *in situ* forming systems *via* solvent exchange mechanism, which self transforms into a solid-like matrix after being exposed to an aqueous environment

of the target site, is one of the useful systems for many purposes since there is the biological fluid located in almost every parts of the creatures.

Table 2 Some in situ forming systems with different trigger mechanisms

System	*In situ* forming material	Solvent	Trigger mechanism	Drug	Target site	Ref
In situ forming gel	poloxamer 407 (pluronic® F127)	deionized water	thermally triggered	carmustine	nose to brain	[71]
In situ forming gel	poloxamer 407 (lutrol® F127)	water	thermally triggered	-	-	[77]
In situ forming gel	low methoxy pectins	ultrapure water	pH, chemical triggered	paracetamol	stomach	[74]
In situ forming micro-particles	bleach shellac	NMP, DMSO, PYR	solvent exchange	doxycycline hyclate	periodontal pocket	[78]
In situ forming micro-particles	PLGA	PYR, NMP, ethyl acetate	solvent exchange	-	-	[80]
In situ forming implants	PLGA	NMP, DMSO	solvent exchange	risperidone, paliperidone	subcutaneously	[5]
In situ forming gel	ethylcellulose, bleached shellac, and eudragit RS	NMP	solvent exchange	doxycycline hyclate	periodontal pocket	[2]
In situ forming gel	eudragit RS (ERS)	NMP	solvent exchange	doxycycline hyclate, metronidazole, benzoyl peroxide	periodontal pocket	[3]

Periodontitis

Nowadays, periodontal diseases affect about 20-50% of global population [87]. During 2009-2014 the prevalence of periodontitis in US adults was 42.2% [88]. The 25.9% of an adult and 36.3% of an elder in Thailand have a health problem on the periodontitis with 4-5 mm depth of periodontal pocket. Over 19.8% and 12.2% of those adult and elder have the severe periodontitis (>6mm deep of periodontal pocket) which can cause more risk of infection, inflammatory, losing teeth and also affect the quality of life. Moreover, it is a risk factor for cardiovascular disease such as coronary heart disease and stroke [89]. Gingivitis is the inflammation of gum caused by bacteria which does not include any loss of bone and tissue. However, it can advance to periodontitis which is a serious gum inflammation and more aggressive than gingivitis. Periodontitis damages the periodontal tissue and destroys the bone that supports the teeth resulting in various size of periodontal pocket which eases for bacteria accumulation [90,91] resulting in more

aggressive condition (Fig. 1). Most of the pathogen of this disease are gram-negative bacteria and some of them are anaerobe bacteria, for example, *P. gingivalis, Prevotella intermedia, Fusabacterium nucleatum* and *Actinobacillus actinomycetemcomitans, Bacteroides forsythus, S. sanguinis, Streptococcus mutans* [40,92,93]. These bacterial infection can cause the periodontium (gingiva, periodontal ligament, dental cementum, and alveolar bone) damages by the bacterial by-product and immune activation [94]. Some of microbes are related to the inflammation and tissue loss including enterobacteria (such as *E.coli, Pseudomonas aeruginosa* and *Klebsiella pneumoniae*), *C. albicans, Neisseria spp., Olsenella uli, Hafnia alvei, Serratia marcescens* and *Filifactor alocis* [95,96]. Moreover, *Staphylococcus aureus* could be found in periodontal pocket; there are 60.5% and 47.6% prevalence of *S. aureus* in non-smoking and smoking aggressive periodontitis patients [97]. Normally, the gap between gingival and tooth is around 1 mm. However, the periodontal pocket of periodontitis is usually exceeding 5 mm [98]. The saliva pH of 6.85 ± 0.27 in a periodontitis is significantly lower than that of the healthy saliva [99] and it is near to the pH in the periodontal pocket of 6.92 ± 0.03 [100].
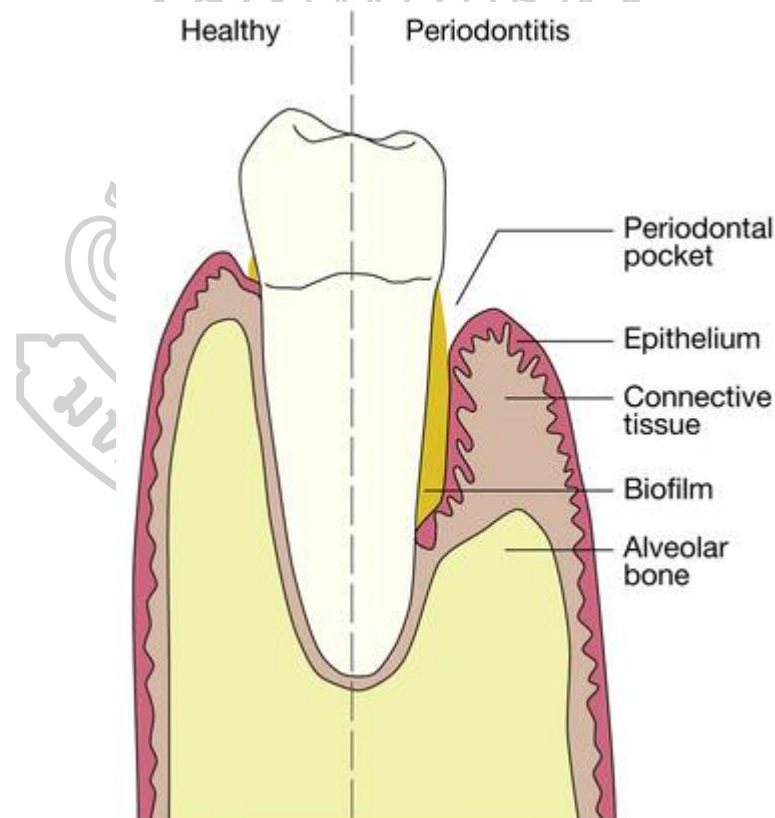
Figure 1 Characteristic of periodontitis
[101]

The treatment techniques for these diseases are recommended as following: mechanical (scaling and root planning, surgery, and root amputation), systemic and local antibiotics treatment [102]. The treatment with the systemic antibiotic treatment is used

to decrease in the pocket depth and attachment loss by eradication of the pathogens. Imidazole analogues, tetracyclines, penicillin, erythromycin, spiramycin, amoxycillin, clavulanic acid and clindamycin are the antibiotics for periodontitis treatment [92]. However, the high oral doses of them are needed for the effective concentrations in the gingival fluid, which can cause a various side effects. Moreover, long term use of the systemic antibiotic leads to the development of resistant bacterial strains [103]. Normally, the local irrigation is ineffective for periodontitis treatment. Although, intra-pocket irrigation is effective in controlling a periodontal infection; nevertheless, the patient compliance with this technique is poor [104]. The local antibiotics delivery systems are interesting to keep a high and effective drug concentration at the target site with minimizing the side effect [39]. The fibre [105], films [106,107], gel [108], strip [109], and *in situ* forming systems [78,110] have been developed or reported for carrying antibiotics as the local drug delivery systems for periodontitis treatment.

The irregular shape and various sizes of periodontal pocket seems to be the problem for mentioned local drug delivery systems. Those of them could not be fitted or well fitted with the various periodontal pockets. Moreover, the solid and semisolid dosage forms are difficult to insert into the tiny pocket. Thus, *in situ* forming drug delivery system, the liquid form at first, demonstrates a beneficial manner over those drug delivery systems due to the goodness of fitting to pocket, ease of use and acceptable clinical effectiveness [111]. There are the commercial products of *in situ* forming gel for periodontal pocket such as Atridox® comprising poly (lactic acid) in NMP as a matrix former for delivering doxycycline to periodontal pocket while Atrisorb® is used for tissue regeneration.

Normally, physiochemical properties of the prepared *in situ* forming system are tested including pH, viscosity, rheology, matrix formation, matrix morphology, adhesiveness and release behavior of active compound [3,35,36,112]. Animal model is used to investigate *in vivo* effectiveness of antibiotic-loaded *in situ* cubic liquid crystal. The rats were induced to become periodontitis by silk ligation combined with high-sugar feeding method before testing [113]. Beagle dogs were selected for *in vivo* study the efficacy of tinidazole-loaded *in situ* forming gel. The gingival index, bleeding on probing and probing depths were measured. The results showed significant decrease in periodontitis evidence [114]. The clinical outcomes of periodontitis treatment could be determined from the change of plaque accumulation, bleeding on probing, probing depths, recession, and clinical attachment loss. The distance from the cemento-enamel junction to the bottom which represents the bone defect is indicated by radiographic measurements. The change in the prevalence of bacterial species before and after treatment was also checked [111,115]. Suitable and well-evaluated formulation of ISM which can provide effectiveness, ease of use and less side effect should be considered for periodontitis treatment. However, the lipid-based ISM has not been reported; thus, it is interesting for developing as the drug delivery system for periodontitis treatment.

Postoperative knee infection

Knee is the main large joint which supports the body weight. The articulated joint is showed in Fig. 2. Lubricating property in the synovial joint is an important factor in the knee function. The biological lubricant components such as hyaluronic acid, lubricin, phospholipid component and protein are found in synovial fluid [116,117]. There are about 4 mL of synovial fluid in human knee joint [118,119] with very high viscosity of about 400 cps [120]. The declined viscosity is due to an inflammation of knee joint [121]. The normal synovial fluid pH is about of 7.35-7.4 [122,123]; whereas, it is more acidic for inflammatory knee joint [123,124]. The synovial fluid pH of septic arthritis appears lower than that of inflammatory or degenerative arthritis. The lower pH causes by the increase of lactic acid [125,126]. Knee joint is one of the most movement parts which gains a larger stress which lead to the degeneration of the articular cartilage, synovial joint and decrease in joint space resulting in knee osteoarthritis. Knee osteoarthritis causes a moderate to severe chronic pain and a disability of a knee function in patients [127-129]. Knee osteoarthritis is a common disease in elder with high prevalence. More than 50% prevalence of woman aged 80-89 years in Japan and the USA suffer from this disease [130]. It is also the most osteoarthritis found among 6 millions of Thai osteoarthritis patients [131]. The treatments with oral administration of NSAIDs and paracetamol, intra-articular corticosteroids injections are supportive care methods to relief the pain [132]. The intra-articular drug delivery can prolong the release of those drugs with ease to be used such as *in situ* forming system. A hydrophobic derivative of hyaluronic acid was used as a gel former of intra-articular *in situ* forming microgel for sustainable release of methylprednisolone over 4 days [133]. Celecoxib-loaded propyl-capped poly(ε-caprolactone-co-lactide)-poly(ethylene glycol)-poly(ε-caprolactone-co-lactide) triblock copolymer has also developed as *in situ* forming hydrogel for synovitis treatment due to its prolongation property over 4 weeks and ease of use [134,135]. However, the end-stage of osteoarthritis treatment needs the total knee arthroplasty. Total knee arthroplasty is the most cost-effective and clinically effective treatment for the end-stage osteoarthritis patients [136] with pain or abnormalities affecting the quality of life. However, the post-operative infection could be found after the arthroplasty affecting the patients in various aspects such as prolonged length of stay in hospital and more complicated condition, and the risk of mortality [137,138]. Serious postoperative knee infection, caused by the methicillin resistant *S. aureus (MRSA)* [139,140], could be treated by various methods including irrigation and debridement with component retention, one-stage or two-stage exchange, resection arthroplasty, and to a lesser extent by arthrodesis or amputation and antibiotic suppression [137,138]. Previously, intra-articular injection of antibiotics has been suggested for treatment of this infection. Intra-articular delivery of vancomycin resulted in a rapid higher peak of drug levels than that of an intravenous route and also resulted in therapeutic synovial fluid levels [41]. Clinically, 1 g of vancomycin was applied intravenously twice daily at least 2 days and intra-articular vancomycin (100-mg vancomycin/30mL sterile water) was used. Intra-

articular vancomycin is safe and effective against MRSA; therefore, it becomes the first choice for the postoperative knee infection treatment in Missouri Bone and Joint Research Foundation Institute [141]. However, the rapid clearance of intra-articular vancomycin should be considered. It might due to the lowering of the viscosity of synovial fluid during septic and inflammatory [118,121]. Gentamicin, vancomycin, tobramycin and cefuroxime have been reported as the active compounds in the impregnated cement which is one of the drug delivery systems that become an alternative method for treatment of this condition [139]. Using the local treatment is known that it has minimal side effect than the other administration routes and also provides an effective therapeutic level at target site. However, antibiotic-loaded *in situ* forming systems which can prolong the drug level in the knee joint with ease to be employed for this infection has not been reported. In the case of the knee with any pain, the synovial fluid volume is up to 7 mL and 20.5 mL with severe pain. The minimal inhibitory concentration of vancomycin against MRSA is 2-4 µg/mL[142] and its tissue distribution is 30% of serum [143]; thus, 7.5-15 µg/mL is needed to achieve for this desired therapeutic manner.

Lipid, one of the components in synovial fluid, is biocompatible and safe as mentioned previously. The self-degradation of lipid in human beings is also interesting, The degradation of fat is found in cartilage *via* oxidation [144] together with the lipolysis at an arthritic knee joint *via* lipid metabolism [145]. Thus, using lipid-based *in situ* forming system to deliver the antibiotics is interesting for postoperative knee infection and this concept idea has not been reported previously.
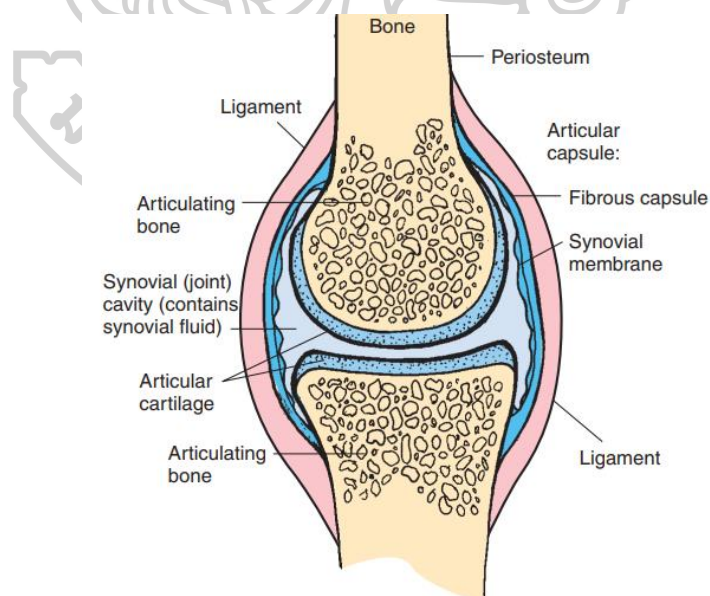
Figure 2 Anatomy of articulated joint
[118]

Vancomycin HCl

Vancomycin HCl (VCM) (Fig. 3), a hydrophilic molecule with a molecular weight of approximately 1450 Daltons, is a glycol-peptide bactericidal antibiotic [142]. VCM appears as a white solid which is soluble in water (200 mg/ml) [146]. The dissociation constant of VCM are 2.6, 7.2, 8.6, 9.6, 10.5, 11.7 for pKa1-6, respectively [147]. VCM diluted with water for injection (10 mg/mL) was stable for at least 84 days at 4°C and was stable at 25°C for 47 days [148]. The mechanism of antibacterial action of VCM is to inhibit bacterial cell wall synthesis, to disturb the permeability of bacterial cell membrane and RNA synthesis. VCM has been widely used for the treatment of infections caused by Gram-positive bacteria either susceptible or resistant Gram-positive bacteria especially, *S. aureus* (including MRSA), *S. epidermidis, Streptococci* spp., viridans group *streptococci.*, Enterococcus spp. [149-152]. It has limited antimicrobial activity against Gram-negative bacteria [153,154]. However, *P. gingivalis* is a VCM-susceptible anaerobic Gram-negative bateria [155,156]. VCM has a very low oral bioavailability (<10%) and its tissue distribution is 30% of serum [143]. It can cause a serious side effect *via* an intravenous route such as hematologic effects, cardiac arrest, shock, red-man syndrome and etc. VCM is used in various preparations such as intravenous, oral route, or extemporaneous formulations including ophthalmic, topical and oral cavity routes [37,38,157]. In the cases of knee infection, it has been reported to be administered this drug *via* the intra-articular route [41]. The minimum inhibitory concentration and minimum bactericidal concentration of VCM for *S. aureus* is 12.5 and 25 μg/mL, respectively [158]. The minimal inhibitory concentration of VCM against MRSA is 2- 4 μg/mL [142]. Antibiotics-microbial assay is the standard method for determine amount of VCM in United States Pharmacopeia [157]. In the research field, there are many research articles using UV-HPLC for VCM determination with UV detector at the wavelength of 280 nm [158,159]. As well as the standalone UV-spectrophotoscopy, this method has been used to investigate the release of VCM from various drug delivery systems in various dissolution media such as the release of VCM from hydrogel scaffold of silk fibroin/oxidized pectin in phosphate buffer saline [160]; biodegradable ß-Tricalcium phosphate-FeAg nanocomposites in tris-buffer solution [161]; cabopol nanogel in phosphate buffer solution [162].

Since VCM has less adverse effect on osteoblasts and skeletal cells, it is widely used to prevent the bone infection or osteomyelitis. The powder of VCM can be applied directly to the intrawound of hip and knee arthroplasty [163]. Intra-articular VCM with safe and effective is the first choice for the postoperative knee infection treatment in some institute [141]. However, the rapid clearance of VCM [41] should be considered since the effectiveness of infectious treatment of VCM depends on both duration of treatment and drug concentration. Impregnation of vancomycin to bone cement and beads has been developed to prevent and treat the knee infection. The release of VCM from the Palacos-cement, widely used cement for this infection, is longer than 2 months

and the release concentration is enough to against *S. aureus* and MRSA but not for high plaque *S. epidermidis* [164]. The VCM-loaded polyurethane scaffold for osteomyelitis was also developed to attain a sustained release of VCM over 7 weeks [146]. VCM-loaded hydrogel scaffold of silk fibroin/oxidized pectin exhibits a sustained release over 8 days with a zero-order release pattern [160]. Copolymers combination with thiolated hyaluronic acid was used to carry VCM with the controlled release pattern over 100 days. However, they needed a surgery to insert or remove the remnant after treatment [158]. Recently, the *in situ* forming system concept with the ease of application/administration without removal of remnant was of interest in field of drug delivery systems such as depot or implant. VCM-loaded PLGA-based *in situ* forming implants were employed for osteomyelitis treatment by using various ratios of acetone:NMP mixed solvents [158]. The developed formula controlled the release of VCM longer than 6 weeks. Thus, VCM is an interestingly antibiotic for periodontitis and post-operative knee infection treatment due to its antimicrobial activities against pathogenic bacteria. Additionally, the VCM-loaded fatty acid ISM has not been reported previously.
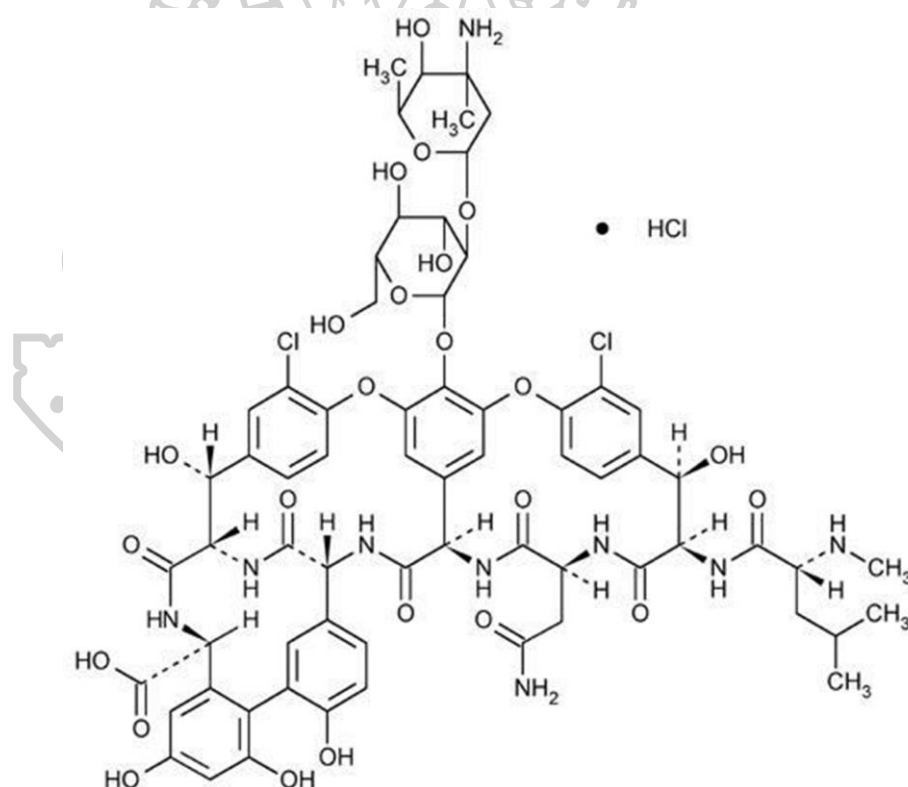
Figure 3 Chemical structure of VCM

Release kinetics

The controlled release systems are developed to maintain the level of the active ingredient in the blood or target sites at the preferred therapeutic value over the desired

period. *In situ* forming system, an outstanding controlled release system, has been developing over past decade. To understand the release behavior of each *in situ* forming system, the release kinetics are investigated. Various release models are studied to understand the mechanism of drug release from developed drug delivery systems and to predict the level of a drug during a period. The high amount of drug release with has no retarding effect from the system refer to the burst release effect. For many controlled systems, the burst release is usually showed at the initial step then the sustaining release is obtained subsequently. The release kinetics are used to fit with the release data or profile to indicate the release behavior of any controlled release system. The main release kinetic including zero order, first order, Higuchi's models, and power-law are well known. The degree of curve fitting is indicated by the coefficient of determination (r^2) in which a high r^2 value indicated a high degree of fit. According to the Korsmeyer–Peppas model, the diffusion exponent (n) from the power-law model indicates the drug transport mechanism [165-167].

1. Zero order release model

Zero order release is an ideal model for controlled release system in which the release rate is constant. The equation for this model is given below:

$$Q_t = Q_0 + k_0 t \qquad ...(Eq.1)$$

Where Q_t is the total amount of drug release at given time (t), Q_0 is initial drug release, k is the release rate constant, and t is given time.

2. First order release model

The release rate of this model is proportional to the rest of drug in system [168]. The equation for this model is given below:

$$Q_t = Q_0 e^{-kt} \qquad ...(Eq.2)$$

Where Q_t is the total amount of drug release at given time (t), Q_0 is initial drug release, k is the release rate constant, and t is given time.

3. Higuchi's model

The release pattern which fit results of Higuchi's model claimed the expedition of active ingredient through the tortuosity system, in which it accounted for the distance to the surface of the drug dissolution region. The Higuchi's model is given below [169,170].

$$Q_t = k\sqrt{t} \ ...(Eq.3)$$

Where Q_t is the total amount of drug release at given time (t), k is the release rate constant, and t is given time.

Taking logarithms of Higuchi's equation to verify the release follows Higuchi's model as:

$$\log Q_t = \log k + \frac{1}{2} \log t \ ...(Eq.4)$$

$$Q=[D\varepsilon/\tau(2A\varepsilon C_s)C_s t]^{\frac{1}{2}}...(Eq.5)$$

Where Q is weight of drug release per unit surface area, D is diffusion coefficient of drug in release medium, ε is porosity of matrix, τ is tortuosity of matrix, Cs is solubility of drug in release medium, and A is concentration of drug in matrix.

4. Semi-empirical equations of Peppas

The power-law model is used along with other models to explore the release kinetic mechanism *via* the semi-empirical equations of Peppas as given below.

$$\frac{M_t}{M_\alpha}=kt^n...(Eq.\ 6)$$

Where the M_t/M_α is the fractional of release of drug at given time (t), k is a constant incorporating the structure and geometric characteristic of system, and n is release exponent which using for indicate the release mechanism. This equation could be modified for application to non-planar geometric which could be used to analyzed the release from cylinders, spheres, tablets, and etc. under sink conditions.

For the non-swelling system with a cylindrical shape, the release exponent (n) implies the transport of drug, where n = 1 indicates the case-II transport mechanism, n = 0.45 indicates Fickian diffusion, 0.45 < n < 1 indicates anomalous diffusion, n < 0.45 indicates quasi-Fickian diffusion and n > 1 indicates super case-II transport (Table 3). In the case of swelling system with a cylindrical shape, n value, the 0.89 is used instead of 1. Fickian diffusion refers to the drug transport mechanism in which the rate of diffusion is more rapid than that of structure relaxation. Case-II transport occurs when the rate of relaxation is greater than that of diffusion. In the case that these two rate are closed to each other, anomalous diffusion is acquired [166,167,171,172].

Table 3 Diffusional exponent and mechanism of diffusional release from various non-swelling/swelling with a cylindrical shape controlled release systems

Diffusional exponent (n)		Drug release mechanism
non-swelling system	swelling system	
<0.45	<0.45	quasi-Fickian diffusion
0.45	0.45	Fickian diffusion
0.45-1	0.45-0.89	anomalous diffusion (non-fickian diffusion)
1	0.89	case-II transport
>1	>0.89	super case-II transport

Nucleation, crystallization and interface interaction

Nucleation is the initial step of crystal creation and then calls as a crystallization once the crystal is going growth. The new interface of a dense liquid in dispersed fluid indicates the nucleation formation. Namely, once the surface free energy presents the

nucleation is started. Nucleus is a single unit that has a complete unique structure. While the growing of smallest size with stable thermodynamics nuclei is the crystallization [173,174] as shown in Fig. 4.

The nucleation can be divided into two types (Fig. 5): primary nucleation which refers to the very first nuclei formation process or very far from any pre-existing nuclei; secondary nuclei are crystal nuclei produced subsequently from a pre-existing crystal. There are two subtypes of primary nucleation, homogeneous nucleation and heterogeneous nucleation. Homogeneous nucleation is the formation process from pure substance while heterogeneous nucleation occurs on a foreign surface or interface. Both of them are based on the same kinetics mechanism but heterogeneous nucleation exhibits a faster formation because of the lower free energy barrier [175,176]. The nucleation relies on thermodynamic and kinetic drives which need enough activation energy [177]. The new interface from various phenomena such as solvent evaporation, anti-solvation, undercooling process, etc. provides an unbalance of forces at the boundary and subsequently thermodynamic driving [177-180].

Nucleation and crystallization have been known as the important phenomena/behavior in the pharmaceutical field. They relate to the expected/unexpected properties of the active ingredient and/or the formula which refer to the manufacturing process and quality of the product as well as in the delivery system development such as nanoparticles, microparticles and macrostructure matrices. More amount of PAL in the formulation of the complex fluid showed more rapid crystallization resulting in different rheological behaviors owing to a different crystal morphologies and inter-particle interactions [69]. The various nucleation behaviors were studied to use as the template for expected structure. The controlled structure forming of nanostructured lipid carriers could be developed by using high-melting lecithin as a template for interfacial nucleation induction. Namely, high-melting lecithin solidified itself at an initial time as a shell then induced the shell-parallel nucleation of inner components as tristearin [181]. High methotrexate loading nanoparticles were developed by using lipid and STR-valine conjugate as a core-shell. The STR-valine conjugated was used as a biosurfactant for initial core-shell forming during the anti-solvation process [60].

There are many factors affecting nucleation and crystallization such as concentration, temperature, temperature changing rate, shear rate, shear stress, seeding agent, etc.; thus, controlling these parameters considerably can achieve the expected formulations. The eudragit L100-based nanoparticle for carrying Biopharmaceutics Classification System type 2 drugs, fenofibrate, was prepared by solvent replacement method. It was found that 1.35% of eudragit L100 reached the critical nucleation concentration but not too high resulted in agglomerate prohibition and expected nanoparticle subsequently [182]. Biphasic-calcium phosphate microspheres with different surface topographies for adjustable drug release were fabricated by controlling the process parameters relating to the nucleation and crystallization. These parameters

included template concentration, heat rate, and stirring speed. Under low heating rate and static conditions, the spherical microparticles with long and short nanosheets on the surfaces were obtained by using the low and high Ethylene diamine tetraacetic acid concentrations, respectively. The prepared microspheres were highly effective for target-substance loading and modulation of the release of both small and large molecules such as dexamethasone and bovine serum albumin, respectively [183]. Adding some agents can modify and control the nucleation. There are various organic molecules reported to control the nucleation and crystallization of the hydroxyapatite nanoparticles. Piperine could initiate the nucleation and control the topography of the nanoparticles. Without piperine, hydroxyapatite nanoparticles exhibit various distribution in the shape and size. Two different concentrations of piperine were used for modifying morphology of hydroxyapatite nanoparticles. The various well-controlled type and shape of hydroxyapatite nanoparticles can be employed as a drug delivery systems [184]. Some of ethylene copolymers, and small molecules with a long alkyl chain could affect the wax formation and can be used as a wax inhibitor of n-$C_{32}H_{66}$ in decane and de-aromatized white oil. The small amount of ethylene-co-vinyl acetate could delay the nucleation due to the minimization for nucleation onset temperature and lowering wax appearance temperature. Moreover, the wax inhibitor could alter the crystal-structure and morphology by adsorbing to the wax surfaces and inhibiting plate growth resulted in a small particle formation; thus, the macro-physical properties such as viscosity and the pour-point of oil were also improved. The impact of wax inhibitors was related to the amount and type of structure-disturbing groups in the copolymers since propylene copolymers, and ethylene copolymers with ethyl acrylate, maleic anhydride, and ethylene glycol showed a weak inhibiting effect [185]. The drug-loading method based on solvent evaporation and crystallization were developed. Functionalized calcium carbonate (FCC) microparticles and four drugs including ibuprofen, nifedipine, losartan potassium, and metronidazole benzoate were used. The heterogeneous nucleation was promoted by a high specific area of carrier and its large pore sizes which could reduce the crystallization pressures and lead to a drug deposition [186]. The immediate and sustained drug release tablets were prepared using poly (ethylene oxide) and poly caprolactone as the polymer, respectively. They were prepared by various thermal histories. The polymer crystallinity was affected by the different preparation methods resulted in the change of microstructure affecting the release from both tablets. Higher polymer crystals were found with higher mold temperatures resulted in decreasing of the metoprolol diffusion rate through the poly caprolactone matrix [22]. Therefore, the controlling nucleation means controlling crystallization influencing the size, size distribution and polymorph of crystal.

Since the pattern of nucleation and crystallization influences on the polymorph of crystal affecting the mechanical, physical, thermal properties of materials [23,24] and thereafter could affect the overall properties such as drug release as mentioned above. Thus, this might be a key parameter of various outcomes of fatty acid-based *in situ*

forming system and plays an important role on its matrix formation mechanistic. Three polymorphic forms are often found in saturated fatty acids including α (alpha), β` (beta prime) and β (beta) which differ in crystallinity, free energy, physical and chemical properties. Characteristic of each polymorph is different from each other such as melting point, re-solidification point, the heat of crystallization, specific volume and X-ray spacing and morphology. These different properties can affect the macro-properties of the products such as hardness, texture, and stability [187]. The α polymorph is most readily formed because of the lower saturation concentration requirement and loose packing structure, but it is very unstable. Normally, it will transform into the β` form within a short time. The β` form exhibits more stable because of the more packing and dense structure while β is the most stable but it is very rarely found because it needs a very slow crystallization rate [23,24].

The surface is the boundary between two phases which one of them cannot be clearly observed such as solid or liquid-vapor interface. The interface is a boundary between two phases which both of them can be clearly observed such as liquid-liquid interface, solid-solid interface and solid-liquid interface. Interfacial tension or surface tension (surface free energy) is the intermolecular attraction forces at the boundary. It has a dimension of force per unit length which the SI unit for interfacial tension is milli-Newtons per meter (mN/m) [188]. To be a well formed crystal, the thermodynamic stable conditions is required. Normally, the unstable cluster can be disappearing step backwards into the non-cluster. The stable or unstable clusters are affected by the surface tension of the cluster and the gain of energy upon crystallization [180]. According to the classical nucleation theory, the rate of nucleation also related to the interfacial tension at the particle-solution interface [177].

Heterogeneous nucleation is the formation on a foreign surface or interface such as on the foreign particle, air bubble, surface of container, etc. as mentioned. Therefore, it is related to the solvent exchange induced fatty acid-based *in situ* forming system which it has to expose to the aqueous environment and transform into fatty acid matrix. The interface between the developed system and the aqueous environment provides the free energy that can activate a nucleation through the thermodynamic drive. However, the relationship between nucleation, crystallization and interface interaction has not been reported for phase inversion of the fatty acid ISM *via* solvent exchange mechanism.
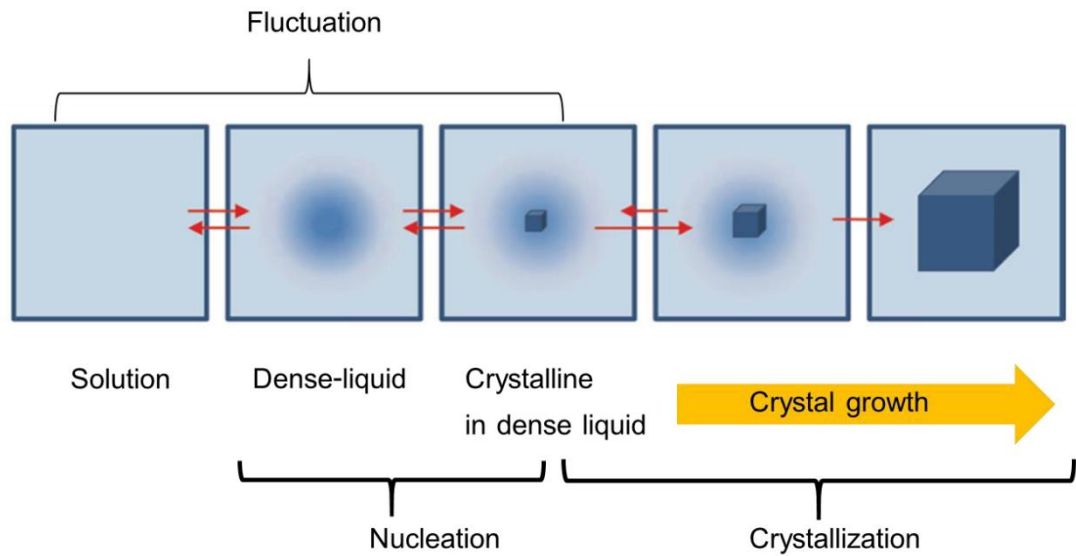
Figure 4 Nucleation and crystallization steps
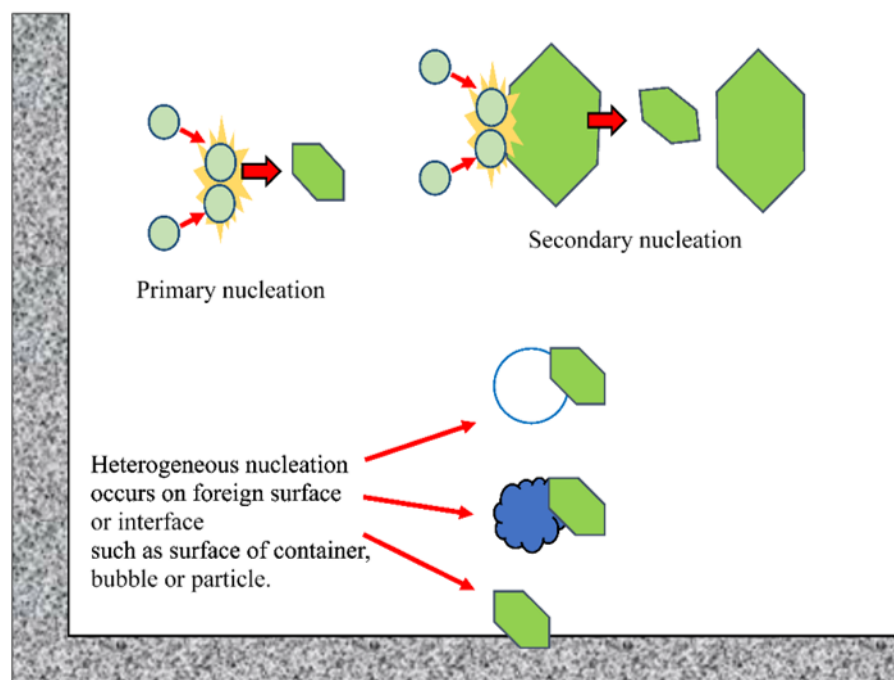
Figure 5 The types of nucleation

Molecular dynamics simulation

Recently, molecular dynamics（MD）simulation has been employed as a necessary tool in the biological and chemical systems, investigating the structure, dynamics, and thermodynamics of biomaterials [189,190]. It is an essential tool to understand and predict critical biochemical processes. MD is a form of computer simulation in which atoms or molecules interact over time, femtoseconds to

milliseconds. To study the displacement of atoms, as the molecular system consists of voluminous units, it is impossible to find the properties of a complex system using analysis. Thus, numerical methods are applied for the determination of system properties [189-192]. MD calculates the properties of the system several atom or molecules by tracking atom motion dynamics with the equations of motion through the force field, resulting in a large number of calculations. Dynamics tracking can be achieved using an integrator such as Verlet method, Rangegatta method, and Gear predictor corrector [193].

MD has been applied in various aspects and scientific fileds, especially in biological researches. It has widely used for understanding allostery, molecular docking and drug design, and refining structure predictions. Since the regulation phenomena in proteins are explained within conformational transitions, the allostery that translates the conformational dynamics in functional implications has been investigated [194]. Because of how a ligand binds to its molecular is a key for understanding the function itself. Thus, in the pharmaceutical field, the practical application of the MD is docking strategies which useful for the drug design phase [195,196]. The other traditional problem in structural bioinformatics is to predict the structure. MD with the long simulations has been used for a macromolecule structure prediction [189,190]. MD was used to explain and explored various phenomenon such as the transient inter-domain motions during the GroEL allosteric cycle [191]; mechanism for hydrophobic gating in ion channels [192] and water permeation through aquaporin [197]; stabilizing the activation of the nicotinic acetylcholine receptor by cholesterol; the binding sites and poses, and allosteric modulators mechanism of the M2 muscarinic acetylcholine receptor [198]. The interaction between amyloid beta (Aβ) peptides could enhance Aβ aggregation related to neurodegenerative disease. Therefore, the adhesion of Aβ40 to a GM1 ganglioside-containing membrane was simulated using MD simulation and found that the secondary structure of Aβ40 was an influenced factor for deeply insert itself into the membrane [199]. MD has also used to simulate the nucleation and crystallization of materials in various conditions. The microscopic mechanism of crystal nucleation and growth behavior of methane hydrate in the porous media was revealed using a couple of simulations [200]. Since the interface-specific phenomena were influenced by the orientation and hydrogen bonding patterns of the interface/near-interface molecules, the arrangement of lauric acid at the water-hexane and water-carbon tetrachloride interfaces were studied using MD simulations. The results showed that the protonation of their headgroups strongly influenced the behavior of lauric acid molecules. [201].

For a briefly MD flow, an initial atom coordinate is received from both experimental structures or similar modeling data in which represented at various levels of detail. Although the atomistic representation could lead to the highly reliable reproduction of the systems, solvent representation is a critical point in system definition [202-204]. The forces acting on every atom (force fields) are calculated subsequently when the initial model is built. The force fields could reveal a various molecular features for example springs for bond length and angles, periodic functions for bond rotations and Lennard-Jones potentials, and the Coulomb's law for van der

Waals and electrostatic interactions [193]. Nowadays, they are parameterized for the simulation, modern force-fields are normally used [205]. Subsequently, accelerations and velocities and to rearrange the atom positions is calculated using the equations of motion (classical Newton's law of motion) through the force field. The most popular simulation codes including CHARMM [206], GROMACS [207], NAMD [208], and AMBER [209] have long been compatible with the messaging passing interface (MPI).

The term Amber refers to the various programs that work together to setup, perform, and analyze MD simulations. The principal flow of information is shown in Fig. 6. The main preparation programs are LEaP and antechamber. LEaP can be used to generate force field files for Amber MD packages and Nucleic Acid Builder. Meanwhile, antechamber is designed to be used with the General Amber Force Field (GAFF) [210], which could assign atom types and attempt to generate missing parameters, automatically. The result of the preparation is two text files including a coordinate (prmcrd) file that contains the Cartesian coordinates of all atoms, and a parameter-topology (prm-top) file that contains all other information required to compute energies and forces (includes atom names and masses, force field parameters, lists of bonds, angles, dihedrals, and additional book keeping information) [211].

Amber now consists of three different MD simulation engines as follows: Sander, the traditional computation platform; pmemd and pmemd.cuda which have focused on maximizing the performance. The additional codes that can be used to carry out a range of simulations are developed as follows: Nucleic Acid Builder, mdgx, Sqm, Pipil, rism1d and rism3d.snglpnt [211].

For the fundamental analysis tools in AMBER, ptraj is the main trajectory analysis tool which is able to perform many types of analyses. An MPI parallel version of this tool is also available as ptraj.MPI. The cpptraj is a complimentary program to ptraj in which written in C++. The benefit of cpptraj is the ability to process trajectory files with different topology files in the same run [211].

Although MD is a computation of properties Systems based on very small numbers of atoms or molecules, recent studies found that the results from MD simulations were not much different from the macro-level experiments [193].

Since the MD is a useful tool for understanding the phenomenon in molecular level and it is difficult to understand the nucleation and growth mechanism of *in situ* forming process by experimental and numerical simulation methods. Therefore, using computer simulation techniques can be linked to the macro-level properties of the *in situ* forming process to complete the mechanism understanding.
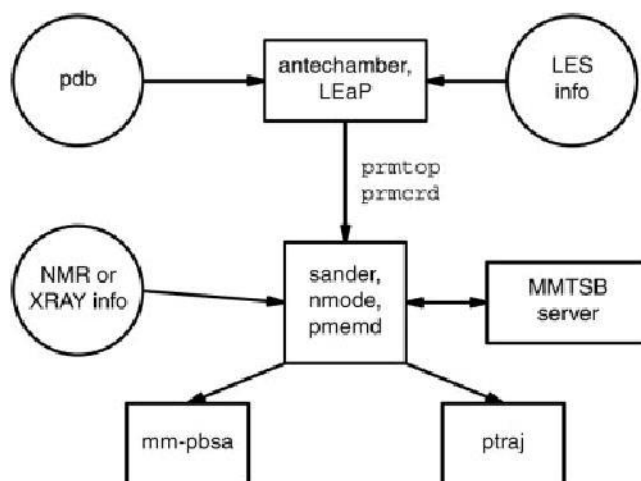
Figure 6 Information flow in the Amber program suite [212].
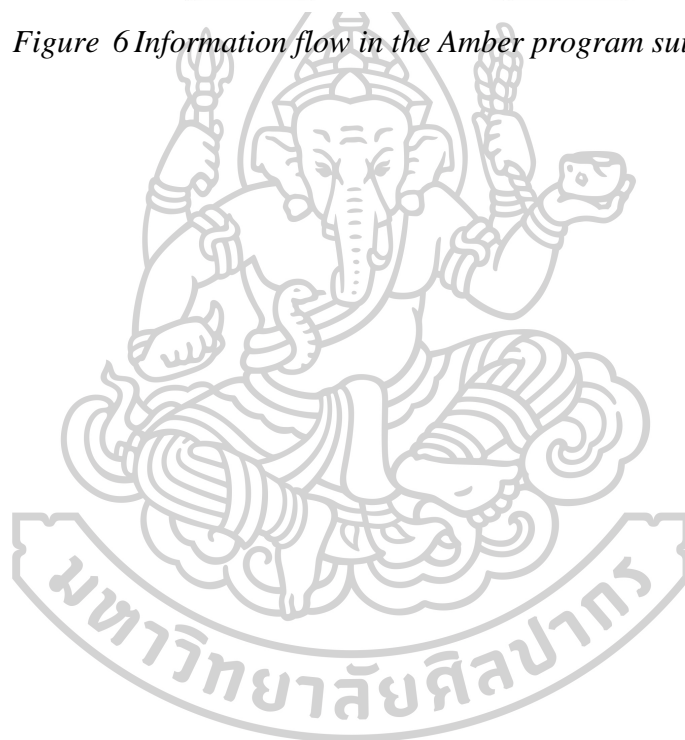
CHAPTER 3

MATERIALS AND METHODS

MATERIALS

CPL (Batch No. 289D1190515A), CPR (Batch No. 219D161222A), LAU (Batch No. 229F170S08A), MYR (Batch No. FPLK437X4S) and PAL (Batch No. 668F180902D), which were procured from Pacific Oleochemicals, Pasir Gudang Johor Darul Takzim, Malaysia and STR (Batch No. 3452018), which was purchased from CT Chemical, Bangkok, Thailand, were used as matrix formers. VCM (Lot No. WXBB5169V, Sigma-Aldrich, Co., USA) was used as a model drug. NMP (Lot No. A0251390, Fluka, New Jersey, USA), PYR (Lot No. BCBF5715V, Fluka, Germany) and DMSO (Lot No. 453035, Fluka, Switzerland) were used as solvents. Muller Hinton agar (Lot No. 1005843, Oxoid, UK) was used as medium for the antimicrobial tests. *S. aureus* ATCC 43300, *S. aureus* DMST 6535, *S. aureus* ATCC 25923, *E. coli* ATCC 8739, *C. albicans* and *P. gingivalis* ATCC 33277 were used as test microbials. Phosphoric acid (Merck KGaA, Darmstadt, Germany) , and acetone (Ajax, Finechem, Australia) were used for mobile phase preparation. Potassium dihydrogen orthophosphate (Lot No. E23W60, Ajax Finechem, Australia) and sodium hydroxide (Lot No. AF 310204, Ajax Finechem, Australia) were used as components of phosphate buffer (PB) with pH 7.4 to simulate the physiological fluid. Agarose (Lot No. H7014714, Vivantis, Malaysia) and sodium-fluorescein (Lot No. MXCG7851, Sigma-Aldrich, USA.) were used for the analysis of matrix formation behavior and solvent diffusion. Atri-III® (Lot AP1907, Yooyoung Pharmaceutical Co., Ltd., Korea), commercial product of hyaluronic intra-articular, was selected to compare the injectability with the developed formula.

EQUIPMENT AND INSTRUMENTS

1. Analytical balance (Sartorius model BP2100S and Sartorius model CP224S, Germany)
2. Anaerobic incubator (Forma anaerobic incubator, marietta, ohio, USA.)
3. Brookfield viscometer DV-III ULTRA (Brookfield Engineering Laboratories.Inc., USA.)
4. Conductometer)SevenCompact, METTLER TOLEDO, USA.(
5. Differential Scanning Calorimetry (Pyris Sapphire DSC, Standard 115V, Perkin Elmer instruments, Japan)
6. Field emission-scanning electron microscope (FE-SEM) (TESCAN MIRA3, Czech Republic)
7. FT-IR spectrophotometer (FT/IR-4100, JASCO International Co., Ltd., Tokyo, Japan)
8. Goniometer (FTA 1000, First Ten Angstroms, USA.)

9. Hot stage microscope (HSM Mettler Toledo, model FP82HT, SNR 5130346892, Switzerland)

10. Microscope (Olympus, Bangkok, Thailand)

11. Inverted microscope)TE-2000U, Nikon, Japan(

12. Pycnometer (Densito 30PX, Mettler Toledo Thailand Ltd, PortableLab TM, Switzerland)

13. pH meter (Professional Meter PP-15 Sartorius, Goettingen, Germany)

14. Shaking incubator Model SI4 (Shel Lab, Cornelius, USA.)

15. Stereo microscope (Motic SMZ-171 Series, Hong kong)

16. Texture analyzer (Charpa Techcenter, Godalming, Stable micro Systems Ltd., UK)

17. Thermal gravimetric analysis (TGA) (Pyris TGA, PerkinElmer, USA.)

18. UV-vis spectrophotometer (Perkin-Elmer, Germany)

19. UV-HPLC (1260 infinitely series, Agilent Technologies Inc., California, USA.) equipped with a C18 column (150 mm × 4.6 mm, 5 µm particle size)

20. Water bath (Julabo, Japan)

21. X-ray powder diffractometer (Miniflex II, Rigaku Corp.Tokyo, Japan)

22. Micropipette 2-20 µL, 20-200 µL, 100-1000 µL (Gilson, Middleton, USA.)

23. Pymol programme (The PyMOL Molecular Graphics System, Version 2.0 Schrödinger, LLC., New York, USA.)

24. Rasmol programme (Roger Sayle, Biomolecular Structures Group, Glaxo Wellcome Research & Development, Stevenage, Hertfordshire, UK)

25. Visual molecular dynamics programme (VMD) (Theoretical and Computational Biophysics Group, Beckman Institute, University of Illinois at Urbana-Champaign, USA.)

26. Amber programme (University of California, San Francisco, USA.)

METHODS

1. Study of fatty acid-based ISM

1.1. *Preparation of fatty acid solutions and fatty acid precipitates*

The saturated fatty acid ISM systems were prepared using different concentrations of fatty acids dissolved in NMP, PYR, DMSO and various ratios of mixed solvent (Table 4-5) then stirred for 24 h until the clear solutions were obtained.

To study the influence of fatty acid concentration and solvent, the concentration-based system was prepared in different solvents. The 10, 20, 30, 40, 50, 60, and 70%w/w fatty acids including CPL, CPR, LAU, MYR, PAL, and STR were prepared by using DMSO, NMP, and PYR as the solvents. The mixtures were stirred for 24 h until the clear solutions were obtained.

For mixed solvent systems, LAU ISM systems were prepared using 50% w/w LAU as the matrix dissolved in mixed solvents with various ratios (1:3, 1:1, 3:1) of NMP, DMSO, and PYR then stirred for 24 h until the clear solutions were obtained.

For the mixed fatty acid systems, the 40% and 50% w/w fatty acids in various ratios of LAU:STR (1:0, 3:1, 1:1, 1:3 and 0:1) as the matrices were dissolved in different ratios of NMP and DMSO (1:0, 1:1 and 0:1) then stirred for 24 h until the clear solutions were obtained.

The effect of various fatty acid aliphatic chain was investigated by the series of 35%w/v, and 1.75mM fatty acids in different solvents.

To prepare the precipitates of the formulations, the prepared solutions were added with the excess distilled water and stirred then the precipitates were collected on membrane after filter through 0.45 μm nylon membrane filter. The precipitates were dried in the desiccator.

Table 4 Composition of formulations of Concentration-based amd Mixed fatty acid/solvent system

Formulation	Amount (%w/w)								
	Fatty acid						Solvent		
	CPL	CPR	LAU	MYR	PAL	STR	PYR	NMP	DMSO
Concentration-based system									
10LD	-	-	10	-	-	-	-	-	90
20LD	-	-	20	-	-	-	-	-	80
30LD	-	-	30	-	-	-	-	-	70
40LD	-	-	40	-	-	-	-	-	60
50LD	-	-	50	-	-	-	-	-	50
60LD	-	-	60	-	-	-	-	-	40
70LD	-	-	70	-	-	-	-	-	30
10LN	-	-	10	-	-	-	-	90	-
20LN	-	-	20	-	-	-	-	80	-
30LN	-	-	30	-	-	-	-	70	-
40LN	-	-	40	-	-	-	-	60	-
50LN	-	-	50	-	-	-	-	50	-
60LN	-	-	60	-	-	-	-	40	-
70LN	-	-	70	-	-	-	-	30	-

Formulation	Amount (%w/w)								
	Fatty acid						Solvent		
	CPL	CPR	LAU	MYR	PAL	STR	PYR	NMP	DMSO
10LP	-	-	10	-	-	-	90	-	-
20LP	-	-	20	-	-	-	80	-	-
30LP	-	-	30	-	-	-	70	-	-
40LP	-	-	40	-	-	-	60	-	-
50LP	-	-	50	-	-	-	50	-	-
60LP	-	-	60	-	-	-	40	-	-
70LP	-	-	70	-	-	-	30	-	-
Mixed fatty acid/solvent system									
40LS1:0-ND1:0 (40LN)	-	-	40	-	-	-	-	60	-
40LS3:1-ND1:0	-	-	30	-	-	10	-	60	-
40LS1:1-ND1:0	-	-	20	-	-	20	-	60	-
40LS1:3-ND1:0	-	-	10	-	-	30	-	60	-
40LS0:1-ND1:0 (40SN)	-	-	-	-	-	40	-	60	-
40LS1:0-ND1:1	-	-	40	-	-	-	-	30	30
40LS3:1-ND1:1	-	-	30	-	-	10	-	30	30
40LS1:1-ND1:1	-	-	20	-	-	20	-	30	30
40LS1:3-ND1:1	-	-	10	-	-	30	-	30	30
40LS0:1-ND1:1	-	-	-	-	-	40	-	30	30
40LS1:0-ND0:1 (40LD)	-	-	40	-	-	-	-	-	60
40LS3:1-ND0:1	-	-	30	-	-	10	-	-	60
40LS1:1-ND0:1 (40LSD)	-	-	20	-	-	20	-	-	60
40LS1:3-ND0:1	-	-	10	-	-	30	-	-	60
40LS0:1-ND0:1 (40SD)	-	-	-	-	-	40	-	-	60
50LS1:0-ND1:0 (50LN)	-	-	50	-	-	-	-	50	-
50LS3:1-ND1:0	-	-	37.5	-	-	12.5	-	50	-

Formulation	Amount (%w/w)								
	Fatty acid						Solvent		
	CPL	CPR	LAU	MYR	PAL	STR	PYR	NMP	DMSO
50LS1:1-ND1:0	-	-	25	-	-	25	-	50	-
50LS1:3-ND1:0	-	-	12.5	-	-	37.5	-	50	-
50LS0:1-ND1:0 (50SN)	-	-	-	-	-	50	-	50	-
50LS1:0-ND1:1	-	-	50	-	-	-	-	25	25
50LS3:1-ND1:1	-	-	37.5	-	-	12.5	-	25	25
50LS1:1-ND1:1	-	-	25	-	-	25	-	25	25
50LS1:3-ND1:1	-	-	12.5	-	-	37.5	-	25	25
50LS0:1-ND1:1	-	-	-	-	-	50	-	25	25
50LS1:0-ND0:1 (50LD)	-	-	50	-	-	-	-	-	50
50LS3:1-ND0:1	-	-	37.5	-	-	12.5	-	-	50
50LS1:1-ND0:1	-	-	25	-	-	25	-	-	50
50LS1:3-ND0:1	-	-	12.5	-	-	37.5	-	-	50
50LS0:1-ND0:1 (50SD)	-	-	-	-	-	50	-	-	50

Table 5 Composition of formulations of Molecular weight-based system

Formula	Amount (%w/v)							
	Fatty acid						VCM	Solvent qs to 100 mL
	CPL	CPR	LAU	MYR	PAL	STR		
Molecular weight-based system								
35CPLD	35.06	-	-	-	-	-	-	DMSO
35CPRD	-	35.06	-	-	-	-	-	DMSO
35LD	-	-	35.06	-	-	-	-	DMSO
35MD	-	-	-	35.06	-	-	-	DMSO
35PD	-	-	-	-	35.06	-	-	DMSO
35SD	-	-	-	-	-	35.06	-	DMSO
1.75CPLD	25.24	-	-	-	-	-	-	DMSO

Formula	Amount (%w/v)							
	Fatty acid						VCM	Solvent qs to 100 mL
	CPL	CPR	LAU	MYR	PAL	STR		
1.75CPRD	-	30.15	-	-	-	-	-	DMSO
1.75LD	-	-	35.06	-	-	-	-	DMSO
1.75MD	-	-	-	39.97	-	-	-	DMSO
1.75PD	-	-	-	-	44.88	-	-	DMSO
1.75SD	-	-	-	-	-	49.78	-	DMSO
35CPLN	35.06	-	-	-	-	-	-	NMP
35CPRN	-	35.06	-	-	-	-	-	NMP
35LN	-	-	35.06	-	-	-	-	NMP
35MN	-	-	-	35.06	-	-	-	NMP
35PN	-	-	-	-	35.06	-	-	NMP
35SN	-	-	-	-	-	35.06	-	NMP
1.75CPLN	25.24	-	-	-	-	-	-	NMP
1.75CPRN	-	30.15	-	-	-	-	-	NMP
1.75LN	-	-	35.06	-	-	-	-	NMP
1.75MN	-	-	-	39.97	-	-	-	NMP
1.75PN	-	-	-	-	44.88	-	-	NMP
1.75SN	-	-	-	-	-	49.78	-	NMP

1.2. Physicochemical characterizations of saturated fatty acids solution

1.2.1. Appearance of prepared formulations

The appearances of formulations including clearity and homogeneity were observed by visual observation.

1.2.2. Determination of pH and density

The prepared solutions were determined for their pH values using a pH meter (n=3). The density of them were measured using a pycnometer (n=3).

1.2.3. Determination of contact angle, surface tension and interfacial tension

The contact angle of formula on glass slide was measured using the goniometer. Contact angle at 5th sec was measured and estimated from the first automatic image of droplet (n=3). The drop shape analysis was employed for checking surface tension and interfacial tension using a goniometer (pump out rate 2.5757 µL/s) (n=3).

1.2.4. Apparent viscosity and rheological behavior

The viscosity was determined using a Brookfield DV-III Ultra programmable rheometer (n=3). The shear stress of samples was measured at various shear rates at 25°C. The flow parameters were characterized using an exponential formula with N as the exponential constant (Farrow's constant) and η´ as the viscosity coefficient.

1.3. Characterization of ISM behaviors

1.3.1. In vitro matrix formation

The 1 mL of prepared ISM was passed through an 18-gauge needle into a 5-mL of various mediums in test tube such as PB pH of 6.8, PB pH of 7.4, and 0.75% w/v hyaluronic acid (HA) solution. The fatty acid matrix formation was then photographed with a digital camera at different time points (0, 1, 5 and 30 min).

1.3.2. Water-tolerance and the influence of KH_2PO_4

The capacity of formulations to endure a phase transformation was investigated by using the titration method. This experiment was set up to magnify the environmental factor influencing the water tolerance property. The high percent of titrated water (%v/v) at the separation point represents a high water tolerance. A total of 10 mL of each formula was filled into a 50 mL Erlenmeyer flask as the titrand and then titrated with the deionised water and various concentrations of KH_2PO_4 solutions (12.5, 25, 50, 100 and 200 mM) until the clear solution turned turbid (separation point). The dropping rate of titration was 0.05 mL/s. The formulation was swirled continuously at 150 rpm using a magnetic stirrer during titration. The amount of titrant required for transformation was recorded and the water amount (%v/v) was calculated using Equation 7.

$$\%\text{Water volume} = \frac{\text{Volume of titrant (mL)}}{10+\text{Volume of titrant (mL)}} \times 100 \quad \text{...(Eq.7)}$$

1.3.3. Rate of matrix formation and solvent diffusion

To determine the matrix formation, an experiment was set up to simulate a periodontal and knee environments using an agarose well, and the matrix fronts of formula at different time intervals under a stereo-microscope were observed. Briefly, 0.6% w/w agarose was dissolved in boiling distilled water, and the obtained solutions were poured into Petri dishes (diameter of 4.5 cm). At the centre of the settled gels, a cylindrical well (diameter of 6 mm) was made and filled with 150 µL of liquid formulation using a micropipette. During solvent exchange, the morphological change

or the matrix front formation was captured using a stereoscope at different time intervals. The distance of matrix formation from the rim of agarose to the inside was measured for five zones in triplicate, and the rate of matrix formation was calculated (n = 3). For the observation of the solvent migration, amaranth tracking approach was applied. The 0.03%w/v amaranth in each formulation was prepared. Its red color diffusion on behalf of the solvent was observed over time using Motic SMZ-171 Serie software. The distance between the matrix rim and the red color rim was measured using the Motic SMZ-171 Series software for five zones, each in triplicate (n = 5).

1.3.4. Injectability test

The minimal force or work of injection could signify the easy injectability. The injectability measurement was performed with a compression mode using a texture analyze. The obtained ISM was filled into a 1-mL syringe with 18 and 27-gauge needle clamped with a stainless stand. The syringe base was compressed with the upper probe of the texture analyzer downwards at a constant speed (1.0 mm s^{-1}) and a constant force of 0.1 N. Maximum force and work of compresion were recorded from the force displacement profiles, with the forces at a distance of 10-mm being selected for analysis (n=3).

1.3.5. Antimicrobial activities

The agar cup diffusion method was used for antimicrobial activity tests (against *S. aureus* ATCC 25923, *S. aureus* ATCC 43300, *S. aureus* DMST 6935, *E. coli* ATCC 8739, *C. albicans*, and *P. gingivalis* ATCC 33277) of the prepared systems with the technique based on the diffusion of the antimicrobial agent from a stainless-steel cylinder through agar gel inoculated with tested microorganism. Briefly, the used bacterial strains were adjusted to a turbidity of the 0.5 McFarland standard and then thoroughly plated on Muller Hinton agar (MHA) (Oxoid, UK). The diffusion of 100 µL of tested preparation from a cylinder placed on the surface of an inoculated agar plate was determined. The MHA plate was then incubated at 35 ºC for 18 h. The inhibition zone margin in mm. was detected with unaided eye. All tests were carried out in triplicate. To follow the quality control recommendations of the Clinical and Laboratory Standards Institute (2017), *S. aureus* ATCC 25923 strain was used as the control species using a disk diffusion method with the standard antibiotic disks including cefoxitin (30 µg/disk), trimethoprim-sulfamethoxazole (1.25/23.75 µg/disk), vancomycin (30 µg/disk), clindamycin (2 µg/disk) and ciprofloxacin (5 µg/disk). For anaerobic bacteria, the test was conducted using an anaerobic incubator.

1.3.6. Study of invert-in situ forming process

The matrix formation ability of various formulations was tested by injecting 0.5 mL of formulation through a 27G needle into the PB pH 6.8 and 7.4. The invert-*in situ*

forming process was observed under 30°C or 37°C at 50 rpm over 7 days using a shaking incubator in which the solid white matrix (formed matrix) transformed into gel.

1.4. Characterization of dried fatty acid precipitates

1.4.1. Determination of surface morphology

In order to observe the systems' morphology, the formed ISM systems were dried overnight at room temperature and kept in a desiccator for one week to avoid their structures melting and collapsing. The dried samples were coated with gold before being examined under a (FE-SEM) at an accelerating voltage of 15 kV.

1.4.2. Morphology change under hot stage microscope (HSM)

The morphology change by temperature of dried various fatty acids and precipitated ISM were observed by HSM with heating rate of 5°C/min. The morphology change of the sample was photographed at any point of temperatures which observed the change including the temperature below the melting point, at the melting point and above the melting point, respectively.

1.4.3. X-ray powder diffractometer (PXRD)

PXRD was used to investigate the crystalline properties of the raw fatty acids and the ISM precipitates. The test samples were grinded into fine particle by mortar and pestle and loaded into aluminium holder. All samples were scanned in the degree of 2θ in the range of 5 to 30 °2θ.

1.4.4. Differential scanning calorimetry (DSC)

All samples were weighed at 2.5 - 4 mg then placed in a non-hermitically aluminium pan. The pan was sealed then the thermal property was determined by DSC. The samples were investigated under 10°C/min of heating rate and the heating range was 30-100°C under 40 mL/min of nitrogen gas flow.

1.4.5. Thermogravimetric analysis (TGA)

The 5 mg of each compound was weighed and placed in non-hermitically aluminium pan and then sealed then thermogravimetric analysis was tested with TGA. Heating rate was 10°C/min with heating range was 30 – 350°C under 200 mL/min of nitrogen gas flow.

1.4.6. Fourier-transform infrared (FT-IR) spectroscopy

The samples were blended with potassium bromide (AR grade for IR) and plunged with plunger and die to make a pellet using hydraulic press at compression force of 4 tons. The % FT-IR transmittance of the sample was recorded using FT-IR. The test was performed with the wave number ranges of 400–4000 cm^{-1} with 32 scans at 4 cm^{-1} resolution.

2. Study of drug-loaded fatty acid-based ISM for perodontitis and postoperative knee infection treatment

2.1. Preparation of drug-loaded ISM systems containing fatty acid

The drug-loaded formulations were prepared as Table 6. The 0.75 and 1%w/w of VCM ISM systems were prepared by dissolved VCM in the solvent and stirring until the clear solution was obtained. The various fatty acids were dissolved by VCM solution with 24 h stirring to obtain the clear solution.

Table 6 Composition of formulations of Drug-loaded system

Formula	Amount (%w/v)							
	Fatty acid						VCM	Solvent qs to 100 mL
	CPL	CPR	LAU	MYR	PAL	STR		
Drug-loaded system								
VD	-	-	-	-	-	-	1	DMSO
0.75VD	-	-	-	-	-	-	0.75	DMSO
VCPLD	35.06	-	-	-	-	-	1	DMSO
VCPRD	-	35.06	-	-	-	-	1	DMSO
VLD	-	-	35.06	-	-	-	1	DMSO
VLD-40	-	-	40	-	-	-	1	DMSO
VMD	-	-	-	35.06	-	-	1	DMSO
VPD	-	-	-	-	35.06	-	1	DMSO
VLSD	-	-	20	-	-	20	0.75	DMSO

2.2. Evaluation of formula

2.2.1. pH and density study

The test was accorded to the pH and density study as mentioned above (1.2.2).

2.2.2. Contact angle, surface and interfacial tension study

The test was accorded to the contact angle, surface and interfacial tension study as mentioned above (1.2.3).

2.3. Evaluation of ISM systems before exposure to solvent exchange

2.3.1. Appearance viscosity and rheological behavior studies

The test was accorded to the viscosity and rheological behavior study as mentioned above (1.2.4).

2.3.2.   Injectability test

The test was accorded to the injectability test as mentioned above (1.3.4).

2.4. Evaluation of ISM systems during exposure to solvent exchange

2.4.1.   In vitro matrix formation

The test was accorded to the *in vitro* matrix formation as mentioned above (1.3.1).

2.4.2.   Rate of matrix formation and Solvent diffusion

The test was accorded to the rate of matrix formation and solvent diffusion as mentioned above (1.3.3).

2.4.3.   Aqueous phase diffusion tracking

In addition, the sodium-fluorescein tracking approach was applied for observation of aqueous phase migration. The 0.003% w/v sodium-fluorescein in 0.6% w/v agarose was prepared. Sodium-fluorescein was added to the boiled PB pH 7.4, together with the agarose. The obtained solution was poured onto a glass slide. The glass slides were coated with 2 mm-thick sodium-fluorescein-loaded agarose. Then, 100 μL formulation was dropped at the boundary of the cut piece of settled agarose. The migration of fluorescence color on behalf of the aqueous phase was time-lapse captured under an inverted microscope with 10x magnification.

2.4.4.   In vitro drug release studies

2.4.4.1. Calibration curve of drugs

Standard stock solutions were prepared by accurately weighted the drug then dissolved in phosphate buffer (pH 6.8 and 7.4). The stock solution was diluted to the various concentrations that cover the range of drug release sample. The optimal concentration range for UV detection was set by plot the relationship between concentration and absorbance/mAU from UV-vis spectrophotometer and UV-HPLC which r^2 value was 0.9990-1.000. (Appendices Figs. 43-45)

2.4.4.2. Drug content determination

The drug amount was analyzed using UV-vis spectroscopy or UV-HPLC. For the test that using UV-spectrophotometer, the samples were tested with wavelength of 280 for VCM. In the case of UV-HPLC was employed, it was equipped with C18 column

(150 mm × 4.6 mm, 5 μm particle size). The 0.1%v/v phosphoric acid (90%) and acetonitrile (10%) were used as mobile phase. The injection volume and the flow rate were set at 20 μL and 1.5 mL/min, respectively. The eluent was detected by UV-detector at a wavelength of 280 nm (n = 6). The detected values were converted to the amount of drug by using a standard curve of the drug.

2.4.4.3. Drug release test with dialysis membrane method

The dialysis tube method was used for determining the VCM release. A total of 1 g selected formulation was filled into a dialysis tube (Spectrapor, MW cut-off: 6000–8000). The filled tube was immersed in 100 mL PB (pH 6.8 and 7.4) at 37°C with a rotational speed of 50 rpm using a shaking incubator. Aliquots, with each having a volume of 10 mL, were withdrawn from the release medium at different time intervals and were replaced with 10 mL fresh medium. The VCM release amount was analysed as Drug content determination section.

2.4.4.4. Drug release test with membraneless method

The 5 mL of 0.6 %w/v agarose solution was prepared. The obtained agarose solution was poured into a 25-mL bottle. At the center of the settled gels, a cylindrical well (diameter of 6 mm) was made and then filled with 300 μL of the formulation. Ten mL of PB pH 7.4 was added to the bottle after the matrix was formed (5 min). The conceptual figure is shown in Appendix Fig. 46. Since the effect of temperature is one of the basic subjects and this study aims to fill the fundamental data of the fatty acid-based *in situ* forming system; therefore, the 30, 37, and 40°C were selected for "effect of temperature on drug release sustainability test". These prepared bottles were incubated at 30 or 37°C (after the date of plateau state, the 37°C system temperature was increased to 40°C) with a rotational speed of 50 rpm using a shaking incubator. Aliquots, each of 1.5 mL, were withdrawn from the release medium at different time intervals and were replaced with 1.5 mL of fresh medium. The VCM release amount was analysed as presented in drug content determination session.

2.4.4.5. Analysis of drug release data

The release data were analyzed by a nonlinear computer program, Scientist® for Windows, version 2.1 (MicroMath Scientific Software, SaltLake City, UT, USA.). Different mathematical release equations are the essential tool for fitting the cumulative percentage of drug release profiles in range of 10% to 80%. Considerable models of mathematic equation for this experiment are power law, zero order, first order, and Higuchi's. The coefficient of determination (r^2) and model selection criteria (msc) are parameters for indicating the degree of curve fittings. The msc was calculated by the equation 8 as given below.

$$msc= \ln\left\{\frac{\sum_{i=1}^{n} w_i\left(Y_{obs_i}-\overline{Y}_{obs}\right)^2}{\sum_{i=1}^{n} w_i\left(Y_{obs_i}-Y_{cal_i}\right)^2}\right\} - \frac{2p}{n} ...(Eq.8)$$

The Y_{obsi} and Y_{cali} are the observed and calculated values of the i-th point, respectively. The w_i was the applies weight to the i-th point. The n and p was number of points and parameters, repectively.

2.4.5. *Antimicrobial activities*

The test was accorded to the antimicrobial activities as mentioned above.

2.5. *Evaluation of drug-loaded ISM systems after exposure to solvent exchange*

Samples were collected after the release studies and they were dried using the desiccator for 7 days to avoid the collapse of porous structures.

2.5.1. *Mechanical property studies*

The mechanical property measurement was performed with a compression mode using a texture analyzer. The samples were pressed with the upper probe of the texture analyzer downwards at a constant speed (1.0 mm s^{-1}) and a constant force of 0.1 N. Maximum force and work of compression were recorded from the force displacement profiles, with the forces at a distance of 10-mm being selected for analysis (n=3).

2.5.2. *Determination of surface morphology*

Determination of topography by SEM according to the above mentioned.

3. Mechanistic phase inversion of fatty acid based ISM

3.1. *Effect of conductivity and ion on phase transformation*

Various conductivities and ions of environment were set. The various concentrations of KH_2PO_4 was prepared. The water-tolerance method which mentioned above uses to indicate the phase inversion point using KH_2PO_4 solutions as titrant instead of distilled water (n=3).

3.2. *Electrical potential difference during phase transformation*

The electrical potential change was investigated using a conductometer. The 4 mL samples of fatty acid solutions were filled in the glass test tube. Then, 50 μL deionised water was added at each time interval and the obtained liquid sample was mixed with Vortex at level 3. The deionised water was added until a turbid liquid was observed (separation point). The electrical potential change was measured at each time interval from the beginning of deionised water addition until the phase inversion was obtained (n=3).

3.3. Determination of contact angle and surface tension

The test data will be collected as the contact angle and surface tension studies as mentioned above for mechanistic phase inversion and the boundary tension relationship investigation (n=3).

3.4. Interface interaction of ISM

3.4.1. Transformation via liquid-liquid interface

Drop shape analyzer (FTA 1000, First Ten Angstroms, USA.) was applied to observe the matrix formation of prepared ISM systems with microscopic change. The 5 µL/sec of ISM feed was pumped out into 1.5 mL of PB pH 6.8 in quart cuvette. The solid-like matrix formation was then observed and photographed with a drop shape analyzer at various times (5, 10, and 40 sec)

3.4.2. Transformation via liquid-semisoild interface

A 0.6% w/v agarose solution was prepared as mentioned above. The obtained solution was poured onto a glass slide with a 2 mm-thick agarose. Then, 100 µL formulation was dropped at the boundary of the cut piece of settled agarose. The interfacial event was time-lapse captured under an inverted microscope with 10x magnification.

3.4.3. Time lapse morphology by SEM

The distilled water was added into the formulation with the initial amount that could induce the phase inversion. The precipitates were collected at the various time points then filtrate with whatman filter No.1. The filtrated sample was washed with excess distilled water for 3 times then dried in desiccator for 7 days. The morphology of various times precipitated samples were determined by SEM. The use of SEM was according to the mentioned above.

3.5. Computer modelling of mechanistic phase inversion

3.5.1. Construction of a computational model

The initial atom coordinate of fatty acids was obtained from Cambridge Crystallographic Data Centre. The accession codes were: CPR, 738369; LAU, 738617; MYR, 738618 and PAL, 738619. For the DMSO, NMP, and VCM, the parameters for the MD simulation were determined by the molecular orbital calculation with Gaussian16. The input data of Gaussian16 was built by Gaussview6. The reduced charges of the atoms in the respective molecules were performed by deducing from the calculation at the level of B3LYP/6-31G**//HF/cc-pVTZ. The simulation models consisted of dozens of fatty acids, solvents molecules, and VCM with various molecular ratios (Table 7). The initial positions of fatty acids were manually arranged with Rasmol

[213] . The solvent molecules were generated around the fatty acids, and the VCM was placed at the central of fatty acid/solvent box.

Table 7 Composition of initial models for MD simulation

Model	Fatty acid	Solvent	Drug	Molecular ratio of Fatty acid:Solvent:Drug
VCPRD	CPR	DMSO	VCM	302:1217:1
VCPRN	CPR	NMP	VCM	302:959:1
VLAUD	LAU	DMSO	VCM	260:1217:1
VLAUN	LAU	NMP	VCM	260:959:1
VMYRD	MYR	DMSO	VCM	228:1217:1
VMYRN	MYR	NMP	VCM	228:959:1
VPALD	PAL	DMSO	VCM	203:1217:1
VPALN	PAL	NMP	VCM	203:959:1

3.5.2. MD simulation details

The force field parameters of the molecules were generated by Antechamber module of Ambertools16 with the general AMBER force field. The topology parameter file and the initial coordinates of the atoms were built by Leap module. The drug-fatty acid-solvent system was placed in a periodic boundary box and solvated with TIP3P water (water box model). The thickness of the generated water layer was more than 10 Å from the boundary wall for the model of high-water-ratio region. For the model of low-water-ratio region, the 1 Å water layer was generated. The energy minimization and the heating up to 310 K were performed with a sander module. Then the production run of MD simulation was executed at 310 K with constant pressure condition using pmemd module. The shell scripts for MD simulation are given in Appendix III: Computational modelling.

3.5.3. Simulation analysis

The hydrogen bond (H-bond) occupancy was calculated by VMD software [214]. The criteria for H-bond formation is that the distance between the acceptor and donor atoms is less than 3.5 Å and the angle made by acceptor, donor, and hydrogen atoms is less than 60° [199]. The root-mean-squared deviation (RMSD) with regard to VCM was obtained by cpptraj module [212]. The diffusion constant of VCM was calculated by ptraj module [212] using the simulation time-evolved trajectory. The diffusion constants of VCM of the various models referred to the distance traveled from its initial position. The last position of each model was deduced from the snapshot at the time point when the VCM was located outside the formed-fat. For visual clarity, the positions of some molecules were transferred to the x-, y-, or z-direction by the length of the periodic boundary box in the drawing of simulation structures. The water, DMSO, and NMP

molecules were omitted in the drawing for clarity. All of the structures were visualized by PyMOL programme [215].

4. Statistical analysis

The SPSS for Window (Version 11.5) was used for the analysis. The statistical significance for the measurement was examined using one-way analysis of variance (ANOVA) followed by a least significant difference (LSD) post hoc test. The statistical significance level was set at $P < 0.05$

CHAPTER 4

RESULTS AND DISCUSSION

pH and density evaluation

Although the pH measurement in the non-aqueous condition is not preferred, it is possible to compare the pH value of non-aqueous mixture in the formulation series. Many research and IUPAC are also interested this issue [216]. This data set is frequently asked in practical.

pH and density of LAU series

There were only CPL, CPR, and LAU which completely dissolved in all solvents at the concentration of 70%w/w. As the preliminary test for matrix formation ability, CPR and CPL could not form; thus, LAU was selected on behalf of fatty acid to study the influent of fatty acid concentration. Whereas all solutions of LAU in DMSO and NMP were clear and colorless, the solutions of 60%–70% (w/w) LAU in PYR were turbid. Therefore, Only DMSO and NMP were selected for the mixed fatty acid/solvent and molecular weight series.

The pH of the systems significantly decreased ($P < 0.05$) as the amount of LAU increased, as shown in (Table 8), due to the decrease in amount of solvent with a high pH (~11) and the abundance of acidic carboxylic groups provided by LAU, the pKa of which is 4.9 [217]. Nevertheless, gingival tissue irritation is not expected to occur because of the rapid transformation of the preparations into the solid state and the application of small injection volume.

Density is related and used to estimate viscosity [218]. It was also used to predict the nucleation rate of soft compound [219]. Thus, the density of the LAU formulations was measured. The density of LAU in the PYR formulations is higher than that of LAU in DMSO and NMP (Table 8). This behavior is related to the density of the solvents, which could be ordered as PYR > DMSO > NMP. Higher amounts of fatty acid resulted in lower-density of the formulations due to apparent low density of LAU (0.82 ± 0.08 g/cm^3, at 23–24°C) [220]. Typically, the density of a mixture at a given temperature is the sum of this characteristic of each pure compound under the mole fraction of those compounds.

Table 8 pH and density of LAU series (n = 3)

Concentration of LAU (% W/W)	pH			Density (g/cm^3)		
	Solvent			Solvent		
	DMSO	NMP	PYR	DMSO	NMP	PYR
0	11.08 ± 0.38[a]	11.77 ± 0.03[b]	11.46 ± 0.19[c]	1.0943 ± 0.0004	1.0277 ± 0.0001	1.1071 ± 0.0006
10	7.19 ± 0.09[a]	7.16 ± 0.12[b]	7.15 ± 0.11[c]	1.0689 ± 0.0003	1.0109 ± 0.0002	1.0809 ± 0.0001
20	6.41 ± 0.10[a]	6.33 ± 0.06[b]	6.6 ± 0.10[c]	1.0445 ± 0.0002	0.9962 ± 0.0001	1.0564 ± 0.0003
30	5.76 ± 0.08[a]	5.68 ± 0.03[b]	6.31 ± 0.17[c]	1.0225 ± 0.0001	0.9825 ± 0.0001	1.0329 ± 0.0004
40	5.51 ± 0.09[a]	5.18 ± 0.02[b]	6.05 ± 0.09[c]	1.002 ± 0.0004	0.9649 ± 0.0002	1.0105 ± 0.0005
50	4.99 ± 0.15[a]	4.8 ± 0.16[b]	5.54 ± 0.08[c]	0.9828 ± 0.0002	0.9581 ± 0.0003	0.9896 ± 0.0002
60	4.46 ± 0.11[a]	4.15 ± 0.04[b]	5.09 ± 0.25[c]	0.9638 ± 0.0001	0.9437 ± 0.0003	ND
70	3.09 ± 0.16[a]	4.00 ± 0.35[b]	ND	0.9459 ± 0.0001	0.9314 ± 0.0001	ND

The superscripts a, b and c indicate a significant difference (P < 0.05); ND = not determined

pH and density for solutions of mixed fatty acid series

According to formation behavior of LAU-based series, 40 and 50 %w/w fatty acid which showed an outstanding formation ability, were selected. Only DMSO and NMP were used as a solvent since PYR-based formulations showed turbid liquid at high fatty acid concentration and high viscous than the others. All prepared drug-free ISM systems were clear and colorless, except 40SD and 50SD were turbid. The pH values of 40% w/w and 50% w/w fatty acids were 4.71–5.57 and 5.32–6.56, respectively. These section showed different trend compared to the previous section wherein the pH of the system increased significantly (P<0.05) when the fatty acid amount increased as presented in Table 9. The increase of fatty acid resulted in aggregation with ionization difficulty resulting in a higher pH. The higher ratio of STR resulted in a lower acidity owing to the its hydrophobicity ratio with longer hydrocarbon chain compared to LAU dominating the acidity from the carboxyl group. Fatty acids with longer aliphatic chain have higher pKa value than short-chain fatty acids [221,222]. Lower protonation of fatty acids occurred due to the longer aliphatic component [223]. In comparison to the same concentration, STR had lower molar amount; therefore, this led to a lower carboxyl functional group and resulted a higher pH value. At a lower LAU concentration with a higher DMSO volume, the pH value of the formulation was higher due to the pH of this solvent, pK$_{HA}$ 32–33 [224].

Using higher DMSO volume in the formulation resulted in a higher density due to its own density value. The density of DMSO was higher than that of NMP (Table 9). The lower density trend of the solution was due to a higher amount of low density compounds such as fatty acids (densities of LAU and STR are 0.82 ± 0.08 and 0.84 ± 0.08 g/cm^3, respectively, at 23°C–24°C) [220]. The density of the mixture was the density summation of each pure matter based on their mass fraction [225].

pH and density for solutions of fatty acid molecular weight series

According to formation behavior of LAU-based series, the concentration of 35%w/v and 1.75 mM were selected. Table 10 shows the apparent pH, density and viscosity of fatty acid solutions. The 35% w/v fatty acid solutions showed an increased

pH when a high-MW fatty acid was used due to the decrease in fatty acid molecules with a carboxyl group. In the case of 1.75 mM fatty acid solutions, the decreasing trend of pH was noted. The decrease in pH resulted from the diminishing of solvent given that NMP and DMSO show a higher pH (11.77 ± 0.03 and 11.08 ± 0.38, respectively). However, several fatty acid solutions, such as 1.75CPLN, 1.75CPLD and 1.75SD showed suspicious results, which possibly arose due to the following reasons. The hydrophobicity of long hydrocarbon chains can dominate the acidity of the carboxyl group and long-chain fatty acids have high pK value [221,222], which results in the low protonation of fatty acids [223]. By contrast, the less carbon amount of CPL showed a less dominating effect on the carboxyl group, with its ionisation resulting in the significantly low pH than the others.

The descending density was distinguished once the concentration of fatty acid was fixed at 1.75 mM. The lowering trend of density was due to the accumulation of fatty acids, which are low-density material. Similarly, the fatty acid solutions using DMSO as a solvent produced a high density due to the high density of this solvent. The densities of NMP, DMSO, CPR, LAU, MYR, PAL and STR were 1.027, 1.100, 0.85 ± 0.08, 0.82 ± 0.08, 0.86 ± 0.09, 0.9 ± 0.09 and 0.84 ± 0.08 g/cm^3, respectively, at 23°C–24°C [220,226].

Viscosity and rheology

To be administered *via* injection, the viscosity of a formulation is one of the key parameters that must be considered [227], wherein a low-viscous formulation is easier to inject [84].

Viscosity of solutions from LAU series

The apparent viscosity of all formulations increased as the concentration of LAU increased (Fig. 7), thus revealing interactions amongst functional groups. For example, the carboxylic groups of LAU may undergo hydrogen bonding amongst themselves [228]. The results corresponded to the density values obtained. The viscosity of all formulas was fairly low due to the lubricating effect of LAU molecules [78] and a markedly low density of LAU. The low density, small size and unsophisticated structure of LAU molecules minimized the molecular interactions. This low viscosity indicates a great ease of injection [84]. LAU in the DMSO and NMP formulations showed a viscosity lower than that observed in the PYR formulas, thereby indicating that the fatty acid dissolves more freely in the former solvents than in the latter. Use of a solvent with good ability to dissolve polymers results in solutions with low viscosity [35]. Substance–substance interactions are dominated by substance–solvent interactions, which lead to lowered viscosity [25]. Polymers such as ethyl cellulose, bleach shellac, Eudragit RS, PLA and PLGA have been widely used as matrix formers in ISM systems; however, these materials have very high viscosity and, thus, poor injectability. For example, the viscosity of 25%–35% (w/w) PLA and PLGA-based ISM is approximately 44200–204400 cPs (measured at 50s^{-1}, 25 °C) [229]. Therefore, the low viscosity of LAU ISM is a beneficial property of using fatty acids rather than polymers in ISM systems.
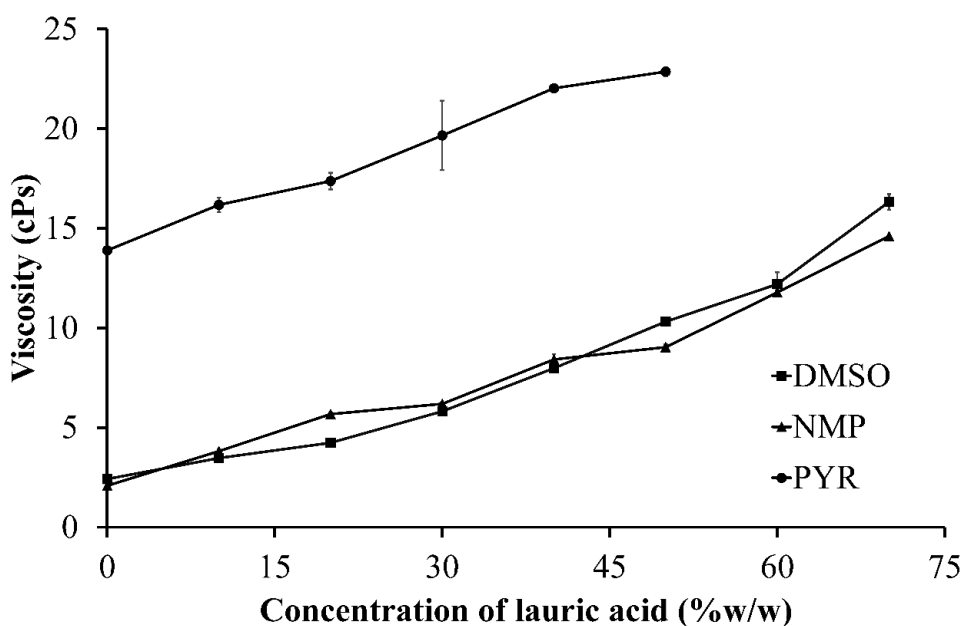
Figure 7 Viscosity of various concentrations of LAU series at room temperature (n=3)

Viscosity and rheological behavior from solutions of mixed fatty acid series

Increasing the apparent viscosity was associated with a higher amount of STR (Table 9). This result was in agreement with a previous study which demonstrated that binary liquid mixtures of fatty acids exhibited more viscosity when a long-chain fatty acid was used [230]. Higher amount of fatty acid promoted a more viscous environment suggested the intramolecular interaction *via* hydrogen bonding between carboxylic groups [228]. The viscosity and density were found to be correlated. In this case, decreasing the density related to the increasing of the viscosity. The relationship was that the more viscous environment was created from lowering the volume of solvent and replacement of higher amount fatty acid. The unique fatty acid characteristics of short-chain molecule and lubricating effect together with having low density evidenced very low viscosity of all formulations. A simpler and smaller molecular structure can reduce the interaction between the molecules. On the other hand, bulky molecules such as long-chain polymers can readily interact with each other or with the adjacent molecules including solvents. For example, Eudragit® RS that was used as a polymer in an *in situ* forming gel exhibited quite a viscous preparation when the concentration was enriched *via* polymer–polymer interaction [231]. The use of NMP as a solvent resulted in lower viscosity due to the solvent is less viscous and fatty acids can be freely dissolved. Typically, good solvent affinity for dissolving the solute can lower the viscosity of the mixture [35] due to the domination of substance–solvent interaction over substance–substance interaction [25]. In general, polymers have been used as a matrix gel former in *in situ* forming

systems; however, they exhibited high viscosity that results in difficulty of injection. Therefore, the low-viscous fatty acid-based ISM indicated convenience of injection that had beneficial properties over traditional polymeric *in situ* forming systems. All the prepared formulations exhibited a flow index (N) that was close to one at an ambient temperature indicating a Newtonian behavior [84], which was an expected pattern in an injection dosage form [232].

Table 9 Physical properties of mixed fatty acid series (n = 3)

Formula	pH	Density (g/mL)	Viscosity (Cp)	Flow index (N)
DMSO	11.08 ± 0.38^a	1.0943 ± 0.0004	2.42 ± 0.01	ND
NMP	11.77 ± 0.03^b	1.0277 ± 0.0001	2.08 ± 0.01	ND
40LS1:0-ND1:0	4.71 ± 0.03	0.9703 ± 0.0003	5.76 ± 0.14	0.850 ± 0.025
40LS3:1-ND1:0	4.85 ± 0.06	0.9688 ± 0.0002	6.00 ± 0.04	0.860 ± 0.036
40LS1:1-ND1:0	5.06 ± 0.06	0.9680 ± 0.0002	6.79 ± 0.48	0.890 ± 0.045
40LS1:3-ND1:0	5.21 ± 0.04	0.9680 ± 0.0001	7.21 ± 0.02	0.940 ± 0.026
40LS0:1-ND1:0	5.44 ± 0.06	0.9661 ± 0.0002	7.25 ± 0.13	0.890 ± 0.052
40LS1:0-ND1:1	4.90 ± 0.09	0.9843 ± 0.0003	6.03 ± 0.26	0.850 ± 0.01
40LS3:1-ND1:1	5.18 ± 0.08	0.9835 ± 0.0001	6.15 ± 0.03	0.880 ± 0.021
40LS1:1-ND1:1	5.26 ± 0.03	0.9828 ± 0.0004	6.73 ± 0.12	0.880 ± 0.080
40LS1:3-ND1:1	5.40 ± 0.07	0.9831 ± 0.0001	7.79 ± 0.15	0.930 ± 0.015
40LS0:1-ND1:1	5.57 ± 0.11	0.9819 ± 0.0002	8.60 ± 0.15	0.940 ± 0.030
40LS1:0-ND0:1	5.06 ± 0.16	1.0021 ± 0.0002	6.64 ± 0.06	0.870 ± 0.020
40LS3:1-ND0:1	5.22 ± 0.09	1.0016 ± 0.0001	7.39 ± 0.04	0.910 ± 0.025
40LS1:1-ND0:1	5.41 ± 0.03	1.0001 ± 0.0003	7.67 ± 0.03	0.840 ± 0.030
40LS1:3-ND0:1	5.56 ± 0.07	0.9978 ± 0.0001	8.66 ± 0.14	0.900 ± 0.021
40LS0:1-ND0:1	ND	ND	11.55 ± 0.17	ND
50LS1:0-ND1:0	ND	ND	82.00 ± 2.00	ND
50LS3:1-ND1:0	5.33 ± 0.04	0.9611 ± 0.0003	8.90 ± 0.04	0.970 ± 0.010
50LS1:1-ND1:0	5.41 ± 0.14	0.9562 ± 0.0002	9.63 ± 0.03	0.980 ± 0.015
50LS1:3-ND1:0	5.32 ± 0.10	0.9555 ± 0.0004	10.56 ± 0.02	0.990 ± 0.012
50LS0:1-ND1:0	5.54 ± 0.02	0.9544 ± 0.0003	11.45 ± 0.04	1.000 ± 0.006
50LS1:0-ND1:1	5.71 ± 0.02	0.9527 ± 0.0003	12.40 ± 0.03	1.000 ± 0.006

Formula	pH	Density (g/mL)	Viscosity (Cp)	Flow index (N)
50LS3:1-ND1:1	5.65 ± 0.14	0.9691±0.0018	8.76±0.03	0.990±0.006
50LS1:1-ND1:1	5.70 ± 0.03	0.9674±0.0002	9.33±0.04	0.990±0.015
50LS1:3-ND1:1	5.53 ± 0.09	0.9654±0.0002	10.74±0.04	0.810±0.115
50LS0:1-ND1:1	5.97 ± 0.11	0.9686±0.0004	10.86±0.06	ND
50LS1:0-ND0:1	6.49 ± 0.04	0.9624±0.0002	12.96±0.03	ND
50LS3:1-ND0:1	5.38 ± 0.07	0.9822±0.0006	8.53±0.03	0.980±0.012
50LS1:1-ND0:1	5.58 ± 0.03	0.9807±0.0003	9.32±0.03	0.990±0.006
50LS1:3-ND0:1	6.56 ± 0.11	0.9802±0.0004	10.52±0.06	0.960±0.020
50LS0:1-ND0:1	6.11 ± 0.08	0.9796±0.0003	13.22±0.02	ND

The superscripts of a, b and c represent a significant difference (P < 0.05); ND = not determined

Viscosity of solutions from fatty acid molecular weight series

The trend of viscosity change was similar to that of density [218]. All the solutions had low viscosity (Table 10) given that a simple and small structure of fatty acid can lessen the inter/intra-molecular interaction, different from bulky molecules such as polymer. Eudragit® RS, a gel forming agent of recently developed *in situ* forming gel, can readily interact with vehicles, resulting in a steep viscous preparation when the concentration was increased [231]. A high viscosity is associated with the use of a higher MW fatty acid. In the study of binary liquid mixtures of fatty acids, the solutions exhibited increased viscosity when the ratio of long-chain fatty acid was increased [230]. Otherwise, the functional group as carboxyl was perceived for behavior of fatty acids in solutions. The interaction between fatty acid which resulted in more viscous environment was reported in another studies. The carboxyl group of fatty acid protruding from the cavity of amylose-lipid complexes can interact with other molecules, resulting in increased viscosity [233,234]. Although the hydrogen bonding between carboxylic groups can typically promote a viscosity [228], the hydrophobic interaction should be decisively considered. The hydrophobic interaction can enhance the environmental viscosity [235]; the long chain length of alkanes induces the increase in hydrophobic interaction, resulting in the high viscosity of silicone oil [236]. Among the 35% w/v fatty acid solutions, the less fatty acid molecules were evident for longer chain fatty acid solutions. Thus, the results might not be distinct. Meanwhile, at the concentration of 1.75 mM, the intermolecular interaction was evident. Hence, at the same amount of the fatty acid molecule, the viscosity flourished when using higher MW fatty acid-loaded solutions.

Table 10 Physical properties of fatty acid molecular weight series (n = 3)

Formulation	pH	Density (g/cm^3)	Viscosity (cPs)
35CPLD	5.55 ± 0.07	1.0240 ± 0.0002	6.29 ± 0.04
35CPRD	6.13 ± 0.02	1.0205 ± 0.0001	7.51 ± 0.02
35LD	6.05 ± 0.11	1.0161 ± 0.0002	8.05 ± 0.05
35MD	6.19 ± 0.11	1.0142 ± 0.0000	9.54 ± 0.17
35PD	6.22 ± 0.05	1.0119 ± 0.0001	10.90 ± 0.05
35SD	6.78 ± 0.01	1.0109 ± 0.0001	ND*
1.75CPLD	5.97 ± 0.02	1.0407 ± 0.0001	5.47 ± 0.12
1.75CPRD	6.44 ± 0.04	1.0345 ± 0.0001	6.08 ± 0.05
1.75LD	6.15 ± 0.03	1.0154 ± 0.0001	7.95 ± 0.10
1.75MD	5.95 ± 0.03	1.0026 ± 0.0002	11.86 ± 0.08
1.75PD	5.98 ± 0.04	0.9899 ± 0.0002	ND*
1.75SD	6.28 ± 0.01	0.9799 ± 0.0002	ND*
35CPLN	5.35 ± 0.01	0.9894 ± 0.0001	7.07 ± 0.20
35CPRN	5.76 ± 0.05	0.9825 ± 0.0002	7.96 ± 0.29
35LN	5.93 ± 0.03	0.9797 ± 0.0001	8.43 ± 0.09
35MN	5.98 ± 0.01	0.9767 ± 0.0001	8.91 ± 0.40
35PN	6.06 ± 0.01	0.9731 ± 0.0001	8.92 ± 0.54
35SN	6.00 ± 0.00	0.9759 ± 0.0001	9.24 ± 0.44
1.75CPLN	6.53 ± 0.05	0.9935 ± 0.0001	5.63 ± 0.06
1.75CPRN	6.53 ± 0.05	0.9947 ± 0.0000	5.73 ± 0.08
1.75LN	5.81 ± 0.04	0.9775 ± 0.0000	7.57 ± 0.16
1.75MN	5.60 ± 0.01	0.9664 ± 0.0001	9.49 ± 0.20
1.75PN	5.41 ± 0.05	0.9579 ± 0.0001	10.90 ± 0.20
1.75SN	5.16 ± 0.01	0.9529 ± 0.0003	13.97 ± 0.05

*ND = not determined (Turbid liquid obtained); By comparison in each group of 35% and 1.75 mM fatty acids in different solvents, the different MW of fatty acid resulted in significantly increased/decresed trend (ANOVA, $P < 0.05$). According to post hoc test, any paired samples showed significant difference ($P < 0.05$) except the following: pH of 1.75MD-1.75PD; pH of 35CPRD-35LD-35MD-35PD; viscosity of 1.75CPLN-1.75CPRN; viscosity of 35LN-35MN-35PN; viscosity of 35MN-35PN-35SN.

Matrix formation behavior and solvent exchange tracking

Macroscopic matrix formation behavior of solutions from LAU series

ISM is alternative drug delivery system for painless administration. The liquid state of an ISM formula transforms into a solid at the injection site through the solvent-exchange mechanism [25]. The matrix formation behavior of LAU solutions in the simulated crevicular fluid is depicted in Fig. 8, which shows that the solution state changes to a semisolid and then to a solid-like state over time. Notably faster transformation occurred by increasing the amount of LAU in the ISM. LAU in DMSO formulations exhibited more rapid transformation than LAU in NMP and PYR formulations. DMSO has higher polarity and greater water miscibility than PYR and

NMP, respectively, which results in faster water diffusion [35,78,237]. The low affinity of NMP and PYR to water delayed LAU nucleation; thus, the system required more water penetration to induce the phase separation of LAU. The several LAU nuclei occurred at the same time, and each of them had to take a solvent. This condition limited the growth of each nucleus [25]. A similar behavior was observed in *in situ*-forming microparticles (ISM) of bleached shellac prepared by using PYR as a solvent due to the virtue of a low affinity of PYR to water [78]. Rapid phase inversion was evident in the low-viscosity formula because of the ease of solvent exchange. The slower solvent-exchange behavior of formulations of 40% and 50% (w/w) LAU in NMP and incomplete transformation into a matrix within 5 min is due to the low affinity of NMP, which has very low polarity, with water [35,78]. The low density of LAU promotes the floating of some formulations prior to transformation. Thus, solvent exchange occurs over a limited surface area, resulting in incomplete transformation. Formulations with 60% and 70% (w/w) LAU in NMP showed the rapid and complete transformation. Rapid transformation during administration is more convenient for periodontitis treatment, improves patient compliance [238,239] and prevents the leakage of the formula from the periodontal pocket.
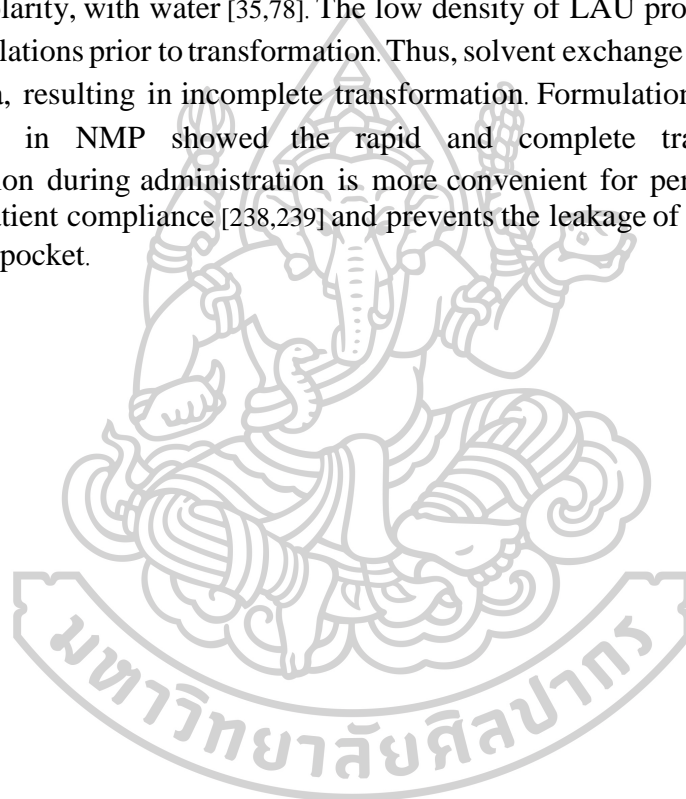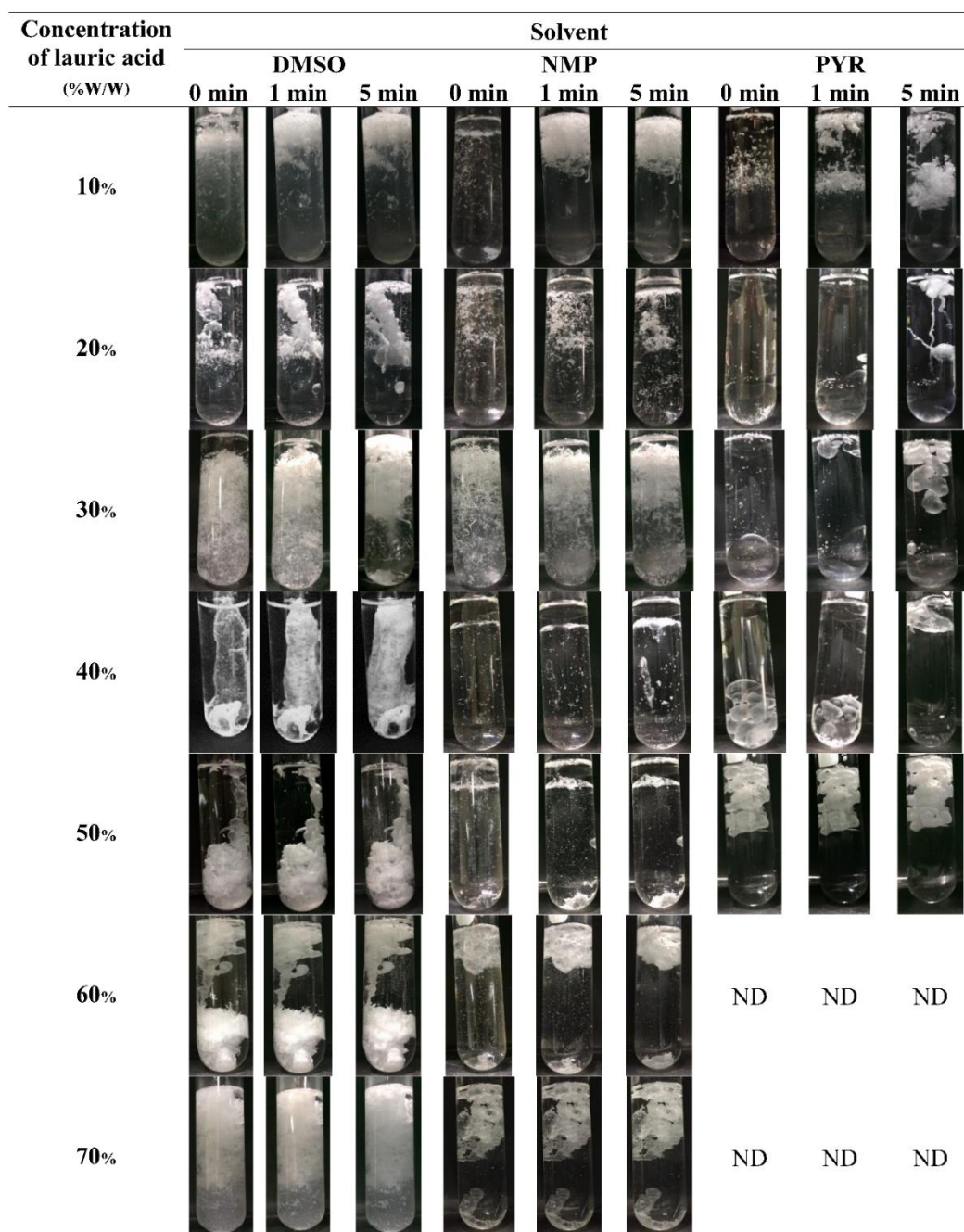
Figure 8 In vitro matrix formation behavior of fatty acid-based ISM (LAU series) in PB pH 6.8 (n=3, ND = not determined)

Microscopic matrix formation behavior of solutions from LAU series

Since practical situations often require only a minimal volume of prepared solution, the transformation behavior might differ from macroscopic transformation [3,75,240]; thus, this evaluation was set to simulate the small volume *in situ* forming once applied via injection to the periodontal pocket. The LAU solutions changed into a gel or solid-like wax matrix at needle tip after injection through the needle of the drop shape analyser into PB pH 6.8 (Fig. 9). Increasing the amount of LAU in the formulation hastened the

transformation and shape change. Floating droplets were evident because of the low density of LAU in PB. However, high concentrations of LAU, such as 60%–70% (w/w) did not yield floating droplets because a surface network formed fast enough to resist the floating force. Droplet expansion occurred as the LAU concentration increased because the network formation rate is properly balanced with the pumped volume. Low concentrations of LAU in the NMP and PYR formulations resulted in relatively slow transformation because of the low affinity of these formulas to water and the small amount of matrix component available. These results correspond with the macroscopic matrix formation behavior of the LAU solutions. The present experiment provides not only a new method which to evaluate ISM systems but also a useful assessment tool for tracking the self-forming behavior of *in situ* forming dosage forms at the microscopic level. The matrix formation character was performed under the influence of density and the mechanical strength of material. It was the important manners to be considered in the developing process of such dosage forms.
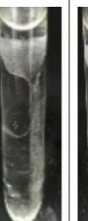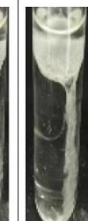
Figure 9 In vitro matrix formation behavior of fatty acid-based ISM (LAU series) in PB pH 6.8 as analysed by a drop shape analyser (n=3)

Macroscopic matrix formation behavior of solutions from mixed fatty acid series

The *in vitro* matrix formation behavior of the prepared formulations in the simulated physiological fluid is shown in Fig. 10A, in which the liquid state of the formulation

transformed into a matrix, and subsequently, as an opaque solid-like fatty acid over time. Increasing the concentration of STR resulted in a faster conversion from liquid into an opaque solid matrix. DMSO while used as the solvent promoted a more rapid transformation. The higher polarity of DMSO together with a greater water-miscible property compared to NMP promoted faster solvent exchange [35,78]. Normally, these fatty acids require water inward to induce a phase separation. Therefore, the nucleation rate of fatty acids in NMP was retarded due to a lower affinity of this solvent to water. Several fatty acid nuclei required to uptake the solvent at the same time; hence, the growth of each nucleus was limited [25]. This result was similar to that of bleached shellac-based *in situ* forming microparticle that showed a slow conversion into solid resin when using PYR as a solvent owing to a low affinity of this solvent to water [78]. Moreover, the VLSD injected into the HA solution, which is a primary component in the knee joint also transformed into matrix (Fig. 10B). In the HA solution, VLSD exhibited a slower transformation than that in PB at pH 7.4 due to the lower amount of water in HA, and the higher viscous environment retarded the solvent exchange [16, 53]. As the lubricating property is an important factor of knee function and the biological lubricants such as HA, lubricin, phospholipids and protein are the components of the synovial fluid [57, 58], the lubrication properties of fatty acids as mentioned here could be beneficial. Furthermore, fat oxidation was found in the cartilage [59], and lipolysis might occur at an arthritic knee joint through lipid metabolism [60]. Therefore, the prepared fatty acid depot could be degradable with time.

A

B

Figure 10 In vitro matrix formation behavior of fatty acid-based ISM (mixed fatty acid/solvent series) in PB pH 7.4 (A); In vitro matrix formation behavior of fatty acid-based ISM in PB pH 7.4 and HA (B) (n=3)

Macroscopic matrix formation behavior of solutions from fatty acid molecular weight series

The results showed the changing state behavior from the liquid state into the solid-like state of fatty acid solutions by time after exposure to aqueous environment by solvent exchange process. The use of different MW fatty acids remarkably affected the *in vitro* matrix formation behavior (Fig. 11). The prerequisite of ISM is the capability to form into a solid-like matrix within the expected time. Within 5 min, all formulations comprising CPL and CPR could not transform into a solid-like state; the same was observed for LAU in NMP. Meanwhile, rapid formation was acquired, if the high-MW fatty acids, including MYR, PAL and STR, were used. LAU, a 12-carbon atom fatty acid, showed a conflicting formation behavior. LN matrix could not be formed, although LD could. LAU located itself amid the solvent effect. Notwithstanding, the inquiry of completed formation or the rate of formation could not be achieved in this experiment. Thus, the determining matrix formation at the cross-sectional view was performed.
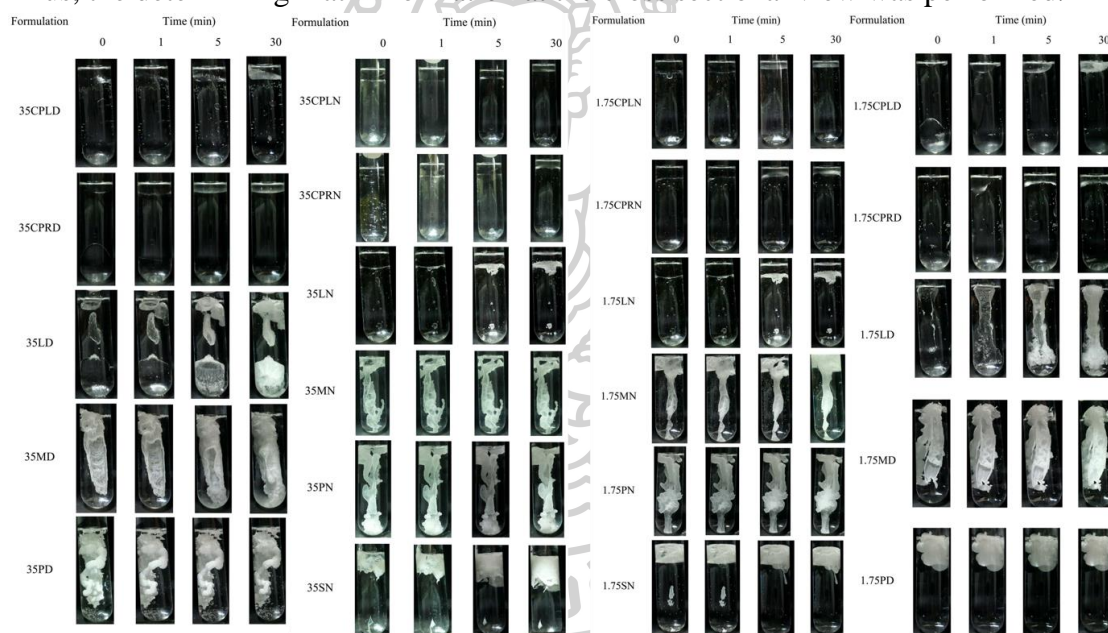
Figure   11 In vitro matrix formation behavior of fatty acid-based ISM (fatty acid molecular weight series) in PB pH 7.4 (n=3)

Matrix formation (cross-sectional view) and solvent diffusion pattern of solutions from LAU series

Phase separation promoting LAU matrix formation was observed after the formula was exposed to the aqueous solution from PB pH 6.8 in agarose gel (Fig. 12). Matrix formation slowed down as the amount of LAU was increased (30% and 40% w/w) due to the immediate formation of a waxy network on the surface of the matrix front, which obstructed the water diffusion from agarose. Moreover, the dense surface of a matrix network retards the inward migration of water [242]. However, highly rapid diffusion was observed when a very high concentration of LAU, such as 50% (w/w), was used; at this

concentration, supersaturation and seeding were evident. The nucleation rate was high in the supersaturated condition, and seeding could increase the crystallisation rate [243,244].
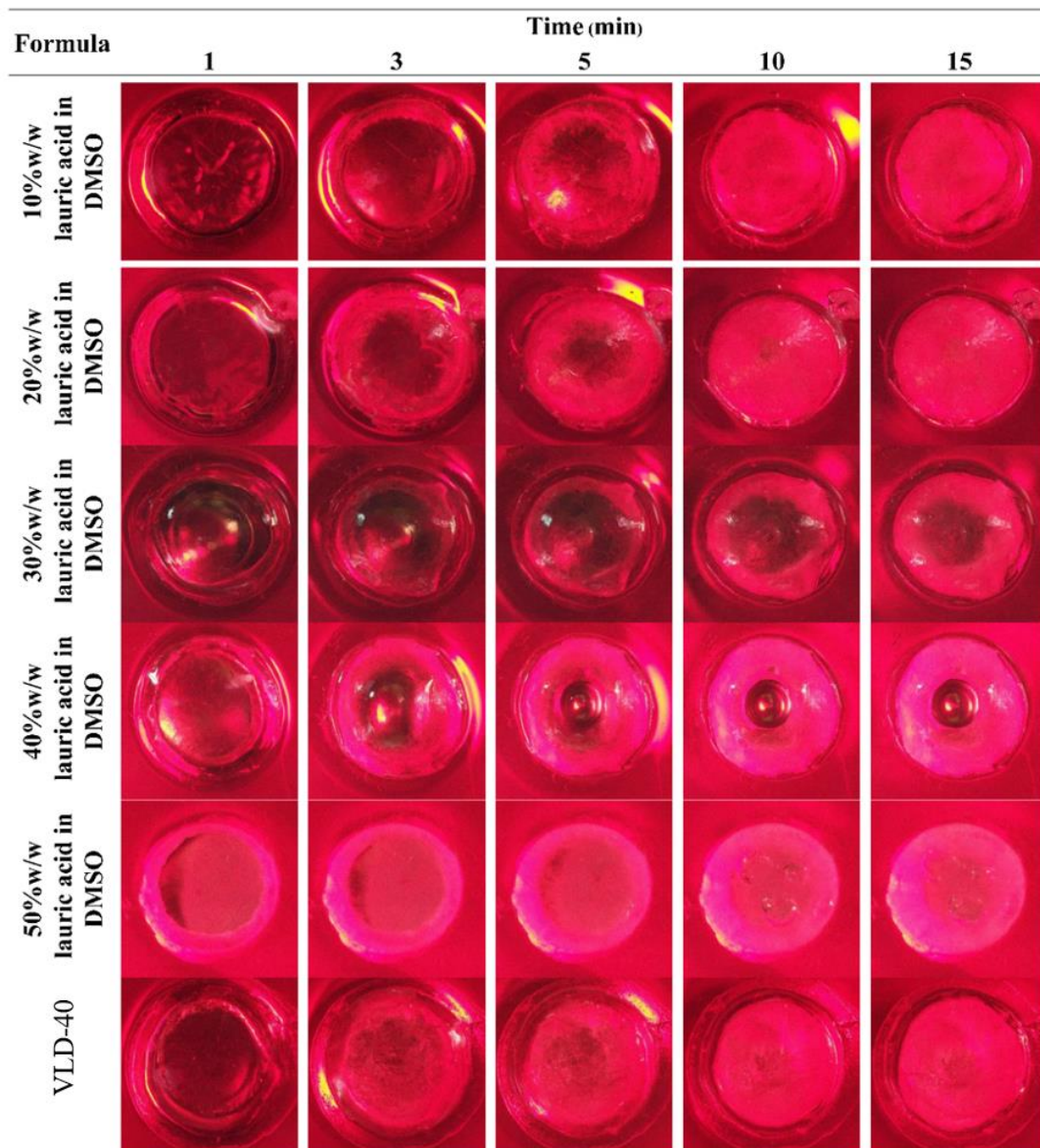
Figure 12 Phase separation of LAU in DMSO and VLD-40 at different time intervals with addition of amaranth

The distance and rate of the solvent diffusion of the ISMs were calculated as a function of time, and the results are illustrated in Fig. 13. Both formulations exhibited a longer diffusion distance with time and a lower rate of solvent diffusion as the concentration of LAU increased because of the thickening of the surface matrix network, which retarded the solvent exchange [231]. The diffusion rate slowed with time because the gradual formation of the matrix induced a much thicker surface network

and inhibited an external aqueous penetration at later stages [240]. The increase in a phase separation of LAU with time resulted in higher tortuosity and/or lower porosity of the LAU matrix, which lower the rate of solvent diffusion [245,246]. However, the formulation of 50% (w/w) LAU in DMSO exhibited a rapid phase separation at the interface between the agarose and the matrix because the dense surface LAU network was adequate to retard a solvent diffusion even at an early phase [242]. This behavior was due to the rapid conversion from solution into the matrix creating a tortuous channel, resulting in a slower and steadier rate than those of other LAU concentrations. The solvent diffusion rate of the VLD-40 formulations was apparently less than that of the 40% (w/w) LAU in DMSO formulation because VCM replaced some mass of the solvent. Such replacement caused a faster LAU matrix formation and inhibited a solvent migration.
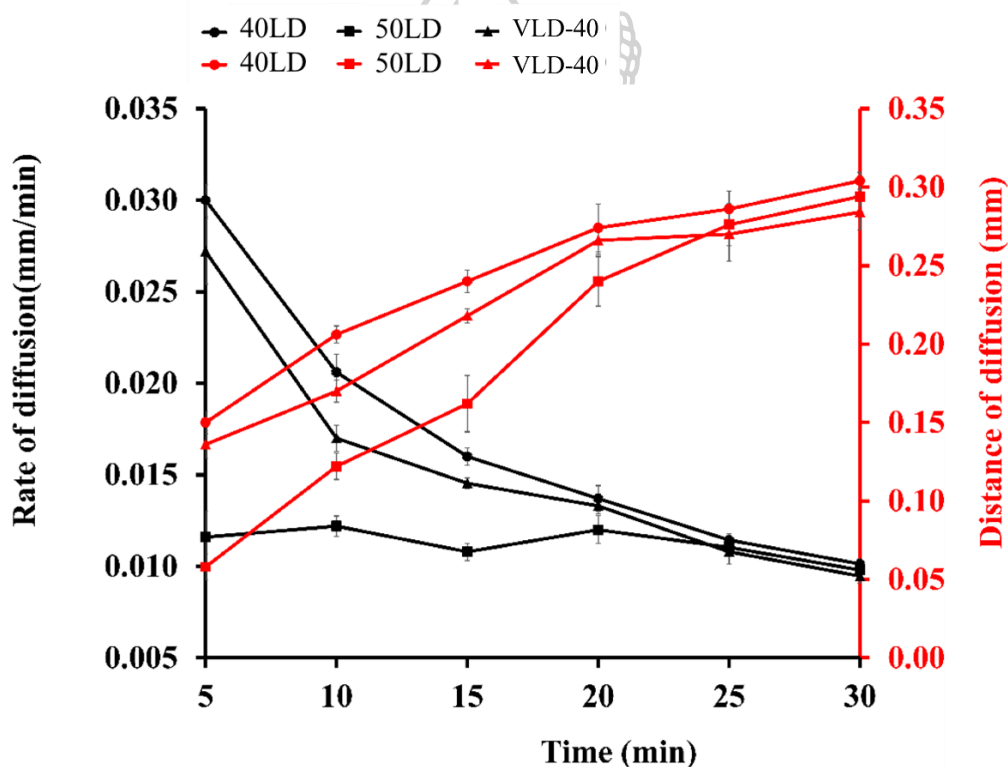
Figure 13 Rate (black line) and distance (red line) of solvent diffusion of 40% and 50% (w/w) LAU in DMSO formulation and VLD-40 (closed circle, square and triangle respectively) (n = 3)

Matrix formation (cross-sectional view) and solvent diffusion pattern of solutions from mixed fatty acid series

Solvent diffusion and gradual matrix formation of VLSD were observed after exposed to the buffer in agarose gel (Fig. 14A). The white matrix ring of the fatty acid formed rapidly together with an appearance of the red color front, indicating that

solvent exchange occurred suddenly after being exposed to an aqueous environment. Although there was a gradual fatty acid matrix formation, the solvent still diffused outwards, indicating that the solvent could escape through the matrix with higher tortuosity and less porosity. VLSD transformation was faster at the initial stage because the solvent was replaced by VCM. The rate of matrix formation decreased, while the distance increased with time as shown in Fig. 14B. The network formation of the fatty acid at the system surface front retarded the solvent exchange. Subsequently, the matrix became denser with higher tortusity and less porosity [242]; thus, the rate of transformation decreased with time. However, the longer distance of matrix formation with time was evident because the solvent and water exchange still remained; thereafter, the crystal growth of the fatty acid matrix occurred continuously [244]. From this test, there was no phase inversion of the formulation into solid fatty acid matrix moving into agarose gel and the opaque matrix was seen at the rim into inner area of agarose well. Practically, the diffusion of the formulation could occure at the initial stage and at a very short distance; however, this evidence was not detected under the stereomicroscope because the matrix at the rim behaved as the barrier against further diffusion out of fatty acid molecules.
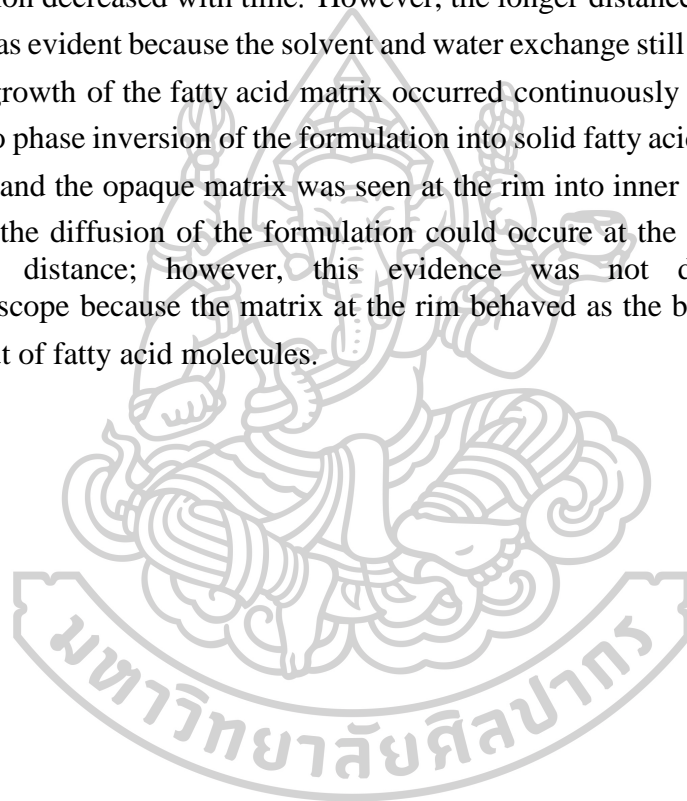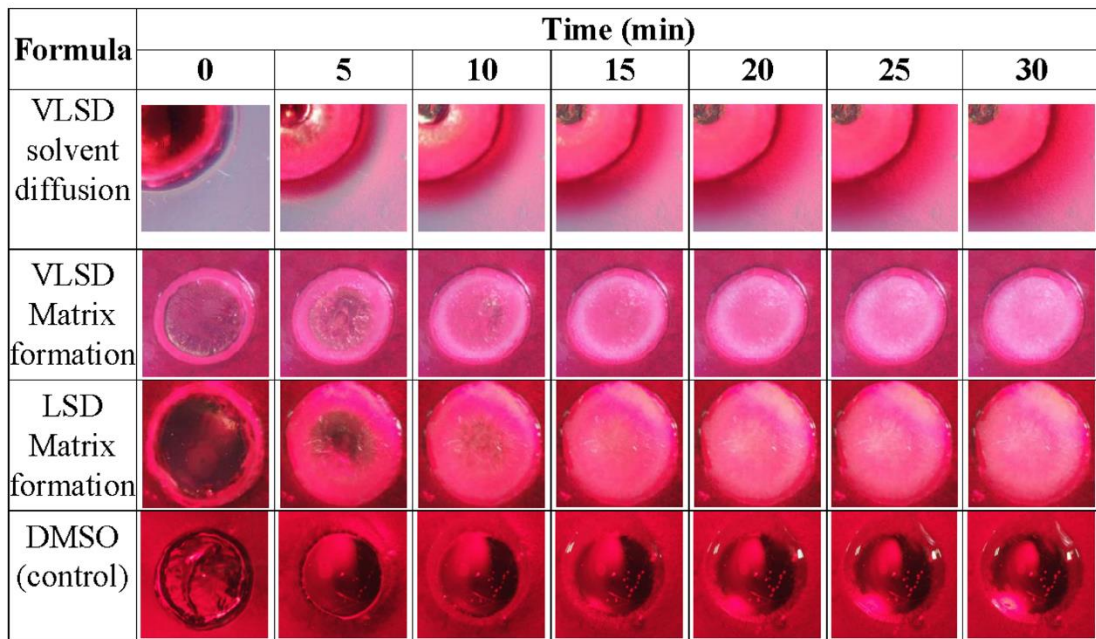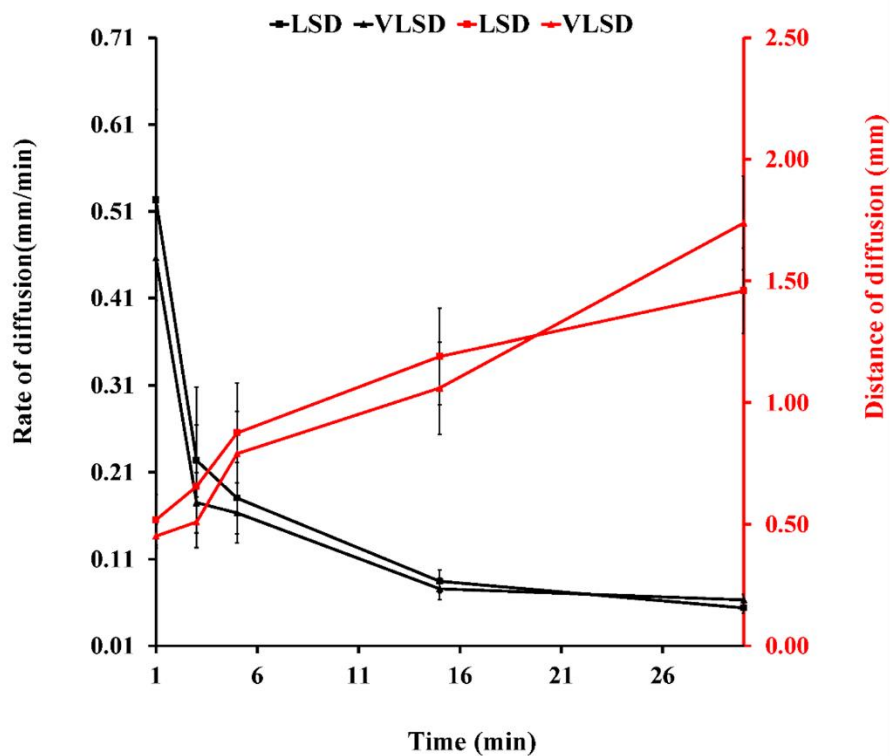
Figure 14 Color diffusion outwards (above) and matrix formation (below) of LSD and VLSD formulations (A); rate (black line) and distance (red line) of matrix formation with time of LSD and VLSD formulation (B) (n = 5) after filling the selected formulation into agarose well

Matrix formation rate (cross-sectional view) of solutions from fatty acid molecular weight series

The transformation behavior of the formulations in the agarose well corresponded with the result of a previous experiment (Macroscopic matrix formation behavior of solutions from fatty acid molecular weight series). The low-MW fatty acid solutions containing CPL and CPR did not change into a solid-like state (Fig. 15A). The trend of diminishing transformation rate by time (Fig. 15B), resulted by the restriction of solvent transfusion through interfacial network of initiated fatty acid matrix, which became denser with higher tortuosity and less porosity by time. Similarly, the dense gelation network also lowered the water diffusion coefficient [242]. Therefore, several formulations, including 35LD, 1.75LD, 35MD and 1.75MD, showed an incomplete formation within 15 min. Crystallisation was another crucial factor. Although the aqueous/solvent diffusion was obstructed, the crystal growth of the fatty acid still occurred continuously. Likewise, the completed PAL and STR matrix rapidly formed. Accordingly, the thermodynamic stability is interrupted by various factors, such as the presence of new interfacial energy from the initial crystal, aqueous surface, bubble surface, etc., together with the supersaturation (during decreasing of solvent); afterward, the system stabilises itself, resulting in crystal formation [244]. In this experiment, the difference in matrix formation between systems using NMP and DMSO as solvent was noticed. At 1–5 min intervals, the formulations using NMP as a solvent did not transform, whereas the formulations using DMSO showed a transformation visibly at the boundary. This behavior was noted in all fatty acid solutions in addition to comparison with high-MW fatty acids such as PAL. The DMSO diffusion rate was higher than that of NMP [247]. The fundamental properties, such as hydrophilicity/lipophilicity, should not be disregarded, especially in the ISM, which involves hydrophobic materials and an aqueous environment. Owing to its higher hydrophilicity (logK_{ow} values of DMSO and NMP are -1.98 and -0.38, respectively [248,249]), DMSO can be mixed with high polarity water more easily, whereas NMP remained still. Otherwise, NMP had a higher carrying capability for fatty acids although the system was mixed with inward water, as mentioned and disclosed in Section " Influence of KH_2PO_4 ion on water tolerance".
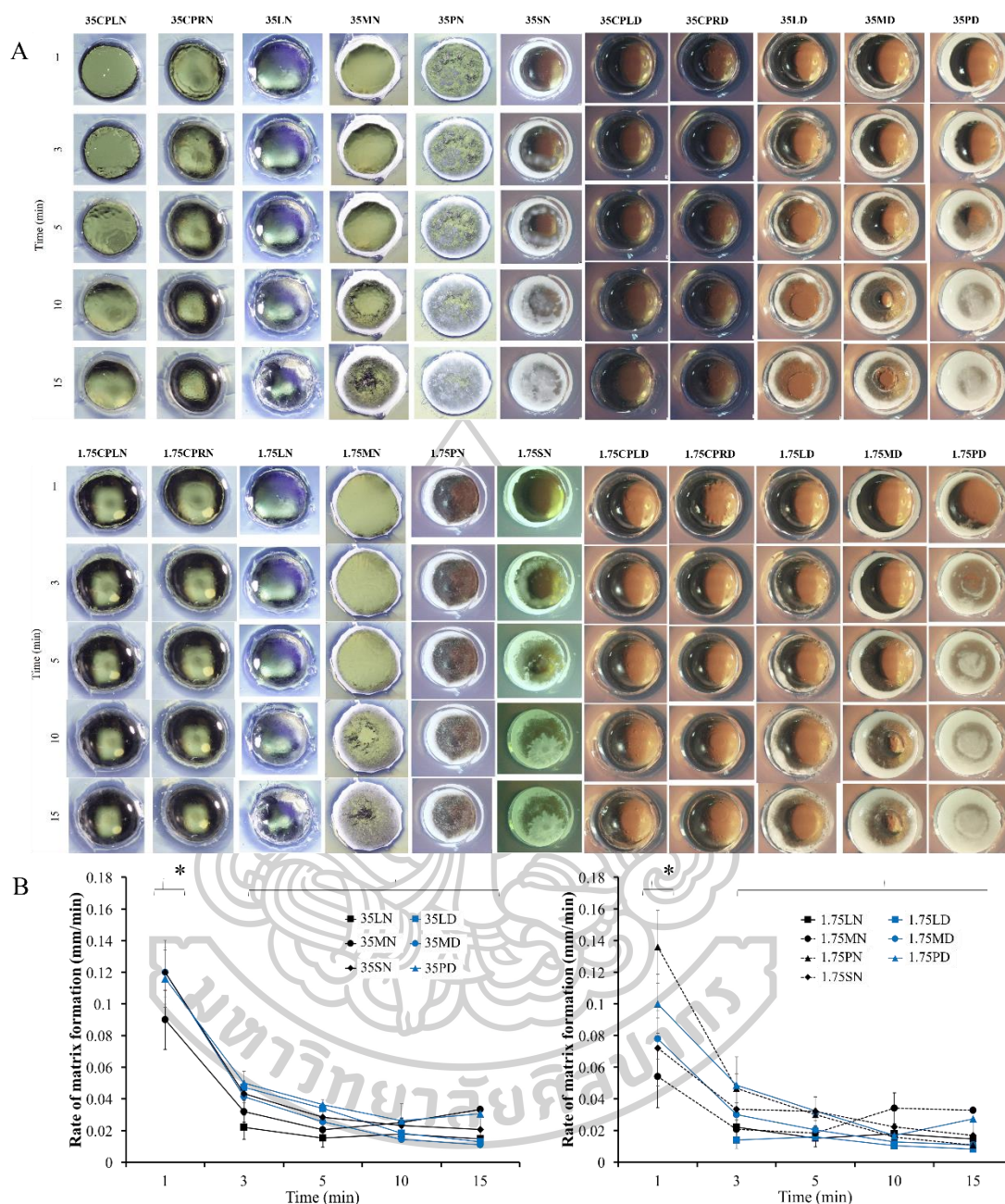
Figure 15 Cross-sectional view of matrix formation (A) and its rate over time in the agarose well (B) of fatty acid molecular weight series (n = 3)

Characterization of dried fatty acid precipitates

Thermal properties from TGA and DSC

The difference of fat crystal forms have the different thermal properties; thus, 40LD, 40LN, 40LP, DMSO, NMP and PRY were determined for their thermal properties in which the effect of solvent-used and *in situ* forming process on fat structure

was investigated. TGA thermogram (Fig. 16A) indicated that the intact LAU degraded slower than LAU precipitates. The maximum degradation temperature of intact LAU was 237°C while those of precipitates were about 227°C. The mass loss of solvents was due to their evaporation. PRY had two steps of mass loss with slower than the others while DMSO showed single step with lower maximum degradation temperature which might due to the viscosity of them. Thus, the thermal properties of LAU precipitates from *in situ* forming process was changed from that of LAU intact form, indicating the different crystal form. From previous report, TGA revealed that the LAU crystal is stable up to 45 °C [65]. DSC analysis in Fig. 16B indicated the lowering of melting temperature of LAU precipitates which that from PYR was lower than NMP and DMSO, respectively. All above mentions signified that the precipitation of LAU with these solvents inferred the crystallization of LAU and decreased the thermal stability of LAU in which the melting temperature and degradation temperature decreased.
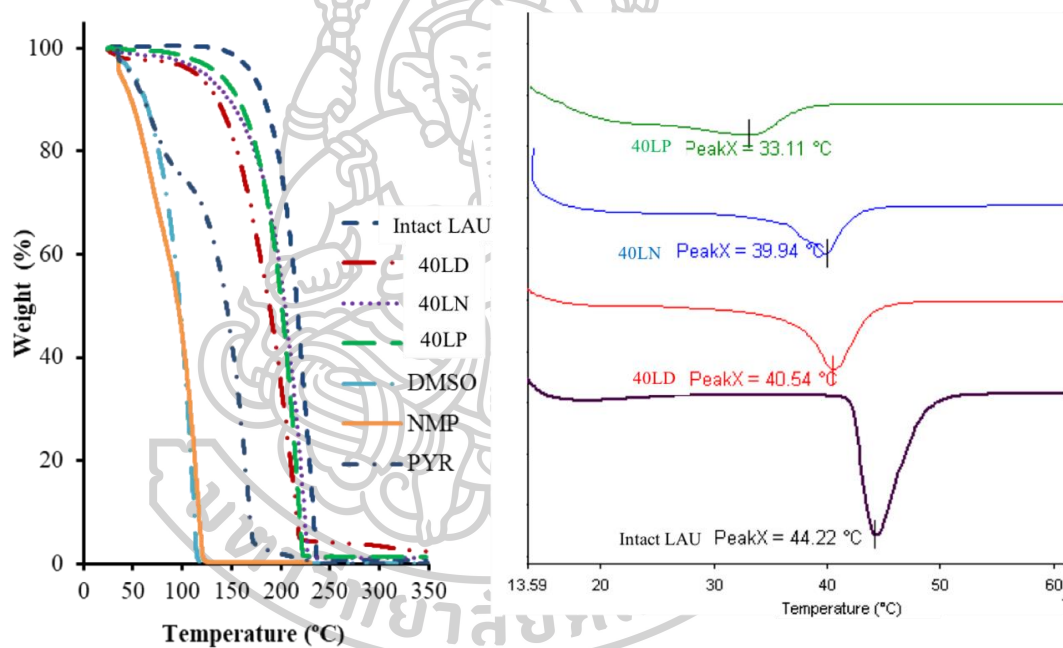
Figure 16 TGA (A) and DSC (B) thermograms of intact LAU and LAU precipitates

PXRD

LAU is known to exhibit polymorphism that its crystal behavior was described as following. Form A, of LAU, is triclinic, with $a = 7.45$, $b = 5.40$, $c = 17.47$ Å; $\alpha = 96°$ 53', $\beta = 113°$ 8', and $\gamma = 81°$ 7' [250]. The space group is Pi. The crystal is built of LAU dimers, which are packed together with the planes of all hydrocarbon chains parallel to each other (triclinie sub-cell), and with the carboxyl groups of one dimer adjacent to methyl groups of neighbouring dimers. The angle of tilt is 67° 20' [250]. While LAU in form C is obtained when LAU is crystallized from the melt or from ethyl alcohol solution at room temperature, which its crystal habit is monoclinic with $a = 9.524$, $b = 4.965$, $c = 35.39$

Å; α = 129° 13'. The cell contains four molecules; density observed 1.032, calculated 1.034 g.cm.$^{-3}$. The angle of tilt T = 54 ° 52' [251]. From PXRD pattern (Fig. 17), the peak intensity at 21.6 and 23.9° 2θ decreased notably for LAU precipitates from three solvents. The peak intensity at 6.5, 9.7 and 16.2° 2θ also decreased in the case of 40LN and 40LP. Thus, the LAU crystal might be interfered with solvent, especially, NMP and PYR during crystallization with slower rate than that from DMSO.
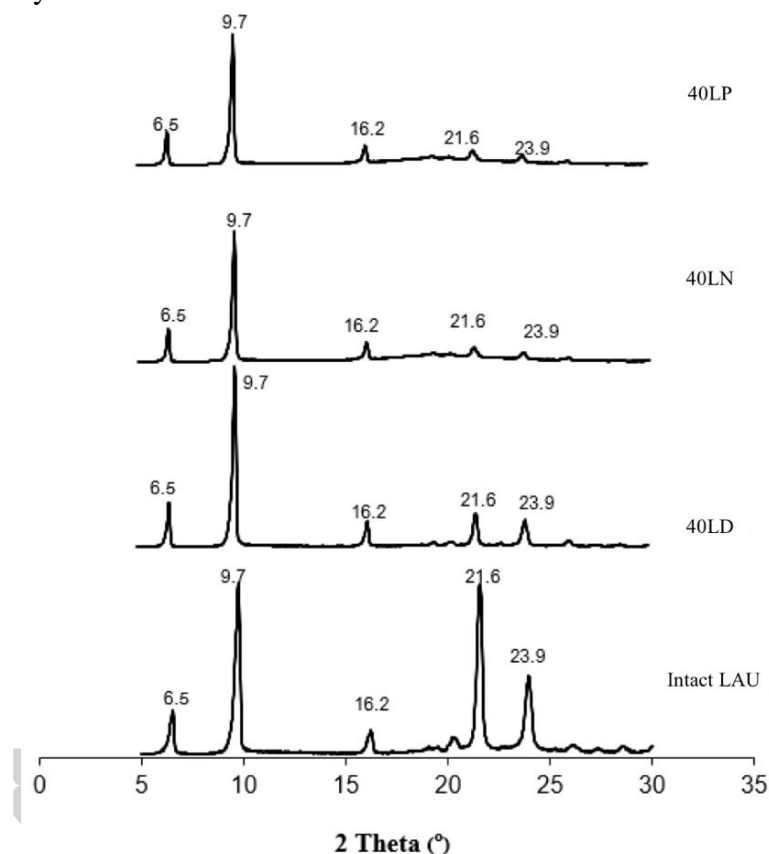
Figure 17 Powder X-ray diffraction patterns of intact LAU and LAU precipitates

FTIR

The characteristic peaks of intact LAU were evident at wave-numbers of 2931, 2851 and 1700 cm^{-1} (Fig. 18). Peaks at 2931, 2851 cm^{-1} were from CH_2 asymmetric stretching. The shift of C=O stretching at 1700 cm^{-1} of intact LAU to lower wave-number was found for LAU precipitates indicated the hydrogen bond formation between LAU and solvent residue in crystals. The H-bonding of H atom on solvent molecule to the carbonyl of LAU promoted a shift of the C=O stretching with decreasing wave-number [252].
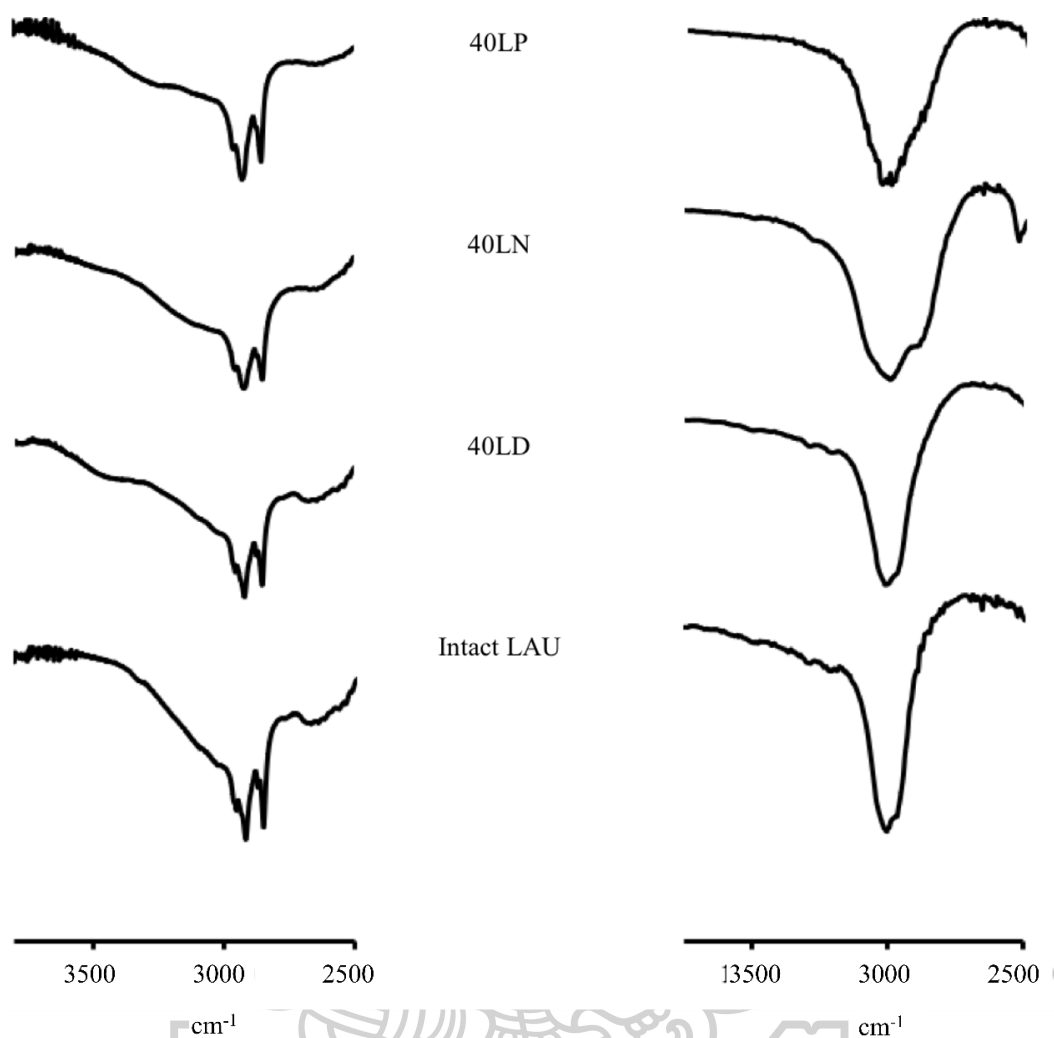
Figure 18 FT-IR spectra of intact LAU and LAU precipitates

HSM

Intact LAU showed temperature at starting for melting and complete melting at 42.9 and 44.7 °C, respectively (Fig. 19). All those complete melting temperatures of LAU precipitates were lower than intact LAU. Thus, these evidences corresponded with above- mentioned thermal properties to indicate the lower temperature of phase transition from solid state to fluid state after heating.

The transformation from LAU solution in different solvents into LAU solid-state influenced the physicochemical properties of LAU precipitate. The melting temperature of LAU precipitates might related with the formation behavior wherein the nucleation and crystallization could be affect to the crystallinity of LAU precipitates. The high crystallinity of intact LAU as showed in PXRD section has higher melting temperature than that of precipitate. The drug delivery systems based on phase inversion using LAU as component should be considered for this alteration for proper design and control the drug release behavior.

	Room temp. at starting point	Temp. at starting for melting	Temp. at completely melting
Intact LAU	30 °C	42.9 °C	44.7 °C
LAU precipitated from 40LD	30 °C	39.3 °C	43.4 °C
LAU precipitated from 40LN	30 °C	38.8 °C	42.3 °C
LAU precipitated from 40LP	30 °C	41.3 °C	44 °C
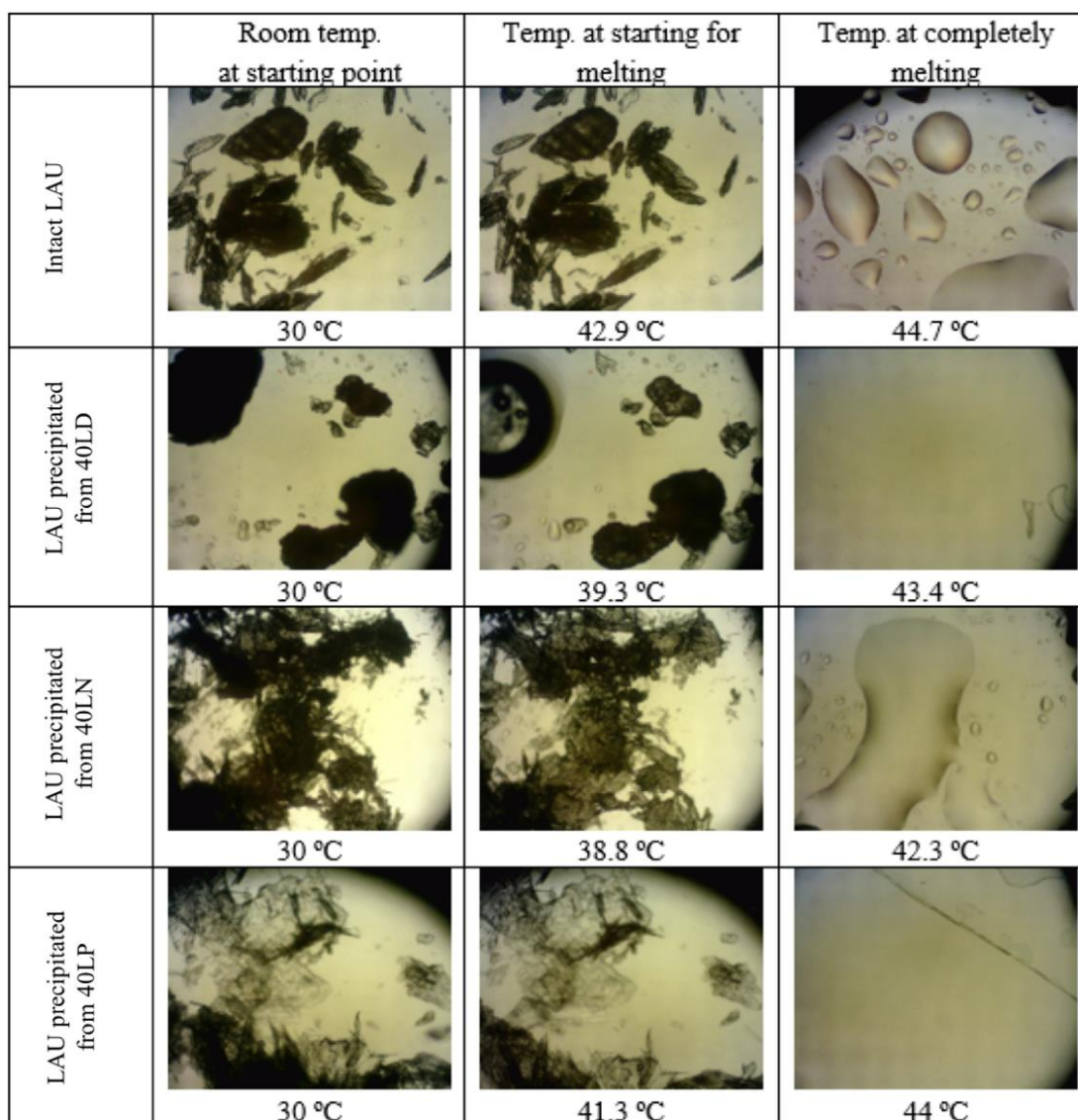
Figure 19 Photomicrograph from HSM of intact LAU and LAU precipitates

Injectability

Injectability of solutions from LAU series

The injection force and work of the drug-loaded formulation, VLD-40, was 0.94 ± 0.20 N and 5.35 ± 0.42 N.mm, respectively. Work and force of injection increased as the LAU concentration was increased (Fig. 20). By comparison, VLD-40 injectability was apparently lower than that of polymeric ISM. The injection work of polymer-based ISM, such as 5%–20% ethyl cellulose, 15%–30% bleach shellac and 15%–35% Eudragit RS ISM are 21.73–41.98, 11.73–27.69, 8.04–23.99 N.mm, respectively [2]. Therefore, the injectability of the developed LAU-based ISM is within the acceptable range (<50 N [80]). The enhanced performance of injectability of the prepared fatty acid-based ISM compared with those of polymeric based ISM indicated that it may be conveniently applied to the periodontal pocket [80].
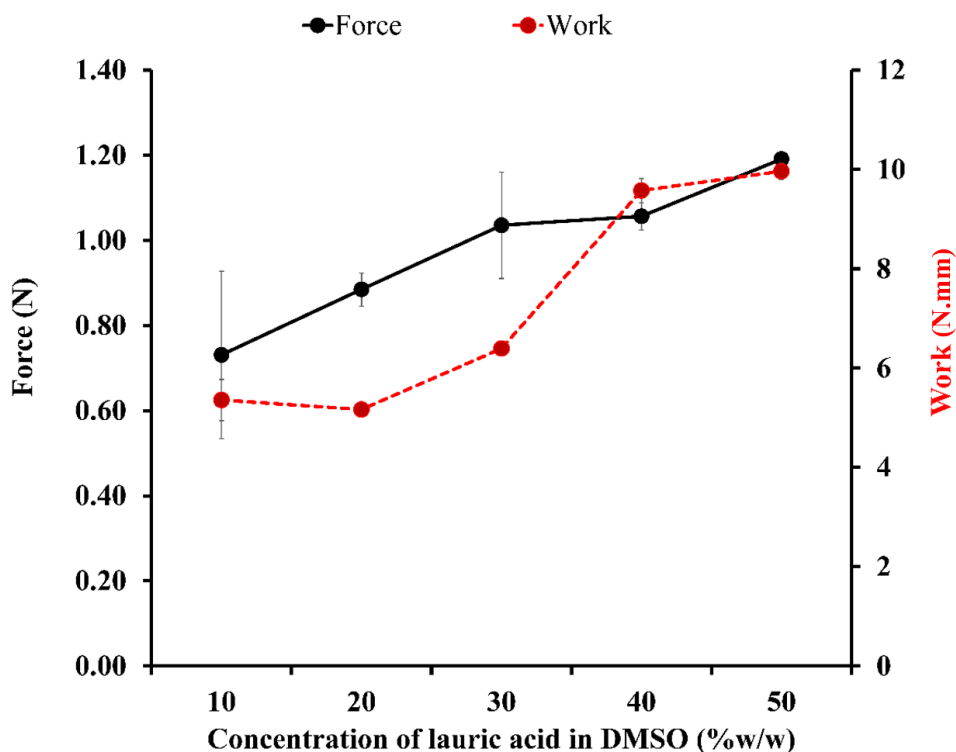
Figure 20 Work (red line) and force (black line) of injections of various concentrations of LAU in DMSO through a 27-gauge needle (n = 3)

Injectability of solutions from mixed fatty acid series

The injectability of prepared formulations (LSD and VLSD) showed remarkably lower than the threshold criteria of 50 N [61]. Thus, the developed formulation exhibited higher injectability than various polymeric- based intra-arthricular solutions such as hyaluronic injections. Famous intra- arthricular HA solution like Synvisc®, Orthovisc®, Atri- III®, and Hyalgan® needed to improve the ease of use (injectability) due to their highly viscous fluids [62]. The crosslinked HA molecules with divinyl sulfone (HA/DVS) showed the injectability about 12.5 N, while the HA solution prepared by traditional method showed about 35 N through 22- G needle [63]. To confirm the ease of use, the commercial product of intra- arthricual hyaluronic acid, Ari- III®, was compared with the developed formula. The developed formala exhibited quite higher injectaility than Atri- III® (Table 11) indicating their easiness for practical application of developed formulations eventhough the 27- G needle was used.

Table 11 Injectability through 18- and 27-gauge needles compared with commercial HA intra-articular of of fatty acid-based ISM.

Formula	Injectability test			
	Maximum force (N)		Work (N.mm)	
	18 G	27 G	18 G	27 G
VLSD	1.079±0.215	1.230±0.145	1.402±0.081	10.522±0.373
LSD	0.608±0.027	0.867±0.010	1.220±0.059	7.682±0.304
Atri-III®	2.853±0.154	27.026±0.339	38.422±1.874	341.991±7.241

Injectability of solutions from fatty acid molecular weight series

The injection force values of fatty acid formulations were in the range of 1.551–3.1182 N, which was extremely lower than acceptable criteria (<50 N [80]) indicating the high or ease injectability, with no significant difference between each formulation ($P < 0.05$). The injection work values of fatty acid-based formulation were in the range of 16.9103–35.3128 N.mm (Fig. 21), in which related to their MW. Lower injeactability trend was obtained as a higher MW fatty acid was employed wherein corresponded to their density and viscosity characters. Another report suggests that this injectability property was due to the lubricating performance of waxy materials [253]. This high injectability of the fatty acid-based *in situ* forming system indicates the ease of administration *via* injection. For example, in the case of knee joint administration, this system is more easily injected through small needle (27-G) than that of other intra-articular dosage forms and hyaluronic acid solutions, such as Atri-III® and Hyalgan®, which are highly viscous fluids [254] where the 12.5 and 35 N were used to inject cross-linked hyaluronic acid molecules with divinyl sulfone and hyaluronic acid solution through a 22-G needle [255].
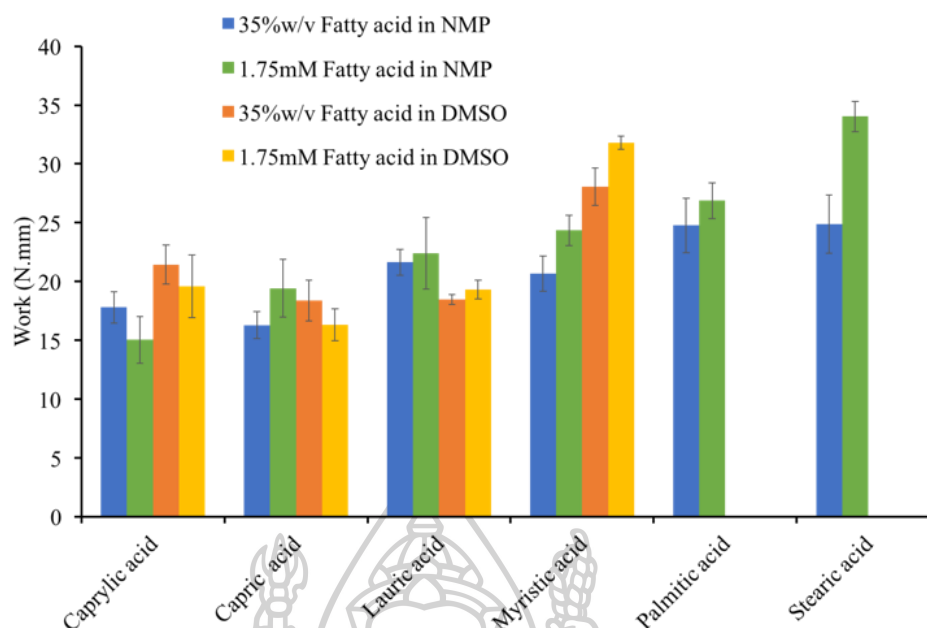
Figure 21 Injectability of preparations (work) (n=3)

Drug release and model fitting

In vitro **drug release of LAU-based formulations**

LAU in DMSO systems exhibited an interesting performance because they showed faster matrix formation with low water tolerance compared with that in other solvent systems. Formulations of 40%–60% (w/w) LAU in DMSO exhibited the advantage of rapid transformation; by contrast, formulations of VCM loaded in 50%–70% LAU in DMSO could not completely dissolve. Thus, 40% LAU in DMSO was selected for the drug release tests. Practically, the drug release from 1% (w/w) VCM-loaded 40% (w/w) LAU in DMSO (VLD-40) was compared with the control of 1% (w/w) VCM in DMSO (VD) (Fig. 22). VCM completely released from VLD-40 after 6 days, which apparently slowered than the drug release rate from VD. VCM was completely released within 1 day for VD. Therefore, LAU as an ISM matrix forming agent effectively prolonged a drug release. The release of VCM and, subsequently, the reduced diffusion of the drug, could be minimised by the hydrophobic property of LAU, which retarded the solvent exchange. Other hydrophobic materials, such as bleached shellac and cholesterol, also retarded a drug diffusion, resulting in an achievement of a sustained drug release [84,240]. Rapid surface network formation reduces the water diffusion and drug migration [240,242]. Rapid solvent exchange could result in the formation of a highly porous LAU matrix, resulting in a burst release. The initial burst release observed in VLD-40 was due to the rapid diffusion of DMSO outward the matrix, and the sustained release of VCM was achieved through the higher tortuosity and/or a lower porosity of the remaining LAU wax matrix after extensive crystallisation of this fatty acid had occurred [245,246]. By comparison, 30% VCM released from PLGA-based implants on the 15th day [256] and 11%–63% VCM released from PLGA *in situ* forming implants within 12 h [257]. PLGA

in situ forming systems showed a burst release and then reached a steady state on the 5th day with 50%–60% drug release. Thus, VLD-40 initially released the drug at a high concentration and then sustained the drug release to nearly 100% on the 6th day. The VCM release data of VLD-40 ISM and VD were fitted to a number of mathematical release models, and the estimated r^2 and msc values are shown in Table 12. The release data from VD fitted a first-order kinetic model, whilst that from VLD-40 ISM fitted Higuchi,s equation. The result indicated the diffusion or penetration characteristics of the water-soluble drug through VLD-40 matrix [258]. The VLD-40 release data also fitted the power law model well, and the exponent value (*n*) was close to 0.45. This finding indicated that drug release occurred through a Fickian diffusion mechanism and that the rate of liquid diffusion was the limiting step of drug release through the insoluble matrix [166,259]. The *n* of VD was between 0.45 and 1, which indicated that the release mechanism was an anomalous (non-Fickian) transport due to the release of the dissolved drug with a concentration gradient through the dialysis membrane [166,260].
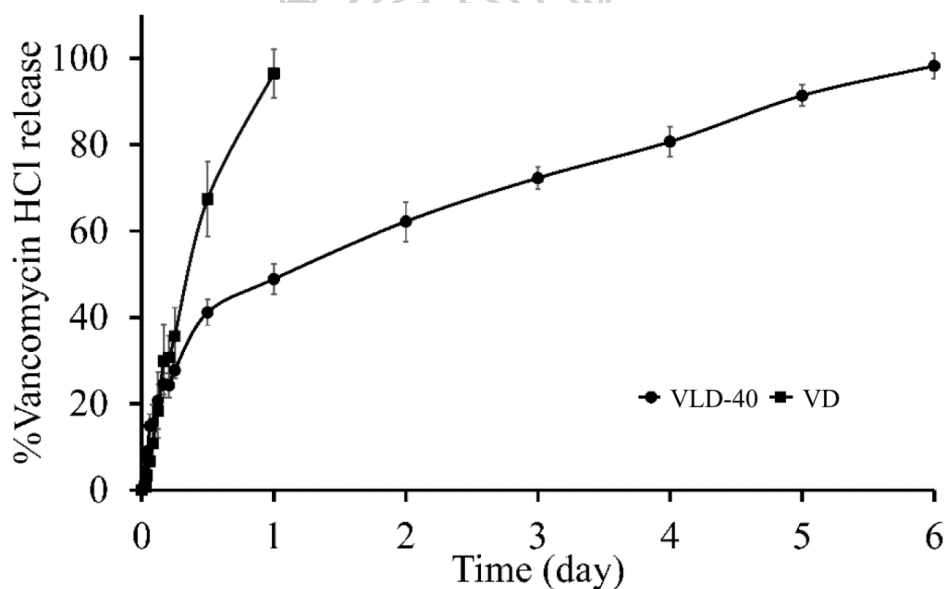
Figure 22 Release of VCM from ISM containing LAU using the dialysis tube method in PB pH 6.8 (n = 3)

Table 12 Comparison of degrees of goodness-of-fit from curve fittings and parameter estimation from curve fittings of the release profiles of VCM from VD and VLD-40 systems in PB (pH 6.8) using the dialysis tube method for different release models

Formula	First order		Higuchi's		Zero order		Power law			
	r^2	msc	r^2	msc	r^2	msc	r^2	msc	n ± S.D.	Release mechanism
VD	0.9870	4.0347	0.8967	1.8703	0.9448	2.5325	0.9705	2.9250	0.7241 ± 0.1160	Non-Fickian diffusion
VLD-40	0.9537	2.8494	0.9748	3.4303	0.8841	1.9326	0.9653	3.0083	0.3957 ± 0.0463	Fickian diffusion

Abbreviation: VD=1% (w/w) VCM in DMSO; VLD-40 = 1% (w/w) VCM with 40% (w/w) LAU in DMSO

In vitro drug release of ISMs from mixed fatty acid series

The drug release from VLSD was compared with 0.75% w/w VCM in DMSO (0.75VD) (Fig. 23). The drug released from 0.75VD by fast diffusion through the dialysis membrane and completed within half day, whereas VLSD extended the release over 6 days, which was significantly slower than that of VD. Thus, 1:1 L:S exhibited an effective ISM to achieve sustained drug release due to the rapid fat network formation at the surface and minimised the water and drug diffusion [240,242]. Hydrophobic property of these fatty acids retarded the water diffusion and also reduced the diffusion of dissolved VCM. Thirty seven percent of vancomycin released from PLGA scaffold in PB pH 7.4 at the first day and slowly released to reach 46% on the 8th day [261]. The vancomycin release from PLGA ophthalmic implant was about of 30% on day 15 [256] while VLSD released VCM for 96.5% on the 6th day.

The release of VCM from PLGA *in situ* forming implants in acetate buffer solution (40mM, pH 6.8) were 11-63% in 12 h depended on the type and ratio of mixed solvent (NMP and acetone) [257]. Those formulations showed a burst release then reached the plateau pattern at 5th day with 50-60% release. Thus, the benefit of the VLSD release pattern over those PLGA formulations was the delivery of suitable release rate for post-operative knee infection. Precisely, VLSD at the first 8 h reached the MIC level then sustained the release to almost 100% at the 6th day. In the case of the longer treatment period (>6 days), VLSD administration could be repeated on the 7th day. This sustainable VCM release was capable of achieving the goal of knee infection treatment as the effectiveness of VCM depended on both the concentration and the duration of the exposed time [41]. The estimated r^2 and msc from the VCM dissolution profile were fitted to different mathematical release models as shown in Table 13A. The higher value of r^2 and msc indicated the superiority of the degree of fit. The release data from VLSD fitted well with the first order kinetic and also fitted well with the power law model, wherein the exponent value (n) was lower than 0.45 (Table 13B). Hence, the drug was

released *via* a quasi-Fickian diffusion mechanism and the limiting step of this non-swelling matrix system was the diffusion of the liquid [166,259]. The MIC of vancomycin against MRSA is 2-4 μg/mL. Since the elimination rate of VCM in synovial fluid is 3.22 hr^{-1} [41,141], the estimate concentration in 30 mL synovial fluid (5.85-250.88 μg/mL) was above MIC level over 6 days (Table 14). Moreover, the estimated AUC/MIC were 7,437 and 3,718 for the MRSA MIC of 2 and 4 μg/mL. Based on the Pharmacokinetic-Pharmacodynamics criteria, AUC/MIC ratio of >400 has been used as the predicted target value to achieve the clinical effectiveness of VCM [262,263]. Thus, 0.3-2 mL of VLSD was sufficient to reach the MIC level against MRSA in 5-30 mL synovial fluid. Since the MIC levels of antibiotics are difficult to reach in synovial fluid *via* intravenous or antibiotic-loaded cement, the intra-articular delivery of antibiotics has been effective because it was directly injected to the target site. Thus, an intra-articular injection of VCM becomes the first choice for the postoperative knee infection treatment in Missouri Bone and Joint Research Foundation Institute [141]. However, to maintain the concentration of VCM in a synovial fluid, the repeated dose of every 12 or 24 h is required. Thus, the developed formulation could be the choice for post-operative knee infection because it could sustain VCM release with sufficient VCM therapeutic amount.
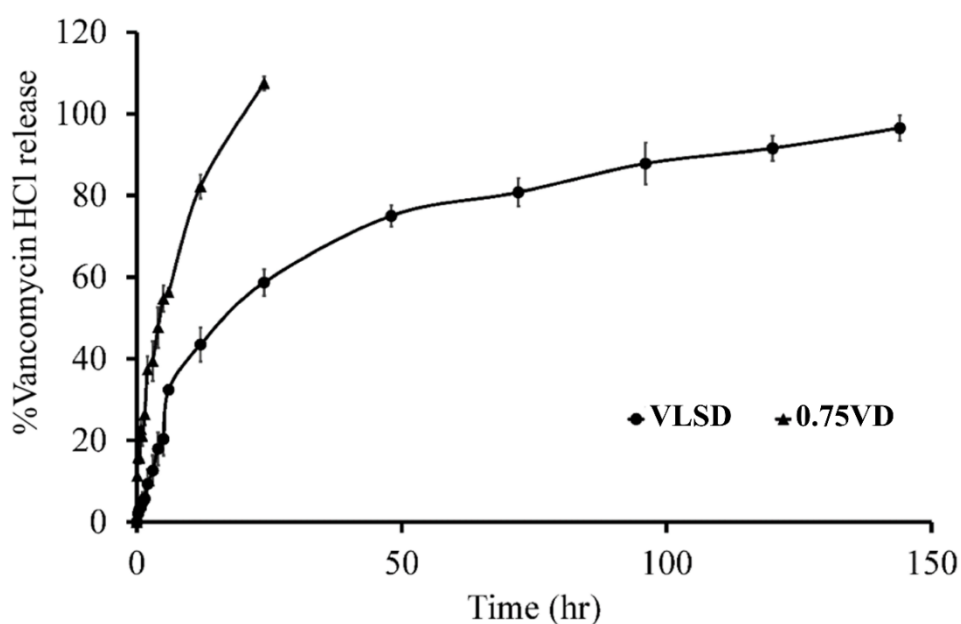
Figure 23 VCM release from LAU/STR-based ISM in PB pH 7.4 using the dialysis tube method (n = 3)

Table 13 Degrees of goodness-of-fit (A) and estimated parameters (B) from curve fittings of the release profiles of VLSD systems in PB pH 7.4 using the dialysis tube method

A											
Zero order			First order			Higuchi's			Power law		
r^2	cd	msc	r^2	cd	msc	r^2	cd	msc	r^2	cd	msc
0.9162	0.8120	1.3379	0.9943	0.9871	4.0187	0.9793	0.9275	2.1801	0.9922	0.9726	2.9291

B		
k±SD	n±SD	Release mechanism
0.0478±0.0148	0.3552±0.0388	quasi-Fickian diffusion

k = constant, and n = diffusional exponent

Table 14 Estimate concentration of VCM in 30 mL synovial knee joint

Time (hr)	C_t (µg/mL)
0	
0.083	17.70051654
0.25	50.30023113
0.5	92.76548825
0.75	128.3437842
1	157.8778949
1.5	201.7248447
2	229.3430009
3	250.8794832
4	244.9206436
5	225.0407345
6	8.596246646
12	10.69539562
24	10.85672069
48	9.644950418
72	8.513695567
96	7.514814803
120	6.633127291
144	5.854885149

The estimated concentrations in table 14 were calculated from the kinetic equation given below based on the synovial fluid volume of 30 mL, elimination half-life 3.22 hr^{-1}, 2 mL of VLSD injection (15,000 µg of VCM), 0.4365 (0-6 hr) and 0.0052 (6-144hr) release rate constant.

$$C_t = \frac{D}{V}\frac{k_r}{k_r - k_e}\left[e^{-k_e(t-t_D)} - e^{-k_r(t-t_D)}\right]$$

, C_t = Concentration at given time (µg/ml)

D = Dose of administration: 15,000µg (2 mL of VLSD)

V = Volume of synovial fluid (30mL)

k_r = release rate constant, 2.303∗slope: 0.4365 (0-6 hr), 0.0052 (6-144hr)

k_e = elimination rate constant (hr^{-1}), 0.693/$t_{1/2}$: 0.693/3.22

t = Given time

t_D = Initial time

In vitro drug release of ISMs from fatty acid molecular weight series

At the initial experimental periods, the VCPLD formula showed the highest burst release because it did not form a solid-like state. The burst release of a well-transformed matrix was influenced by the type of fatty acid. VPD, VMD, VCPRD and VLD

presented a descending burst release (Fig. 24). Although, the crystal network at the contacted surface was rapidly formed, as described in another sections " Matrix formation (cross-sectional view) and solvent diffusion pattern of solutions from mixed fatty acid series" and "Interfacial phenomenon during initial transformation period". VMD and VPD exhibited more burst release than VLD. The rapid matrix formation signified the rapid movement of DMSO with the crystallisation of fatty acid. Therefore, the rapid DMSO outflux carried this drug with its diffusion. Moreover, the evidently large passage of high fatty acid-based formulation might be formed. The topography of the obtained matrix under SEM revealed this evidence. According to the results in " Influence of KH_2PO_4 on water tolerance", 35LD had a higher separation point, signifying a lower degree of supersaturation than 35MD and 35PD. Thus, VLD needed more water penetration to induce phase separation, resulting in a high water-containing volume at the given time. Then, the high number of fatty acid nuclei coincided with the slowed crystal growth rate of each other [25]. Each crystallisation origin grew with vignettes, resulting in less porosity and high tortuosity. By contrast, the rapid formation had less crystallisation origin. Thus, the large passage mentioned above can be obtained *via* continuous crystal growth. Thereafter, with a completed matrix formation, the drug liberation attained as a sustaining release pattern, whereas the control group showed a fast and complete VCM release within the first day. VMD and VPD prolonged the drug release over seven days, with about 80% cumulative drug release, whereas VLD showed 56% cumulative drug release. The formulations gained a sustainable capability through the restriction of water and drug migration [240,242]. The hydrophobicity of fatty acid and the obtained hard waxy matrix retarded the water-drug movement. This movement retardation was also observed when using the other hydrophobic matrix formers, such as bleached shellac and cholesterol [84,240]. Hydrogen bonding was also considered given that fatty acid and VCM molecules contained the functional groups including COOH, OH and NH. Although the formulations prolonged the drug release over seven days with a 56%–80% drug release, repeated administration could only be conducted if the treatment period would be extended.
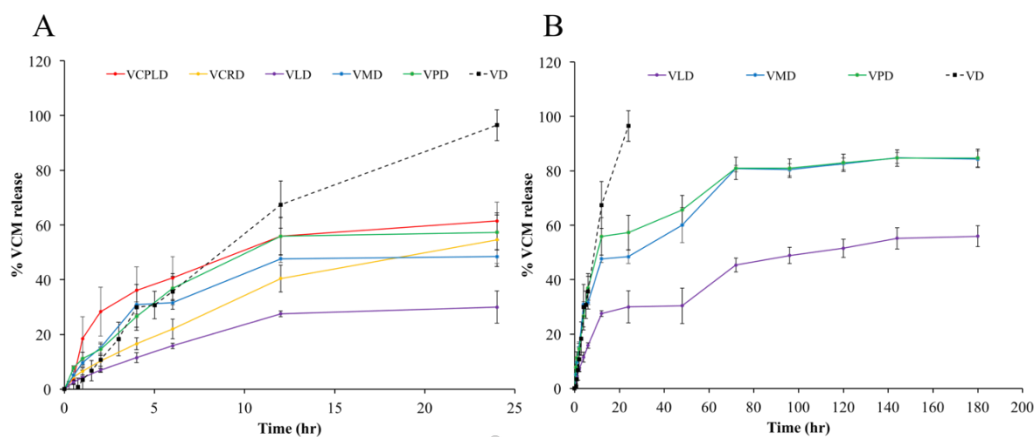
Figure 24 VCM release from ISM at the initial experimental period (A) and over 7 days (B) in PB at pH 7.4 using dialysis tube method

In vitro **drug release of ISMs from fatty acid molecular weight series (membraneless method)**

To acquire a sustainable drug release from the *in situ* formation system, the ability to form a matrix is a prerequisite. The results showed that VCPLD was a non-sustainable drug release system. The drug release trend was directly related to the molecular weight of fatty acids; the lower molecular weight fatty acid-based formulation showed higher drug release sustaining capability, except the VLD that was tested under 37°C (Fig. 25). This was explained more in the next section. The VPD, which formed matrix faster than others, presented a burst release and reached the plateau pattern within 3 days. In comparison, VMD and VLD (tested under 30°C) showed higher drug release sustaining capability. These implied an inverse relation between formation ability and sustainable release. The inverse relation was basically understood by the movement of the solvent and the formation of the matrix pattern. The VPD could generate the continuous crystal wall due to its high ability to form a matrix; however, the solvent also desperated moving out. The only way to move out during this rapidly forming wall was to head directly and move massively, whereby, the large uncomplex channel was generated and subsequently resulted in a less sustainable release. The more slowly forming VMD and VLD (tested under 30 °C) showed a different matrix pattern formation. According to the previous investigation, the lower molecular weight of the fatty acid-based formulation had a higher separation point or a higher water tolerance, which contained a higher volume of water/solvent mix at the specified time resulting in an altogether high number of fatty acid nucleation when the water ratio was reached the separation point and, thereafter, slowed the crystal growth rate [25]. Consequently, each crystal was growing with confusedly resulting in a complex interior structure, which was suitable for prolonging the drug release. It is known that formulations gain a sustainable ability through the restriction of water and drug migration [240,242]. Moreover, the hydrophobicity of fatty acids could play a crucial role for retarding solvent movement

and drug diffusion as another reported using bleached shellac and cholesterol as the matrix forming agents [84,240].

Effect of temperature on drug release sustainability

There are no statistically significant differences ($P<0.05$) between the drug release series formulation under 30°C and 37°C except VLD (Fig. 25). Since the VD (control group) and VCPLD could not form a matrix, they released the drug completely on the first day. In the case of the high molecular weight fatty acid-based formula such as VMD and VPD, the temperature had no affect because the melting point of MYR and PAL are near 51.80 °C and 60.42 °C [56], respectively.

In contrast, VLD exhibited dramatically different release patterns when test conditions were between 30°C and 37°C ($P<0.05$). Under 30°C, VLD showed a remarkable ability to sustain a drug release compared to others. Meanwhile under 37°C, VLD reached 87% cumulative release on the 3rd day. This was due to the invert-*in situ* forming process of VLD under specific conditions; namely, the solid matrix was secondarily transformed into a swelling-gel-like matrix (Fig. 26). This swelling-gel-like matrix with a very loose network of fat resulted in significantly reduced ability to sustain the drug release than that of a solid matrix ($P<0.05$). However, the swelling-gel-like matrix still provided some ability to sustain the VCM, which relied on the slow transformation process; thereby, either invert-formation or some interaction of VCM/fat could be a reason, which was discussed in the next section. Considering the release pattern of the two types of VLD matrix, gel-like and solid-like, it confirmed in the SEM results that the formulation's sustainability was mainly affected by the tortuosity and porosity of the transformed fat matrix.
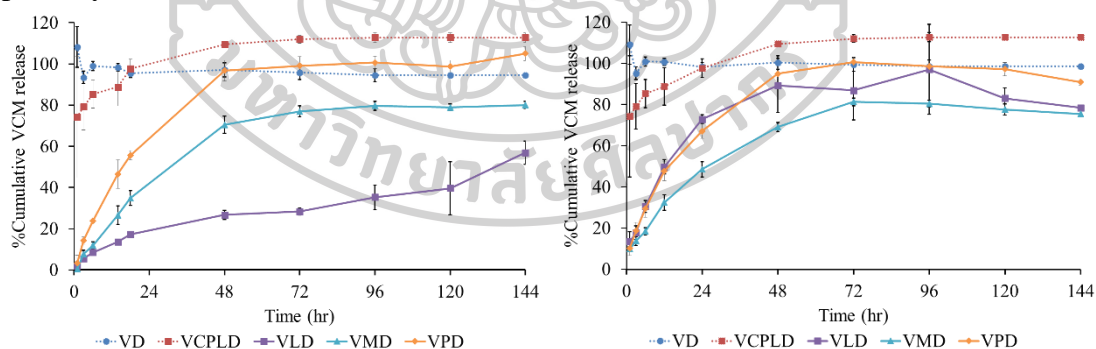
Figure 25 VCM release from ISM at 30°C (left) and 37°C (right) in phosphate buffer pH 7.4 using membranless method

Invert *in situ* forming process

The swelling-gel-like matrix was obtained for some specific conditions. The secondary transformation was slowly processed, and the obtained gel maintained its state over 7 days (Fig. 26) with some sustaining release ability. Since it formed into the solid-like matrix, then loosen its structure and became semisolid, whereby, this manner characteristic was named as an invert-*in situ* forming process. The reason being that

there was no invert-*in situ* forming process in the sections of LAU-based and LAU/STR-based ISM, tested under 37°C with a medium of pH 6.8 and 7.4 phosphate buffer. Some specific conditions were achieved in this scenario, such as the coincidence of medium pH, temperature, and type of fatty acid (Table 15). It is known that the pKa of any acids is directly related to thermodynamics of the dissociation reaction. The relation between pKa and temperature is based on Le Châtelier's principle [264]. The shift of the dissociation constant in the function of temperature has been proved over time [265,266]. Thence, the following reasons synergized each other and resulted in the slow invert-*in situ* process of VLD. According to the equation of acid-based dissociation, the high pH medium (pH=7.4) caused more dissociation of lower pKa substance as LAU (5.3, at 20°C). Meanwhile the other fatty acid, which has a higher pKa value due to its longer aliphatic chain [267] (MYR pKa=7.0, PAL pKa=7.2 [268]) exhibited less dissociation in the same pH medium. Secondly, the melting temperature of LAU is 43.55 °C [55] while the melting point of MYR and PAL is about 51.80 °C and 60.42 °C [56]. This also means more energy is required at a higher molecular weight to break the structure of those matrices. Thirdly, at the higher temperature (37°C), the less of pKa value of LAU resulted in more dissociation. Although, the conditions synergized to break the crystal network of LAU, it still had a function of time since the formed-matrix has less surface area than that of a small particle. Thus, the slow invert process was obtained. To clarify, this phenomenon could be obtained in any of the fatty acid-based ISM under the function of temperature and medium pH; however, in this study, the condition was specified to VLD.
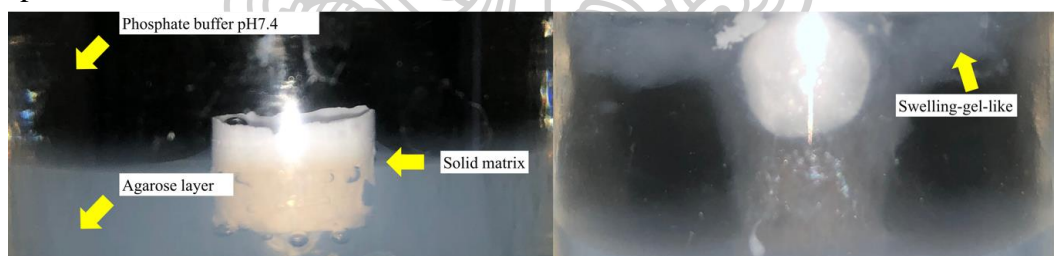
Figure 26 Formed solid matrix (left) and invert-in situ forming process (right)

Table 15 Matrix formation ability and invert-in situ forming process at different temperatures and pH

Formulation	Medium pH	Matrix formation (within 5 min)		Invert-*in situ* forming process (within 7 day)	
		At 25°C	At 37°C	At 30°C	At 37°C
VCPLD	7.4	Not obtained	Not obtained	Not obtained	ND
VLD	7.4	Obtained	Obtained	Not obtained	Obtained (on 2nd day)
VLD-40	6.8	Obtained	Obtained	Not obtained	Not obtained
VLSD	6.8	Obtained	Obtained	Not obtained	Not obtained
VMD	7.4	Obtained	Obtained	Not obtained	Not obtained
VPD	7.4	Obtained	Obtained	Not obtained	Not obtained

Drug release profile fitting

The estimated r^2 from the VCM cumulative release data fitted to different mathematical release models is shown in Table 16. All release profiles in both 30ºC and 37ºC fitted well with Higuchi's equation except that of VLD (tested under 30ºC), which fitted well with a zero-order model. The fit results of Higuchi's model claimed the expedition of VCM through the tortuosity matrix in which it accounted for the distance to the surface of the drug dissolution region [169,170]. The good zero-order fit indicated the rate of VCM release from VLD was an ideal concentration/time-independent for contolled-drug release. Power-law model was used along with other models to explore the release kinetic mechanism. According to those cited, the VCM released from most formulations *via* anomalous diffusion revealed both of drug diffusion (pure Fickian diffusion) and structure relaxation. Only VMD (tested under 30ºC) presented a case-II transport. However, the r^2 of fitting with power-law was quite lower than 0.9; thereby, it should be deserted and focused only on Higuchi's model. The interpretation of VLD (tested under 37ºC) differentiated to others since it showed obvious swelling over time. In that case, the release mechanism relied on VCM diffusion and swelling of the fat network since the n value indicated the anomalous mechanism. Even the n value was over 0.45; however, it was also very closed, which likely indicated Fickian diffusion. This phenomenon was due to the apparently loosed fat network from the invert-*in situ* forming process that resulted in more free VCM diffusion over time. Speaking of which, these all results indicated that most of the fatty acid-based ISM exhibited the release pattern of the matrix as a Higuchi's model for which the dissolution, diffusion, and distance were accounted.

Table 16 Degrees of goodness-of-fit and estimated parameters from curve fittings of the release profiles of VCM-loaded in situ forming systems in PB pH 7.4 using the membrane-less method

	Zero order		First order		Higuchi's		Power law		
	r^2	k	r^2	k	r^2	k	r^2	k	n
At 30ºC									
VLD	0.9460	0.3309	0.7048	0.0072	0.8794	4.6305	0.9769	0.0247	0.6075
VMD	0.8976	0.8931	0.4839	0.0153	0.9699	9.4970	0.8784	0.0112	1.0358
VPD	0.8331	1.0808	0.5517	0.0109	0.9563	11.8450	0.9387	0.0525	0.7269
At 37ºC									
VLD	0.7785	0.9281	0.6421	0.0076	0.9362	10.3530	0.9602	0.1312	0.4709
VMD	0.9300	1.0836	0.7975	0.0119	0.9945	9.9350	0.9839	0.0845	0.5308
VMD	0.9252	1.8732	0.7046	0.0175	0.9961	14.1470	0.9969	0.1013	0.5913

Antibacterial activity

Antibacterial activity of LAU series

The inhibition zone diameters of the prepared ISM systems against various microorganisms are shown in Table 17. Whereas VLD-40 exhibited the excellent antibacterial activities against all *S. aureus* and *P. gingivalis* strains with a similar clear zone diameter, 40% (w/w) LAU in DMSO exhibited a significantly smaller clear zone against *P. gingivalis* ($P < 0.05$). Because DMSO shows no antibacterial activity against *S. aureus* and *P. gingivalis*, the occurrence of the clear zone in the LAU in DMSO system indicates that LAU exhibited the antimicrobial activities against the tested bacteria. LAU could disturb the uptake of amino acids and similar molecules into bacterial cells [269], disturb membrane fluidity [270] and affect the optimal conformation of potential proteins [270]. VCM inhibits cell wall synthesis in bacteria by limiting the polymerisation of the phosphodisaccharide-pentapeptide lipid complex [151]. Practically, the antimicrobial activity obtained from an agar diffusion assay (cylinder plate method) related to the diffusion of antimicrobial agent; therefore, the sustainable VCM release from VLD-40 promoted a less inhibition zone than VD. NMP and PYR exhibited the antimicrobial activities against *S. aureus*, *P. gingivalis*, *E. coli* and *C. albicans*, whilst DMSO inhibited the growth of *E. coli* and *C. albicans* only. These solvents could solubilise the lipid components in bacterial and fungal cell membranes owing to their high solubilising power [84,271]. When NMP is replaced with LAU, a significantly larger clear zone compared with that obtained by using pure NMP is observed ($P < 0.05$) for all bacterial strains except *S. aureus* ATCC 25923. The synergistic behavior between LAU and NMP is an interesting topic to explore in future work. ISM comprising LAU exhibited very large clear zones against *C. albicans*. Previous reports revealed that LAU exhibits antimicrobial activities against *S. aureus*, including MRSA [269,272], *E. coli* [272,273], *P. gingivalis* and *C. albicans* [15]. VLD-40 appropriately sustained drug release and effectively inhibited MRSA (*S. aureus* ATCC 43300). Thus, the LAU in DMSO series was selected to further investigate their matrix formation, solvent diffusion and injectability. Once the periodontal pocket is filled with the

formulation, the volume of crevicular fluid in the pocket is limited, resulting in the drug concentration reaching the minimum inhibitory concentration (*MIC*) of all *pathogen*s (4 µg/mL for *P. gingivalis* [274]). In the presence of periodontitis, the gingival crevicular fluid volume is approximately 0.5–1.0 µL [275]. Assuming that the pocket is filled with 1 µL of VLD-40, the lowest amount of VCM released from 1 µL of VLD-40 is approximately 0.06 µg (from 90–120 min) thus the least concentration was nearly 60 µg/ml which above the MIC.

Table 17 Inhibition zone diameters of the tested formulations from LAU series and standard discs of antibiotics against S. aureus, E. coli, C. albicans and P. gingivalis (n=3)

Formula	Clear zone diameter (mean ± S.D.) (mm.)					
	S. aureus ATCC 25923	*S. aureus* ATCC 43300	*S. aureus* DMST 6935	*E. coli* ATCC 8739	*C. albicans*	*P. gingivalis* ATCC 33277
Vancomycin disc (30µg)	19.00 ± 2.00	ND	ND	ND	ND	ND
VD	ND	ND	25.30 ± 1.50	16.70 ± 0.60	18.30 ± 0.60	ND
VLD-40	26.67 ± 0.47[b]	26.33 ± 1.53[b]	24.67 ± 0.58[b]	11.20 ± 0.80	12.3 ± 1.50	31.0 ± 1.41[a,b]
40LN	19.00 ± 0.00	25.33 ± 0.58	23.33 ± 0.58	23.50 ± 0.90	40.30 ± 2.10[c]	ND
40LP	14.33 ± 0.47	18.33 ± 0.58	11.00 ± 0.58	19.80 ± 0.80	40.00 ± 1.00	ND
40LD	17.67 ± 0.47	19.33 ± 0.58	18.33 ± 0.58	-	16.70 ± 2.50	8.50 ± 0.71[a]
NMP	20.67 ± 1.15	13.33 ± 1.15	14.33 ± 0.58	20.0 ± 0.50	30.70 ± 1.76[c]	19.00 ± 1.41
PYR	21.33 ± 1.15	20.00 ± 0.00	12.33 ± 0.58	20.0 ± 0.00	32.20 ± 2.84	20.50 ± 0.71
DMSO	-	-	-	13.20 ± 1.30	11.80 ± 1.76	-

The superscripts a, b, c, d and e indicate a significant difference (P<0.05)
Based on CLSI 2017; quality control ranges for *S. aureus* ATCC 25923 include cefoxitin 23–29 mm, trimethoprim–sulphamethoxazole 24–32 mm, vancomycin 17–21 mm, clindamycin 24–30 mm, ciprofloxacin 22-30 mm. *S. aureus* ATCC 25923 control species could be clearly inhibited by cefoxitine (28 mm), trimethoprim–sulphamethoxazole (28 mm), vancomycin (17 mm), clindamycin (25 mm) and ciprofloxacin (29 mm) discs within the acceptable range of diameter according to CLSI 2017 guidelines.
Abbreviation: VD=1%VCM in DMSO; VLD-40=1%VCM in 40%w/w Lauric acid in DMSO; 40LN=40%w/wLauric acid in NMP; 40LP= 40%w/w Lauric acid in PYR; 40LD= 40%w/w Lauric acid in DMSO; ND = not determined

Antibacterial activities of ISMs from mixed fatty acid series

The antibacterial activities of the prepared formulations were shown in Table 18. VLSD exhibited a significantly higher antibacterial activity against *S. aureus* ATCC 25923 and MRSA strains (*S. aureus* ATCC 43300) than the drug-free formulation (LSD) (P < 0.05), except against *S. aureus* DMST 6935. VCM is an antibiotic that has been used for the treatment of *S. aureus*, especially MRSA infections [149-151]. The antimicrobial activities against the tested bacteria of LAU in DMSO series represented an activity

against MRSA of LAU. Owing to the antimicrobial activity of medium-chain fatty acid such as LAU, the LSD also exhibited the clear zone. Therefore, VLSD did not only prolong the drug release but also effectively inhibited MRSA. Since the infection occurring after total knee arthroplasty treatment is complicated, expensive, and requires additional surgery [137], the use of VLSD could potentially become an alternative treatment. DMSO has been reported as a solvent of various dosage forms such as risperidone and paliperidone-loaded *in situ* forming implants for treatment of the atypical antipsychotics [5], osthole-loaded *in situ* forming implants using polylactide, poly(lactide-co-glycolide), polycaprolactone, or poly(trimethylene carbonate) as the forming polymers, [276] *in situ* forming microparticle loading a selective leukotriene receptor antagonist such as montelukast sodium [27], and rapamycin-loaded intra-arthricular injection [277]. Moreover, US FDA has approved to use 50%w/w DMSO (RIMSO-50®) for human interstitial/chronic cystitis treatment. The topical solution of various DMSO concentration has been used for flap ischemia (60% DMSO), herpes zoster (5% idoxuridine in DMSO), and injection site extravasation (99%DMSO) treatment [278]. In the field of veterinary, DMSO has been used as the anti-inflammatory agent in equine by intra-arthricular injection [279]. From cell recovery with toxicity kinetic study of DMSO in an intact articular cartilage, the 1 M DMSO did not cause a toxic to the chondrocytes [280]. The estimate DMSO concentration after injection of 0.3 - 2.0 mL VLSD into 5-30 mL synovial fluid was in the rank of 0.0025-0.0167 M. Although the safety data and applications of DMSO indicate the probability of using DMSO as the solvent for injectable dosage forms, the effect of DMSO from an intra-articular formulation such as the developed VLSD needs to be determined more in a clinical experiment.

Table 18 Inhibition zone diameter of tested formulations from mixed fatty acid series and standard discs of antibiotics against S. aureus, E. coli, C. albicans and P. gingivalis strains (n = 3)

Formula	Clear zone diameter (mm.) mean±SD		
	S. aureus ATCC 25923	*S. aureus* ATCC 43300	*S. aureus* DMST 6935
VLSD	25.33 ± 0.94^a	28.67 ± 1.53^b	24.67 ± 1.53
LSD	20.00 ± 0.00^a	24.33 ± 1.15^b	26.67 ± 1.15
40LN	19.00 ± 0.00	25.33 ± 0.58	23.33 ± 0.58
40LD	17.67 ± 0.47	19.33 ± 0.58	18.33 ± 0.58
Cefoxitin (30 µg)	28	ND	ND
Trimethoprim-sulfamethoxazole (1.25/23.75 µg)*	28	ND	ND
VCM (30µg)*	17	ND	ND
Clindamycin (2µg)*	25	ND	ND
Ciprofloxacin (5µg)*	29	ND	ND

The superscripts a and b indicate a significant difference (P<0.05)
Abbreviation: VLSD=0.75%VCM in 40% of 1:1 Lauric acid:Stearic acid in DMSO; LSD=40% of 1:1 Lauric acid:Stearic acid in DMSO; 40LN=40%w/wLauric acid in NMP; 40LD= 40%w/w Lauric acid in DMSO; ND = not determined
*Antimicrobial agent for microbe validation. Based on CLSI 2017; quality control ranges for *S. aureus* ATCC 25923 included, cefoxitin 23–29 mm, trimethoprim–sulfamethoxazole 24–32 mm, vancomycin 17–21 mm, clindamycin 24–30 mm, ciprofloxacin 22–30 mm.

Antimicrobial activity studies of ISMs from fatty acid molecular weight series

Table 19 presents the antibacterial activities for drug-loaded and drug-free formulations. The drug-loaded formulation exhibited a significantly higher antibacterial activity against *S. aureus* DMST 6935, *S. aureus* ATCC 25923, *E. coli* ATCC 8739 and MRSA strains (*S. aureus* ATCC 43300) than the drug-free formulations ($P < 0.05$). No statistical difference ($P < 0.05$) was observed between the antimicrobial activity of drug-loaded and drug-free formulation against *C. albicans,* which indicates that the drug showed no effect on *C. albicans*. Thus, the activity against *C. albicans* was due to the short-chain fatty acids. Short-chain fatty acids exert activity against *C. albicans* by inhibiting germ tube and hyphae formation and reducing the metabolic activity [281]. The descending trend of antimicrobial activity was related to the use of higher MW fatty acids, which retarded the VCM release. Notably, the activity of VMD and VPD against MRSA significantly decreased compared with that of VD (P<0.05). Although this activity of most drug-loaded formulations was no different from that of VD, the following formulations provoked a significantly high activity ($P < 0.05$), indicating a

synergistic effect: VLD (against *S. aureus* DMST 6935); VCPLD and VCPRD (against *S. aureus* ATCC 43300 and *S. aureus* ATCC 25923). Several microbes are highly sensitive, resulting in the synergistic effect. Therefore, the use of a VCM-loaded fatty acid-based ISM not only modulated the drug release capability but also effectively inhibited various pathogens, especially MRSA. However, a significant difference was noted in multiple properties that rely on the MW of fatty acid. Hence, to design a proper fatty acid-based ISM for any aspect of drug delivery applications, the MW of this matrix former should be considered.

Table 19 Inhibition zone diameter of tested formulations from fatty acid molecular weight series against S. aureus, E. coli and C. albicans (n = 3)

Formula	Clear zone diameter (mean ± SD)				
	S .aureus ATCC 25923	*S .aureus* ATCC 43300	*S .aureus* DMST 6935	*E .coli* ATCC 8739	*C .albicans*
35CPLD	11.00 ± 0.00	10.00 ± 0.00	10.00 ± 0.00	10.33 ± 0.58	40.33 ± 2.52
35CPRD	7.67 ± 0.58	7.00 ± 0.00	7.00 ± 0.00	0.00	24.33 ± 0.58
35LD	7.33 ± 0.58	8.33 ± 2.31	10.00 ± 0.00	0.00	16.33 ± 0.58
35MD	7.00 ± 0.00	7.00 ± 0.00	7.00 ± 0.00	0.00	16.67 ± 1.53
35PD	7.00 ± 0.00	7.00 ± 0.00	7.00 ± 0.00	0.00	13.67 ± 1.53
VCPLD	30.33 ± 1.53	30.00 ± 0.00	27.33 ± 2.08	17.33 ± 0.58	39.33 ± 1.15
VCPRD	31.67 ± 2.08	29.67 ± 0.58	28.00 ± 2.00	16.33 ± 0.58	28.00 ± 2.00
VLD	28.00 ± 3.61	28.00 ± 1.00	34.67 ± 3.06	16.67 ± 0.58	16.67 ± 0.58
VMD	27.00 ± 1.73	27.00 ± 0.00	31.67 ± 2.08	15.33 ± 1.53	15.33 ± 1.15
VPD	26.33 ± 1.53	27.67 ± 1.53	26.67 ± 0.58	13.00 ± 1.00	14.33 ± 0.58
VD	27.33 ± 0.58	29.67 ± 0.58	28.33 ± 1.15	16.67 ± 0.58	18.33 ± 0.58
DMSO	7.67 ± 1.15	6.67 ± 0.58	7.00 ± 0.00	13.00 ± 1.00	19.67 ± 0.58

Based on CLSI 2017; quality control ranges for S. aureus ATCC 25923: cefoxitin, 23-29 mm; trimethoprim-sulphamethoxazole, 24-32 mm; vancomycin 17-21 mm, clindamycin 24-30 mm; ciprofloxacin, 22-30 mm. S. aureus ATCC 25923 control species could be clearly inhibited by cefoxitine (28 mm), trimethoprim-sulphamethoxazole (28 mm), vancomycin (17 mm), clindamycin (25 mm) and ciprofloxacin (29 mm) discs within the acceptable range of diameter in CLSI 2017 guidelines.

Topography of transformed-matrices

Topography of transformed-matrices of ISMs from LAU series

The surface topography of VCM-loaded LAU ISM within the first h (initial period) exhibited a highly porous and loose network Fig. 27, whilst the remnants of the matrix after the release test exhibited a compact agglomeration of LAU crystal. Such a structure clearly confirms that the release of VCM is prolonged after an initial period through crystallisation over time after LAU changes into a solid matrix. A tight network of LAU crystals could retard the release of VCM through higher tortuosity and/or lower porosity.
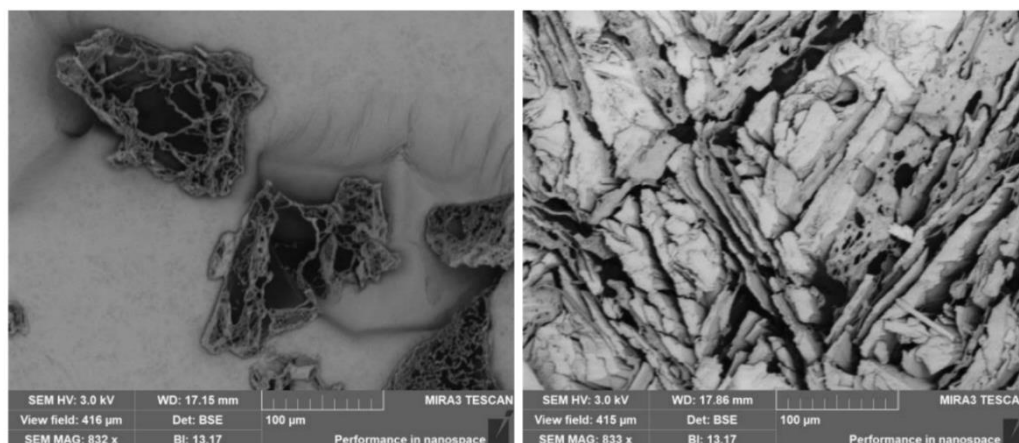
Figure 27 SEM micrograph of VLD-40 at the initial period of transformation of the ISM (left); and dried after the release test (right)

Topography of transformed matrices of ISM from mixed fatty acid series

It has been demonstrated that tortuosity and porosity affect the drug migration rate [245]. The topography of VLSD after the release test revealed a compact agglomerated LAU and STR (Fig. 28). LAU exhibited high porosity, whereas VLSD exhibited a tight formation of fatty acid compaction after the injection into the simulated physiological fluid with solvent exchang. This topography supported that higher tortuosity and/or lower porosity retarded a drug migration [246].
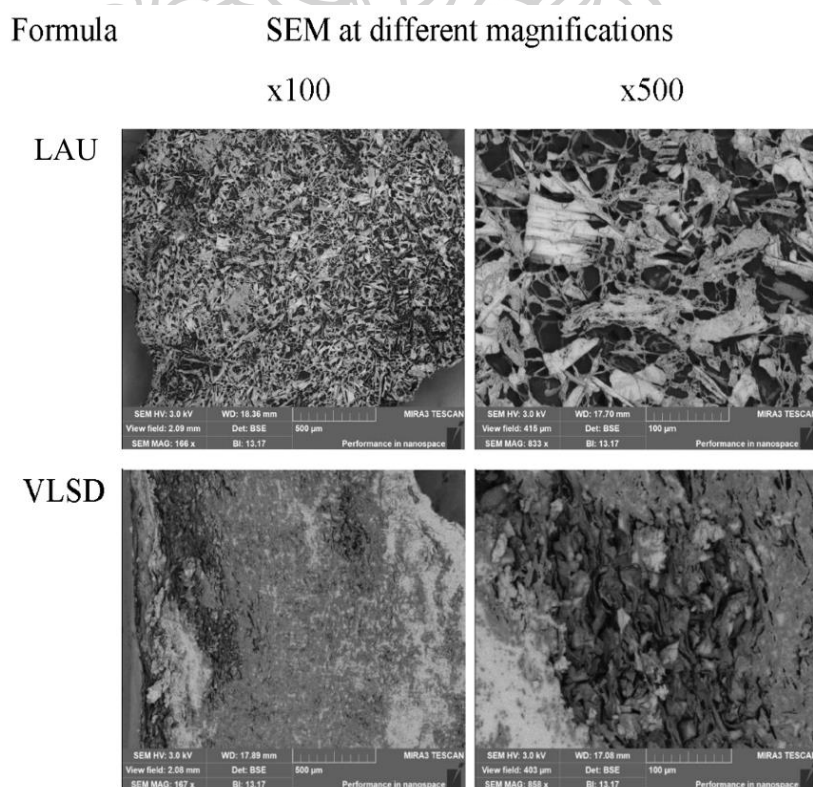
Figure 28 SEM of formulation after release test in PB pH 7.4 using the dialysis tube method

Topography of transformed matrices of fatty acid molecular weight series

On behalf of low-MW fatty acid-based formulation, the dried matrix after the release test of VLD was selected to compare with the higher one as VPD (Fig. 29). The VLD dried matrix presented a needle-shaped crystal agglomerate with a continuously intricated matrix. However, VPD showed an enclosed sheath crystal with a large and simple aperture. The excavation of VPD confirmed the low tortuosity that resulted in a burst drug release and low sustainable drug liberation as mentioned in Section "Drug release and model fitting". The continuously intricated matrix of VLD prolonged the release of VCM owing to its high tortuosity and less porosity, whereas the pattern of VLD crystal formation related to the following step. Firstly, the water diffused inward in high unit per volume, which sufficiently generated a large number of nuclei per volume simultaneously. Secondly, the nuclei growth individually showed with a competition to each other, resulting in a slow crystal growth. Thirdly, the tangled structure of the matrix was formed *via* a lot of crystallisation origin. By contrast, according to the above results, VPD was ready to generate a crystal with a high crystal growth capability and that the nuclei were formed rapidly at the interface of water/formulation. When the initial nuclei were formed, a rapid crystal growth occurred consequently with no competition effect because it contained less nuclei per volume. Thus, VPD had a less crystal origin, which resulted in a matrix topography with high porosity and low tuotosity, in which the drug leaked easily.
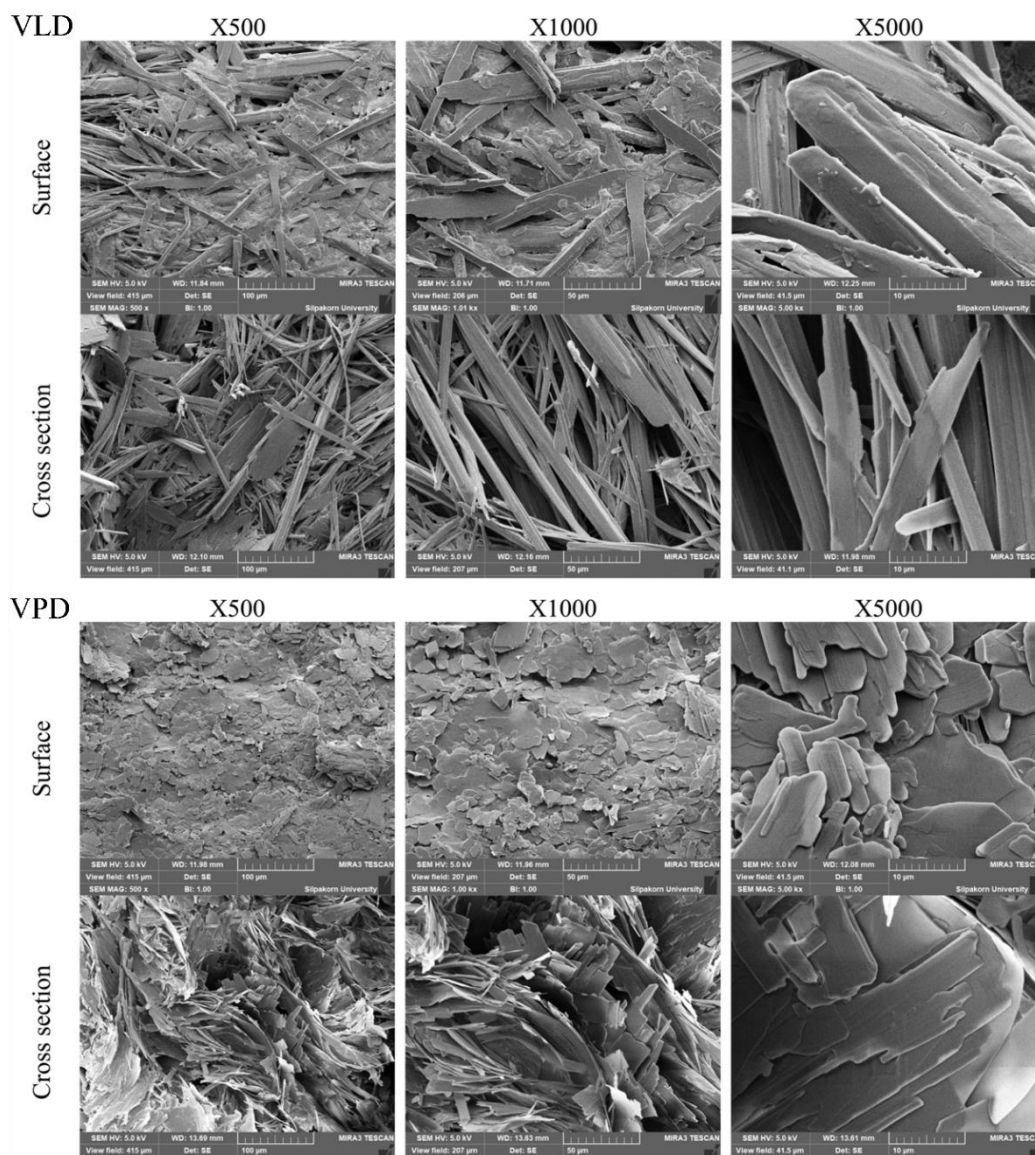
Figure 29 Topography under scanning electron microscope of formed matrix (VLD and VPD) after release test

The VLD dried matrix from the drug release test (under 30ºC), presented as a needle-shaped crystal agglomerate with a continuously intricated matrix and the VMD, showed a small hexagon crystal with a narrow size distribution (Fig. 30). Meanwhile, VPD exhibited a large and simple crystal wall with a large passage. The VPD interior structure with this large and simple aperture confirmed that less tortuosity resulted in a less ability to sustain the drug release. The continuously intricated matrix of VLD and VMD prolonged the release of VCM owing to the complex interior structure. The crystallization pattern of the lower molecular weight-based fatty acid formulation slowed the crystal growth rate and promoted a complex interior structure which corresponded with the results as cited in "*In vitro* drug release of fatty acid molecular weight series". The topography of formed-fatty acid matrices, release pattern, and model

fitting were supported by each other where the release rate constant was quite a bit lower than that fabricated from higher molecular weight fatty acid.
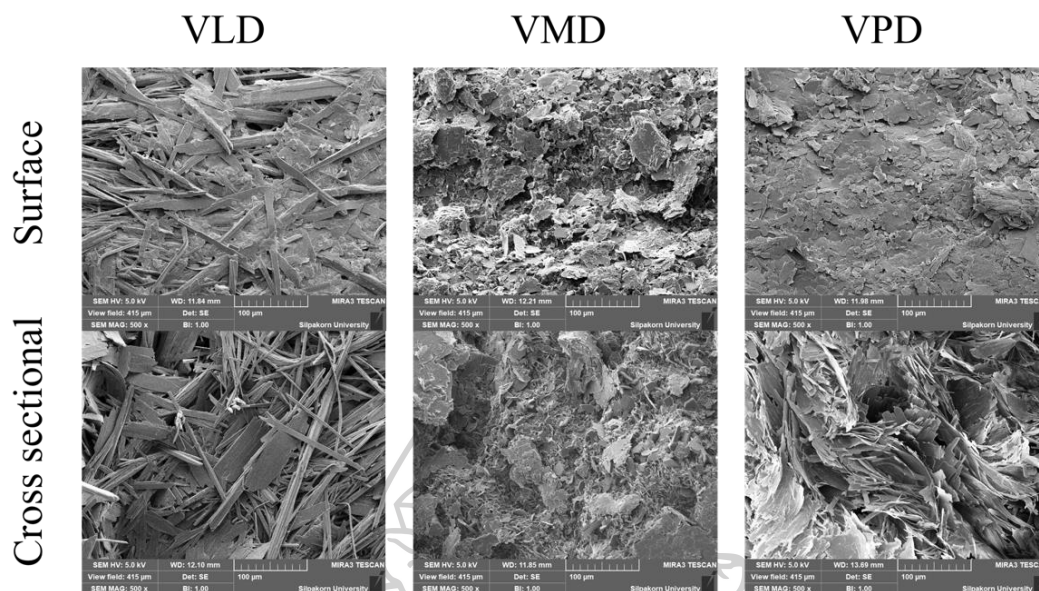
Figure 30 Topography under SEM of formed-fatty acid matrix of drug-loaded formulation after release test (under 30°C)

Surface tension and contact angle

Effect of fatty acid concentration on surface tension

The surface tension was significantly decreased ($P<0.05$) with the incorporation of LAU in all solvent systems because of the solvent-solvent interaction was disturbed by LAU (Fig. 31). Increasing the concentration of LAU in any solvent caused lower in surface tension. It is known as one of the surfactants that can reduce the surface tension as the increase of LAU concentration [282], due to the tendency of amphiphilic molecules to locate itself at the surface [283]. Since the longer chain of fatty acid has a higher steric hindrance effect, the surface tension showed a decreasing trend when the long-chain fatty acid was used. DMSO-based formulations showed the lower surface tension than others since it has a higher polar than that of NMP and PYR; therefore, DMSO-based formulations were mostly affected by the hydrophobic part of LAU then PYR and NMP-based formulation, respectively.

Effect of fatty acid concentration on contact angle

All contact angle values of fatty acid solution were lower than that of the pure solvent except 10LN. The higher concentration of LAU caused less surface tension resulted in higher spreadability [282]. The wettability of preparations might be promoted by the carboxyl group of LAU [284]. However, for the DMSO-based system, the contact angle showed an increasing trend; even the surface tension showed a decreasing trend. It might be related to the viscosity value of preparation where the high concentration

formulations possessed a higher viscous manner where the fluid flow was retarded at the initial time. Although this concept had some conflict since the NMP and PYR-based showed the different patterns from that of DMSO, the viscosity-contact angle relation should not be oblivion. Because of DMSO and pyridine group exhibits the different properties. DMSO has a lower logP than pyridine [248,249]; thus, LAU's higher concentration caused lower hydrophilicity of preparation. In contrast, for the pyridines-based system, the higher concentration of LAU caused more wettability due to the carboxyl group.
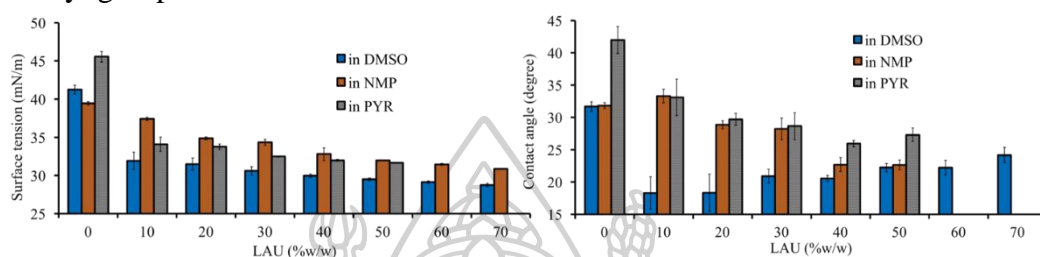
Figure 31 Surface tension (left) and contact angle (right) of LAU concentration series in DMSO, NMP and PYR (n=3) at room temperature

Effect of fatty acid molecular weight on surface tension

Since the steric hindrance played a role in intermolecular force interruption, the surface tension presented a decreasing trend ($P<0.05$) when the longer chain fatty acid was incorporated in DMSO (Fig. 32). It was reported that there was a low surface tension when the higher molecular weight fatty acid was employed at the same concentration [285,286]. For the NMP-based 35% w/v fatty acid formulations, there was no difference in surface tension except 35% w/v PAL and STR ($P<0.05$). The long chain as PAL and STR has a high hydrophobicity and steric hindrance effect; therefore, the tension was reduced even its molecule amount was low. For 1.75 mM fatty acid in NMP, the decreasing trend of surface tension was notably marked because each fatty acid's molecule amount was equal. However, the MYR, PAL, and STR-based formulations showed steep high surface tension ($P<0.05$), wherein the main intermolecular force was changed from the solvent to fatty acid. Various factors could influence the surface tension, but the molecular weight is one of the crucial factors [286].
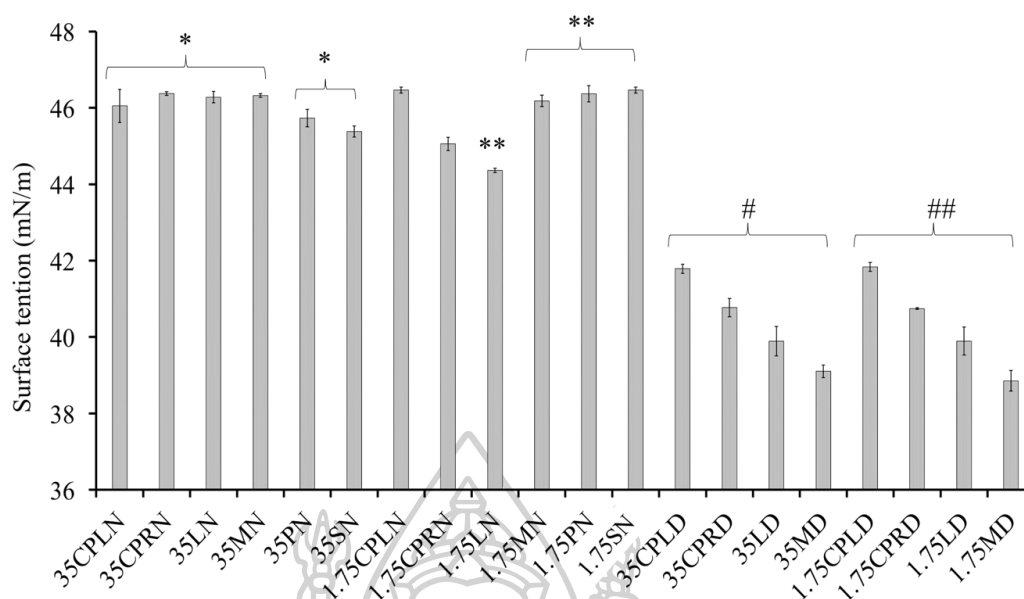
Figure 32 Surface tension of fatty acid molecular weight series in DMSO and NMP (n=3)

Effect of fatty acid molecular weight on contact angle

The contact angle presented a decreasing trend when the longer chain fatty acid was incorporated, which related to the less surface tension (Fig. 33). However, the inversion pattern was obtained when the high molecular weight fatty acids such as MYR and PAL were used ($P<0.05$), since the main intermolecular force was changed from the solvent to fatty acid. This trend was similar to the results of surface tension measurement. However, the high molecular weight fatty acid-based formulation possessed a high contact angle that related to the higher viscous of preparation and thereafter lower spreading ability. The high molecular weight fatty acid-based in NMP showed lower viscosity than using DMSO as a solvent that resulted in different contact angles. The high hydrophobicity, which depends on how long the fatty acid aliphatic chain is the other factor, wherein the carboxyl group of fatty acid was dominated and resulted in less adhesion force to the hydrophilic glass slide [284]. STR was used to coated the calcite; the more coverage percent resulted in higher contact angle (tested with water, dichloromethane, and formamide) [287].
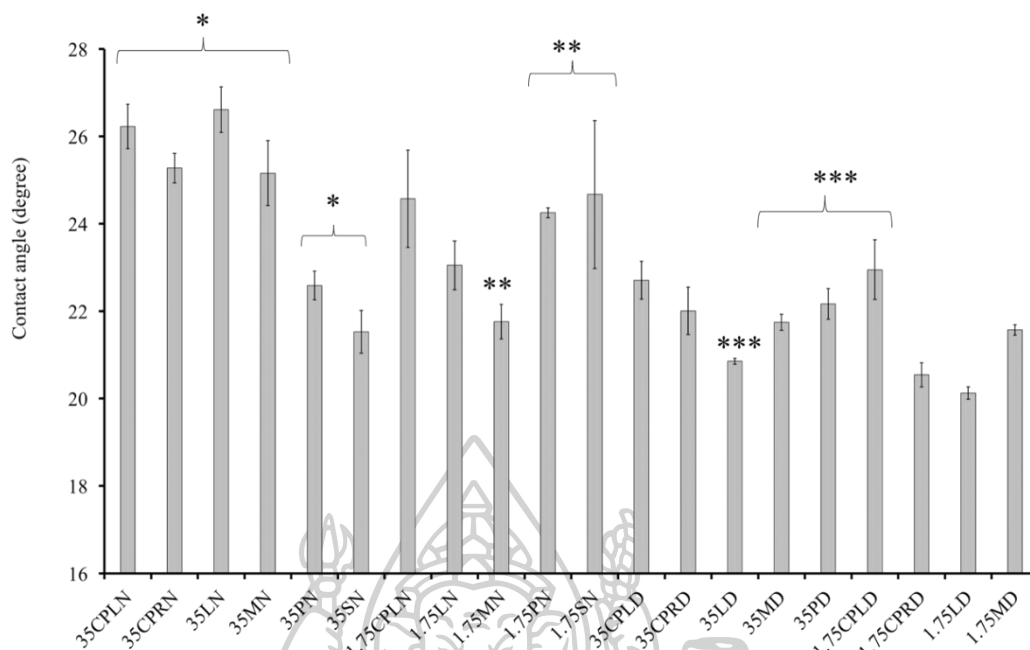
Figure 33 Contact angle of fatty acid molecular weight series in DMSO and NMP (n=3) at room temperature.
*Statistic symbol: *, **,*** = significantly different (P<0.05)*

Phase inversion

Water tolerance of ISMs from LAU series

A solvent exchange-induced ISM transforms from a liquid state into the solid state by the inward diffusion of water together with outward diffusion of solvent; thus, water content at the transformation point is a clue of phase transformation. Water tolerance refers to the capacity to endure a phase change influenced by water. In this work, the volume of water (%, v/v) necessary to achieve phase transformation was used to indicate the water tolerance property of the prepared ISM systems. The requirement of a larger volume of water to achieve turbidity (endpoint) indicates higher water tolerance. The concentration of LAU and the water miscibility of the solvent affected the water tolerance of an ISM. All ISM systems showed lower water tolerance when the concentration of LAU was higher (Table 20). At higher fatty acid concentrations, the solvents were not enough to dissolve LAU whenever the solvent leave out. The LAU in DMSO systems required less water than the systems using NMP and PYR as the solvents to reach the endpoint. DMSO has higher water miscibility than NMP or PYR due to its high polarity [35,78,237], resulting in the rapid phase separation of LAU. These results confirmed and corresponded to the transformation behavior of LAU ISM in microscopic matrix formation.

Table 20 Water volume at transformation point of the formulas (n = 3)

Concentration of LAU (% w/w)	Water volume (%v/v) Solvent		
	DMSO	NMP	PYR
10	28.31 ± 2.56 [a]	45.85 ± 0.45 [b]	51.05 ± 1.08 [c]
20	22.75 ± 1.68	41.10 ± 0.75	41.74 ± 3.14
40	22.19 ± 4.37 [d,e]	34.38 ± 0.15 [d]	41.91 ± 3.88 [e]
50	18.26 ± 1.64 [a]	35.86 ± 0.66 [b]	37.59 ± 3.55 [c]

The superscript of a, b, c, d and e represent a significant difference (P<0.05)

Influence of KH_2PO_4 ion on water tolerance

KH_2PO_4 was used to prepare buffer of various pH and a simulated physiological fluid [231,247]. Typically, ions could induced the separation of hydrophobic material from the solution [288]. Therefore, the effect of KH_2PO_4 on a water tolerance of the fatty acid solutions was evaluated. The high concentration of KH_2PO_4 notably lowered the transformation point of all formulations (Fig. 34). The ionic kosmotropes of HPO_4^{2-} promoted the high stability and proper structure of water–water interactions; therefore, this electrolyte forced the phase separation of hydrophobic substances [288]. In other words, kosmotrope promoted the interfacial tension [289]; thus, the transformation point of these fatty acids occurred earlier when the concentration of KH_2PO_4 increased. With the increased hydrophobicity and low aqueous solubility of long-chain saturated fatty acids, a supersaturated point was easily obtained. Hence, the component of aqueous environment should be considered along with the properties of the formulation to govern the solvent exchange-induced *in situ* formation process of fatty acid.
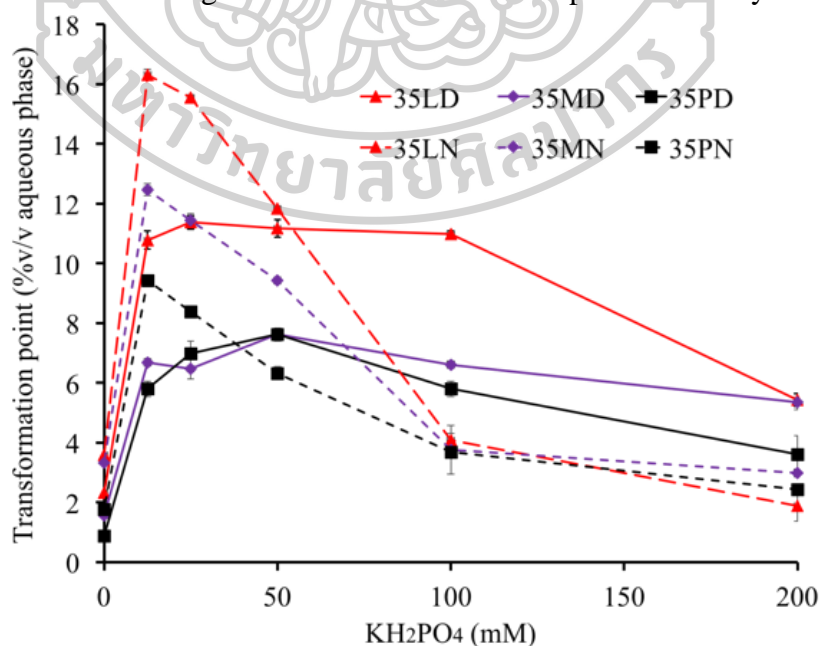
Figure 34 Effect of KH_2PO_4 concentrations on transformation point

Electrical potential difference during phase transformation

When the systems meet the aqueous environment, the solvent diffuses outward while the water diffuses inward, leading to the *in situ* formation with solvent exchange process, that is, the water ratio increases over time. For this reason, in this experiment, the water volume (% v/ v) was implied to correspond with the time of phase transformation. The interfacial tension is related to nucleation [177] and the relation between electrical potential and interfacial tension was pointed out [289,290]; thereby, the electrical potential difference was applied to track the nucleation process. The increase in electrical potential values (Fig. 35A) is related to the enriched high polarity phase owing to the high amount of water and the ionisation of fatty acid molecules [291]. When the polarity of the system reached the point at which the hydrophobic part could not be retained, the two liquids separated, resulting in a new water solvent/lipid solvent interface. The appearance of the interface before was detected (Fig. 35B). It was called a "dense liquid" in another study [175]. The boundary between the two liquids gained a free energy; as a result, they desperated to reduce the energy *via* nucleation and crystallisation [291]. Lastly, at the point of phase separation, the value steeply decreased owing to the absence of a polar group as carboxyl because of the crystallisation into solid fatty acid. By comparison, the separation point of long-chain fatty acids was obtained at a low electrical potential difference. The dissolved long-chain fatty acids might have shown less tolerance during electrical change given that they have a lower polarity than short-chain fatty acids. This result corresponded to that of another report, which indicated that a less surface charge contributed to the water interface of long-chain fatty acids [292]. Given the relation of interfacial tension and electrical potential, this experiment assumed that the interface of two liquids, that is, water solvent/lipid solvent, was generated *via* a difference in voltage value. This assumption also means that an electrical property can be one of the factors that induce the phase separation of fatty acid-based *in situ* forming systems.
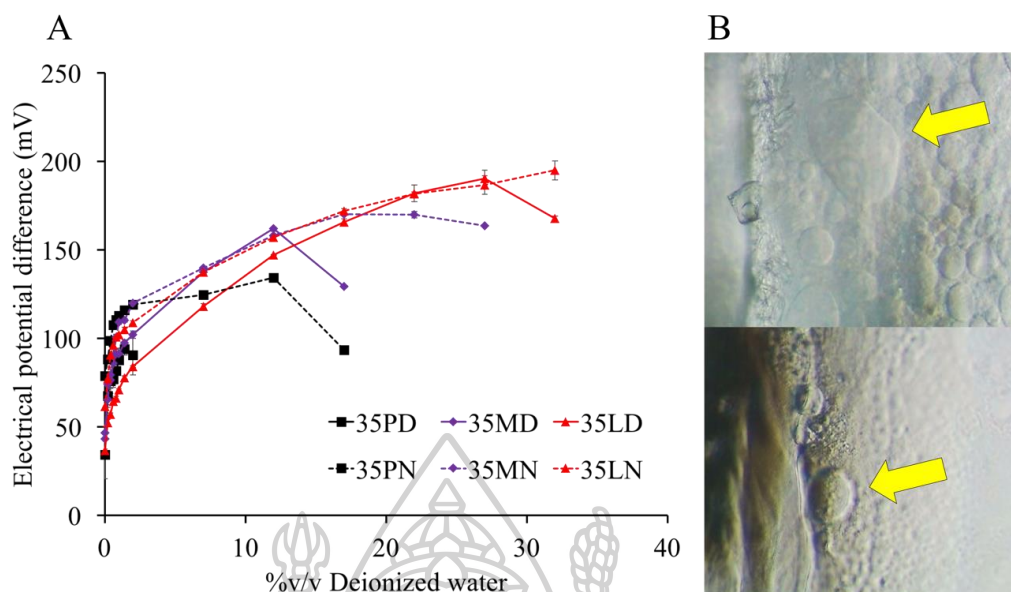
Figure 35 Electrical potential difference of systems (preparation and water) during in situ formation process (A) (n = 3). The appearance of dense liquid at 45th sec of 35LD (top) and 35LN (beneath) (B)

Interfacial phenomenon during initial transformation period

This experiment was set up to simulate the phenomenon at the boundary of formulation, which faced the target site containing the biological fluid. The agarose platform referred to the simulated biological site for which the *in situ* forming systems were administered and transformed into solid-like material to modulate drug release as mentioned previously. Comparison between solvents using DMSO (Fig. 36) caused an outright liquid movement, whereas the delayed fluid movement was evident for all formulations using NMP as a solvent. At the early initial experimental period, these events confirmed the previously mentioned phenomenon indicating that DMSO was more readily mixed with the aqueous phase than NMP. Although the liquid movement in NMP-used formulations was slightly noticed, the transformation continued. The faster rim crystal formation of 35PN compared with 35MN indicates that using higher MW fatty acid promoted a more rapid phase inversion with solvent exchange process. Considering the results in Sections "Macroscopic matrix formation behavior of solutions from fatty acid molecular weight series" and "Matrix formation (cross-sectional view) and solvent diffusion pattern of solutions from mixed fatty acid series", the MW and solvent type played the considerable roles in matrix formation. The type of solvent influenced intensely the matrix formation of LAU-loaded solution. The rapid crystallisation dominated massively in the long-chain fatty acid solution. Theoretically, an energy exists at the boundary between any unmixable objects; this energy can provoke nucleation and subsequently, crystallisation through a thermodynamic driving

force [180]. Thence, not only the external interface comprising agarose and initial crystal interface but also the interface of unmixed liquids can induce continuous crystallisation.
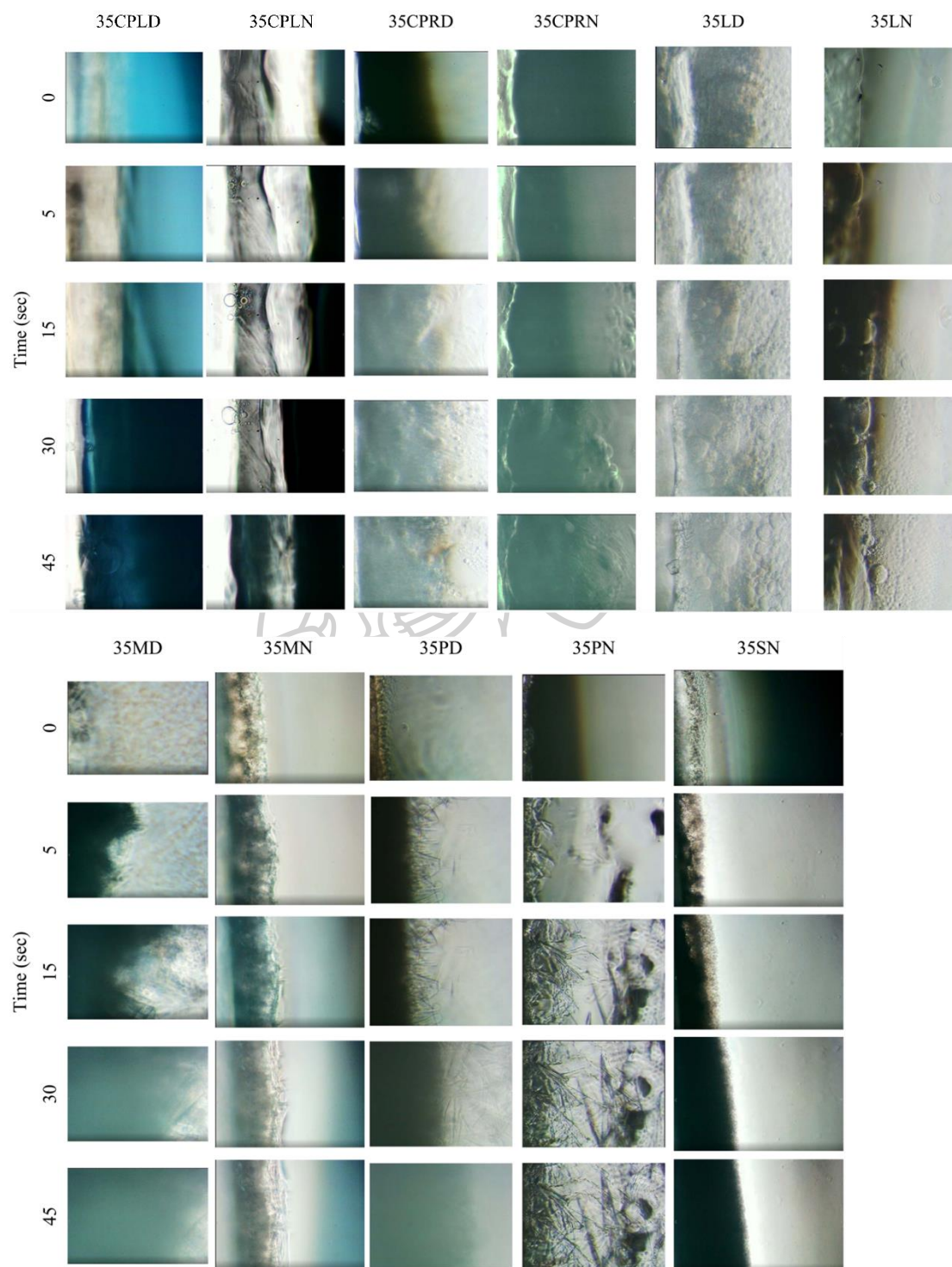
Figure 36 Behaviors of preparations at the boundary of aqueous phase and in situ forming systems during the initial period (0-45 sec)

Aqueous phase influx tracking

Albeit the solvent exchange was mentioned in many reports [25,247] and the solvent tracking inquiry was done [231], the movement of aqueous phase has not been profoundly understood. Thus, in this study, the aqueous influx tracking of the following formulations was investigated (Fig. 37). The fluorescence color represented the aqueous phase from the agarose stage, which gradually moved inward. VCPLD and VCPRD, which did not form a matrix, presented a rapid aqueous influx at the beginning of the experiment. VLD showed a classical pattern. Firstly, the aqueous influx diffused inward; secondly, the surface network was formed and aqueous diffusion was retarded consequently. For the transformation of VMD and VPD, the crystal edge near the aqueous front indicated the high transformation capability of these long-chain fatty acids. VMD showed a faster crystal formation along with aqueous diffusion than VPD, which confirmed the rapid dense network of high-MW fatty acids such as PAL and the retardation of aqueous-solvent migration. Although the solvent exchange was prohibited *via* dense waxy network of PAL at the initial experimental period, the notable crystallisation capability of PAL appeared and accomplished the completed matrix formation, as described in Section "Matrix formation (cross-sectional view) and solvent diffusion pattern of solutions from mixed fatty acid series". Generally, if a high-MW fatty acid (PAL) formed a rapid dense network and gradually retarded the solvent exchange process, the transformation from a solution into a solid would be prohibited owing to the restriction of water diffusion. However, this phenomenon was not observed. Once the first crystal was formed, the crystal growth initiated its self-transformation capability, which was significantly more dominating than solvent exchange, as described above and in Section "Matrix formation rate (cross-sectional view) of fatty acid molecular weight series". These results confirm that solvent exchange and crystallisation capability were the crucial parameters influencing the self-formation process of the fatty acid-based ISM. MYR-based formulation showed a well-balanced effect on solvent exchange and crystallisation. By contrast, VLD, which had high free migration of solvent at the initial time of the experiment, exhibited less crystallisation capability with a higher number of nuclei formation; once these nuclei grew, a very dense network was obtained and the burst drug release was minimised subsequently, as mentioned in Section "Drug release and model fitting". Therefore, solvent exchange and crystallisation should be managed and considered compulsively for designing further solvent exchange-induced ISM systems.
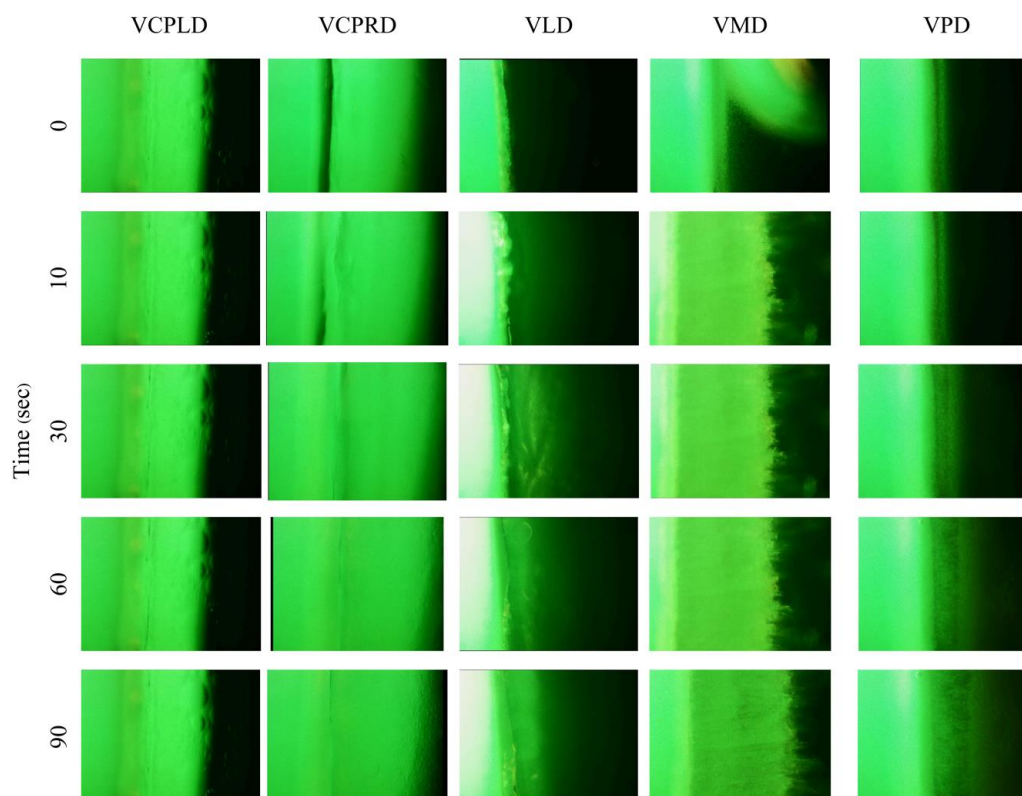
Figure 37 Influx behavior of aqueous phase at boundary of drug-loaded fatty acid ISM

Computational modelling

Computational results of MD simulation

Fatty acids rearranged and ordered their molecular patterns during the MD simulation (Fig. 38 and Appendices Figs. 47-55). The degree of the order and formation rate depended on their aliphatic chain length, and solvent type. The traditional perspective of the solvent exchange-induced *in situ* formation process was the influx migration of water and outflux diffusion of solvent. In this simulation, however, the results showed another concept of this mechanism. Considering the $logK_{ow}$ of the solvents, the water appealed the outward migration of all solvent molecules and forced the hydrophobic matter as fatty acid away *via* its strong hydrophilic force. The different $logK_{ow}$ among the solvents determined the rate of solvent migration. The DMSO, which possessed the lower a $logK_{ow}$ than that of NMP, exhibited faster migration as shown in Fig. 38C, D ($logK_{ow}$ value of DMSO and NMP is -1.98 and -0.38, respectively [248,249]). This corresponded to another solvent diffusion tracking experiment at macroscopic level [231]. Likewise, the hydrophobic force of fatty acid also played a role in this process; the longer chain fatty acid as PAL showed a faster and straight matrix formation. Meanwhile, the shortest one as CPR

showed a tangled structure (Fig. 38A, B). The higher hydrophobic interaction of longer aliphatic chains (MYR, and PAL) caused more orderly arrangement with faster than that of the shorter one (LAU, and CPR) as shown in Appendices Fig. 47-55.

At the given time, waters penetrated into the bulk of fatty acids, which resulted in different water ratios at the various sites, where the region of low-water-ratio referred to an area that was far from the initial interface, as shown in Fig. 39. Under the lower-water-ratio simulation (1Å, TIP3P box), the VLAUN was not formed within 100ns, which was due to the following reason. At the equilibrium of NMP/water/lipid distribution, the rest of the NMP in the lipid phase was still able to dissolve the LAU. Otherwise, VLAUD formed into matrix within 10ns, which indicated that, at the equilibrium, DMSO was more likely to be located in the water phase. Subsequently, the lipid formation occurred since the rest of the DMSO in the lipid phase was not enough to dissolve LAU. The VPALN and VPALD exhibited a faster formation than that of the LAU-based system. These simulations suggested that the solvent and fatty acid type played a dominant role in each other. Namely, the low molecular weight fatty acid-based system was dominated by the solvent effect, and this effect was also governed by the high molecular weight. However, the results, which were acquired from the high-water-ratio simulation (10Å, TIP3P box), depicted a more rapid fat formation than that of low-water-ratio simulation. Thus, it was also buried by the high-water-ratio condition as the 5ns of most of the system formation was shown in Fig. 39 and Appendices Fig. 47-55.

The VCM moved out of from the fatty acid structure within 5-20 ns, but it still laid with the formed-fat until the simulation ended. According to the position of VCM, this signified the H-bonding between COOH, OH, and NH of VCM and the COOH of fatty acid. Hydrogen bonding was investigated by VMD software with the criteria that the distance between the acceptor and donor atoms were less than 3.5 Å, and the angle made by acceptor, donor, and hydrogen atoms was less than 60° [199,214]. Results showed the number of H-bonds over time. The H-bonding between the COOH group of fatty acid and the various OH/NH groups of VCM (Fig. 40-41) confirmed that not only the fat matrix but also a mild attachment force between VCM and fatty acid retarded the VCM diffusion. Therefore, the sustaining release of VCM was also obtained in the apparently loose fat network such as VLD (tested under 37ºC). Speaking of which, this simulation demonstrated that VCM was not incorporated in the fat crystal but was attached alongside of fat. The VCM was incorporated with mild-interaction in the complex matrix and moved out with a water diffusion through the porous matrix (Fig. 39). Thus, in the case of the VCM-loaded fatty acid-based ISM, the sustaining drug release ability of each formulation was differentiated by the tortuosity and porosity of the formed matrix, which relied on the type of fatty acid and solvent as described in the previous study [293,294] and as mentioned in Drug release and model fitting.

These simulation results confirmed the previous macro/micro level studies as follows: separation point, cros-sectional-view matrix formation, aqueous tracking, and topography of dried matrix [293,294]. The following steps briefly explain the macro/micro levels of *in situ* forming process as shown in Fig. 39. Firstly, at the initial

interface, where the water and system first interacted, the water penetrated into the system and the solvent penetrated into the water phase, resulting in a mixed water/solvent region. Secondly, the initial crystal occurred at the high-water-ratio area. The lower molecular weight-based system had a greater water/system mass mix before this occurrance than that of a higher molecular weight-based system as well as the type of solvent. The difference in water/solvent mass mix resulted in a different number of nucleation origins and subsequently affected its matrix growth rate. At the time of formation, at the molecular level, VCM and solvents moved out from the region of the fatty acid while the fat formation pattern in molecular level was differentiated by its molecular weight. Thirdly, crystallization occurred continuously, which resulted in any matrix having a complex/non-complex interior structure as seen in SEM results. These interior structures depended on the fatty acid type and number of nucleation. Besides, VCM laid itself down along with the fat-structure. Hereby, the burst release was obtained from the VCM, which settled at the external site while the inner VCM slowly moved through the complex interior structure, as shown in Fig. 39. However, the VPALD showed a simple passage that resulted in a less sustainable ability of VCM release. This release pattern and topography were confirmed by each other and were subsequently supported by the mathematical calculation. This molecular-level simulation could verify the previous phenomenon of the micro/macroscopic matrix formation of fatty acids and reveal the *in situ* formation mechanism at the initial time.
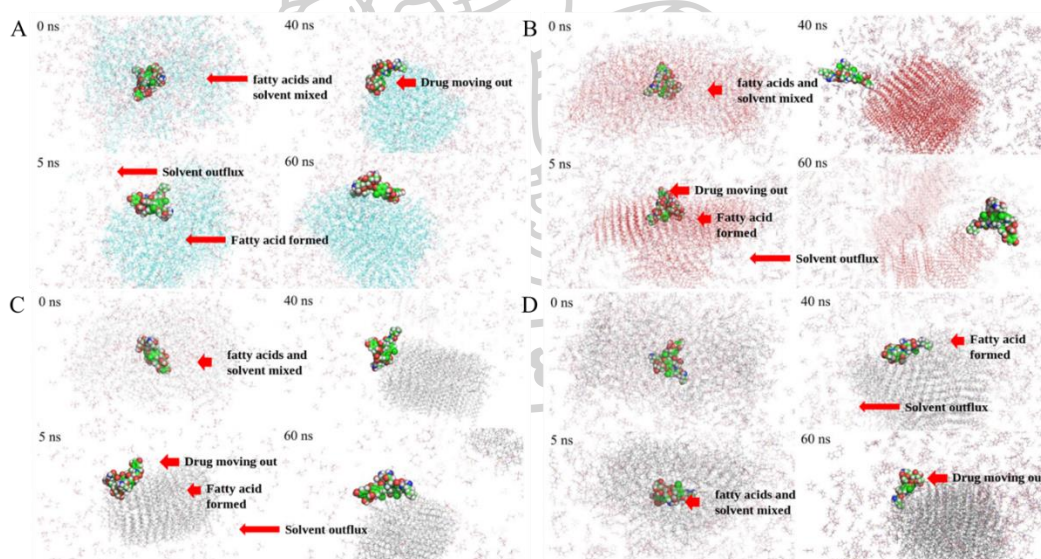
Figure 38 Snapshot structures at 0, 5, 40, and 60 ns of the MD simulation of the in situ formation process of VCPRD (A), VPALD (B), VLAUD (C), and VLAUN (D) with forming matrices
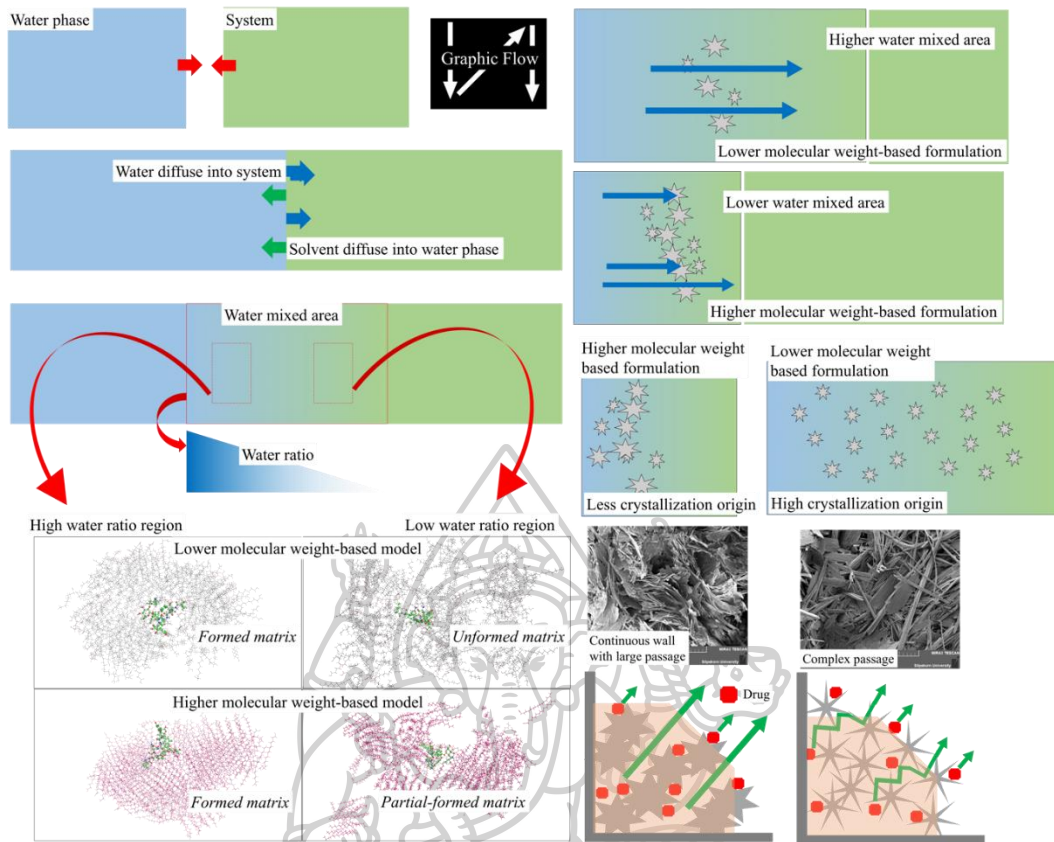
Figure 39 Over all steps of fatty acid-based ISM and its release pattern
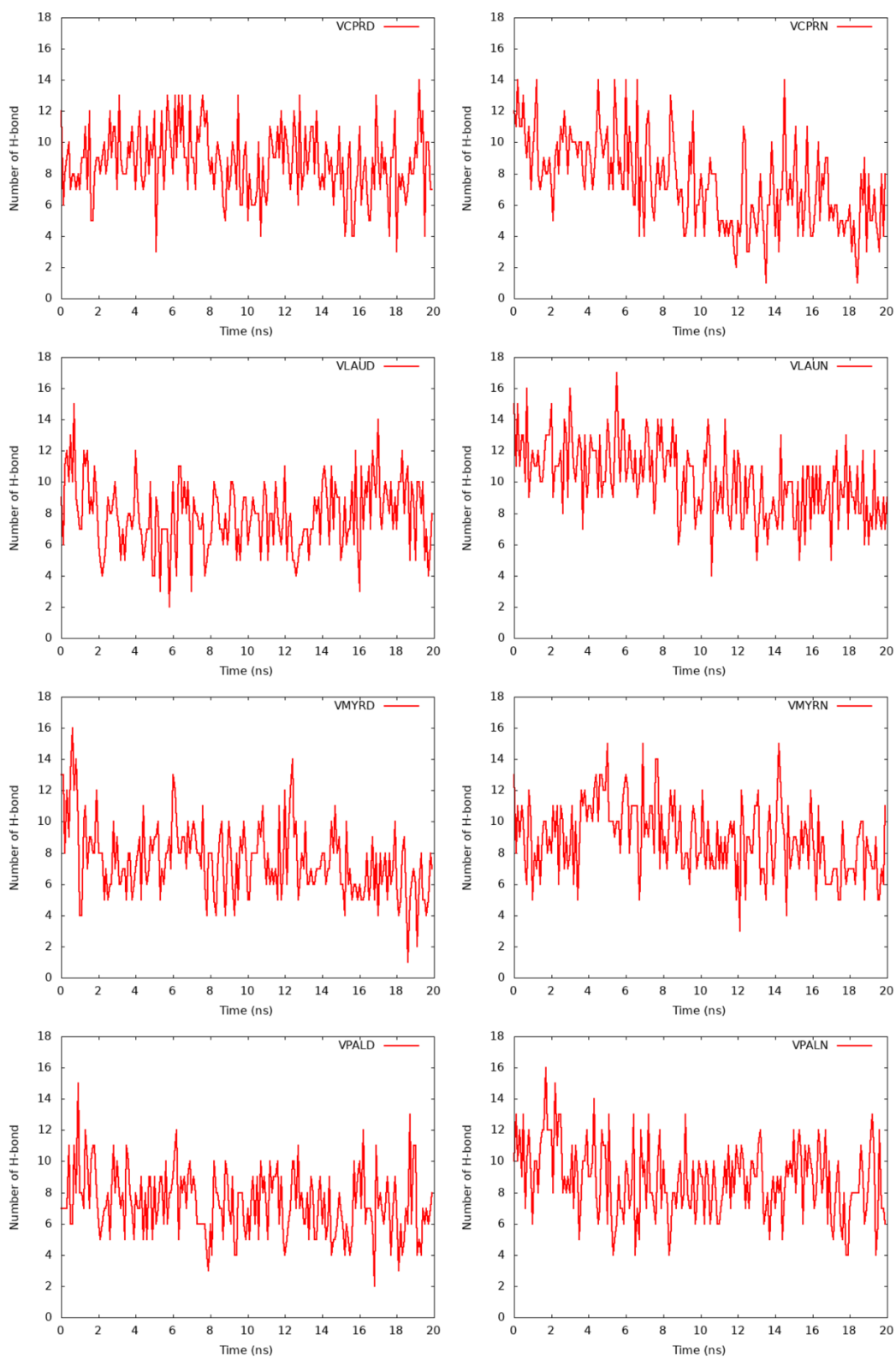
Figure 40 Change in number of hydrogen bonds during the MD simulation
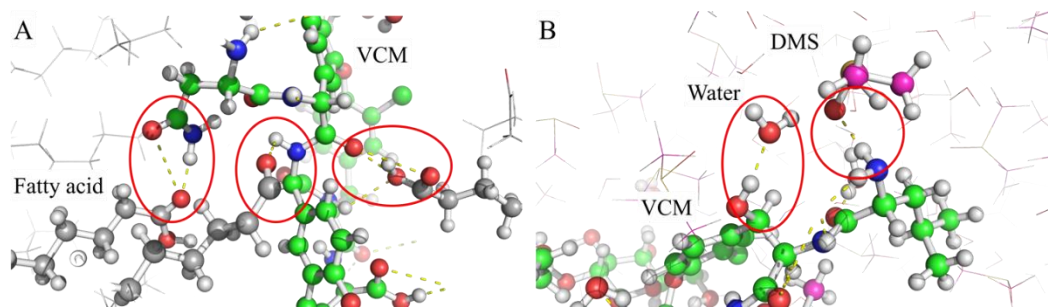
Figure 41 H-bonding between fatty acid and VCM (A) H-bonding between VCM and water/solvent

VCM diffusion constant and its topology change by time

As can be seen in Table 21 and Fig. 42, the results of the VCM movement depended on the formation behavior of any models. As previously stated, the PAL and MYR based models rapidly formed an orderly structure, while the LAU-based model did not. Thus, this rapid formation and orderly formation pattern forced VCM to move out more quickly. Nevertheless, the VCPRD exhibited a different pattern. The high diffusion constant in this case was a freely moving of VCM since this model had less formation ability. The results from RMSD showed the topography change over time while VCM moved out from those fat matrix formations because the force from moving molecules interacted with VCM (Fig. 42). After the fat matrix formation and the VCM laid itself beside that fat, the VCM topography showed a more stable conformation. However, there were still some interaction between VCM and water/solvent (Fig. 40-41), which resulted in a bit VCM conformation change over the time in the range of ± 2 Å.

Table 21 Diffusion constant of VCM during the early stage of the in situ formation process

Formulation	VCPRD	VCPRN	VLAUD	VLAUN	VMYRD	VMYRN	VPALD	VPALN
Diffusion constant (Å²/ps)	0.9416	0.4954	0.0697	0.2461	0.2649	0.2912	0.4358	0.5196
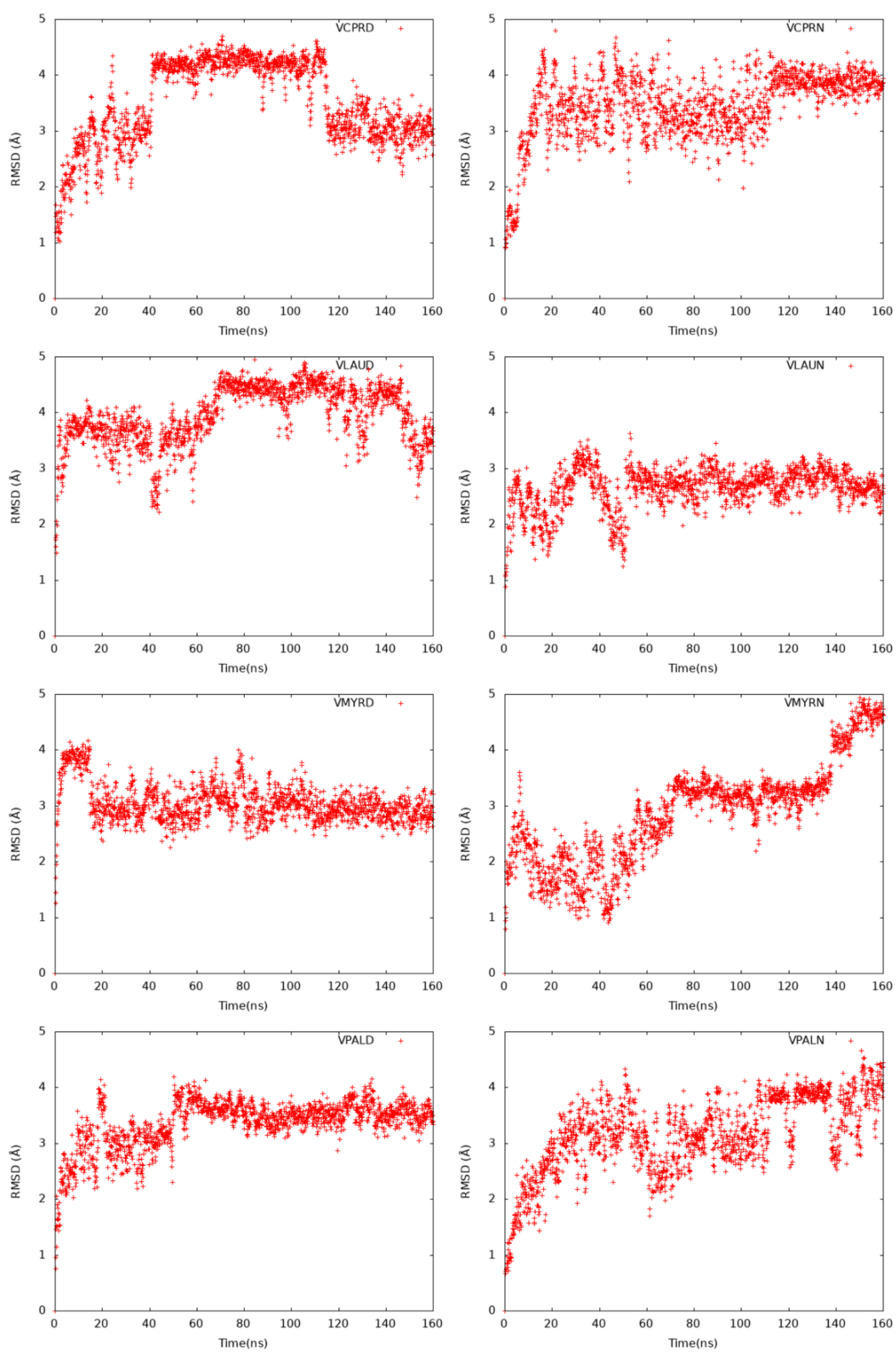
Figure 42 RMSD of the VCM conformation relative to the starting point of the MD simulations

SUMMARY AND GENERAL CONCLUSION

Fatty acids are considered beneficial materials because of their biocompatability, biodegradability and versatile usefulness. The use of fatty acid as a matrix former for ISM resulted in an apparent low viscosity formulation. The solvent type affected the behavior and properties of ISM. Using DMSO as a solvent promoted a faster matrix formation, compared with NMP and PYR. Although rapid transformation into a matrix-like gel occurred with increasing amounts of LAU, the complete matrix formation was impeded by the immediate formation of a surface network, which obstructed an inward water migration. The hydrophobic property of LAU and the rapid surface network formation retarded the diffusion and prolongation of the release of VCM. LAU loaded into DMSO or NMP exhibited the high antimicrobial activities against MRSA, *P. gingivalis* and *C. albicans via* their own activities; addition of VCM enhanced such activities against MRSA and *P. gingivalis*.

In the case of mixed fatty acid/solvent system, LAU- and STR-based ISM systems in various solvent ratios of DMSO and NMP exhibited a very low viscosity (7.89 ± 0.09 cps) together with Newtonian flow behavior. This promoted the ease for injection than the typical polymeric ISM and became more convenience for both patient and medical staff. Changing the ratio of STR and/or DMSO affected the transformation behavior and matrix formation rate. VLSD ISM exhibited a rapid matrix formation in both PB (pH 7.4) and HA solution (less than 1 min and 5 min, respectively) and prolonged the release of VCM over 6 days due to its hydrophobicity and the high tortuosity together with the low-porosity characteristic of the fatty acid matrix. This VCM-loaded fatty acid ISM exhibited the effective antimicrobial activities against MRSA with the inhibition zone of 28.67 ± 1.53 mm. Moreover, VLSD exhibited the ease of injection through the needle; hence, it was suitable for the intra-articular administration of VCM for treating patients with infections occurring after total knee arthroplasty.

The solvent mixture for dissolving LAU showed the important role to achieve the desired properties of prepared ISM. LAU loading decreased the pH and density values of solvent while increased the viscosity. Changing in the ratio of mixed solvent affected the density and viscosity of preparations. In the case of the mixed solvent systems, there was no different in surface tension but contact angle of NMP/PYR mixed solvent systems was greater than the other. LAU ISM in NMP or solvent mixture with high ratio of NMP formed into matrix-like apparently slower than the other preparations after exposure to aqueous fluid. LAU matrix could retard the antimicrobial activities of NMP and PYR.

The fatty acid molecular weight series ISM showed markedly low viscosity and apparent high injectability promoting their ease for injection. The type of fatty acids affected the transformation behaviors at both microscopic and macroscopic levels. Its transformation rate has relied on MW and solvent characters. The VLD, VMD and VPD prolonged the release of VCM over seven days due to its hydrophobicity and high matrix tortuosity. The release pattern of VLD was different from that of VMD and VPD

due to the nucleation/crystallisation and solvent exchange behaviors. The VCM-loaded fatty acid ISM *via* antisolvent process showed efficient antimicrobial activities against various pathogens including MRSA. The molecular weight of fatty acid affected the sustained drug release ability *via* its various matrix formation patterns. The VCM release patterns fitted well with Higuchi's model depicting drug diffusion through the matrix with the relation of distance over time. The LAU and MYR-based formulations facilitated more drug release retardation than PAL-based formulation. In addition, the PAL-based formulation provoked the continuous wall and large non-complex passage, which decreased the release rate. The change in a high environmental temperature did not affect the release of high-molecular-weight fatty acid-based formulations (VMD and VPD). However, the LAU-based formulation showed a significant change in the VCM release pattern *via* the invert *in situ* process when the environment temperature was increased. The invert *in situ* process produced a swelling-gel-like matrix over time resulting in easier VCM diffusion. The MD simulation revealed a correlation between fatty acid formation and fatty acid/solvent type. The low molecular weight-fatty acid based model exhibited a slower and more orderly rearrangement than those of the high molecular weight-fatty acid based model. The solvent with low logP (DMSO) moved more rapidly to the water region, and resulted in faster fat matrix formation, compared with the system using NMP. The MD simulation of the low- and high-water-ratio regions elucidated the *in situ* formation process in which the mixed water/solvent region, initial crystal at the high-water-ratio area, matrix growth, occurred respectively. Then the VCM and solvents moved out from the region of the fatty acid. In macroscopic level, crystallization occurred continuously resulted in various interior structure and sustained VCM release, subsequently. The hydrogen bonding could then be generated between VCM and the transformed fatty acid.

The ease of injection of the developed ISM is attributed to its unique low viscosity and convenient for administration. Fatty acids are less expensive than biodegradable polymers and also exhibited the interesting antibacterial activities. Hence, the developed preparations, such as VLD, VLD-40, VMD, and VPD can become the suitable local antimicrobial delivery systems for various Gram-positive bacterial infection sites, such as joints, crevicular pockets and post-surgery sites. The administration amount can be adjusted based on the following considerations: the fluid volume at the target site, the minimum inhibition concentration of any bacteria at the infection site and the pharmacokinetics of VCM at the target site. However, further investigation for the safety and clinical efficacy of a particular infection site should be investigated. This study provided fundamental information on further development using various fatty acids as a matrix former for solvent exchange-induced in situ forming system for other group of active compounds in which the drug release sustainability is required such as anticancer, hormonal drug and other non-communicable disease drugs.

REFERENCES

1. Kempe, S.; Metz, H.; Mader, K. Do *in situ* forming PLG/NMP implants behave similar *in vitro* and *in vivo*? A non-invasive and quantitative EPR investigation on the mechanisms of the implant formation process. *Journal of Controlled Release* **2008**, *130*, 220-225, doi:10.1016/j.jconrel.2008.06.006.

2. Srichan, T.; Phaechamud, T. Designing solvent exchange-induced *in situ* forming gel from aqueous insoluble polymers as matrix base for periodontitis treatment. *American Association of Pharmaceutical Scientists journal* **2017**, *18*, 194-201, doi:10.1208/s12249-016-0507-1.

3. Phaechamud, T.; Jantadee, T.; Mahadlek, J.; Charoensuksai, P.; Pichayakorn, W. Characterization of antimicrobial agent loaded eudragit RS solvent exchange-induced *in situ* forming gels for periodontitis treatment. *American Association of Pharmaceutical Scientists journal* **2017**, *18*, 494-508, doi:10.1208/s12249-016-0534-y.

4. Fogueri, L.R.; Singh, S. Smart polymers for controlled delivery of proteins and peptides: a review of patents. *Recent patents on drug delivery & formulation* **2009**, *3*, 40-48.

5. Wang, L.; Wang, A.; Zhao, X.; Liu, X.; Wang, D.; Sun, F.; Li, Y. Design of a long-term antipsychotic *in situ* forming implant and its release control method and mechanism. *International Journal of Pharmaceutics* **2012**, *427*, 284-292, doi:10.1016/j.ijpharm.2012.02.015.

6. White, B. Dietary fatty acids. *American Family Physician* **2009**, *80*, 345-350.

7. Xie, F.M.; Zeng, K.; Li, G.F.; Lin, Z.F.; Sun, L.D. Preparation of stearic acid solid lipid nanoparticles containing podophyllotoxin. *Di 1 Jun Yi Da Xue Xue Bao. Academic Journal of the First Medical College of Pla* **2005**, *25*, 99-101.

8. Yuan, H.; Lu, L.-J.; Du, Y.-Z.; Hu, F.-Q. Stearic acid-g-chitosan polymeric micelle for oral drug delivery: *in vitro* transport and *in vivo* absorption. *Molecular Pharmaceutics* **2011**, *8*, 225-238, doi:10.1021/mp100289v.

9. Desai, D.; Kothari, S.; Chen, W.; Wang, J.; Huang, M.; Sharma, L. Fatty acid and water-soluble polymer-based controlled release drug delivery system. *Journal of Pharmaceutical Sciences* **2011**, *100*, 1900-1912, doi:10.1002/jps.22397.

10. Beare-Rogers, J.L.; Dieffenbacher, A.; Holm, J.V. Lexicon of lipid nutrition (IUPAC Technical Report). *Pure and Applied Chemistry* **2001**, *73*, 685, doi:10.1351/pac200173040685.

11. Kingsbury, K.J.; Paul, S.; Crossley, A.; Morgan, D.M. The fatty acid composition of human depot fat. *Biochemical Journal* **1961**, *78*, 541-550.

12. Elmadfa, I.; Kornsteiner, M. Fats and fatty acid requirements for adults. *Annals of Nutrition and Metabolism* **2009**, *55*, 56-75, doi:10.1159/000228996.

13. Burdock, G.A.; Carabin, I.G. Safety assessment of myristic acid as a food ingredient. *Food and Chemical Toxicology* **2007**, *45*, 517-529, doi:10.1016/j.fct.2006.10.009.

14. Yang, D.; Pornpattananangkul, D.; Nakatsuji, T.; Chan, M.; Carson, D.; Huang, C.M.; Zhang, L. The antimicrobial activity of liposomal lauric acids against *Propionibacterium acnes*. *Biomaterials* **2009**, *30*, 6035-6040, doi:10.1016/j.biomaterials.2009.07.033.

15. Huang, C.B.; Alimova, Y.; Myers, T.M.; Ebersole, J.L. Short- and medium-chain fatty acids exhibit antimicrobial activity for oral microorganisms. *Archives of Oral Biology* **2011**, *56*, 650-654, doi:10.1016/j.archoralbio.2011.01.011.

16. Anneken David, J.; Both, S.; Christoph, R.; Fieg, G.; Steinberner, U.; Westfechtel, A. Fatty acids. In *Ullmann's Encyclopedia of Industrial Chemistry*, Wiley VCH Verlag GmbH & Co KGaA: Weinheim, 2006; Vol. 14, pp. 74-116.

17. Costa, M.C.; Sardo, M.; Rolemberg, M.P.; Coutinho, J.A.P.; Meirelles, A.J.A.; Ribeiro-Claro, P.; Krähenbühl, M.A. The solid–liquid phase diagrams of binary mixtures of consecutive, even saturated fatty acids. *Chemistry and Physics of Lipids* **2009**, *160*, 85-97, doi:10.1016/j.chemphyslip.2009.05.004.

18. Vervaeck, A.; Saerens, L.; De Geest, B.G.; De Beer, T.; Carleer, R.; Adriaensens, P.; Remon, J.P.; Vervaet, C. Prilling of fatty acids as a continuous process for the development of controlled release multiparticulate dosage forms. *European Journal of Pharmaceutics and Biopharmaceutics* **2013**, *85*, 587-596, doi:10.1016/j.ejpb.2013.02.003.

19. Vervaeck, A.; Monteyne, T.; Siepmann, F.; Boone, M.N.; Van Hoorebeke, L.; De Beer, T.; Siepmann, J.; Remon, J.P.; Vervaet, C. Fatty acids for controlled release applications: A comparison between prilling and solid lipid extrusion as manufacturing techniques. *European Journal of Pharmaceutics and Biopharmaceutics* **2015**, *97*, 173-184, doi:10.1016/j.ejpb.2015.09.011.

20. Pandya, N.T.; Jani, P.; Vanza, J.; Tandel, H. Solid lipid nanoparticles as an efficient drug delivery system of olmesartan medoxomil for the treatment of hypertension. *Colloids and Surfaces B: Biointerfaces* **2018**, *165*, 37-44, doi:10.1016/j.colsurfb.2018.02.011.

21. Bayón, B.; Bucalá, V.; Castro, G.R. Development of antimicrobial hybrid mesoporous silver phosphate–pectin microspheres for control release of levofloxacin. *Microporous and Mesoporous Materials* **2016**, *226*, 71-78, doi:10.1016/j.micromeso.2015.12.041.

22. Van Renterghem, J.; Dhondt, H.; Verstraete, G.; De Bruyne, M.; Vervaet, C.; De Beer, T. The impact of the injection mold temperature upon polymer crystallization and resulting drug release from immediate and sustained release tablets. *International Journal of Pharmaceutics* **2018**, *541*, 108-116, doi:10.1016/j.ijpharm.2018.01.053.

23. Herrera, M.L.; Hartel, R.W. Effect of processing conditions on crystallization kinetics of a milk fat model system. *Journal of the American Oil Chemists' Society* **2000**, *77*, 1177-1188, doi:10.1007/s11746-000-0184-4.

24. Herrera, M.L.; Hartel, R.W. Effect of processing conditions on physical properties of a milk fat model system: Microstructure. *Journal of the American Oil Chemists' Society* **2000**, *77*, 1197-1205, doi:10.1007/s11746-000-0186-2.

25. Parent, M.; Nouvel, C.; Koerber, M.; Sapin, A.; Maincent, P.; Boudier, A. PLGA *in situ* implants formed by phase inversion: Critical physicochemical parameters to modulate drug release. *Journal of Controlled Release* **2013**, *172*, 292-304, doi:10.1016/j.jconrel.2013.08.024.

26. Sanghvi, R.; Narazaki, R.; Machatha, S.G.; Yalkowsky, S.H. Solubility improvement of drugs using *N*-methyl pyrrolidone. *American Association of Pharmaceutical Scientists journal* **2008**, *9*, 366-376, doi:10.1208/s12249-008-9050-z.

27.   Ahmed, T.A.; Ibrahim, H.M.; Samy, A.M.; Kaseem, A.; Nutan, M.T.H.; Hussain, M.D. Biodegradable injectable *in situ* implants and microparticles for sustained release of montelukast: *in vitro* release, pharmacokinetics, and stability. *American Association of Pharmaceutical Scientists journal* **2014**, *15*, 772-780, doi:10.1208/s12249-014-0101-3.

28.   Lee, D.K.; Wang, D.P. Formulation development of allopurinol suppositories and injectables. *Drug Development and Industrial Pharmacy* **1999**, *25*, 1205-1208, doi:10.1081/ddc-100102289.

29.   Strickley, R.G. Solubilizing excipients in oral and injectable formulations. *Pharmaceutical Research* **2004**, *21*, 201-230, doi:10.1023/B:PHAM.0000016235.32639.23.

30.   Jouyban, A.; Fakhree, M.A.; Shayanfar, A. Review of pharmaceutical applications of *N*-methyl-2-pyrrolidone. *J Pharm Pharm Sci* **2010**, *13*, 524-535.

31.   Bartsch, W.; Sponer, G.; Dietmann, K.; Fuchs, G. Acute toxicity of various solvents in the mouse and rat. LD50 of ethanol, diethylacetamide, dimethylformamide, dimethylsulfoxide, glycerine, *N*-methylpyrrolidone, polyethylene glycol 400, 1,2-propanediol and Tween 20. *Arzneimittelforschung* **1976**, *26*, 1581-1583.

32.   Jain, P.; Yalkowsky, S.H. Solubilization of poorly soluble compounds using 2-pyrrolidone. *International Journal of Pharmaceutics* **2007**, *342*, 1-5, doi:10.1016/j.ijpharm.2007.03.056.

33.   Kranz, H.; Brazeau, G.A.; Napaporn, J.; Martin, R.L.; Millard, W.; Bodmeier, R. Myotoxicity studies of injectable biodegradable *in-situ* forming drug delivery systems. *Int J Pharm* **2001**, *212*, 11-18.

34.   Agostini, E.; Winter, G.; Engert, J. Water-based preparation of spider silk films as drug delivery matrices. *Journal of Controlled Release* **2015**, *213*, 134-141, doi:10.1016/j.jconrel.2015.06.025.

35.   Camargo, J.A.; Sapin, A.; Nouvel, C.; Daloz, D.; Leonard, M.; Bonneaux, F.; Six, J.L.; Maincent, P. Injectable PLA-based in situ forming implants for controlled release of Ivermectin a BCS Class II drug: solvent selection based on physico-chemical characterization. *Drug Development and Industrial Pharmacy* **2013**, *39*, 146-155, doi:10.3109/03639045.2012.660952.

36.   Liu, Q.; Zhang, H.; Zhou, G.; Xie, S.; Zou, H.; Yu, Y.; Li, G., et al. *In vitro* and *in vivo* study of thymosin alpha1 biodegradable *in situ* forming poly(lactide-co-glycolide) implants. *International Journal of Pharmaceutics* **2010**, *397*, 122-129, doi:10.1016/j.ijpharm.2010.07.015.

37.   Argenziano, M.; Banche, G.; Luganini, A.; Finesso, N.; Allizond, V.; Gulino, G.R.; Khadjavi, A., et al. Vancomycin-loaded nanobubbles: A new platform for controlled antibiotic delivery against methicillin-resistant *Staphylococcus aureus* infections. *International Journal of Pharmaceutics* **2017**, *523*, 176-188, doi:10.1016/j.ijpharm.2017.03.033.

38.   Parente, D.M.; Laplante, K.L. 145 - Glycopeptides. In *Infectious Diseases (Fourth Edition)*, Cohen, J., Powderly, W.G., Opal, S.M., Eds. Elsevier: 2017; 10.1016/B978-0-7020-6285-8.00145-3pp. 1249-1255.e1242.

39.   Zilberman, M.; Elsner, J.J. Antibiotic-eluting medical devices for various applications. *Journal of Controlled Release* **2008**, *130*, 202-215, doi:10.1016/j.jconrel.2008.05.020.

40. Jain, N.; Jain, G.K.; Javed, S.; Iqbal, Z.; Talegaonkar, S.; Ahmad, F.J.; Khar, R.K. Recent approaches for the treatment of periodontitis. *Drug Discovery Today* **2008**, *13*, 932-943, doi:10.1016/j.drudis.2008.07.010.

41. Roy, M.E.; Peppers, M.P.; Whiteside, L.A.; LaZear, R.M. Vancomycin concentration in synovial fluid: direct injection into the knee vs. intravenous infusion. *The Journal of Arthroplasty* **2014**, *29*, 564-568, doi:10.1016/j.arth.2013.08.017.

42. Bruniera, F.R.; Ferreira, F.M.; Saviolli, L.R.; Bacci, M.R.; Feder, D.; da Luz Goncalves Pedreira, M.; Sorgini Peterlini, M.A., et al. The use of vancomycin with its therapeutic and adverse effects: a review. *European Review for Medical and Pharmacological Sciences* **2015**, *19*, 694-700.

43. Guse, C.; Koennings, S.; Maschke, A.; Hacker, M.; Becker, C.; Schreiner, S.; Blunk, T.; Spruss, T.; Goepferich, A. Biocompatibility and erosion behavior of implants made of triglycerides and blends with cholesterol and phospholipids. *International Journal of Pharmaceutics* **2006**, *314*, 153-160, doi:10.1016/j.ijpharm.2005.12.050.

44. Clayton, G.D.a.C., F.E. . In *Patty's Industrial Hygiene and Toxicology*, 3rd ed.; John Wiley & Sons: New York, 1982; Vol. 2C: Toxicology.

45. 3: Final report on the safety assessment of oleic acid, lauric Acid, palmitic acid, myristic acid, and stearic Acid. *Journal of the American College of Toxicology* **1987**, *6*, 321-401, doi:10.3109/10915818709098563.

46. Skřivanová, E.; Marounek, M.; Dlouhá, G.; Kaňka, J. Susceptibility of Clostridium perfringens to C2–C18 fatty acids. *Letters in Applied Microbiology* **2005**, *41*, 77-81, doi:10.1111/j.1472-765X.2005.01709.x.

47. Bergsson, G.; Arnfinnsson, J.; SteingrÍMsson, Ó.; Thormar, H. Killing of Gram-positive cocci by fatty acids and monoglyceridesNote. *APMIS* **2001**, *109*, 670-678, doi:10.1034/j.1600-0463.2001.d01-131.x.

48. Kalitheertha Thevar, J.-T.; Nik Malek, N.A.N.; Abdul Kadir, M.R. *In vitro* degradation of triple layered poly (lactic-co-glycolic acid) composite membrane composed of nanoapatite and lauric acid for guided bone regeneration applications. *Materials Chemistry and Physics* **2019**, *221*, 501-514, doi:10.1016/j.matchemphys.2018.09.060.

49. Hoshimoto, A.; Suzuki, Y.; Katsuno, T.; Nakajima, H.; Saito, Y. Caprylic acid and medium-chain triglycerides inhibit IL-8 gene transcription in Caco-2 cells: Comparison with the potent histone deacetylase inhibitor trichostatin A. *British Journal of Pharmacology* **2002**, *136*, 280-286, doi:10.1038/sj.bjp.0704719.

50. Kandula, M.; Sunil Kumar, K.B.; Palanichamy, S.; Rampal, A. Discovery and preclinical development of a novel prodrug conjugate of mesalamine with eicosapentaenoic acid and caprylic acid for the treatment of inflammatory bowel diseases. *International Immunopharmacology* **2016**, *40*, 443-451, doi:10.1016/j.intimp.2016.09.013.

51. Aungst, B.J.; J. Rogers, N.; Shefter, E. Enhancement of naloxone penetration through human skin *in vitro* using fatty acids, fatty alcohols, surfactants, sulfoxides and amides. *International Journal of Pharmaceutics* **1986**, *33*, 225-234, doi:10.1016/0378-5173(86)90057-8.

52. Li-Ren, H.; Yaw-Bin, H.; Pao-Chu, W.; Yi-Hung, T. Percutaneous absorption of piroxicam from FAPG base through rat skin: effects of fatty acid added to FAPG

base. *International Journal of Pharmaceutics* **1994**, *106*, 1-6, doi:10.1016/0378-5173(94)90269-0.

53.   Inoue, T.; Hisatsugu, Y.; Suzuki, M.; Wang, Z.; Zheng, L. Solid–liquid phase behavior of binary fatty acid mixtures: 3. Mixtures of oleic acid with capric acid (decanoic acid) and caprylic acid (octanoic acid). *Chemistry and Physics of Lipids* **2004**, *132*, 225-234, doi:10.1016/j.chemphyslip.2004.07.004.

54.   Karaipekli, A.; Sari, A. Capric acid and palmitic acid eutectic mixture applied in building wallboard for latent heat thermal energy storage. *Journal of scientific and industrial research* **2007**, *66*, 470-476.

55.   Zuo, J.; Li, W.; Weng, L. Thermal properties of lauric acid/1-tetradecanol binary system for energy storage. *Applied Thermal Engineering* **2011**, *31*, 1352-1355, doi:doi.org/10.1016/j.applthermaleng.2011.01.008.

56.   Sari, A.; Alkan, C.; Kolemen, U.; Uzun, O. Eudragit S (methyl methacrylate methacrylic acid copolymer)/fatty acid blends as form-stable phase change material for latent heat thermal energy storage. *Journal of Applied Polymer Science* **2006**, *101*, 1402-1406, doi:10.1002/app.23478.

57.   Le, N.D.T.; Tran, P.H.L.; Lee, B.-J.; Tran, T.T.D. Solid lipid particle-based tablets for buccal delivery: The role of solid lipid particles in drug release. *Journal of Drug Delivery Science and Technology* **2019**, *52*, 96-102, doi:doi.org/10.1016/j.jddst.2019.04.037.

58.   Dew, N.; Bramer, T.; Edsman, K. Catanionic aggregates formed from drugs and lauric or capric acids enable prolonged release from gels. *Journal of Colloid and Interface Science* **2008**, *323*, 386-394, doi:10.1016/j.jcis.2008.04.008.

59.   Sagiri, S.S.; Singh, V.K.; Pal, K.; Banerjee, I.; Basak, P. Stearic acid based oleogels: A study on the molecular, thermal and mechanical properties. *Materials Science and Engineering: C* **2015**, *48*, 688-699, doi:doi.org/10.1016/j.msec.2014.12.018.

60.   Katiyar, S.S.; Kushwah, V.; Dora, C.P.; Jain, S. Novel biosurfactant and lipid core-shell type nanocapsular sustained release system for intravenous application of methotrexate. *International Journal of Pharmaceutics* **2019**, *557*, 86-96, doi:10.1016/j.ijpharm.2018.12.043.

61.   Qiu, Q.; Li, C.; Song, Y.; Shi, T.; Luo, X.; Zhang, H.; Hu, L., et al. Targeted delivery of ibrutinib to tumor-associated macrophages by sialic acid-stearic acid conjugate modified nanocomplexes for cancer immunotherapy. *Acta Biomaterialia* **2019**, *92*, 184-195, doi:doi.org/10.1016/j.actbio.2019.05.030.

62.   Killen, B.U.; Corrigan, O.I. Effect of soluble filler on drug release from stearic acid based compacts. *International Journal of Pharmaceutics* **2006**, *316*, 47-51, doi:doi.org/10.1016/j.ijpharm.2006.02.048.

63.   Monteyne, T.; Adriaensens, P.; Brouckaert, D.; Remon, J.-P.; Vervaet, C.; De Beer, T. Stearic acid and high molecular weight PEO as matrix for the highly water soluble metoprol tartrate in continuous twin-screw melt granulation. *International Journal of Pharmaceutics* **2016**, *512*, 158-167, doi:doi.org/10.1016/j.ijpharm.2016.07.035.

64.   Wang, R.; Ren, M.; Gao, X.; Qin, L. Preparation and properties of fatty acids based thermal energy storage aggregate concrete. *Construction and Building Materials* **2018**, *165*, 1-10, doi:doi.org/10.1016/j.conbuildmat.2018.01.034.

65. Maheswari, J.U.; Krishnan, C.; Kalyanaraman, S.; Selvarajan, P. Growth and characterization of an organic nonlinear optical material—lauric acid crystal. *Materials Research Express* **2016**, *3*, 105101.

66. Maheswari, J.U.; Krishnan, C.; Kalyanaraman, S.; Selvarajan, P. Physical properties of lauric acid crystals grown with KBr in aqueous solution. *Bulletin of Materials Science* **2018**, *41*, 46, doi:10.1007/s12034-018-1565-7.

67. Narine, S.S.; Marangoni, A.G. Relating structure of fat crystal networks to mechanical properties: a review. *Food Research International* **1999**, *32*, 227-248, doi:10.1016/S0963-9969(99)00078-2.

68. Marangoni, A.G.; Rousseau, D. Is plastic fat rheology governed by the fractal nature of the fat crystal network? *Journal of the American Oil Chemists' Society* **1996**, *73*, 991-994, doi:10.1007/BF02523406.

69. Thareja, P.; Street, C.B.; Wagner, N.J.; Vethamuthu, M.S.; Hermanson, K.D.; Ananthapadmanabhan, K.P. Development of an *in situ* rheological method to characterize fatty acid crystallization in complex fluids. *Colloids and Surfaces A: Physicochemical and Engineering Aspects* **2011**, *388*, 12-20, doi:10.1016/j.colsurfa.2011.07.038.

70. Dadwal, A.; Joy, P.A. Influence of chain length of long-chain fatty acid surfactant on the thermal conductivity of magnetite nanofluids in a magnetic field. *Colloids and Surfaces A: Physicochemical and Engineering Aspects* **2018**, *555*, 525-531, doi:10.1016/j.colsurfa.2018.07.034.

71. Akilo, O.D.; Kumar, P.; Choonara, Y.E.; du Toit, L.C.; Pradeep, P.; Modi, G.; Pillay, V. In situ thermo-co-electroresponsive mucogel for controlled release of bioactive agent. *International Journal of Pharmaceutics* **2019**, *559*, 255-270, doi:10.1016/j.ijpharm.2019.01.044.

72. Ritter Jones, M.; Messersmith, P.B. *In situ* forming biomaterials. *Oral and Maxillofacial Surgery Clinics of North America* **2002**, *14*, 29-38, doi:10.1016/S1042-3699(02)00015-8.

73. Wang, Q.; Zuo, Z.; Cheung, C.K.C.; Leung, S.S.Y. Updates on thermosensitive hydrogel for nasal, ocular and cutaneous delivery. *International Journal of Pharmaceutics* **2019**, *559*, 86-101, doi:10.1016/j.ijpharm.2019.01.030.

74. Kubo, W.; Konno, Y.; Miyazaki, S.; Attwood, D. *In situ* gelling pectin formulations for oral sustained delivery of paracetamol. *Drug Development and Industrial Pharmacy* **2004**, *30*, 593-599, doi:10.1081/DDC-120037490.

75. Phaechamud, T.; Mahadlek, J.; Tuntarawongsa, S. Peppermint oil/doxycycline hyclate-loaded Eudragit RS *in situ* forming gel for periodontitis treatment. *Journal of Pharmaceutical Investigation* **2018**, *48*, 451-464, doi:10.1007/s40005-017-0340-x.

76. Guo, J.-H.; Skinner, G.W.; Harcum, W.W.; Barnum, P.E. Pharmaceutical applications of naturally occurring water-soluble polymers. *Pharmaceutical Science & Technology Today* **1998**, *1*, 254-261, doi:10.1016/S1461-5347(98)00072-8.

77. Phaechamud, T.; Mahadlek, J.; Charoenteeraboon, J.; Choopun, S. Characterization and antimicrobial activity of *N*-methyl-2-pyrrolidone-loaded ethylene oxide-propylene oxide block copolymer thermosensitive gel. *Indian Journal of Pharmaceutical Sciences* **2012**, *74*, 498-504, doi:10.4103/0250-474x.110574.

78. Phaechamud, T.; Chanyaboonsub, N.; Setthajindalert, O. Doxycycline hyclate-loaded bleached shellac *in situ* forming microparticle for intraperiodontal pocket local delivery. *European Journal of Pharmaceutical Sciences* **2016**, *93*, 360-370, doi:10.1016/j.ejps.2016.08.034.

79. Praphanwittaya, P.; Phaechamud, T. Bleached shellac as an alternative polymeric matrix for *in situ* microparticle. *Key Engineering Materials* **2015**, *659*, 8-12, doi:10.4028/www.scientific.net/KEM.659.8.

80. Rungseevijitprapa, W.; Bodmeier, R. Injectability of biodegradable *in situ* forming microparticle systems (ISM). *European Journal of Pharmaceutical Sciences* **2009**, *36*, 524-531, doi:10.1016/j.ejps.2008.12.003.

81. Zou, Q.; Hou, F.; Wang, H.; Liao, Y.; Wang, Q.; Yang, Y. Microfluidic one-step preparation of alginate microspheres encapsulated with in situ-formed bismuth sulfide nanoparticles and their photothermal effect. *European Polymer Journal* **2019**, *115*, 282-289, doi:10.1016/j.eurpolymj.2019.03.040.

82. Kamali, H.; Khodaverdi, E.; Hadizadeh, F.; Mohajeri, S.A. In-vitro, ex-vivo, and in-vivo evaluation of buprenorphine HCl release from an in situ forming gel of PLGA-PEG-PLGA using N-methyl-2-pyrrolidone as solvent. *Materials Science and Engineering: C* **2019**, *96*, 561-575, doi:10.1016/j.msec.2018.11.058.

83. Agossa, K.; Lizambard, M.; Rongthong, T.; Delcourt-Debruyne, E.; Siepmann, J.; Siepmann, F. Physical key properties of antibiotic-free, PLGA/HPMC-based in-situ forming implants for local periodontitis treatment. *International Journal of Pharmaceutics* **2017**, *521*, 282-293, doi:10.1016/j.ijpharm.2017.02.039.

84. Phaechamud, T.; Setthajindalert, O. Cholesterol *in situ* forming gel loaded with doxycycline hyclate for intra-periodontal pocket delivery. *European Journal of Pharmaceutical Sciences* **2017**, *99*, 258-265, doi:10.1016/j.ejps.2016.12.023.

85. Li, H.; Liu, T.; Zhu, Y.; Fu, Q.; Wu, W.; Deng, J.; Lan, L.; Shi, S. An *in situ*-forming phospholipid-based phase transition gel prolongs the duration of local anesthesia for ropivacaine with minimal toxicity. *Acta Biomaterialia* **2017**, *58*, 136-145, doi:10.1016/j.actbio.2017.06.013.

86. Zhang, T.; Luo, J.; Peng, Q.; Dong, J.; Wang, Y.; Gong, T.; Zhang, Z. Injectable and biodegradable phospholipid-based phase separation gel for sustained delivery of insulin. *Colloids and Surfaces B: Biointerfaces* **2019**, *176*, 194-201, doi:10.1016/j.colsurfb.2019.01.003.

87. Nazir, M.A. Prevalence of periodontal disease, its association with systemic diseases and prevention. *International journal of health sciences* **2017**, *11*, 72-80.

88. Eke, P.I.; Thornton-Evans, G.O.; Wei, L.; Borgnakke, W.S.; Dye, B.A.; Genco, R.J. Periodontitis in US adults: National health and nutrition examination survey 2009-2014. *The Journal of the American Dental Association* **2018**, *149*, 576-588.e576, doi:doi.org/10.1016/j.adaj.2018.04.023.

89. Janket, S.-J.; Baird, A.E.; Chuang, S.-K.; Jones, J.A. Meta-analysis of periodontal disease and risk of coronary heart disease and stroke. *Oral Surgery, Oral Medicine, Oral Pathology, Oral Radiology, and Endodontology* **2003**, *95*, 559-569, doi:10.1067/moe.2003.107.

90. Ji, Q.X.; Zhao, Q.S.; Deng, J.; Lü, R. A novel injectable chlorhexidine thermosensitive hydrogel for periodontal application: preparation, antibacterial activity and toxicity evaluation. *Journal of Materials Science: Materials in Medicine* **2010**, *21*, 2435-2442, doi:10.1007/s10856-010-4098-1.

91. Farhan, J.A.; Zeenat, I.; Nilu, J.; Gaurav, K.J.; Sushama, T.; Alka, A.; Roop, K.K. Dental therapeutic systems. *Recent patents on drug delivery & formulation* **2008**, *2*, 58-67, doi:10.2174/187221108783331366.

92. Slots, J. Selection of antimicrobial agents in periodontal therapy. *Journal of Periodontal Research* **2002**, *37*, 389-398, doi:10.1034/j.1600-0765.2002.00004.x.

93. Haffajee, A.D.; Socransky, S.S. Attachment level changes in destructive periodontal diseases. *Journal of Clinical Periodontology* **1986**, *13*, 461-472, doi:10.1111/j.1600-051X.1986.tb01491.x.

94. Vyas, S.P.; Sihorkar, V.; Mishra, V. Controlled and targeted drug delivery strategies towards intraperiodontal pocket diseases. *Journal of Clinical Pharmacy and Therapeutics* **2000**, *25*, 21-42, doi:10.1046/j.1365-2710.2000.00261.x.

95. Vieira Colombo, A.P.; Magalhães, C.B.; Hartenbach, F.A.R.R.; Martins do Souto, R.; Maciel da Silva-Boghossian, C. Periodontal-disease-associated biofilm: A reservoir for pathogens of medical importance. *Microbial Pathogenesis* **2016**, *94*, 27-34, doi:10.1016/j.micpath.2015.09.009.

96. Yacoubi, D.A.; Bouziane, D.; Leila, M.; Bensoltane, A. *Microbiological study of periodontitis in the west of algeria*; 2010; Vol. 5.

97. Fritschi, B.Z.; Albert-Kiszely, A.; Persson, G.R. *Staphylococcus aureus* and other bacteria in untreated periodontitis. *Journal of Dental Research* **2008**, *87*, 589-593, doi:10.1177/154405910808700605.

98. Friedman, M.; Steinberg, D. Sustained-release delivery systems for treatment of dental diseases. *Pharmaceutical Research* **1990**, *7*, 313-317.

99. Mayuri Prasad, T., Rajat Sehgal, Manisha Mallik, Aaysha Tabinda Nabi, Sneha Singh. Periodontal disease and salivary pH: Case control study. *International Archives of Integrated Medicine* **2019**, *6*, 1-6.

100. Eggert, F.M.; Drewell, L.; Bigelow, J.A.; Speck, J.E.; Goldner, M. The pH of gingival crevices and periodontal pockets in children, teenagers and adults. *Archives of Oral Biology* **1991**, *36*, 233-238, doi:10.1016/0003-9969(91)90091-8.

101. Yucel-Lindberg, T.; Båge, T. Inflammatory mediators in the pathogenesis of periodontitis. *Expert Reviews in Molecular Medicine* **2013**, *15*, e7, doi:10.1017/erm.2013.8.

102. Michael Newman, H.T., Perry Klokkevold, Fermin Carranza. *Carranza's Clinical Periodontology*; Elsevier Health Sciences: 2014; pp. 904.

103. Goodson, J.M. Antimicrobial strategies for treatment of periodontal diseases. *Periodontology 2000* **1994**, *5*, 142-168, doi:10.1111/j.1600-0757.1994.tb00022.x.

104. Lang, N.P.; LÖE, H. Clinical management of periodontal diseases. *Periodontology 2000* **1993**, *2*, 128-139, doi:10.1111/j.1600-0757.1993.tb00225.x.

105. Reise, M.; Wyrwa, R.; Müller, U.; Zylinski, M.; Völpel, A.; Schnabelrauch, M.; Berg, A., et al. Release of metronidazole from electrospun poly(l-lactide-co-d/l-lactide) fibers for local periodontitis treatment. *Dental Materials* **2012**, *28*, 179-188, doi:10.1016/j.dental.2011.12.006.

106. Ghavami-Lahiji, M.; Shafiei, F.; Najafi, F.; Erfan, M. Drug-loaded polymeric films as a promising tool for the treatment of periodontitis. *Journal of Drug Delivery Science and Technology* **2019**, *52*, 122-129, doi:10.1016/j.jddst.2019.04.034.

107. Khajuria, D.K.; Patil, O.N.; Karasik, D.; Razdan, R. Development and evaluation of novel biodegradable chitosan based metformin intrapocket dental film for the management of periodontitis and alveolar bone loss in a rat model. *Archives of Oral Biology* **2018**, *85*, 120-129, doi:10.1016/j.archoralbio.2017.10.009.

108. Cosyn, J.; Sabzevar, M.M. A Systematic Review on the Effects of Subgingival Chlorhexidine Gel Administration in the Treatment of Chronic Periodontitis. *Journal of Periodontology* **2005**, *76*, 1805-1813, doi:10.1902/jop.2005.76.11.1805.

109. Moran, J.; Addy, M.; Wade, W.; Newcombe, R. The use of antimicrobial acrylic strips in the non-surgical management of chronic periodontitis. *Clinical Materials* **1990**, *6*, 123-135, doi:10.1016/0267-6605(90)90003-E.

110. Swain, G.P.; Patel, S.; Gandhi, J.; Shah, P. Development of moxifloxacin hydrochloride loaded *in-situ* gel for the treatment of periodontitis: *in-vitro* drug release study and antibacterial activity. *Journal of Oral Biology and Craniofacial Research* **2019**, *9*, 190-200, doi:10.1016/j.jobcr.2019.04.001.

111. Yadav, S.K.; Khan, G.; Bansal, M.; Thokala, S.; Bonde, G.V.; Upadhyay, M.; Mishra, B. Multiparticulate based thermosensitive intra-pocket forming implants for better treatment of bacterial infections in periodontitis. *International Journal of Biological Macromolecules* **2018**, *116*, 394-408, doi:10.1016/j.ijbiomac.2018.04.179.

112. Kilicarslan, M.; Koerber, M.; Bodmeier, R. *In situ* forming implants for the delivery of metronidazole to periodontal pockets: formulation and drug release studies. *Drug Development and Industrial Pharmacy* **2014**, *40*, 619-624, doi:10.3109/03639045.2013.873449.

113. Yang, Z.; Liang, X.; Jiang, X.; Guo, J.; Tao, Y.; Wang, S.; Cao, Y.; Gui, S. Development and evaluation of minocycline hydrochloride-loaded *In situ* cubic liquid crystal for intra-periodontal pocket administration. *Molecules* **2018**, *23*, 2275, doi:10.3390/molecules23092275.

114. Qin, Y.; Yuan, M.; Li, L.; Li, W.; Xue, J. Formulation and evaluation of *in situ* forming PLA implant containing tinidazole for the treatment of periodontitis. *Journal of Biomedical Materials Research Part B: Applied Biomaterials* **2012**, *100B*, 2197-2202, doi:10.1002/jbm.b.32788.

115. Aimetti, M.; Romano, F.; Torta, I.; Cirillo, D.; Caposio, P.; Romagnoli, R. Debridement and local application of tetracycline-loaded fibres in the management of persistent periodontitis: results after 12 months. *Journal of Clinical Periodontology* **2004**, *31*, 166-172, doi:10.1111/j.0303-6979.2004.00457.x.

116. Yarimitsu, S.; Nakashima, K.; Sawae, Y.; Murakami, T. Influence of phospholipid and protein constituents on tribological properties of artificial hydrogel cartilage material. *Journal of Biomechanical Science and Engineering* **2013**, *8*, 257-267, doi:10.1299/jbse.8.257.

117. Yarimitsu, S.; Sasaki, S.; Murakami, T.; Suzuki, A. Evaluation of lubrication properties of hydrogel artificial cartilage materials for joint prosthesis. *Biosurface and Biotribology* **2016**, *2*, 40-47, doi:10.1016/j.bsbt.2016.02.005.

118. Lillian A. Mundt, K.S. Synovial fluid. In *Graff's Textbook of Routine Urinalysis and Body Fluids*, Goucher, J., Ed. Lippincott William & Wilkins: 530 Walnut Street, Philadelphia, PA 19106 USA, 2011.

119. Kraus, V.B.; Stabler, T.V.; Kong, S.Y.; Varju, G.; McDaniel, G. Measurement of synovial fluid volume using urea. *Osteoarthritis and Cartilage* **2007**, *15*, 1217-1220, doi:10.1016/j.joca.2007.03.017.

120. Jiang, S.; Gan, R.Z. Dynamic properties of human incudostapedial joint—Experimental measurement and finite element modeling. *Medical Engineering & Physics* **2018**, *54*, 14-21, doi:10.1016/j.medengphy.2018.02.006.

121. Jebens, E.H.; Monk-Jones, M.E. On the viscosity and pH of synovial fluid and the pH of blood. *The Journal of Bone and Joint Surgery. British volume* **1959**, *41-B*, 388-400, doi:10.1302/0301-620X.41B2.388.

122. Cummings, N.A.; Nordby, G.L. Measurement of synovial fluid pH in normal and arthritic knees. *Arthritis & Rheumatism* **1966**, *9*, 47-56, doi:10.1002/art.1780090106.

123. Roman, M.; Fleaca, R.S.; Boicean, A.; Bratu, D.; Birlutiu, V.; Rus, L.L.; Tantar, C.; Mitariu, S.I.C. *Assesment of synovial fluid pH in osteoarthritis of the HIP and knee*; 2017; Vol. 68, pp. 1340-1342.

124. Treuhaft, P.S.; McCarty, D.J. Synovial fluid pH, lactate, oxygen and carbon dioxide partial pressure in various joint diseases. *Arthritis & Rheumatism* **1971**, *14*, 475-484, doi:10.1002/art.1780140407.

125. Brook, I.; Reza, M.J.; Bricknell, K.S.; Bluestone, R.; Finegold, S.M. Synovial fluid lactic acid. a diagnostic aid in septic arthritis. *Arthritis & Rheumatism* **1978**, *21*, 774-779, doi:10.1002/art.1780210706.

126. Niinikoski, J.; Einola, S. Postoperative synovial fluid metabolic response to meniscectomy or synovectomy. *Acta Orthopaedica Scandinavica* **1977**, *48*, 129-137, doi:10.3109/17453677708985123.

127. Coggon, D.; Reading, I.; Croft, P.; McLaren, M.; Barrett, D.; Cooper, C. Knee osteoarthritis and obesity. *International Journal of Obesity and Related Metabolic Disorders* **2001**, *25*, 622-627, doi:10.1038/sj.ijo.0801585.

128. Sadeghi, A.; Rad, Z.A.; Sajedi, B.; Heydari, A.H.; Akbarieh, S.; Jafari, B. Effect of weight losing on the clinical status improvement of patients with knee osteoarthritis. *Reumatologia Clinica* **2019**, *15*, 73-76, doi:10.1016/j.reuma.2017.06.016.

129. Omoumi, P.; Michoux, N.; Thienpont, E.; Roemer, F.W.; Vande Berg, B.C. Anatomical distribution of areas of preserved cartilage in advanced femorotibial osteoarthritis using CT arthrography (Part 1). *Osteoarthritis and Cartilage* **2015**, *23*, 83-87, doi:doi.org/10.1016/j.joca.2014.10.006.

130. Yoshida, S.; Aoyagi, K.; Felson, D.T.; Aliabadi, P.; Shindo, H.; Takemoto, T.-I. Comparison of the prevalence of radiographic osteoarthritis of the knee and hand between Japan and the United States. *The Journal of Rheumatology* **2002**, *29*, 1454.

131. Nimit-arnun, N. The epidemiological situation and risk assessment of knee osteoarthritis among Thai people. *Journal of The Royal Thai Army Nurses* **2014**, *15*, 185-193.

132. Practitioners, T.R.A.C.o.G. *The Royal Australian College of General Practitioners*, 2 ed.; RACGP: East Melbourne, Victoria, Autralia, 2018.

133. Pitarresi, G.; Palumbo, F.S.; Fiorica, C.; Calascibetta, F.; Di Stefano, M.; Giammona, G. Injectable *in situ* forming microgels of hyaluronic acid-g-

polylactic acid for methylprednisolone release. *European Polymer Journal* **2013**, *49*, 718-725, doi:10.1016/j.eurpolymj.2012.12.001.

134. Cokelaere, S.M.; Plomp, S.G.M.; de Boef, E.; de Leeuw, M.; Bool, S.; van de Lest, C.H.A.; van Weeren, P.R.; Korthagen, N.M. Sustained intra-articular release of celecoxib in an equine repeated LPS synovitis model. *European Journal of Pharmaceutics and Biopharmaceutics* **2018**, *128*, 327-336, doi:10.1016/j.ejpb.2018.05.001.

135. Cokelaere, S.; Plomp, S.G.; de Leeuw, M.; van Weeren, R.; Korthagen, N.M. Sustained intra-articular release of celecoxib from *in situ* forming hydrogels made of acetyl-capped PCLA-PEG-PCLA triblock copolymers in an equine model of osteoarthritis. *Osteoarthritis and Cartilage* **2016**, *24*, S525-S526, doi:10.1016/j.joca.2016.01.960.

136. Ruiz, D.J.; Koenig, L.; Dall, T.M.; Gallo, P.; Narzikul, A.; Parvizi, J.; Tongue, J. The direct and Indirect costs to society of treatment for end-stage knee osteoarthritis. *JBJS* **2013**, *95*, 1473-1480, doi:10.2106/jbjs.L.01488.

137. Kalore, N.V.; Gioe, T.J.; Singh, J.A. Diagnosis and management of infected total knee arthroplasty. *The Open Orthopaedics Journal* **2011**, *5*, 86-91, doi:10.2174/1874325001105010086.

138. Alijanipour, P.; Parvizi, J. Infection post-total knee replacement: current concepts. *Current Reviews in Musculoskeletal Medicine* **2014**, *7*, 96-102, doi:10.1007/s12178-014-9217-z.

139. Aggarwal, V.K.; Bakhshi, H.; Ecker, N.U.; Parvizi, J.; Gehrke, T.; Kendoff, D. Organism profile in periprosthetic joint infection: pathogens differ at two arthroplasty infection referral centers in Europe and in the United States. *Journal of Knee Surgery* **2014**, *27*, 399-406, doi:10.1055/s-0033-1364102.

140. Bjerke-Kroll, B.T.; Christ, A.B.; McLawhorn, A.S.; Sculco, P.K.; Jules-Elysee, K.M.; Sculco, T.P. Periprosthetic joint infections treated with two-stage revision over 14 years: an evolving microbiology profile. *J Arthroplasty* **2014**, *29*, 877-882, doi:10.1016/j.arth.2013.09.053.

141. Whiteside, L.A.; Roy, M.E.; Nayfeh, T.A. Intra-articular infusion. *The Bone & Joint Journal* **2016**, *98-B*, 31-36, doi:10.1302/0301-620X.98B.36276.

142. Rybak, M.J. The pharmacokinetic and pharmacodynamic properties of vancomycin. *Clinical Infectious Diseases* **2006**, *42*, S35-S39, doi:10.1086/491712.

143. Skhirtladze, K.; Hutschala, D.; Fleck, T.; Thalhammer, F.; Ehrlich, M.; Vukovich, T.; Müller, M.; Tschernko, E.M. Impaired target site penetration of vancomycin in diabetic patients following cardiac surgery. *Antimicrobial Agents and Chemotherapy* **2006**, *50*, 1372, doi:10.1128/AAC.50.4.1372-1375.2006.

144. Ahlqvist, J. Swelling of synovial joints — An anatomical, physiological and energy metabolical approach. *Pathophysiology* **2000**, *7*, 1-19, doi:10.1016/S0928-4680(00)00044-4.

145. Yin, H.; Wang, L.; Li, Q.-l.; Zhang, J.-h.; Zhang, L.; Wang, X. Metabolomic analysis of biochemical changes in urine of osteoarthritis rat and interventional effects of bushen-huoxue herb couple. *Chinese Herbal Medicines* **2017**, *9*, 369-375, doi:10.1016/S1674-6384(17)60117-5.

146. Li, B.; Brown, K.V.; Wenke, J.C.; Guelcher, S.A. Sustained release of vancomycin from polyurethane scaffolds inhibits infection of bone wounds in a

rat femoral segmental defect model. *Journal of Controlled Release* **2010**, *145*, 221-230, doi:10.1016/j.jconrel.2010.04.002.

147. Dodd, M.C.; Buffle, M.-O.; von Gunten, U. Oxidation of antibacterial molecules by aqueous ozone: moiety-specific reaction kinetics and application to ozone-based wastewater treatment. *Environmental Science & Technology* **2006**, *40*, 1969-1977, doi:10.1021/es051369x.

148. Wood, M.J.; Lund, R.; Beavan, M. Stability of vancomycin in plastic syringes measured by high–performance liquid chromatography. *Journal of Clinical Pharmacy and Therapeutics* **1995**, *20*, 319-325, doi:10.1111/j.1365-2710.1995.tb00705.x.

149. Lin, H.-R.; Ou, L.-H.; Lin, Y.-J.; Ling, M.-H. Hollow, pH-sensitive calcium–alginate/poly(acrylic acid) hydrogel beads as drug carriers for vancomycin release. *Journal of Applied Polymer Science* **2010**, *118*, 1878-1886, doi:10.1002/app.32574.

150. Shukla, A.; Fang, J.C.; Puranam, S.; Hammond, P.T. Release of vancomycin from multilayer coated absorbent gelatin sponges. *Journal of Controlled Release* **2012**, *157*, 64-71, doi:10.1016/j.jconrel.2011.09.062.

151. Watanakunakorn, C. Mode of action and *in-vitro* activity of vancomycin. *Journal of Antimicrobial Chemotherapy* **1984**, *14 Suppl D*, 7-18.

152. Rybak, M.; Lomaestro, B.; Rotschafer, J.C.; Moellering, R., Jr.; Craig, W.; Billeter, M.; Dalovisio, J.R.; Levine, D.P. Therapeutic monitoring of vancomycin in adult patients: a consensus review of the American Society of Health-System Pharmacists, the Infectious Diseases Society of America, and the Society of Infectious Diseases Pharmacists. *American Journal of Health-System Pharmacy* **2009**, *66*, 82-98, doi:10.2146/ajhp080434.

153. García-González, C.A.; Barros, J.; Rey-Rico, A.; Redondo, P.; Gómez-Amoza, J.L.; Concheiro, A.; Alvarez-Lorenzo, C.; Monteiro, F.J. Antimicrobial properties and osteogenicity of vancomycin-loaded synthetic scaffolds obtained by supercritical foaming. *ACS Applied Materials and Interfaces* **2018**, *10*, 3349-3360, doi:10.1021/acsami.7b17375.

154. Liu, K.S.; Lee, C.H.; Wang, Y.C.; Liu, S.J. Sustained release of vancomycin from novel biodegradable nanofiber-loaded vascular prosthetic grafts: *In vitro* and *in vivo* study. *International Journal of Nanomedicine* **2015**, *10*, 885-891, doi:10.2147/IJN.S78675.

155. Könönen, E.; Conrads, G.; Nagy, E. *Bacteroides, Porphyromonas, Prevotella, Fusobacterium* and other anaerobic Gram-negative rods. In *Manual of Clinical Microbiology*, Versalovic J, C.K., Funke G, Jorgensen J, Landry M, Warnock D, Ed. ASM Press: Washington, DC, 2011; 10.1128/9781555816728pp. 967-993.

156. Jung, Y.-J.; Jun, H.-K.; Choi, B.-K. *Porphyromonas gingivalis* suppresses invasion of *Fusobacterium nucleatum* into gingival epithelial cells. *Journal of Oral Microbiology* **2017**, *9*, 1320193, doi:10.1080/20002297.2017.1320193.

157. Rockville, M.U.S.P.C. *United States Pharmacopeia : National Formulary*, USP 36 NF 31 ed.; 2013.

158. Darestani-Farahani, M.; Vasheghani-Farahani, E.; Mobedi, H.; Ganji, F. The effect of solvent composition on vancomycin hydrochloride and free base vancomycin release from *in situ* forming implants. *Polymers for Advanced Technologies* **2016**, *27*, 1653-1663, doi:10.1002/pat.3845.

159. Chauhan MK, B.N. A simple and modified method development of vancomycin using high performance liquid chromatography. *Journal of Chromatography & Separation Techniques* **2015**, *6*, doi:10.4172/2157-7064.1000296.

160. Ahadi, F.; Khorshidi, S.; Karkhaneh, A. A hydrogel/fiber scaffold based on silk fibroin/oxidized pectin with sustainable release of vancomycin hydrochloride. *European Polymer Journal* **2019**, *118*, 265-274, doi:10.1016/j.eurpolymj.2019.06.001.

161. Swain, S.K.; Gotman, I.; Gutmanas, E.Y. Vancomycin release from biodegradable βTCP-FeAg nanocomposites. *Materials Letters* **2019**, *252*, 260-263, doi:10.1016/j.matlet.2019.05.143.

162. Mohammed, W.; Ali, W.; Al-Awady, M. Evaluation of *in vitro* drug release kinetics and antibacterial activity of vancomycin HCl-loaded nanogel for topical application. *Journal of Pharmaceutical Sciences and Research* **2018**, *11*, 2747-2756.

163. Patel, N.N.; Guild, G.N.; Kumar, A.R. Intrawound vancomycin in primary hip and knee arthroplasty: a safe and cost-effective means to decrease early periprosthetic joint infection. *Arthroplasty Today* **2018**, *4*, 479-483, doi:10.1016/j.artd.2018.07.011.

164. Bishop, A.R.; Kim, S.; Squire, M.W.; Rose, W.E.; Ploeg, H.-L. Vancomycin elution, activity and impact on mechanical properties when added to orthopedic bone cement. *Journal of the Mechanical Behavior of Biomedical Materials* **2018**, *87*, 80-86, doi:10.1016/j.jmbbm.2018.06.033.

165. MicroMath. *MicroMath scientist handbook Rev. 7EEF*; MicroMath: Salt Lake City, 1995.

166. Ritger, P.L.; Peppas, N.A. A simple equation for description of solute release I. Fickian and non-fickian release from non-swellable devices in the form of slabs, spheres, cylinders or discs. *Journal of Controlled Release* **1987**, *5*, 23-36, doi:10.1016/0168-3659(87)90034-4.

167. Costa, P.; Sousa Lobo, J.M. Modeling and comparison of dissolution profiles. *European Journal of Pharmaceutical Sciences* **2001**, *13*, 123-133, doi:https://doi.org/10.1016/S0928-0987(01)00095-1.

168. Wagner, J.G. Interpretation of percent dissolved-time plots derived from in vitro testing of conventional tablets and capsules. *Journal of Pharmaceutical Sciences* **1969**, *58*, 1253-1257, doi:10.1002/jps.2600581021.

169. Higuchi, T. Rate of release of medicaments from ointment bases containing drugs in suspension. *Journal of Pharmaceutical Sciences* **1961**, *50*, 874-875, doi:https://doi.org/10.1002/jps.2600501018.

170. Higuchi, T. Mechanism of sustained-action medication. Theoretical analysis of rate of release of solid drugs dispersed in solid matrices. *Journal of Pharmaceutical Sciences* **1963**, *52*, 1145-1149, doi:10.1002/jps.2600521210.

171. Thomas, N.L.; Windle, A.H. A theory of case II diffusion. *Polymer* **1982**, *23*, 529-542, doi:10.1016/0032-3861(82)90093-3.

172. M. Padmaa, P.; Preethy Ani, J.; Cm, S.; G.V. Peter, C. Release Kinetics - concepts and applications. *IJPRT* **2018**, *8*, 12-20, doi:10.31838/ijprt/08.01.02.

173. Petsev, D.N.; Wu, X.; Galkin, O.; Vekilov, P.G. Thermodynamic functions of concentrated protein solutions from phase equilibria. *The Journal of Physical Chemistry B* **2003**, *107*, 3921-3926, doi:10.1021/jp0278317.

174. Bonnett, P.E.; Carpenter, K.J.; Dawson, S.; Davey, R.J. Solution crystallisation via a submerged liquid–liquid phase boundary: oiling out. *Chemical Communications* **2003**, 10.1039/B212062C, 698-699, doi:10.1039/B212062C.

175. Törnquist, M.; Michaels, T.C.T.; Sanagavarapu, K.; Yang, X.; Meisl, G.; Cohen, S.I.A.; Knowles, T.P.J.; Linse, S. Secondary nucleation in amyloid formation. *Chemical Communications* **2018**, *54*, 8667-8684, doi:10.1039/C8CC02204F.

176. Muschol, M.; Rosenberger, F. Liquid–liquid phase separation in supersaturated lysozyme solutions and associated precipitate formation/crystallization. *The Journal of Chemical Physics* **1997**, *107*, 1953-1962, doi:10.1063/1.474547.

177. Kakran, M.; Sahoo, N.G.; Tan, I.L.; Li, L. Preparation of nanoparticles of poorly water-soluble antioxidant curcumin by antisolvent precipitation methods. *Journal of Nanoparticle Research* **2012**, *14*, 757, doi:10.1007/s11051-012-0757-0.

178. Zhu, J.; Hayward, R.C. Interfacial tension of evaporating emulsion droplets containing amphiphilic block copolymers: Effects of solvent and polymer composition. *Journal of Colloid and Interface Science* **2012**, *365*, 275-279, doi:10.1016/j.jcis.2011.09.020.

179. Yao, W.J.; Ye, Z.P.; Wang, N.; Lee, J.H. Phase-field simulation on the heteroepitaxial nucleation of (Fe,Co) solid solution on facet phase in undercooled liquid. *Journal of Alloys and Compounds* **2013**, *577*, 701-709, doi:10.1016/j.jallcom.2013.06.188.

180. Ovrutsky, A.M.; Prokhoda, A.S.; Rasshchupkyna, M.S. 2 - Basic Concepts of Theory of Phase Transformations. In *Computational Materials Science*, Ovrutsky, A.M., Prokhoda, A.S., Rasshchupkyna, M.S., Eds. Elsevier: Oxford, 2014; 10.1016/B978-0-12-420143-9.00002-8pp. 35-69.

181. Salminen, H.; Helgason, T.; Kristinsson, B.; Kristbergsson, K.; Weiss, J. Formation of solid shell nanoparticles with liquid ω-3 fatty acid core. *Food Chemistry* **2013**, *141*, 2934-2943, doi:10.1016/j.foodchem.2013.05.120.

182. Torres-Flores, G.; Türeli Nazende, G.; Akif Emre, T. Preparation of Fenofibrate loaded Eudragit L100 nanoparticles by nanoprecipitation method. *Materials Today* **2019**, *13*, 428-435, doi:10.1016/j.matpr.2019.03.176.

183. Zarkesh, I.; Ghanian, M.H.; Azami, M.; Bagheri, F.; Baharvand, H.; Mohammadi, J.; Eslaminejad, M.B. Facile synthesis of biphasic calcium phosphate microspheres with engineered surface topography for controlled delivery of drugs and proteins. *Colloids and Surfaces B: Biointerfaces* **2017**, *157*, 223-232, doi:10.1016/j.colsurfb.2017.05.067.

184. Subramanian, R.; Sathish, S.; Murugan, P.; Mohamed Musthafa, A.; Elango, M. Effect of piperine on size, shape and morphology of hydroxyapatite nanoparticles synthesized by the chemical precipitation method. *Journal of King Saud University - Science* **2018**, 10.1016/j.jksus.2018.01.002, doi:10.1016/j.jksus.2018.01.002.

185. Jung, T.; Kim, J.-N.; Kang, S.-P. Influence of polymeric additives on paraffin wax crystallization in model oils. *Korean Journal of Chemical Engineering* **2016**, *33*, 1813-1822, doi:10.1007/s11814-016-0052-3.

186. Preisig, D.; Haid, D.; Varum, F.J.O.; Bravo, R.; Alles, R.; Huwyler, J.; Puchkov, M. Drug loading into porous calcium carbonate microparticles by solvent evaporation. *European Journal of Pharmaceutics and Biopharmaceutics* **2014**, *87*, 548-558, doi:10.1016/j.ejpb.2014.02.009.

187. Devi, A.; Khatkar, B.S. Physicochemical, rheological and functional properties of fats and oils in relation to cookie quality: a review. *Journal of Food Science and Technology* **2016**, *53*, 3633-3641, doi:10.1007/s13197-016-2355-0.

188. Speight, J.G. Chapter 4 - Test methods for asphalt binders. In *Asphalt Materials Science and Technology*, Speight, J.G., Ed. Butterworth-Heinemann: Boston, 2016; 10.1016/B978-0-12-800273-5.00004-0pp. 137-203.

189. Dorn, M.; e Silva, M.B.; Buriol, L.S.; Lamb, L.C. Three-dimensional protein structure prediction: Methods and computational strategies. *Computational Biology and Chemistry* **2014**, *53*, 251-276, doi:10.1016/j.compbiolchem.2014.10.001.

190. Bonneau, R.; Baker, D. Ab initio protein structure prediction: progress and prospects. *Annual Review of Biophysics and Biomolecular Structure* **2001**, *30*, 173-189, doi:10.1146/annurev.biophys.30.1.173.

191. Ma, J.; Sigler, P.B.; Xu, Z.; Karplus, M. A dynamic model for the allosteric mechanism of GroEL11Edited by A. Fersht. *Journal of Molecular Biology* **2000**, *302*, 303-313, doi:10.1006/jmbi.2000.4014.

192. Beckstein, O.; Biggin, P.C.; Sansom, M.S.P. A hydrophobic gating mechanism for nanopores. *The Journal of Physical Chemistry B* **2001**, *105*, 12902-12905, doi:10.1021/jp012233y.

193. Hospital, A.; Goñi, J.R.; Orozco, M.; Gelpí, J.L. Molecular dynamics simulations: advances and applications. *Advances and applications in bioinformatics and chemistry : AABC* **2015**, *8*, 37-47, doi:10.2147/AABC.S70333.

194. Koshland, D.E.; Némethy, G.; Filmer, D. Comparison of experimental binding data and theoretical models in proteins containing subunits*. *Biochemistry* **1966**, *5*, 365-385, doi:10.1021/bi00865a047.

195. Fenollosa, C.; Otón, M.; Andrio, P.; Cortés, J.; Orozco, M.; Goñi, J.R. SEABED: Small molecule activity scanner web service based. *Bioinformatics* **2015**, *31*, 773-775, doi:10.1093/bioinformatics/btu709.

196. Chaudhuri, R.; Carrillo, O.; Laughton, C.A.; Orozco, M. Application of drug-perturbed essential dynamics/molecular dynamics (ED/MD) to virtual screening and rational drug design. *Journal of Chemical Theory and Computation* **2012**, *8*, 2204-2214, doi:10.1021/ct300223c.

197. Tajkhorshid, E.; Nollert, P.; Jensen, M.Ø.; Miercke, L.J.W.; Connell, J.; Stroud, R.M.; Schulten, K. Control of the selectivity of the aquaporin water channel family by global orientational tuning. *Science* **2002**, *296*, 525, doi:10.1126/science.1067778.

198. Dror, R.O.; Green, H.F.; Valant, C.; Borhani, D.W.; Valcourt, J.R.; Pan, A.C.; Arlow, D.H., et al. Structural basis for modulation of a G-protein-coupled receptor by allosteric drugs. *Nature* **2013**, *503*, 295-299, doi:10.1038/nature12595.

199. Vahed, M.; Neya, S.; Matsuzaki, K.; Hoshino, T. Analysis of physicochemical interaction of Aβ(40) with a GM1 ganglioside-containing lipid membrane. *The Journal of Physical Chemistry B* **2018**, *122*, 3771-3781, doi:10.1021/acs.jpcb.8b00139.

200. Yan, K.-F.; Li, X.-S.; Chen, Z.-Y.; Xia, Z.-M.; Xu, C.-G.; Zhang, Z. Molecular dynamics simulation of the crystal nucleation and growth behavior of methane hydrate in the presence of the surface and nanopores of porous sediment. *Langmuir* **2016**, *32*, 7975-7984, doi:10.1021/acs.langmuir.6b01601.

201. Holte, L.K.; Kuran, B.A.; Richmond, G.L.; Johnson, K.E. Computational modeling of lauric acid at the organic–water Interface. *The Journal of Physical Chemistry C* **2014**, *118*, 10024-10032, doi:10.1021/jp411985c.

202. Haberthür, U.; Caflisch, A. FACTS: Fast analytical continuum treatment of solvation. *Journal of Computational Chemistry* **2008**, *29*, 701-715, doi:10.1002/jcc.20832.

203. Luchko, T.; Gusarov, S.; Roe, D.R.; Simmerling, C.; Case, D.A.; Tuszynski, J.; Kovalenko, A. Three-dimensional molecular theory of solvation coupled with molecular dynamics in Amber. *Journal of Chemical Theory and Computation* **2010**, *6*, 607-624, doi:10.1021/ct900460m.

204. Kleinjung, J.; Fraternali, F. Design and application of implicit solvent models in biomolecular simulations. *Current Opinion in Structural Biology* **2014**, *25*, 126-134, doi:10.1016/j.sbi.2014.04.003.

205. Pérez, A.; Lankas, F.; Luque, F.J.; Orozco, M. Towards a molecular dynamics consensus view of B-DNA flexibility. *Nucleic Acids Research* **2008**, *36*, 2379-2394, doi:10.1093/nar/gkn082.

206. Brooks, B.R.; Brooks, C.L., 3rd; Mackerell, A.D., Jr.; Nilsson, L.; Petrella, R.J.; Roux, B.; Won, Y., et al. CHARMM: the biomolecular simulation program. *Journal of Computational Chemistry* **2009**, *30*, 1545-1614, doi:10.1002/jcc.21287.

207. Hess, B.; Kutzner, C.; van der Spoel, D.; Lindahl, E. GROMACS 4: Algorithms for highly efficient, load-balanced, and scalable molecular simulation. *Journal of Chemical Theory and Computation* **2008**, *4*, 435-447, doi:10.1021/ct700301q.

208. Nelson, M.T.; Humphrey, W.; Gursoy, A.; Dalke, A.; Kalé, L.V.; Skeel, R.D.; Schulten, K. NAMD: a parallel, object-oriented molecular dynamics program. *The International Journal of Supercomputer Applications and High Performance Computing* **1996**, *10*, 251-268, doi:10.1177/109434209601000401.

209. D.A. Case, T.A.D., T.E. Cheatham, III, C.L. Simmerling, J. Wang, R.E. Duke, R. Luo, R.C. Walker, W. Zhang, K.M. Merz, B. Roberts, S. Hayik, A. Roitberg, G. Seabra, J. Swails, A.W. Götz, I. Kolossváry, K.F. Wong, F. Paesani, J. Vanicek, R.M. Wolf, J. Liu, X. Wu, S.R. Brozell, T. Steinbrecher, H. Gohlke, Q. Cai, X. Ye, J. Wang, M.-J. Hsieh, G. Cui, D.R. Roe, D.H. Mathews, M.G. Seetin, R. Salomon-Ferrer, C. Sagui, V. Babin, T. Luchko, S. Gusarov, A. Kovalenko, and P.A. Kollman *AMBER 12*, University of California, San Francisco: 2012.

210. Wang, J.; Wolf, R.M.; Caldwell, J.W.; Kollman, P.A.; Case, D.A. Development and testing of a general amber force field. *Journal of Computational Chemistry* **2004**, *25*, 1157-1174, doi:10.1002/jcc.20035.

211. Salomon-Ferrer, R.; Case, D.A.; Walker, R.C. An overview of the Amber biomolecular simulation package. *WIREs Computational Molecular Science* **2013**, *3*, 198-210, doi:10.1002/wcms.1121.

212. Case, D.A.; Cheatham, T.E., 3rd; Darden, T.; Gohlke, H.; Luo, R.; Merz, K.M., Jr.; Onufriev, A., et al. The Amber biomolecular simulation programs. *Journal of Computational Chemistry* **2005**, *26*, 1668-1688, doi:10.1002/jcc.20290.

213. Sayle, R.A.; Milner-White, E.J. RASMOL: biomolecular graphics for all. *Trends Biochem Sci* **1995**, *20*, 374, doi:10.1016/s0968-0004(00)89080-5.

214. Humphrey, W.; Dalke, A.; Schulten, K. VMD: visual molecular dynamics. *Journal of Molecular Graphics* **1996**, *14*, 33-38, 27-38, doi:10.1016/0263-7855(96)00018-5.

215. Schrodinger, LLC. The PyMOL Molecular Graphics System, Version 1.8. 2015.

216. Rondinini, S. pH measurements in non-aqueous and aqueous–organic solvents – definition of standard procedures. *Analytical and Bioanalytical Chemistry* **2002**, *374*, 813-816, doi:10.1007/s00216-002-1455-z.

217. Domínguez de María, P.; Fernández-Álvaro, E.; ten Kate, A.; Bargeman, G. Role of apparent pKa of carboxylic acids in lipase-catalyzed esterifications in biphasic systems. *Journal of Molecular Catalysis B: Enzymatic* **2009**, *59*, 220-224, doi:10.1016/j.molcatb.2009.03.004.

218. Rodenbush, C.M.; Hsieh, F.H.; Viswanath, D.S. Density and viscosity of vegetable oils. *Journal of the American Oil Chemists Society* **1999**, *76*, 1415-1419.

219. Obeidat, A.; Jaradat, A.; Hamdan, B.; Abu-Ghazleh, H. Effect of cutoff radius, long range interaction and temperature controller on thermodynamic properties of fluids: Methanol as an example. *Physica A: Statistical Mechanics and its Applications* **2018**, *496*, 243-248, doi:10.1016/j.physa.2018.01.001.

220. Kahwaji, S.; Johnson, M.B.; Kheirabadi, A.C.; Groulx, D.; White, M.A. Fatty acids and related phase change materials for reliable thermal energy storage at moderate temperatures. *Solar Energy Materials and Solar Cells* **2017**, *167*, 109-120, doi:10.1016/j.solmat.2017.03.038.

221. Stainsby, G.; Alexander, A.E. Studies of soap solutions. Part I. The fatty acid soaps and their hydrolysis in aqueous solutions. *Transactions of the Faraday Society* **1949**, *45*, 585-597, doi:10.1039/TF9494500585.

222. Mukerjee, P.; Mysels, K.J.; Dulin, C.I. Dilute solutions of amphipathic ions. I. conductivity of strong salts and dimerization. *The Journal of Physical Chemistry* **1958**, *62*, 1390-1396, doi:10.1021/j150569a010.

223. Craven, D.M.S.B.M. Physical properties of fatty acids and their extracellular and intracellular distribution. In *Polyunsaturated Fatty Acids in Human Nutrition*, Workshop, N.N., Ed. Nestec Ltd., Vevey/Raven Press. Ltd.. New York, 1992; Vol. 28, pp. 25-39.

224. Stewart, R.; Jones, J.R. Ionization of dimethyl sulfoxide. *Journal of the American Chemical Society* **1967**, *89*, 5069-5071, doi:10.1021/ja00995a059.

225. Eiteman, M.A.; Goodrum, J.W. Density and viscosity of low-molecular weight triglycerides and their mixtures. *Journal of the American Oil Chemists Society* **1994**, *71*, 1261, doi:10.1007/BF02540548.

226. *The Merck Index: An encyclopedia of chemicals, drugs, and biologicals*; O'Neil, M.J., Ed. Royal Society of Chemistry, Cambridge: UK, 2013; pp. 2708.

227. Wagh, V.D.; Deshmukh, K.H.; Wagh, K.V. Formulation and evaluation of *in situ* gel drug delivery system of sesbania grandiflora flower extract for the treatment of bacterial conjunctivitis. *Journal of Pharmaceutical Sciences & Research* **2012**, *4*, 1880-1884.

228. Small, D.M. The physical chemistry of lipids : from Alkanes to phospholipids. In *Handbook of lipid research*, Plenum Press: New York, 1986; Vol. 4, p. 264.

229. Gad, H.A.; El-Nabarawi, M.A.; Abd El-Hady, S.S. Formulation and evaluation of PLA and PLGA *in situ* implants containing secnidazole and/or doxycycline for

treatment of periodontitis. *American Association of Pharmaceutical Scientists journal* **2008**, *9*, 878, doi:10.1208/s12249-008-9126-9.

230. Iwahashi, M.; Takebayashi, S.; Taguchi, M.; Kasahara, Y.; Minami, H.; Matsuzawa, H. Dynamical dimer structure and liquid structure of fatty acids in their binary liquid mixture: decanoic/octadecanoic acid and decanoic/dodecanoic acid systems. *Chemistry and Physics of Lipids* **2005**, *133*, 113-124, doi:10.1016/j.chemphyslip.2004.09.022.

231. Phaechamud, T.; Thurein, S.M.; Chantadee, T. Role of clove oil in solvent exchange-induced doxycycline hyclate-loaded Eudragit RS *in situ* forming gel. *Asian Journal of Pharmaceutical Sciences* **2018**, *13*, 131-142, doi:10.1016/j.ajps.2017.09.004.

232. Elnaggar, Y.S.R.; El-Refaie, W.M.; El-Massik, M.A.; Abdallah, O.Y. Lecithin-based nanostructured gels for skin delivery: An update on state of art and recent applications. *Journal of Controlled Release* **2014**, *180*, 10-24, doi:10.1016/j.jconrel.2014.02.004.

233. Raphaelides, S.N.; Georgiadis, N. Effect of fatty acids on the rheological behaviour of amylomaize starch dispersions during heating. *Food Research International* **2008**, *41*, 75-88, doi:10.1016/j.foodres.2007.10.004.

234. Meng, S.; Ma, Y.; Sun, D.-W.; Wang, L.; Liu, T. Properties of starch-palmitic acid complexes prepared by high pressure homogenization. *Journal of Cereal Science* **2014**, *59*, 25-32, doi:10.1016/j.jcs.2013.10.012.

235. Viken, A.L.; Spildo, K.; Reichenbach-Klinke, R.; Djurhuus, K.; Skauge, T. Influence of weak hydrophobic interactions on *in situ* viscosity of a hydrophobically modified water-soluble polymer. *Energy & Fuels* **2018**, *32*, 89-98, doi:10.1021/acs.energyfuels.7b02573.

236. Liang, Y.; Yuan, X.; Wang, L.; Zhou, X.; Ren, X.; Huang, Y.; Zhang, M.; Wu, J.; Wen, W. Highly stable and efficient electrorheological suspensions with hydrophobic interaction. *Journal of Colloid and Interface Science* **2020**, *564*, 381-391, doi:10.1016/j.jcis.2019.12.129.

237. George, J.; Sastry, N.V. Densities, viscosities, speeds of sound, and relative permittivities for water + cyclic amides (2-pyrrolidinone, 1-methyl-2-pyrrolidinone, and 1-vinyl-2-pyrrolidinone) at different temperatures. *Journal of Chemical & Engineering Data* **2004**, *49*, 235-242, doi:10.1021/je0340809.

238. Gokulanathan, S.; Balan, N.; Aravind, R.; Thangavelu, K. Patient compliance and supportive periodontal therapy: Study among young adults of Namakkal district. *Journal of Pharmacy And Bioallied Sciences* **2014**, *6*, 171-173, doi:10.4103/0975-7406.137443.

239. Philippot, P.; Lenoir, N.; D'Hoore, W.; Bercy, P. Improving patients' compliance with the treatment of periodontitis: a controlled study of behavioural intervention. *Journal of Clinical Periodontology* **2005**, *32*, 653-658, doi:10.1111/j.1600-051X.2005.00732.x.

240. Phaechamud, T.; Mahadlek, J.; Chuenbarn, T. *In situ* forming gel comprising bleached shellac loaded with antimicrobial drugs for periodontitis treatment. *Materials & Design* **2016**, *89*, 294-303, doi:10.1016/j.matdes.2015.09.138.

241. **!!! INVALID CITATION !!!** .

242. Yamamoto, S.; Saeki, T.; Inoshita, T. Drying of gelled sugar solutions - Water diffusion behavior. *Chemical Engineering Journal* **2002**, *86*, 179-184, doi:10.1016/S1385-8947(01)00286-8.

243. Hachiya, I.; Koyano, T.; Sato, K. Seeding effects on solidification behavior of cocoa butter and dark chocolate. I. Kinetics of solidification. *Journal of the American Oil Chemists Society* **1989**, *66*, 1757-1762, doi:10.1007/BF02660743.

244. Himawan, C.; Starov, V.M.; Stapley, A.G.F. Thermodynamic and kinetic aspects of fat crystallization. *Advances in Colloid and Interface Science* **2006**, *122*, 3-33, doi:10.1016/j.cis.2006.06.016.

245. Yang, L.; Fassihi, R. Examination of drug solubility, polymer types, hydrodynamics and loading dose on drug release behavior from a triple-layer asymmetric configuration delivery system. *International Journal of Pharmaceutics* **1997**, *155*, 219-229, doi:10.1016/S0378-5173(97)00164-6.

246. Reza, M.S.; Quadir, M.A.; Haider, S.S. Comparative evaluation of plastic, hydrophobic and hydrophilic polymers as matrices for controlled-release drug delivery. *Journal of Pharmacy and Pharmaceutical Sciences* **2003**, *6*, 282-291.

247. Phaechamud, T.; Senarat, S.; Puyathorn, N.; Praphanwittaya, P. Solvent exchange and drug release characteristics of doxycycline hyclate-loaded bleached shellac *in situ*-forming gel and -microparticle. *International Journal of Biological Macromolecules* **2019**, *135*, 1261-1272, doi:10.1016/j.ijbiomac.2018.11.098.

248. Cumming, H.; Rücker, C. Octanol–water partition coefficient measurement by a simple 1H NMR method. *ACS Omega* **2017**, *2*, 6244-6249, doi:10.1021/acsomega.7b01102.

249. Sasaki, H.; Kojima, M.; Mori, Y.; Nakamura, J.; Shibasaki, J. Enhancing effect of pyrrolidone derivatives on transdermal drug delivery. I. *International Journal of Pharmaceutics* **1988**, *44*, 15-24, doi:https://doi.org/10.1016/0378-5173(88)90095-6.

250. Goto, M.; Asada, E. The crystal structure of the A-super form of lauric acid. *Bulletin of the Chemical Society of Japan* **1978**, *51*, 70-74, doi:10.1246/bcsj.51.70.

251. Vand, V.; Morley, W.M.; Lomer, T.R. The crystal sructure of lauric acid. *Acta Crystallographica* **1951**, *4*, 324-329, doi:10.1107/S0365110X51001069.

252. Ghaedi, H.; Ayoub, M.; Sufian, S.; Lal, B.; Uemura, Y. Thermal stability and FT-IR analysis of Phosphonium-based deep eutectic solvents with different hydrogen bond donors. *Journal of Molecular Liquids* **2017**, *242*, 395-403, doi:10.1016/j.molliq.2017.07.016.

253. Zhang, Y.; Li, C.; Yang, M.; Jia, D.; Wang, Y.; Li, B.; Hou, Y.; Zhang, N.; Wu, Q. Experimental evaluation of cooling performance by friction coefficient and specific friction energy in nanofluid minimum quantity lubrication grinding with different types of vegetable oil. *Journal of Cleaner Production* **2016**, *139*, 685-705, doi:10.1016/j.jclepro.2016.08.073.

254. Fakhari, A.; Phan, Q.; Thakkar, S.V.; Middaugh, C.R.; Berkland, C. Hyaluronic acid nanoparticles titrate the viscoelastic properties of viscosupplements. *Langmuir* **2013**, *29*, 5123-5131, doi:10.1021/la304575x.

255. Borzacchiello, A.; Russo, L.; Malle, B.; Schwach-Abdellaoui, K.; Ambrosio, L. Hyaluronic acid based hydrogels for regenerative medicine applications. *BioMed Research International* **2015**, *2015*, 1-12, doi:10.1155/2015/871218.

256. Resende, A.F.C.; Pereira, A.F.; Moreira, T.P.; Patricio, P.S.O.; Fialho, S.L.; Cunha, G.M.F.; Silva-Cunha, A.; Magalhaes, J.T.; Silva, G.R. PLGA Implants containing vancomycin and dexamethasone: development, characterization and bactericidal effects. *Pharmazie* **2016**, *71*, 439-446, doi:10.1691/ph.2016.6009.

257. Darestani-Farahani, M.; Vasheghani-Farahani, E.; Mobedi, H.; Ganji, F. The effect of solvent composition on vancomycin hydrochloride and free base vancomycin release from *in situ* forming implants: The effect of solvent composition on vancomycin release from ISI. *Polymers for Advanced Technologies* **2016**, 10.1002/pat.3845, doi:10.1002/pat.3845.

258. Shoaib, M.H.; Tazeen, J.; Merchant, H.A.; Yousuf, R.I. Evaluation of drug release kinetics from ibuprofen matrix tablets using HPMC. *Pakistan Journal of Pharmaceutical Sciences* **2006**, *19*, 119-124.

259. Perioli, L.; Ambrogi, V.; Rubini, D.; Giovagnoli, S.; Ricci, M.; Blasi, P.; Rossi, C. Novel mucoadhesive buccal formulation containing metronidazole for the treatment of periodontal disease. *Journal of Controlled Release* **2004**, *95*, 521-533, doi:10.1016/j.jconrel.2003.12.018.

260. Pahwa, R.; Piplani, M.; Garg, V.K.; Rao, R.; Lamba, H.S. Formulation and evaluation of orally disintegrating tablets: Comparison of natural and synthetic superdisintegrants. *Der Pharmacia Lettre* **2011**, *3*, 407-418.

261. Du, L.; Yang, S.; Li, W.; Li, H.; Feng, S.; Zeng, R.; Yu, B., et al. Scaffold composed of porous vancomycin-loaded poly(lactide-co-glycolide) microspheres: A controlled-release drug delivery system with shape-memory effect. *Materials Science and Engineering: C* **2017**, *78*, 1172-1178, doi:10.1016/j.msec.2017.04.099.

262. Men, P.; Li, H.-B.; Zhai, S.-D.; Zhao, R.-S. Association between the AUC0-24/MIC ratio of vancomycin and its clinical effectiveness: A systematic review and meta-analysis. *PloS One* **2016**, *11*, e0146224-e0146224, doi:10.1371/journal.pone.0146224.

263. Prybylski, J.P. Vancomycin trough concentration as a predictor of clinical outcomes in patients with *Staphylococcus aureus* bacteremia: A meta-analysis of observational studies. *Pharmacotherapy: The Journal of Human Pharmacology and Drug Therapy* **2015**, *35*, 889-898, doi:10.1002/phar.1638.

264. Reineke, K.; Mathys, A.; Knorr, D. Shift of pH-value during thermal treatments in buffer solutions and selected foods. *International Journal of Food Properties* **2011**, *14*, 870-881, doi:10.1080/10942910903456978.

265. Nagai, H.; Kuwabara, K.; Carta, G. Temperature dependence of the dissociation constants of several amino acids. *Journal of Chemical & Engineering Data* **2008**, *53*, 619-627, doi:10.1021/je700067a.

266. Reijenga, J.; van Hoof, A.; van Loon, A.; Teunissen, B. Development of methods for the determination of pKa values. *Analytical Chemistry Insights* **2013**, *8*, 53-71, doi:10.4137/ACI.S12304.

267. Rahman, M.A.; Ghosh, A.K.; Bose, R.N. Dissociation constants of long chain fatty acids in methanol-water and ethanol-water mixtures. *Journal of Chemical Technology and Biotechnology* **1979**, *29*, 158-162, doi:10.1002/jctb.503290307.

268. Pure, I.U.o.; IUP., A.C. *Ionisation constants of organic acids in aqueous solution*; Oxford, Pergamon Press: 1979.

269. Umerska, A.; Cassisa, V.; Matougui, N.; Joly-Guillou, M.-L.; Eveillard, M.; Saulnier, P. Antibacterial action of lipid nanocapsules containing fatty acids or monoglycerides as co-surfactants. *European Journal of Pharmaceutics and Biopharmaceutics* **2016**, *108*, 100-110, doi:10.1016/j.ejpb.2016.09.001.

270. Ibarguren, M.; Lopez, D.J.; Escriba, P.V. The effect of natural and synthetic fatty acids on membrane structure, microdomain organization, cellular functions and human health. *Biochim Biophys Acta* **2014**, *1838*, 1518-1528, doi:10.1016/j.bbamem.2013.12.021.

271. Phaechamud, T.; Mahadlek, J.; Aroonrerk, N.; Choopun, S.; Charoenteeraboon, J. Antimicrobial activity of ZnO-doxycycline hyclate thermosensitive gel. *ScienceAsia* **2012**, *38*, 64-74, doi:10.2306/scienceasia1513-1874.2012.38.064.

272. Nitbani, F.O.; Jumina; Siswanta, D.; Solikhah, E.N. Isolation and antibacterial activity test of lauric acid from crude coconut oil (*Cocos nucifera L.*). *Procedia Chemistry* **2016**, *18*, 132-140, doi:10.1016/j.proche.2016.01.021.

273. Salleh, E.; Muhammad, I.I.; Pahlawi, Q.A. Spectrum activity and lauric acid release behaviour of antimicrobial starch-based film. *Procedia Chemistry* **2014**, *9*, 11-22, doi:10.1016/j.proche.2014.05.003.

274. Citron, D.M.; Tyrrell, K.L.; Merriam, C.V.; Goldstein, E.J.C. *In vitro* activities of CB-183,315, vancomycin, and metronidazole against 556 strains of *Clostridium difficile*, 445 other intestinal anaerobes, and 56 *Enterobacteriaceae* species. *Antimicrobial agents and chemotherapy* **2012**, *56*, 1613-1615, doi:10.1128/AAC.05655-11.

275. Bevilacqua, L.; Biasi, M.D.; Lorenzon, M.G.; Frattini, C.; Angerame, D. Volumetric analysis of gingival crevicular fluid and peri-implant sulcus fluid in healthy and diseased sites: A cross-sectional split-mouth pilot study. *The open dentistry journal* **2016**, *10*, 131-138, doi:10.2174/1874210601610010131.

276. Zhang, X.; Yang, L.; Zhang, C.; Liu, D.; Meng, S.; Zhang, W.; Meng, S. Effect of polymer permeability and solvent removal rate on *in situ* forming implants: drug burst release and microstructure. *Pharmaceutics* **2019**, *11*, 520, doi:10.3390/pharmaceutics11100520.

277. Takayama, K.; Kawakami, Y.; Kobayashi, M.; Greco, N.; Cummins, J.H.; Matsushita, T.; Kuroda, R., et al. Local intra-articular injection of rapamycin delays articular cartilage degeneration in a murine model of osteoarthritis. *Arthritis Research & Therapy* **2014**, *16*, 482-482, doi:10.1186/s13075-014-0482-4.

278. Micromedex. Dimethyl Sulfoxide. Thomson Micromedex.: Greenwood Village, CO, 2020.

279. Moore, R.M., Walesby, H.A. Pharmacotherapy of joint and tendon disease. In *Equine Sports Medicine and Surgery*, 2004; 10.1016/B978-0-7020-2671-3.50027-1pp. 486-514.

280. Elmoazzen, H.Y.; Poovadan, A.; Law, G.K.; Elliott, J.A.W.; McGann, L.E.; Jomha, N.M. Dimethyl sulfoxide toxicity kinetics in intact articular cartilage. *Cell and Tissue Banking* **2006**, *8*, 125, doi:10.1007/s10561-006-9023-y.

281. Guinan, J.; Wang, S.; Hazbun, T.R.; Yadav, H.; Thangamani, S. Antibiotic-induced decreases in the levels of microbial-derived short-chain fatty acids correlate with increased gastrointestinal colonization of *Candida albicans*. *Scientific Reports* **2019**, *9*, 8872, doi:10.1038/s41598-019-45467-7.

282. Sy Mohamad, S.F.; Mohamad, S.; Aziz, A.A. The susceptibility of aphids, aphis gossypii glover to lauric acid based natural pesticide. *Procedia Engineering* **2013**, *53*, 20-28, doi:10.1016/j.proeng.2013.02.004.

283. Pletnev, M. Chemistry of surfactants, in: surfactants - chemistry, interfacial properties and application (studies in interface science, Vol. 13). Ed. by V.B. Fainerman, D. Möbius, and R. Miller, Elsevier Publishing, Amsterdam, 2001, pp. 1-98. 2015.

284. Fowkes, F.M. Acid–base interactions in polymer adhesion. In *Physicochemical Aspects of Polymer Surfaces*, Kittal, K.L., Ed. Plenum Press: 1983; Vol. 2, pp. 583-603.

285. Danov, K.D.; Kralchevsky, P.A.; Ananthapadmanabhan, K.P.; Lips, A. Interpretation of surface-tension isotherms of n-alkanoic (fatty) acids by means of the van der Waals model. *Journal of Colloid and Interface Science* **2006**, *300*, 809-813, doi:10.1016/j.jcis.2006.04.026.

286. Ahn, C.; Morya, V.K.; Kim, E.-K. Tuning surface-active properties of bio-surfactant sophorolipids by varying fatty-acid chain lengths. *Korean Journal of Chemical Engineering* **2016**, *33*, 2127-2133, doi:10.1007/s11814-016-0082-x.

287. Jeon, C.W.; Park, S.; Bang, J.H.; Chae, S.; Song, K.; Lee, S.W. Nonpolar surface modification using fatty acids and its effect on calcite from mineral carbonation of desulfurized gypsum. *Coatings* **2018**, *8*, doi:10.3390/coatings8010043.

288. Moelbert, S.; Normand, B.; De Los Rios, P. Kosmotropes and chaotropes: modelling preferential exclusion, binding and aggregate stability. *Biophysical Chemistry* **2004**, *112*, 45-57, doi:10.1016/j.bpc.2004.06.012.

289. dos Santos, A.P.; Levin, Y. Surface and interfacial tensions of Hofmeister electrolytes. *Faraday Discussions* **2013**, *160*, 75-87, doi:10.1039/C2FD20067H.

290. Pimienta, V.; Lavabre, D.; Buhse, T.; Micheau, J.-C. Correlation between electric potential and interfacial tension oscillations in a water-oil-water system. *The Journal of Physical Chemistry B* **2004**, *108*, 7331-7336, doi:10.1021/jp0374859.

291. Roger, K.; Cabane, B. Why are hydrophobic/water interfaces negatively charged? *Angewandte Chemie International Edition* **2012**, *51*, 5625-5628, doi:10.1002/anie.201108228.

292. Pashkovskaya, A.A.; Vazdar, M.; Zimmermann, L.; Jovanovic, O.; Pohl, P.; Pohl, E.E. Mechanism of long-chain free fatty acid protonation at the membrane-water interface. *Biophysical Journal* **2018**, *114*, 2142-2151, doi:10.1016/j.bpj.2018.04.011.

293. Chantadee, T.; Santimaleeworagun, W.; Phorom, Y.; Chuenbarn, T.; Phaechamud, T. Vancomycin HCl-loaded lauric acid *in situ*-forming gel with phase inversion for periodontitis treatment. *Journal of Drug Delivery Science and Technology* **2020**, *57*, 101615, doi:10.1016/j.jddst.2020.101615.

294. Chantadee, T.; Sawangsri, P.; Santimaleeworagun, W.; Phaechamud, T. Vancomycin hydrochloride-loaded stearic acid/lauric acid *in situ* forming matrix for antimicrobial inhibition in patients with joint infection after total knee arthroplasty. *Materials Science and Engineering: C* **2020**, *115*, 110761, doi:10.1016/j.msec.2020.110761.
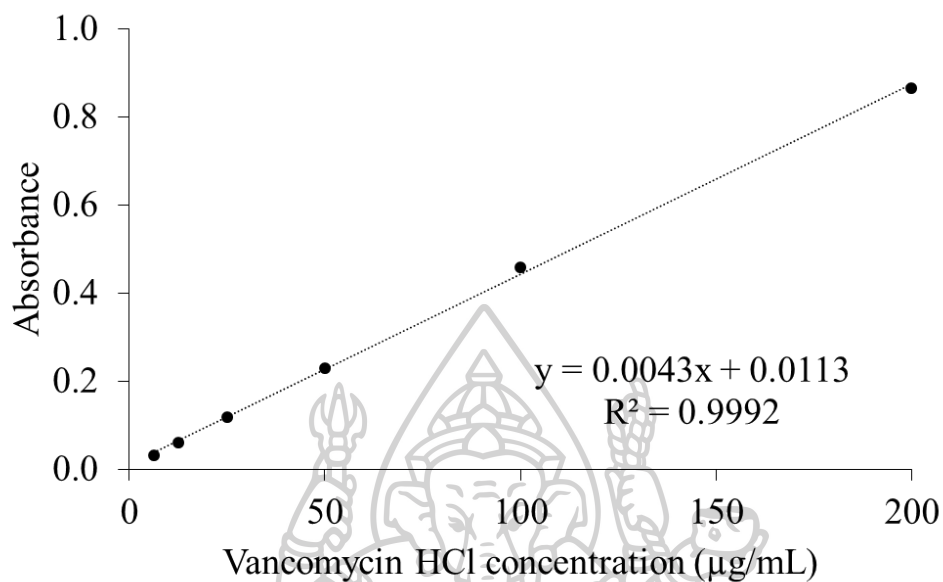
APPENDICES

Appendix I: **Calibration curve for *in vitro* release study**

Figure 43 Calibration curve of VCM in phosphate buffer pH 6.8 for the in vitro release study (UV-vis at 280 nm)
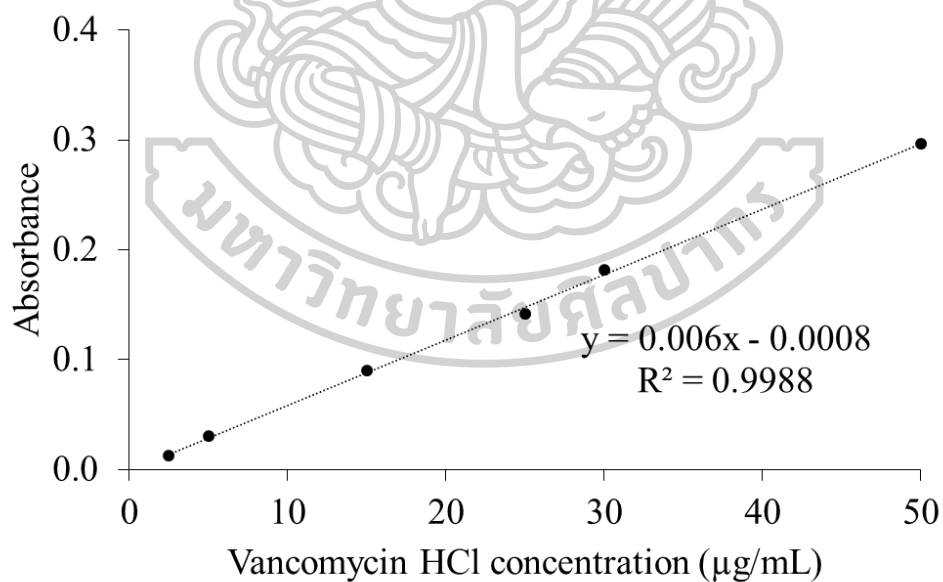

Figure 44 Calibration curve of VCM in phosphate buffer pH 7.4 for the in vitro release study (UV-vis at 280 nm)
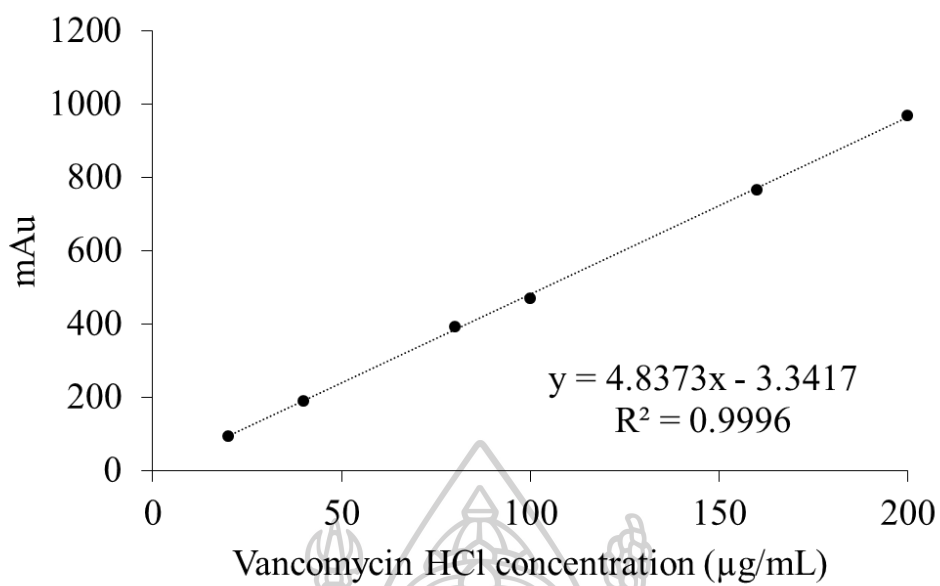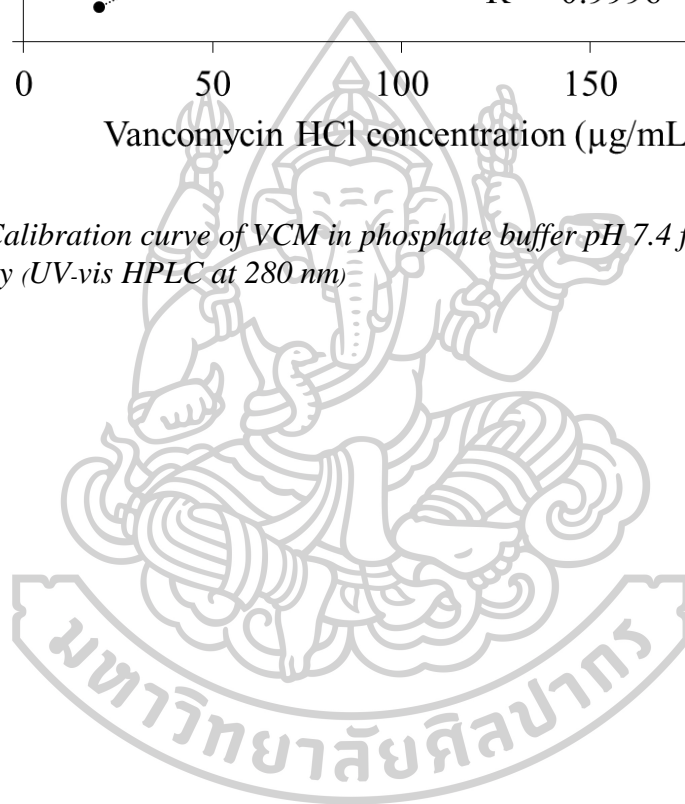
Figure 45 Calibration curve of VCM in phosphate buffer pH 7.4 for the in vitro release study (UV-vis HPLC at 280 nm)
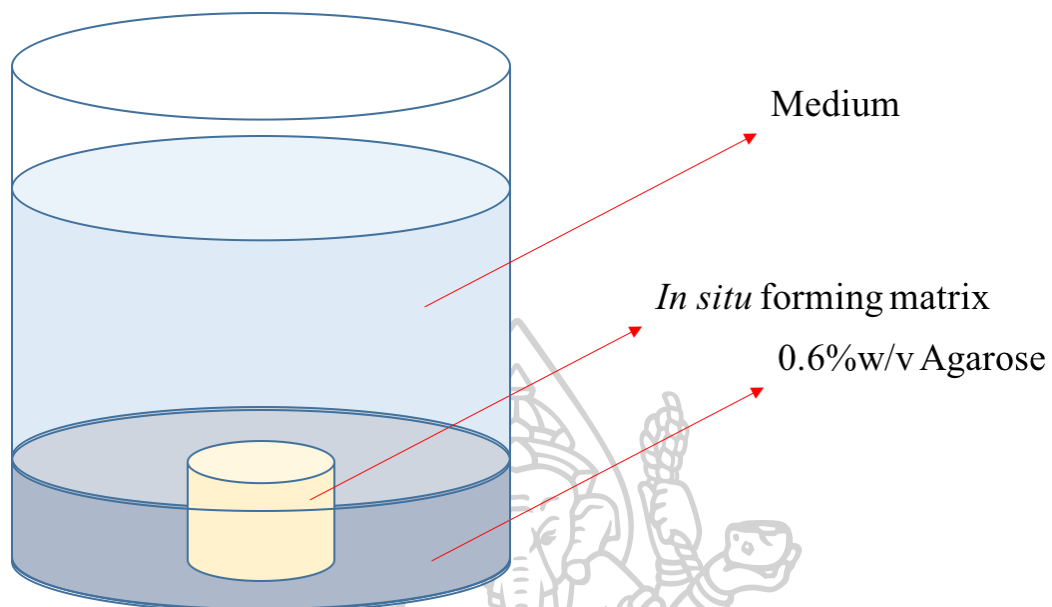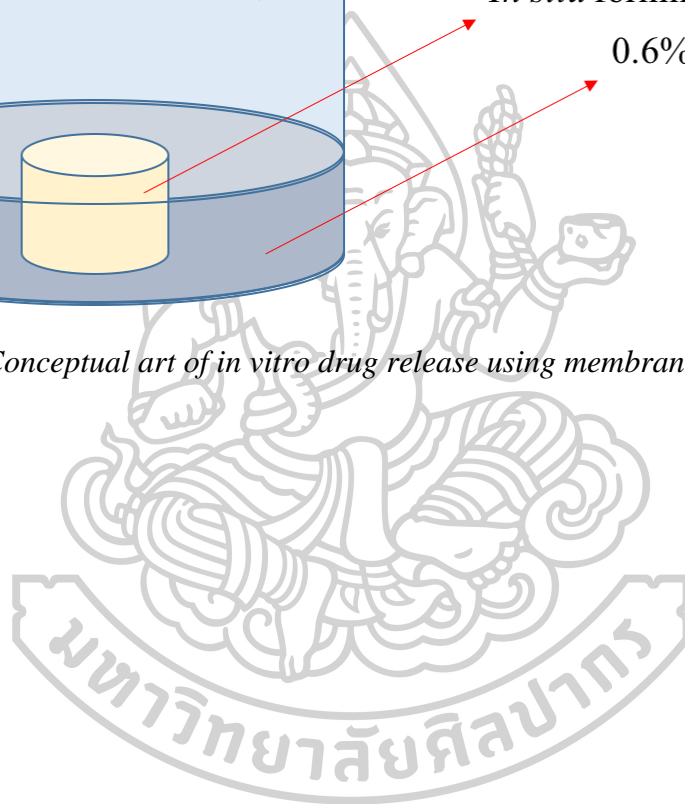
Appendix II: *In vitro* **drug release using membraneless method**

Medium

In situ forming matrix

0.6%w/v Agarose

Figure 46 Conceptual art of in vitro drug release using membraneless method

Appendix III: Computational modelling

Force field generation

/home/RandD/Linux_x86_64/amber16/bin/antechamber -i *molecule-charge*.log if gout -o *molecule*.prep -

fo prepi -c resp -rn *XXX*(residue name, 3 characters) -at gaff2

$AMBERHOME/bin/parmchk -i *molecule-charge*.prep -f prepi -o *molecule-charge*.frcmod

LEAP

source leaprc.protein.ff14SB

source leaprc.water.tip3p

source leaprc.gaff source leaprc.gaff2

loadamberprep *fatty acid*.prep

loadamberprep *VCM*.prep

loadamberprep *Solvent*.prep

Lipids = loadpdb *model (Fatty acid-VCM-Solvent)*.pdb

solvateBox Lipids TIP3PBOX 10.0

frcmod_*XXX(residue name of fat)* = loadamberparams *fatty acid*.frcmod

frcmod_*VCM* = loadamberparams *VCM*.frcmod

frcmod_ *XXX(residue name of solvent)*= loadamberparams *solvent*.frcmod

loadAmberparams frcmod.ionsjc_tip3p

solvateBox Lipids TIP3PBOX 10.0
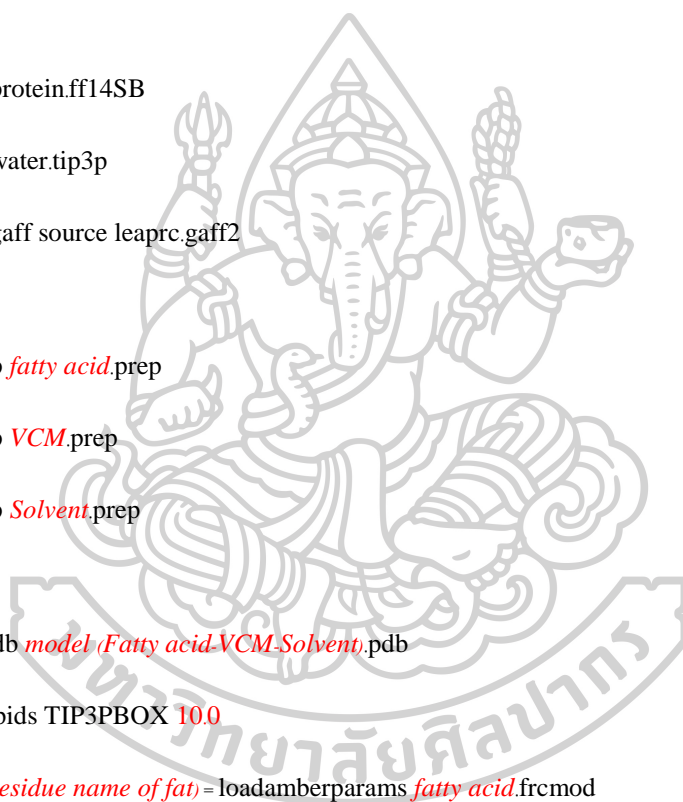
addions Lipids Na+ 0.0

addions Lipids Cl- 0.0

saveamberparm Lipids *MODEL*.top *MODEL*.crd

savepdb Lipids *MODEL*.pdb   quit

Heating

heat.in

```
#heating,
&cntrl
   irest=0, ntx=1,
   nstlim=50000,
   ntpr=5000, ntwr=50000, ntwx=50000,
   t=0.0, dt=0.0020, vlimit=20.0,
   ntt=1, tautp=0.2,
   ntb=1, ntp=0, ntc=2, ntf=2,
   cut=12.0, iwrap=1, nmropt=1,
 &end
 &wt type='TEMP0', istep1=0,istep2=50000,
      value1=0.0,value2=310.0, /
 &wt type='END' /
```

heat_NPT.in

```
# equilibrating
 &cntrl
   irest=1, ntx=5, ntr=0,
   nstlim=200000,
```

```
        ntpr=5000, ntwr=50000,  ntwx=50000,

        t=0.0, dt=0.0020, vlimit=20.0,

        ntt=1, temp0=310.0, tautp=0.5,

        ntb=2, ntp=1, ntc=2, ntf=2,

        cut=12.0, iwrap=1,

     &end
```

Minimization

Minwat.in

```
# minimization
 &cntrl
    irest=0, ntx=1, ibelly=1,

    imin=1, ntmin=1,

    maxcyc=20000, ncyc=10000,

    ntpr=1000, ntwr=5000, ntwx=5000,

    t=0.0, dt=0.0010, vlimit=20.0,

    ntt=1,

    ntb=1, ntp=0,

    ntc=1, tol=0.0005, ntf=1,

    cut=12.0,

    bellymask=":WAT",

 &end
```

Minall.in

```
# minimization
 &cntrl
    irest=0, ntx=1, ibelly=0,
```
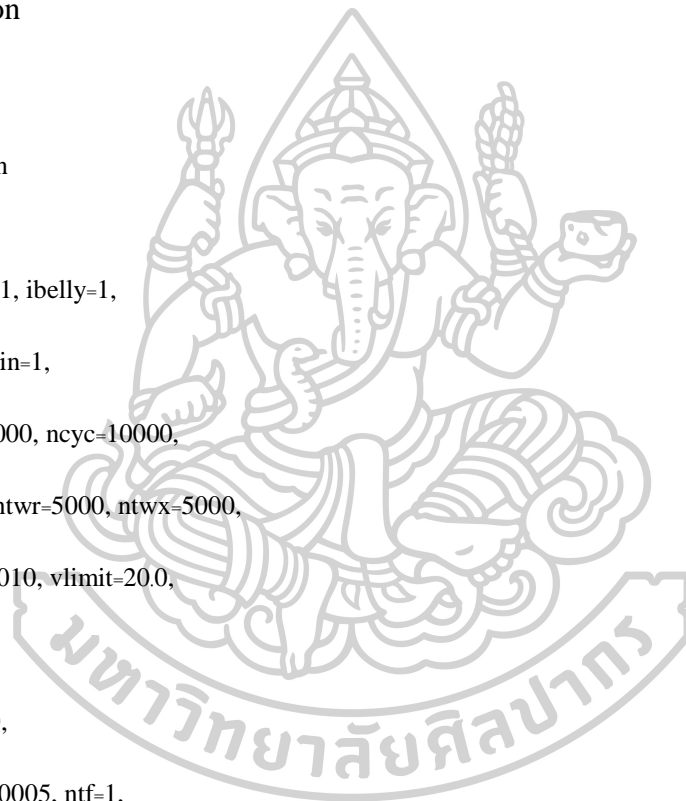
imin=1, ntmin=1,

maxcyc=20000, ncyc=10000,

ntpr=1000, ntwr=5000, ntwx=5000,

t=0.0, dt=0.0010, vlimit=20.0,

ntt=1,

ntb=1, ntp=0,

ntc=1, tol=0.0005, ntf=1,

cut=12.0,

&end

Run minimization

    set AMBER_DIR = '/home/RandD/Linux_x86_64/amber16/bin'

    set MPI_DIR = '/home/RandD/Linux_x86_64/openmpi-1.4.2/bin'

    setenv LD_LIBRARY_PATH /home/RandD/Linux_x86_64/openmpi-

1.4.2/lib:/home/RandD/Linux_x86_64/intel/composer_2011/mkl/lib/intel64:/home/RandD/Linux_x86_64/i

ntel/composer_2011/lib/intel64:${LD_LIBRARY_PATH}

    set BASENAME = 'MODEL'

minimization for water only

    set FILENAME = 'minWAT'

    set INPCOORD = 'MODEL.crd'

    ${MPI_DIR}/mpirun -np 8 ${AMBER_DIR}/sander.MPI -O \

     -i ${FILENAME}.in \

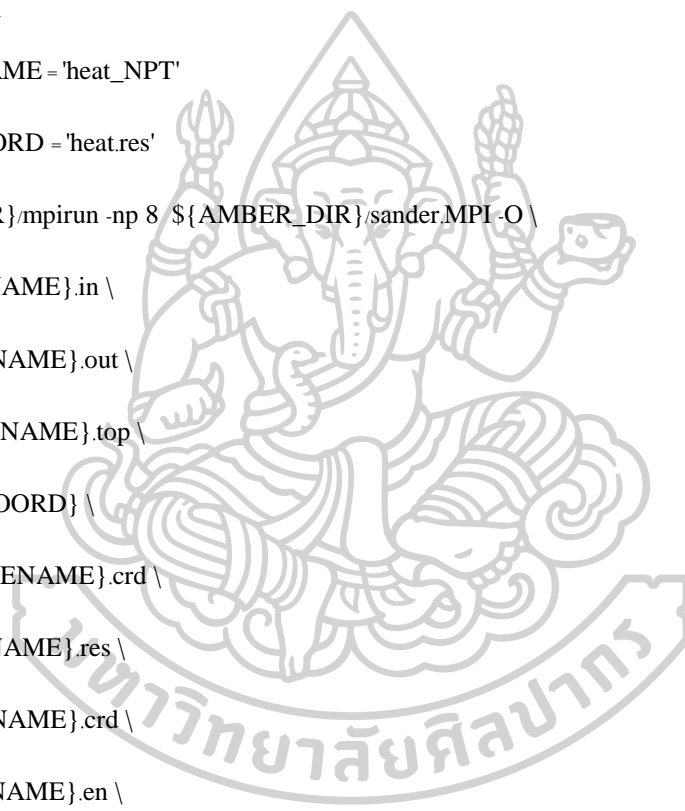   -o ${FILENAME}.out \

```
    -p ${BASENAME}.top \

    -c ${INPCOORD} \

    -ref ${BASENAME}.crd \

    -r ${FILENAME}.res          || goto error


# minimization for all

  set FILENAME = 'minALL'

  set INPCOORD = 'minWAT.res'

  ${MPI_DIR}/mpirun -np 8  ${AMBER_DIR}/sander.MPI -O \

    -i ${FILENAME}.in \

    -o ${FILENAME}.out \

    -p ${BASENAME}.top \

    -c ${INPCOORD} \

    -ref ${BASENAME}.crd \

    -r ${FILENAME}.res          || goto error


# heating

  set FILENAME = 'heat'

  set INPCOORD = 'minALL.res'

  ${MPI_DIR}/mpirun -np 8  ${AMBER_DIR}/sander.MPI -O \

    -i ${FILENAME}.in \

    -o ${FILENAME}.out \

    -p ${BASENAME}.top \

    -c ${INPCOORD} \

    -ref ${BASENAME}.crd \
```
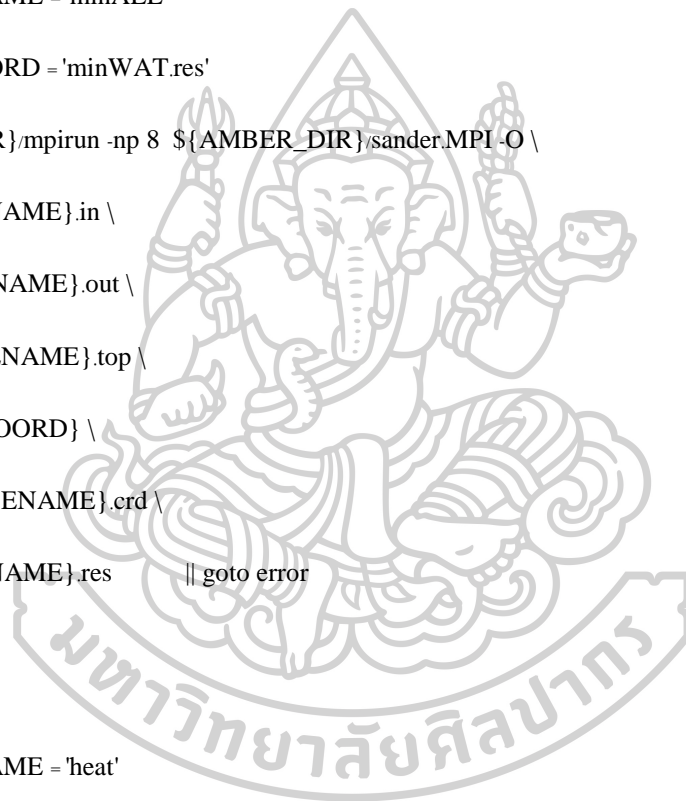
```
    -r ${FILENAME}.res \

    -x ${FILENAME}.crd \

    -e ${FILENAME}.en \

    -v ${FILENAME}.vel \

    -inf ${FILENAME}.info || goto error


# equilibration
  set FILENAME = 'heat_NPT'

  set INPCOORD = 'heat.res'

  ${MPI_DIR}/mpirun -np 8  ${AMBER_DIR}/sander.MPI -O \

   -i ${FILENAME}.in \

   -o ${FILENAME}.out \

   -p ${BASENAME}.top \

   -c ${INPCOORD} \

   -ref ${BASENAME}.crd \

   -r ${FILENAME}.res \

   -x ${FILENAME}.crd \

   -e ${FILENAME}.en \

   -v ${FILENAME}.vel \

   -inf ${FILENAME}.info || goto error



echo "No errors reported"

exit(0)
```

error:

echo " --Program failed - fix problem and run this script again"

exit(1)

Simulation production

set AMBER_DIR = '/home/RandD/Linux_x86_64/amber16'

  setenv LD_LIBRARY_PATH /home/RandD/Linux_x86_64/cuda-

8.0/lib64:/home/RandD/Linux_x86_64/intel/composer_2011/mkl/lib/intel64:/home/RandD/Linux_x86_64/

intel/composer_2011/lib/intel64:${LD_LIBRARY_PATH}

  setenv CUDA_VISIBLE_DEVICES 0

  set BASENAME = 'MODEL'

  set REFCOORD = 'heat_NPT.crd'

production run

set LASTNAME = "heat_NPT.res"

set NUM = 1

while (${NUM} <= 10)

    set NUM = `printf '%02d' ${NUM}`

    set FILENAME = "${BASENAME}-MD${NUM}"

    cp MD310K.in "${FILENAME}.in"

    echo "EQUILIBRATING: ${FILENAME}"

```
if (-f ${FILENAME}.res) then

    set LASTNAME = ${FILENAME}.res

    set NUM = `expr ${NUM} + 1`

    continue

endif


 ${AMBER_DIR}/bin/pmemd.cuda -O \

-i ${FILENAME}.in \

-o ${FILENAME}.out \

-p ${BASENAME}.top \

-c ${LASTNAME} \

-r ${FILENAME}.res \

-ref ${REFCOORD} \

-x ${FILENAME}.crd \

-e ${FILENAME}.en \

-v ${FILENAME}.vel \

-inf ${FILENAME}.info || goto error


set LASTNAME = "${FILENAME}.res"


set NUM = `expr ${NUM} + 1`

end
```
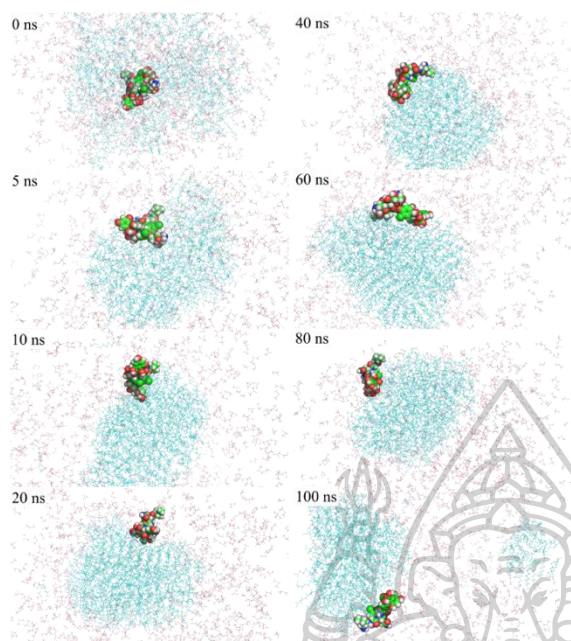
Figure 47 Snapshot structures at 0, 5, 10, 20, 40, 60, 80 and 100 ns of the MD simulation on the in situ formation process of VCPRD
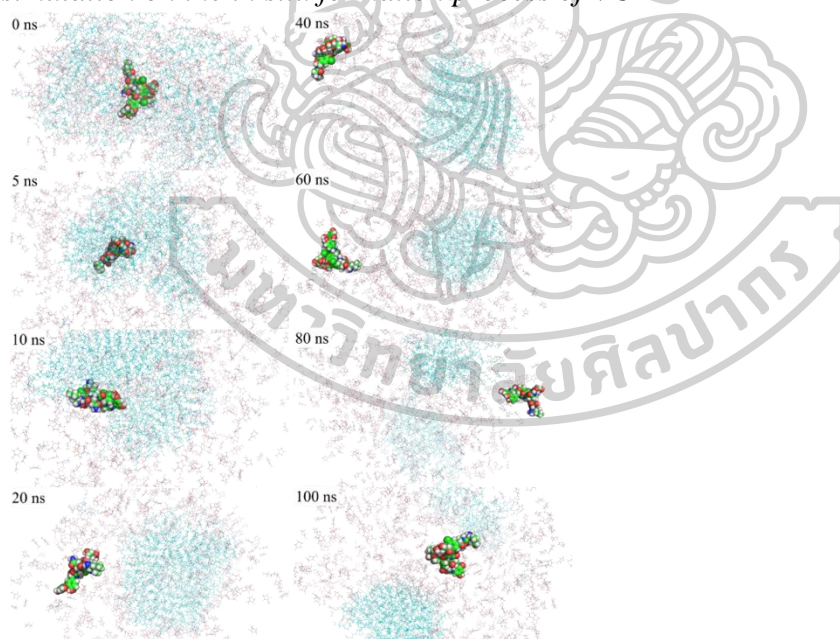
Figure 48 Snapshot structures at 0, 5, 10, 20, 40, 60, 80 and 100 ns of the MD simulation on the in situ formation process of VCPRN
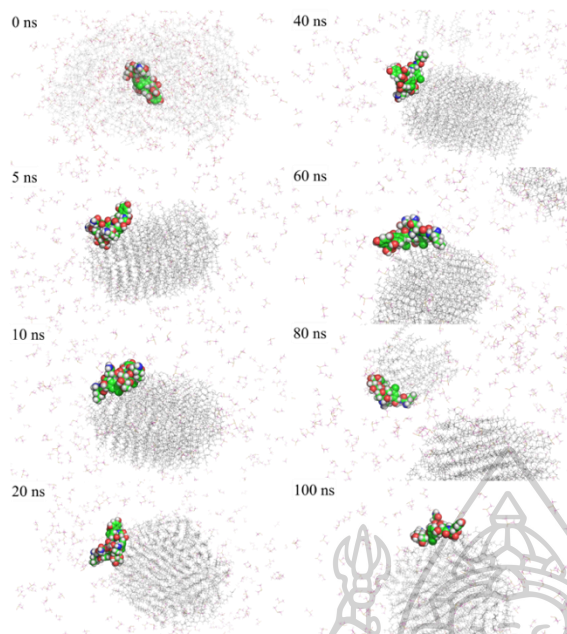
Figure 49 Snapshot structures at 0, 5, 10, 20, 40, 60, 80 and 100 ns of the MD simulation on the in situ formation process of VLAUD
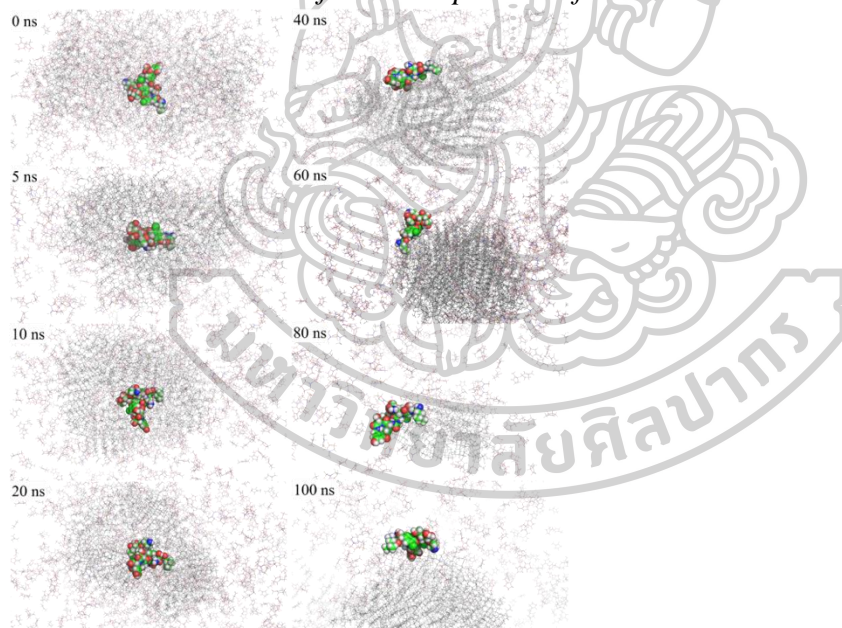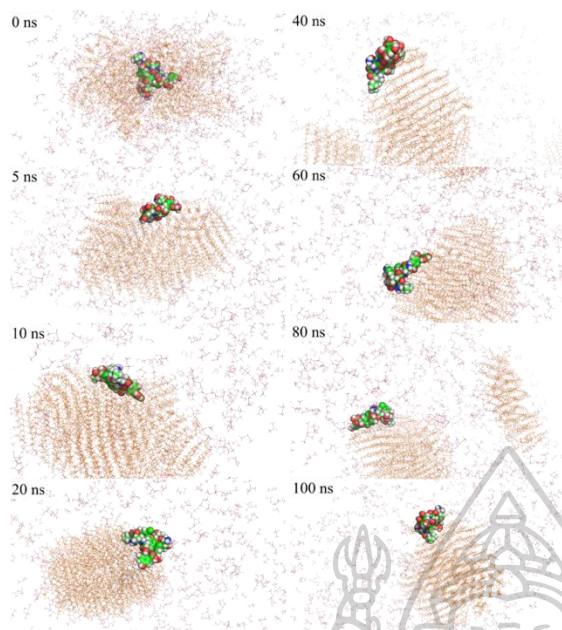

Figure 50 Snapshot structures at 0, 5, 10, 20, 40, 60, 80 and 100 ns of the MD simulation on the in situ formation process of VLAUN

Figure 51 Snapshot structures at 0, 5, 10, 20, 40, 60, 80 and 100 ns of the MD simulation on the in situ formation process of VMYRD
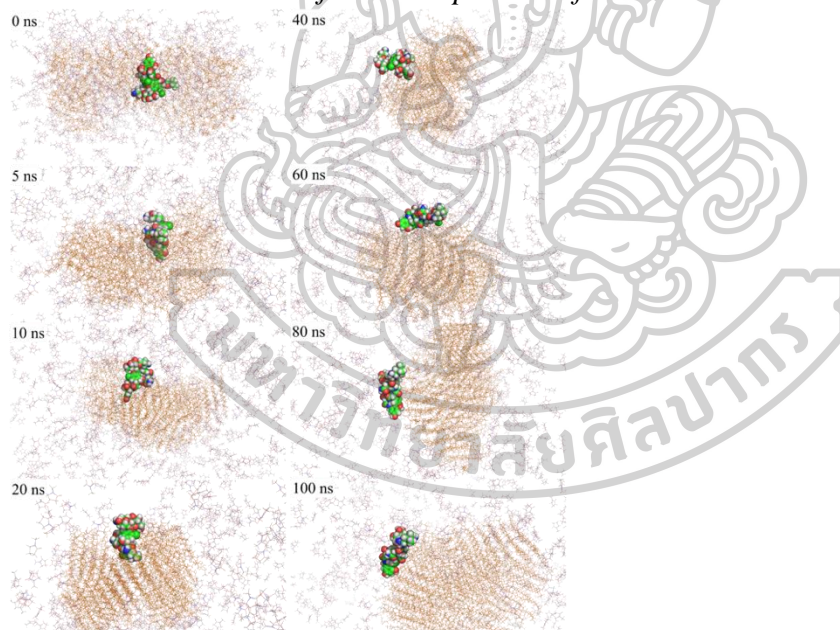

Figure 52 Snapshot structures at 0, 5, 10, 20, 40, 60, 80 and 100 ns of the MD simulation on the in situ formation process of VMYRN
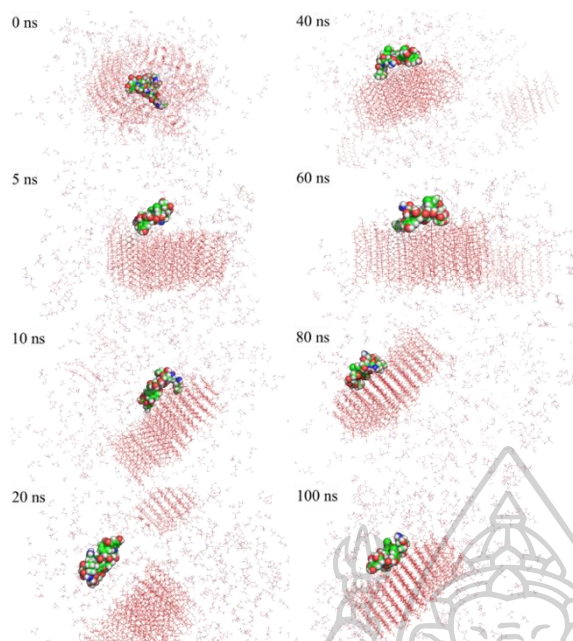
Figure 53 Snapshot structures at 0, 5, 10, 20, 40, 60, 80 and 100 ns of the MD simulation on the in situ formation process of VPALD
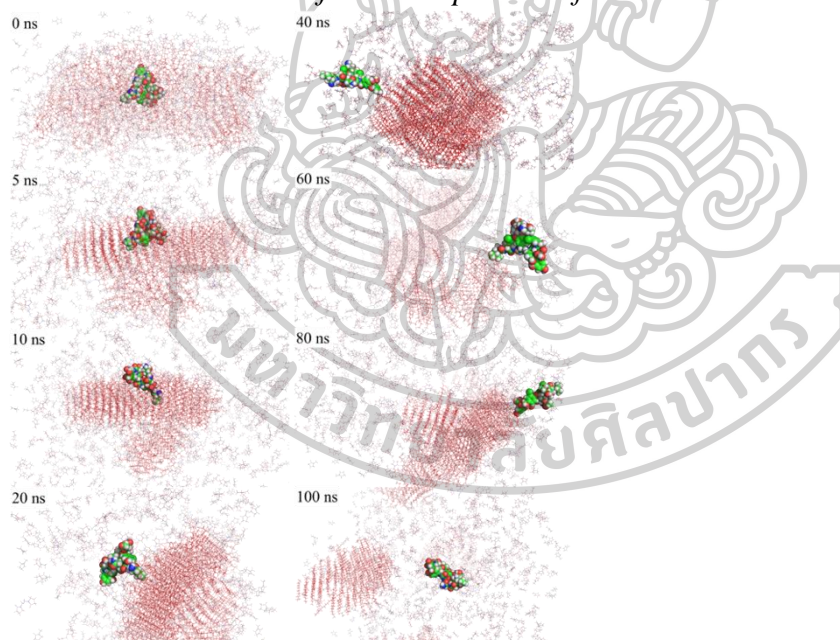

Figure 54 Snapshot structures at 0, 5, 10, 20, 40, 60, 80 and 100 ns of the MD simulation on the in situ formation process of VPALN
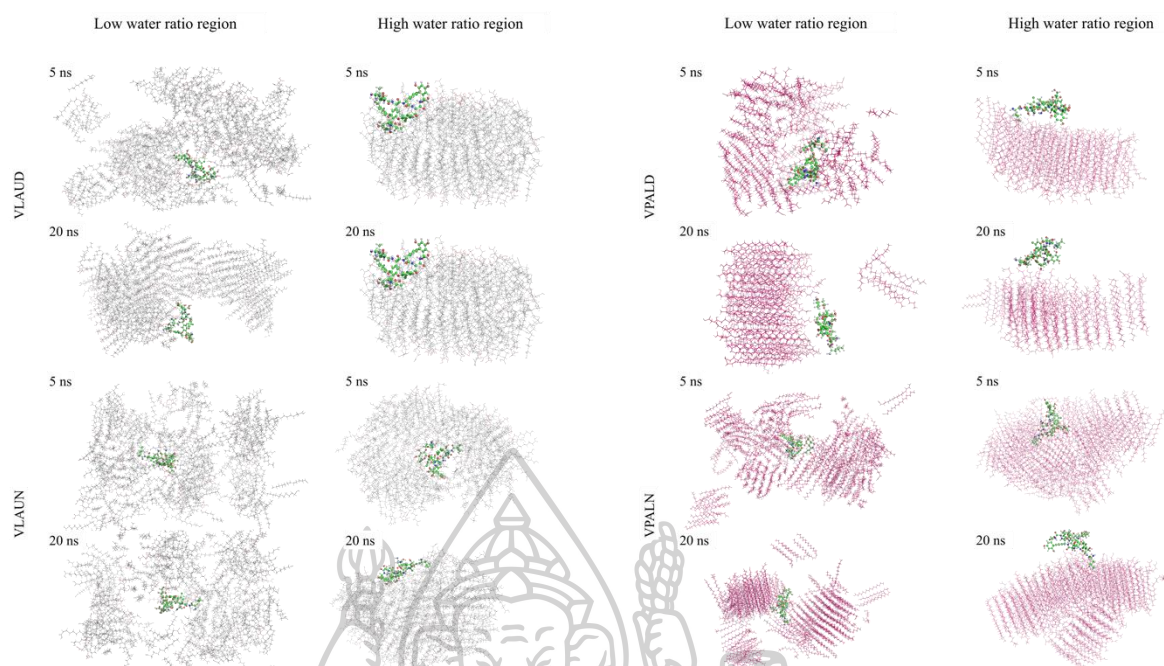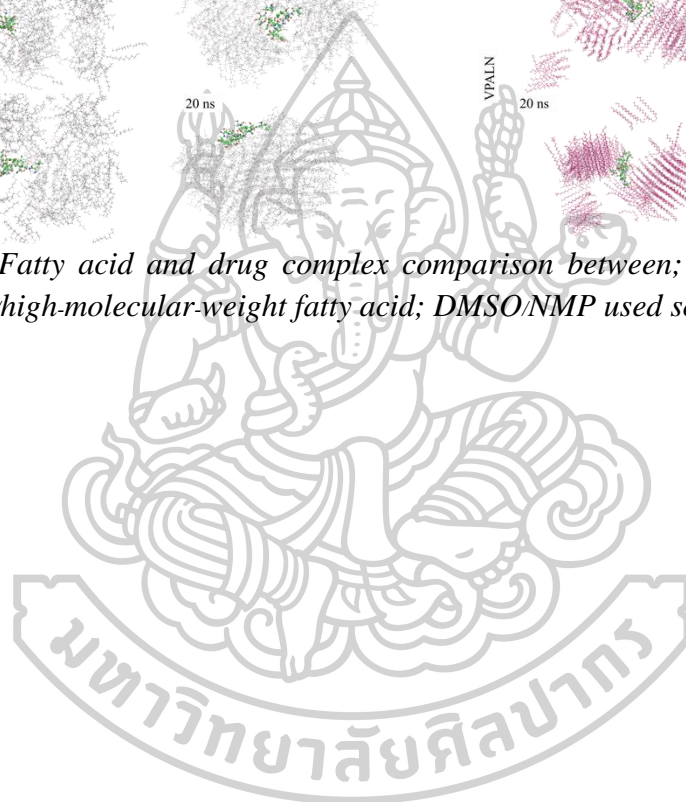
Figure 55 Fatty acid and drug complex comparison between; low/high-water-ratio region; low/high-molecular-weight fatty acid; DMSO/NMP used solvent

VITA

NAME	Takron Chantadee
DATE OF BIRTH	07 Sep 1992
PLACE OF BIRTH	Bangkok
INSTITUTIONS ATTENDED	Doctor of Pharmacy (Pharm. D.), Faculty of Pharmacy, Silpakorn University, Nakorn Pathom Thailand
HOME ADDRESS	37 Romklao road, Sansab, Minburi, Bangkok, 10510

PUBLICATION

Chantadee T, Sirirak J, Hoshino T, Phaechamud T. Augmentative molecular aspect for phase inversion of vancomycin hydrochloride-loaded fatty acid in situ forming matrices (Accepted)

Chantadee T, Santimaleeworagun W, Phorom Y, Phaechamud T. Saturated fatty acid-based in situ forming matrices for localized antimicrobial delivery. Pharmaceutics 2020; 12, article 808. https://doi.org/10.3390/pharmaceutics12090808

Chantadee T, Santimaleeworagun W, Phorom Y, Chuenbarn T, Phaechamud T. Vancomycin HCl-loaded lauric acid in situ-forming gel with phase inversion for periodontitis treatment. Journal of Drug Delivery Science and Technology 2020;57: article 101615. https://doi.org/10.1016/j.jddst.2020.101615

Chantadee T, Santimaleeworagun W, Phaechamud T. Vancomycin hydrochloride-loaded stearic acid/lauric acid in situ forming matrix for antimicrobial inhibition in patients with joint infection after total knee arthroplasty. Materials Science & Engineering C 2020;115: article 110761. https://doi.org/10.1016/j.msec.2020.110761

Chantadee T, Santimaleeworagun W, Phorom Y, Phaechamud T. Mixed solvent-lauric acid solvent-exchange induced in situ forming gel. Key Engineering Materials 2019;819:195-201.

Chantadee T, Lertsuphovanit N, Phaechamud T. Application of fatty acid for pharmaceuticals. Thai Bulletin of Pharmaceutical Sciences 2019;14(1):1-11.

Puyathorn N, Chantadee T, Senarat S, Phaechamud T.

Characterization of lauric acid precipitated from biocompatible solvents. Key Engineering Materials 2019;819:209-14.

Phaechamud T, Lertsuphotvanit N, Issarayungyuen P, Chantadee T. Design, fabrication and characterization of xanthan gum/liquid-loaded porous natural rubber film. Journal of Pharmaceutical Investigation 2018;49(1):149-60.

Senarat S, Chantadee T, Santimaleeworagun W, Phorom Y, Phaechamud T. Alpha-mangostin phase inversion induced in situ forming gel. Key Engineering Materials 2019;819:202-8.

Khaing EM, Chantadee T, Intaraphairot T, Phaechamud T. Gamboge resin-based phase separation in situ forming gel. Key Engineering Materials 2019;819:215-20.

Rojanarata T, Laiwattanapaisal W, Ngawhirunpat T, Opanasopit P, Worrawethanakul K, Chantadee T, Fuangwattana T. Fast, affordable and eco-friendly enzyme kinetic method for the assay of α-ketoglutaric acid in medical product and sports supplements. Enzyme and Microbial Technology 2018;116:72-6.

Phaechamud T, Thurein SM, Chantadee T. Role of clove oil in solvent exchange-induced doxycycline hyclate-loaded eudragit rs in situ forming gel. Asian Journal of Pharmaceutical Sciences 2018;13(2):131-42.

Phaechamud T, Jantadee T, Mahadlek J, Charoensuksai P, Pichayakorn W. Characterization of antimicrobial agent loaded eudragit rs solvent exchange-induced in situ forming gels for periodontitis treatment. AAPS PharmSciTech 2017;18(2):494-508.

Jantadee T, Savetkairop C, Lertsuphovanit N, Phaechamud T. Key factors to be considered in pharmaceutical suspensions. Thai Pharmaceutical and Health Science Journal 2017;12(2).:91-99.

Granted by Faculty of Pharmacy, Silpakorn University (Bond-free Scholarships)

Outstanding poster award 2018in title "Designing fatty acid solvent exchange-induced in situ forming gel comprising vancomycin HCl for periodontal pocket targeted delivery", ISPE Thailand 15th Anniversary Annual Meeting. 2018 July 16th, 2018, Ambassador hotel, Bangkok, Thailand.

Best poster presentation award for undergraduate students (Gold Medal) 2019 (together with Setthapong Senarat, Wichai Santimaleeworagun, Yaowarak Phorom and Thawatchai Phaechamud) in title "Alpha-mangostin phase inversion induced in situ forming gel" the International Conference and Exhibition on Pharmaceutical Sciences and Technology 2019 (PST2019), 18-19 June, 2019, Ambassador Hotel, Bangkok, Thailand.

Silver Medal 2019 of Thailand Inventors' Day (together withThawatchai Phaechamud and Wichai Santimaleeworagun) in title "Saturated fatty acid phase inversion-induced in situ forming matrix for periodontitis treatment", Thailand Inventors' Day, National Research Council of Thailand, 2-6 February, 2019, Event Hall 102 – 104. BITEC, Bangkok, Thailand.

Outstanding poster presentation award 2018 (together with Nutdanai Lertsuphotvanit, Pongsathorn Issarayungyuen and Thawatchai Phaechamud) in title 'Emerging role of xanthan gum in triethyl citrate or glycerin-loaded porous natural rubber film", 34th International Annual Meeting in Pharmaceutical Sciences and 2nd cuFphS- RIKEN cDB Symposium "Advances in cellular and Molecular Biology", Arnoma hotel, 8 March, 2018, Bangkok, Thailand